Oligonuclear complexes derived from aroylbis(*N,N*-dialkylthioureas)

Freie Universität Berlin

Fachbereich Biologie, Chemie, Pharmazie

Institute of Chemistry and Biochemistry

Berlin

Pham Chien Thang

Berlin, April 2016

1. Supervisor: Prof. Dr. Ulrich Abram

2. Supervisor: Prof. Dr. Dieter Lentz

Date of the oral examination: 10.05.2016

Acknowledgement

Table of contents

Abbreviations

1 D	one dimensional
2 D	two dimensional
br	broad
calcd.	calculated
d	doublet
DEPT	Distortionless Enhancement by Polarization Transfer
EPR	Electron Paramagnetic Resonance
ESI	Electrospray Ionization
IR	Infrared
m (in IR spectroscopy)	medium
m (in NMR spectroscopy)	multiplet
MS	Mass Spectroscopy
NMR	Nuclear Magnetic Resonance
q	quartet
s (in IR spectroscopy)	strong
s (in NMR spectroscopy)	singlet
SCC	Supramolecular Coordination Complex
t	triplet
vs	very strong
w	weak

Abstract

This thesis contains synthesis and characterization of well-ordered and multinuclear coordination systems derived from three aroylbis(N,N-dialkylthiourea) ligands, namely isopthaloylbis(N,N-diethylthiourea) H_2L^1, dipicolinoylbis(N,N-diethylthiourea) H_2L^2 and the catechol-spacered H_2L^3. Various oligometallic complexes with different structural topologies have been synthesized by one-pot reactions of the ligands with a large variety of mixtures of two cations including main group, transition, rare earth metal ions and even the non-metal ion NH_4^+. The systematic variation of cations indicates that the rational compositions and structures of such assemblies can be controlled following basic rules of coordination chemistry, such as the Pearson acid and base concept, ionic radii, preferred coordination numbers and coordination environments of metal ions. Besides structural characterization, studies on dynamic properties in solution as well as physiochemical, i.e. redox and magnetic, properties of some representative multinuclear systems were performed.

x

Chapter 1
Introduction

1.1 Supramolecular coordination compounds

The recent decades have witnessed an explosive growth of coordination chemistry with emergence of numerous new branches. One of them is the Supramolecular Coordination Chemistry, which describes Supramolecular Coordination Complexes (SCCs) possessing structural diversity and fascinating physical properties, which are generally inaccessible with organic compounds.[1]
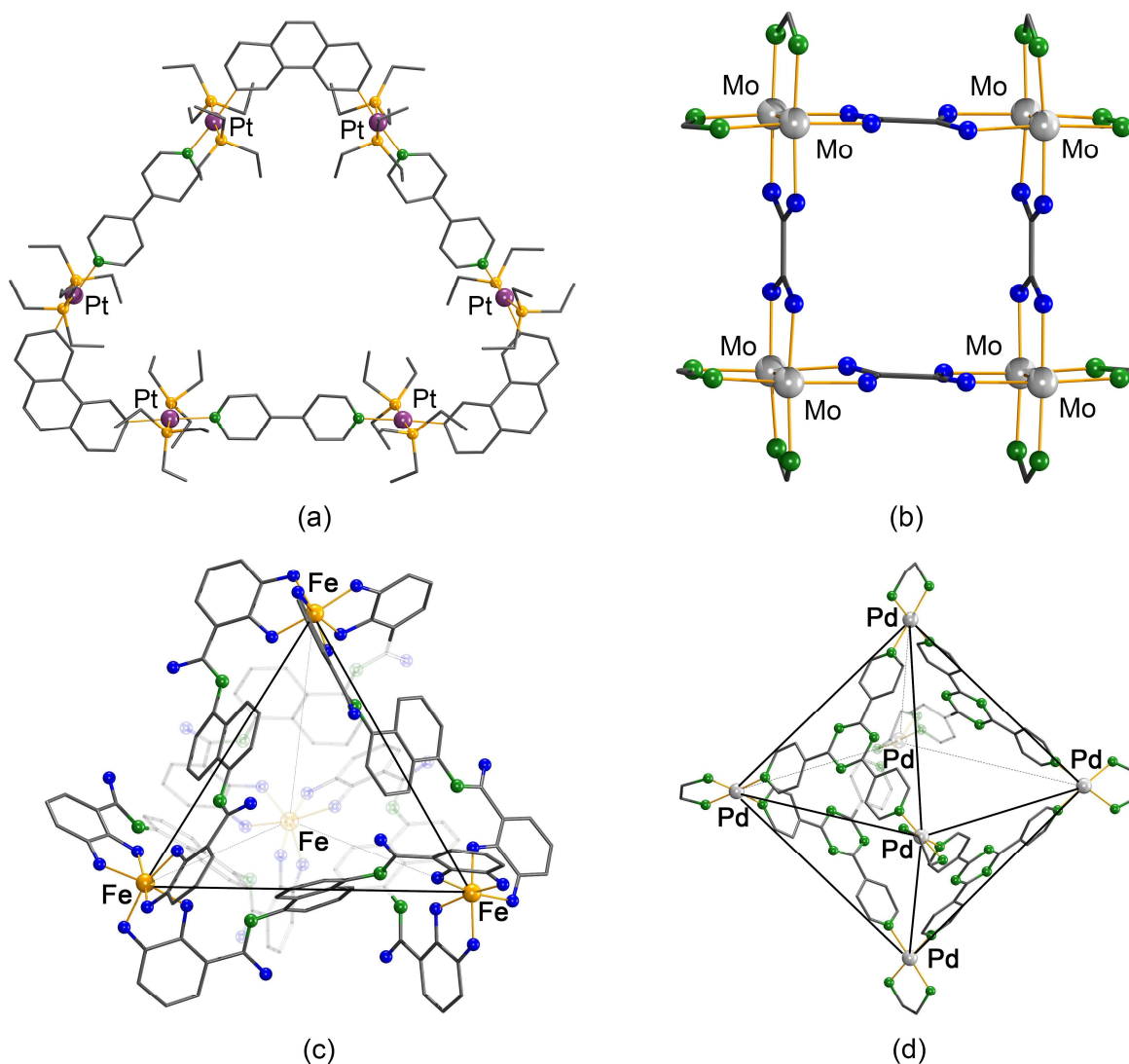
Figure 1.1 Self-assembled polygons and polyhedra: (a) Molecular triangle by Stang *et al.*[2] (b) Molecular square by Cotton *et al.*[3] (c) Tetrahedral cage by Raymond *et al.*[4] (d) Octahedral cage by Fujita *et al.*[5]

SCCs can be defined as discrete supramolecular assemblies, typically obtained in one-pot reactions in high yields by mixing soluble metal ions and ligands, which spontaneously self-assemble under formation of single thermodynamically favored products.[1] Five major strategies, namely i) Stang's directional binding approach,[6] ii) Fujita's molecular paneling procedure,[7] iii) Raymond's symmetry-interaction method,[8] iv) Cotton's use of dimetallic building blocks,[9] and v) Mirkin's weak-link approach,[10] have been developed and widely used for rational syntheses of aesthetic SCCs with predetermined shapes, sizes and functionalities. Representative structural topologies are introduced in Figure 1.1. Due to the strict requirements of chemical information being encoded in the subunits, however, the selection of appropriate building blocks continues to be a challenge of designing large and complex coordination systems. In this study, the potential exploitation of aroylbis(*N,N*-dialkylthioureas) as molecular components for the construction of such systems will be discussed.

1.2 Coordination chemistry of aroyl-*N,N*-dialkylthioureas

The first acyl/aroyl-*N,N*-dialkylthiourea has been synthesized in 1873 and, then the synthetic procedure was simplified by Dixon and Taylor in 1908 and later by Douglass and Dains in 1934.[11-13]
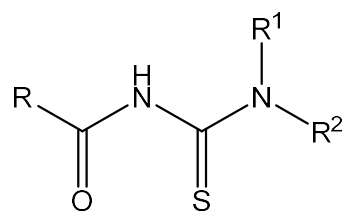
R, R^1, R^2: alkyl or aryl

Figure 1.2 General formula of acyl/aroyl-*N,N*-dialkylthioureas.

In spite of the age of this class of compounds, their coordination chemistry has been only explored in the last four decades, pioneered by the work of Beyer and Hoyer.[14] The hard (*O*) and soft (*S*) donor atoms as well as of a dissociable proton in the weakly acidic amido group –NH– provide various coordination possibilities. In the majority of structurally characterized complexes, aroyl-*N,N*-dialkylthioureas (HL) act as monoanionic, bidentate *S,O* chelates, which form dominantly *cis* square-planar complexes **1** of the general composition *cis*-[M(L-*S,O*)$_2$] with d^8 or d^9 metal ions such as Ni(II), Pd(II), Pt(II), or Cu(II),[15-18] and facial octahedral complexes *fac*-[M(L-*S,O*)$_3$] (**2**) with trivalent metal ions such as Fe(III), Co(III), Tc(III), Ru(III)

or Rh(III).[19-23] There is only one example of a tricarbonylrhenium(I) complex **3**, where chelate formation is observed with the neutral ligand HL.[24] Moreover, coordination as neutral, monodentate *S*-ligands is found in a few complexes with Ag(I), Au(I) and Pt(II) (Figure 1.3).[25-27]

1

2

3

4
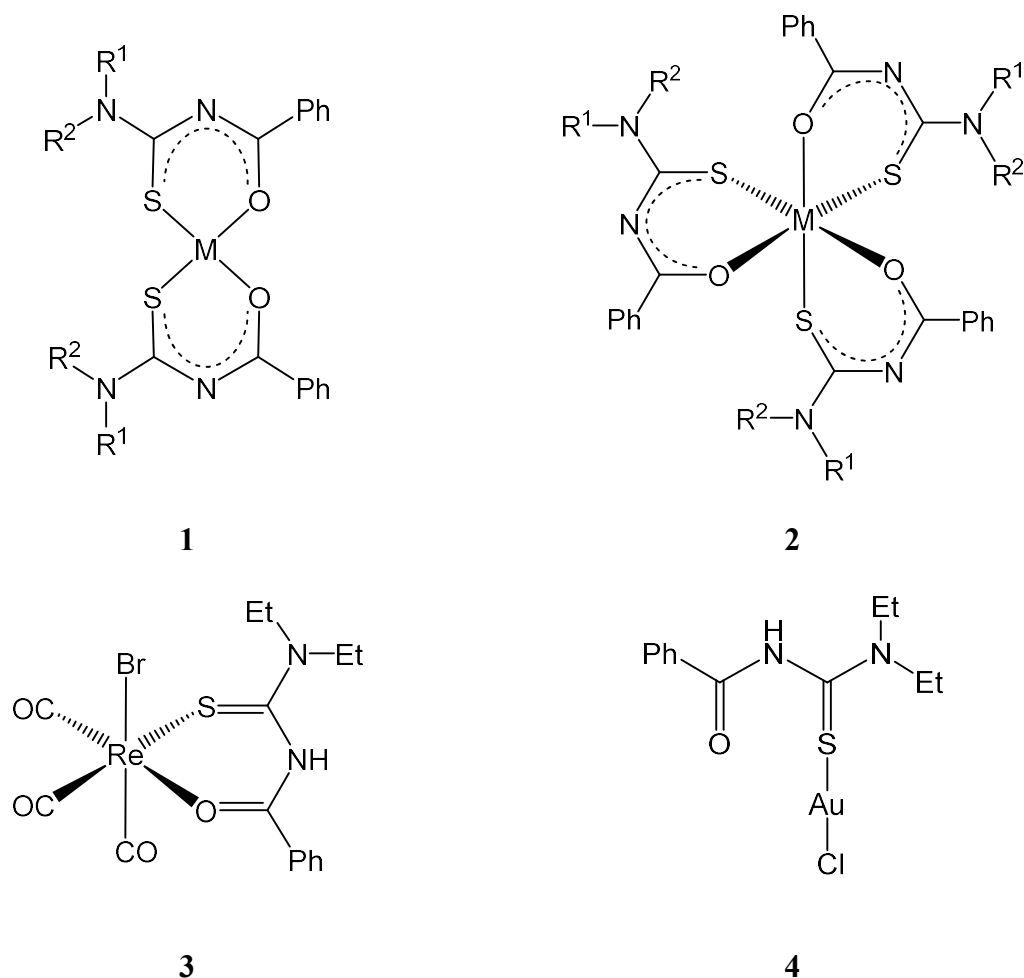
Figure 1.3 Representative coordination modes of benzoyl-*N,N*-dialkylthioureas.

Interestingly, the symmetrical bipodal aroylthiourea derivatives **5** and **6** with two *S,O*-chelating moieties are well suitable for the synthesis of multinuclear complexes. The self-assembly of these ligands with metal ions, which preferably form square-planar or pseudo square-planar complexes such as Ni(II), Pd(II), Pt(II) or Cu(II), results in discrete metallamacrocyclic complexes the basic structures of which strongly depend on the relative positions of the aroylthiourea moieties at the central benzene ring. Particularly, *para* substituted phthaloylbis(*N,N*-dialkylthioureas) **5** are able to form trinuclear metallamacrocycles [M(*p*-L-*S,O*)]₃ (**7**),[28-31] while *meta* substitution as in compounds **6** give rise to binuclear metallamacrocyclic complexes [M(*m*-L-*S,O*)]₂ (**8**).[30, 32-34] In all structurally characterized bi- and trinuclear complexes, the metal ions adopt square-planar geometry with *cis* arrangement

of the donor atoms, which effectively prevents the formation of coordination polymers as have recently been isolated from the reaction of the diethyl derivative of **6** and Pb(II).[35]

5   *p*-H₂L

7

6   *m*-H₂L

8
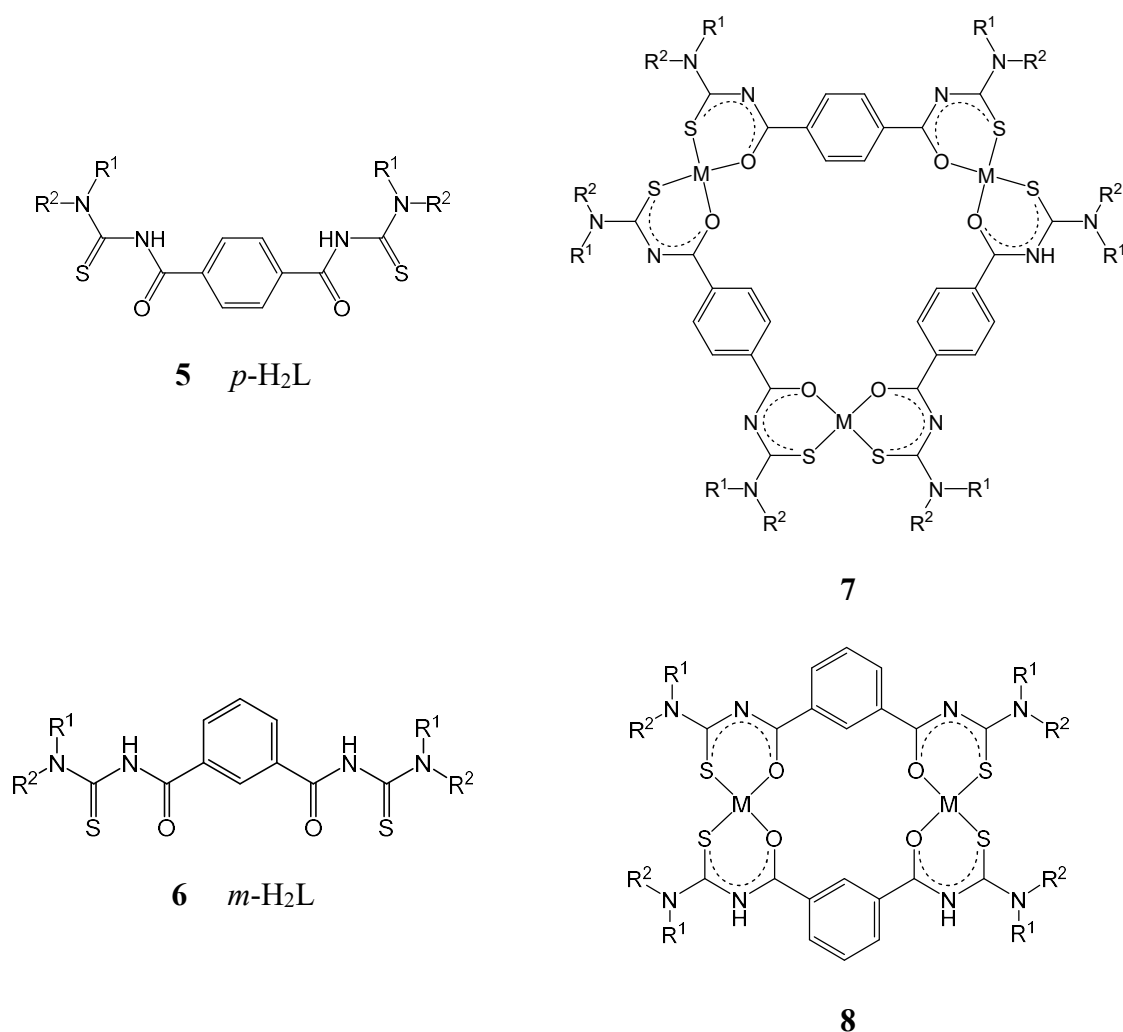
Figure 1.4 Phthaloylbis(*N,N*-dialkylthioureas) and corresponding metallamacrocyclic complexes.

It is noteworthy that the bimetallamacrocycles **8** containing oxidorhenium(V) cores can undergo reversible hydrolytic dimerization under formation of tetranuclear compounds possessing cage-like structures. Nevertheless, the central voids built up by eight oxygen donor atoms with an approximate diameter of 6 Å is empty.[36] With the aim of extending the coordination abilities of such systems, the ligands **6** have been modified using heterocyclic rings, for example pyrrole or pyridine, instead of the benzene ring. The efficiency of the modification strategy has been indicated by recent reports on similar molecular cages, however, in form of host-guest compounds with guest water molecule and alkali metal ions for pyrrole- and pyridine-spacered aroylbis(*N,N*-dialkylthioureas), respectively (Figure 1.5).[37-38]

9 H$_2$L^{pyrrole} **10** H$_2$L^2

{H$_2$O $\subset$ {[ReO(L^{pyrrole})]$_2$O}$_2$}   {K $\subset$ {[ReO(L^2)]$_2$O}$_2$}$^+$
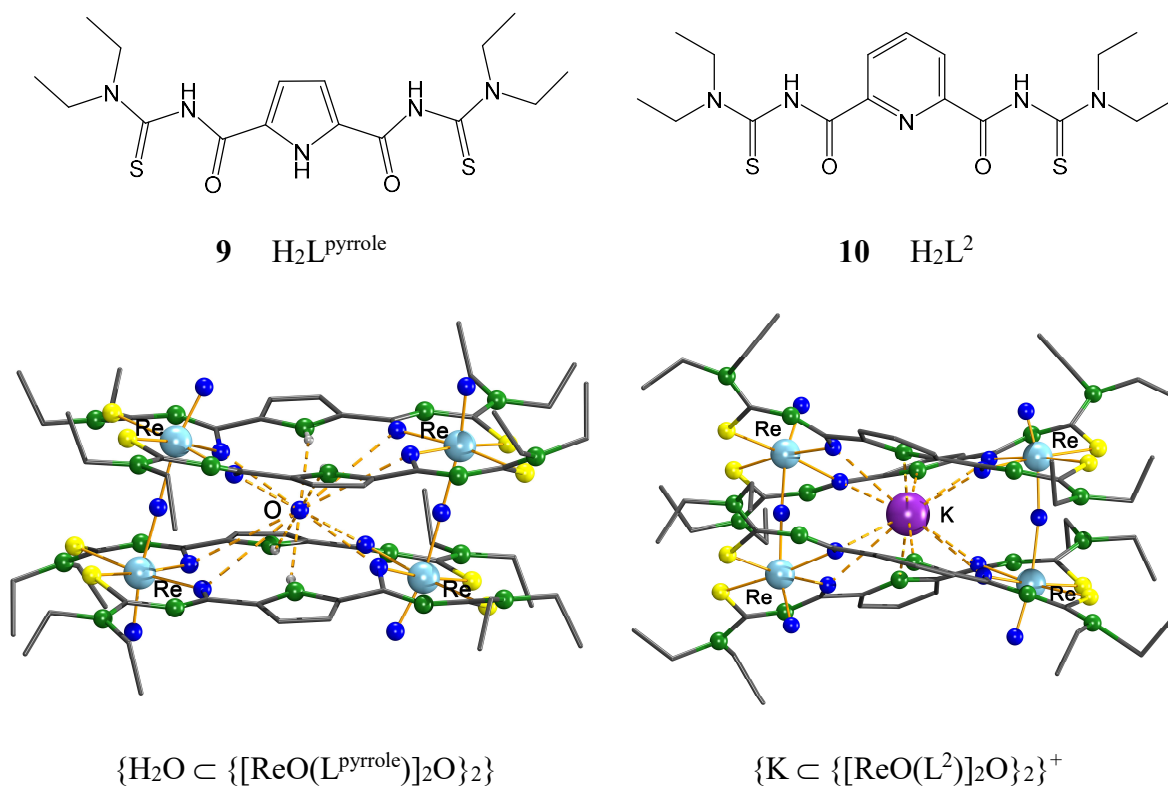
Figure 1.5 Recent aroylbis(*N,N*-diethylthioureas) and corresponding host-guest species.[37-38]

Furthermore, it is remarkable that self-assembly of the ligand **10** with mixtures of two metal ions enables the construction of a variety of novel trinuclear mixed-metal complexes, which could be perceived as inclusion complexes between metallamacrocycles and hard metal ions, with rational compositions and molecular structures.[38]

1.3 Goal of the present research

The hitherto done work on the coordination chemistry of aroylbis(*N,N*-dialkylthioureas) demonstrates their considerable potential for the construction of SCCs. This prospect stimulates the present research on exploiting this class of ligands as molecular components for the assembling of well-ordered and multinuclear coordination systems. For this purpose, aroylbis(*N,N*-dialkylthioureas) with respect to increasing order of denticity, size and flexibility of the backbones of their spacers are used (Figure 1.6). This will allow the synthesis of various ligand-metal assemblies with different topologies. Moreover, the key factors, which control the self-assembling processes and, consequently, determine topologies of resulting assemblies, can be determined and effectively utilized in the synthetic routes.
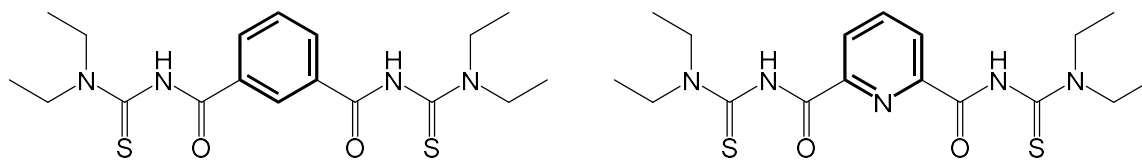
H₂L¹

H₂L²
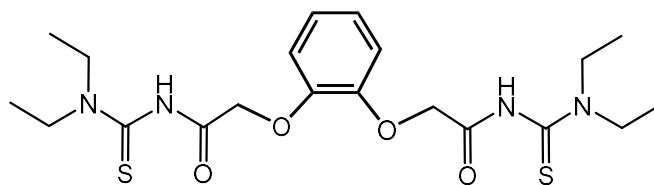
H₂L³

Figure 1.6 Aroylbis(*N,N*-diethylthioureas) used throughout this study.

Chapter 2

Aroylbis(*N,N*-diethylthioureas)

One of the most attractive features of aroyl-*N,N*-dialkylthiourea ligands is their facile synthesis according to the procedure proposed by Douglas and Dain in 1934.[13] The compounds can be prepared from a two-step, one-pot synthesis starting from readily available and inexpensive starting materials, namely aroyl chlorides, NH_4SCN or KSCN, and secondary amines. Pure products are usually obtained with good yields. This straightforward route has been successfully applied to the synthesis of a few aroylbis(*N,N*-dialkylthioureas), for example the isophthaloyl derivative H_2L^1 (Scheme 2.1).[30, 32]
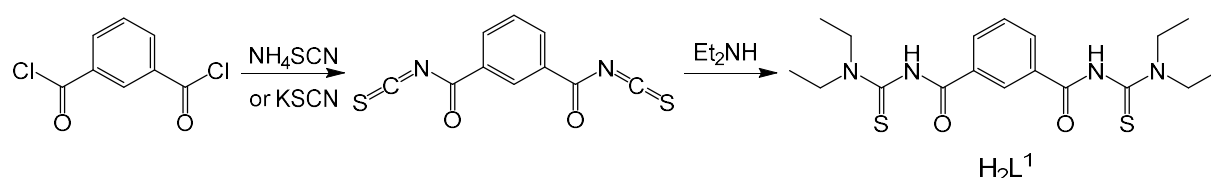
Scheme 2.1 Application of the Douglas and Dain procedure for the synthesis of H_2L^1.

Such a synthetic method, however, is not effective for compounds containing heteroatoms in the backbones of their spacer, for instance the ligand H_2L^2.[39] Therefore, the synthesis of such compounds is performed by an alternative procedure published by Dixon and Taylor with slight modifications.[12, 40] This general procedure starts with the synthesis of the corresponding *N,N*-disubstituted thioureas from hydrolysis of the intermediates ethoxycarbonyl *N,N*-dialkylthioureas, which are prepared following the Douglas and Dain route for chloroformic acid ethylester and secondary amines, under strongly acidic conditions.[41] Details are given in Scheme 2.2 for *N,N*-diethylthiourea, which can be obtained with 50% yield.
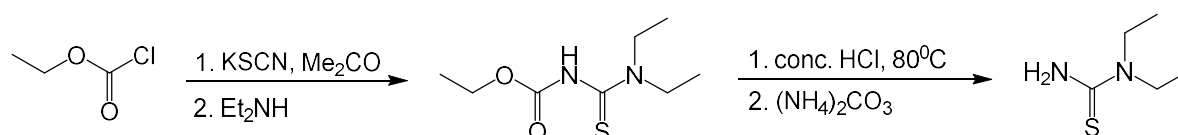
Scheme 2.2 Synthesis of *N,N*-diethylthiourea.

N,N-Dialkylthioureas readily react with carboxylic acid chlorides in the presence of a supporting base under the formation of corresponding aroyl(*N,N*-dialkylthioureas). The possibility of applying such an approach for the synthesis of bisubstituted aroylthiourea derivatives has been proven with H_2L^2 and the novel H_2L^3 ligands (Schemes 2.3 and 2.4).
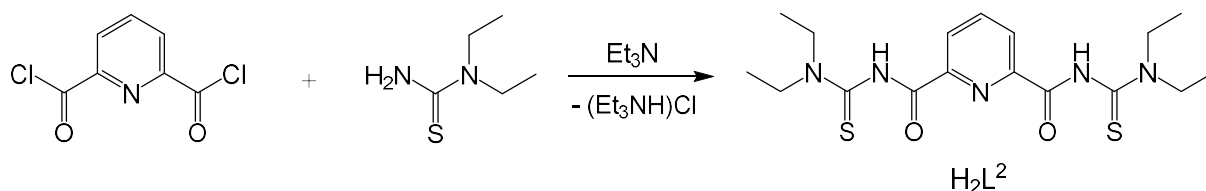
Scheme 2.3 The Dixon and Taylor procedure for synthesis of H_2L^2.

Synthesis as well as spectroscopic and structural characterization of the isophthaloyl- and dipicolinoylbis(*N,N*-diethylthioureas), H_2L^1 [30, 32] and H_2L^2, have been reported previously.[38-39]

The synthesis of H_2L^3 starts with the preparation of the dicarboxylic acid **11** from catechol.[42] Then, **11** is converted into its dichloride **12** by refluxing it in an excess of $SOCl_2$. The reaction of **12** with *N,N*-diethylthiourea in the presence of Et_3N gives the ligand H_2L^3 in 70% yield (Scheme 2.4).
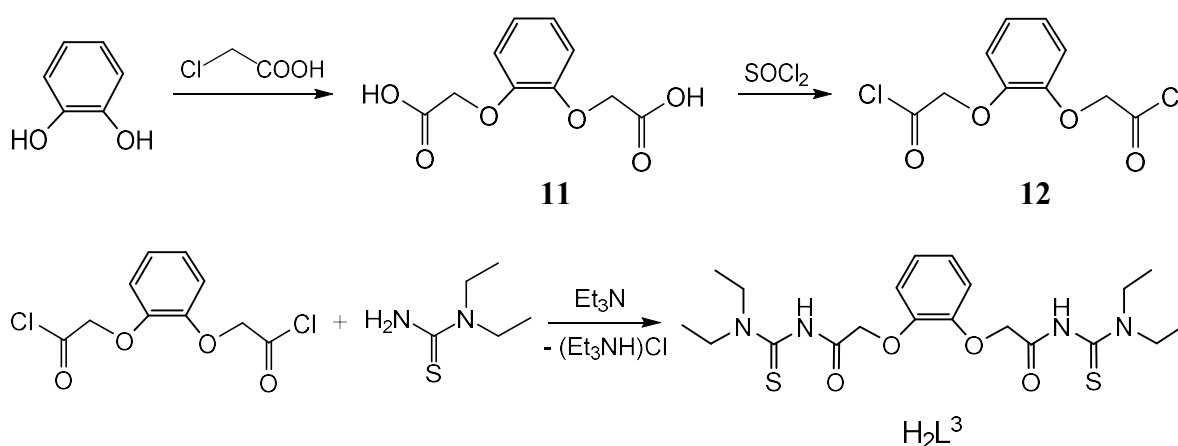
Scheme 2.4 Synthesis of H_2L^3.

The IR spectrum of H_2L^3 is characterized by a medium broad absorption at 3163 cm^{-1} and a strong absorption at 1659 cm^{-1}, which can be assigned to the stretching vibrations of the NH and C=O groups, respectively. The ^1H NMR spectrum of H_2L^3 in CDCl$_3$ presents a broad signal at 8.92 ppm, which confirms the presence of NH protons. Another broad signal at 4.66 ppm is assigned to the methylene protons of OCH$_2$. Two well-separated signal sets of two ethyl groups indicate the hindered rotation around the C(S)–NEt$_2$ bond, which is normally also observed for other aroyl-*N,N*-dialkylthioureas.[21, 30] The successful synthesis of H_2L^3 demonstrates that the procedure of Dixon and Taylor is also appropriate for the preparation of bisubstituted aroylthiourea derivatives.

In the following Chapters, metal-ligand assemblies derived from the three ligands in Figure 1.6 will be discussed. The two hitherto known ligands, H_2L^1 and H_2L^2, are used as probe for the

synthetic routes. Subsequently, the expertise acquired is applied to the novel catechol-spacered aroylbis(N,N-diethylthiourea) H_2L^3. The resulting coordination systems are classified according to their topologies as introduced by Saalfrank *et al.*[43] and organized in terms of coordination number or electronic properties of transition metal ions:

(i)   Assemblies with six-coordinate octahedral metal ions

(ii)   Assemblies with four-coordinate metal ions

(iii)   Assemblies with four- or six-coordinate metal ions

(iv)   Assemblies with thiophilic metal ions

Chapter 3

Assemblies with six-coordinate octahedral metal ions

The versatility of ligand-interaction modes of six-coordinate octahedral metal ions allows the straightforward access to different architectures.[44] Surprisingly less is known about complexes of aroylbis(*N,N*-dialkylthioureas) with this type of metal ions. Indeed, there is only one binuclear In(III) complex with the ligand H_2L^1 recently reported.[35] X-ray structure analysis of the complex reveals that distorted octahedral coordination of In(III) ions with three bis(bidentate) chelators leads to a metallamacrocylce with a cryptand-like structure (Figure 3.1). This hitherto unprecedented structure type in the chemistry of aroylbis(*N,N*-dialkylthioureas) is the prototype of metal-ligand assemblies discussed in this Chapter.

$[In_2(L^1)_3]$ 2, 2, 2-Cryptand
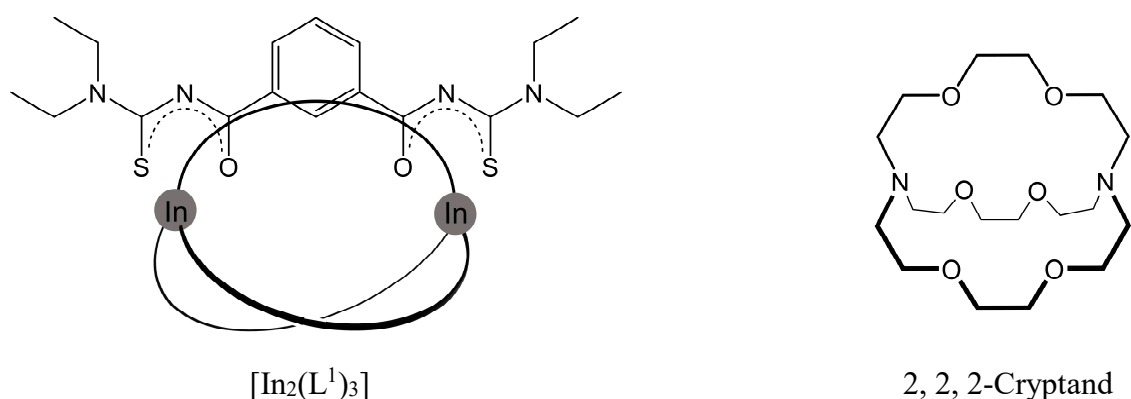
Figure 3.1 Metallamacrocycle with cryptand-like structure.

3.1 An iron(III)-containing macrocycle $[Fe_2(L^1)_3]$

Taking into account the coordination chemistry of metal ions and redox properties of resulting complexes, Fe^{3+} ions should be representative of six-coordinate octahedral transition metal ions. When the same procedure reported for the In(III) complex is applied for reaction between iron(III) chloride and the ligand H_2L^1, pure $[Fe_2(L^1)_3]$ deposits directly from reaction mixture as a dark-red solid. In the IR spectrum of the compound, no absorptions in the region above 3100 cm^{-1} corresponding to v_{NH} stretches are observed. This is a sign of the deprotonation of the ligand during complexation. A bathochromic shift of the $v_{C=O}$ band from 1690 cm^{-1} in H_2L^1 to 1504 cm^{-1} in the complex strongly reflects the formation of *S,O* chelates after the coordination with the metal ions. The result of the elemental analysis and the detection of the expected molecular ions as well as corresponding $[M + Na]^+$ and $[M + K]^+$ ions in the ESI$^+$ MS

spectrum are clear evidences for the formation of a neutral complex with the composition of $[Fe_2(L^1)_3]$. This is confirmed by an X-ray diffraction analysis of single crystals obtained from slow evaporation of a solution of the complex in DMF. Figure 3.2 depicts the molecular structure of the compound and selected bond lengths and torsion angles are given in Table 3.1. The coordination geometry of the metal ions is similar to that in the In(III) complex. In particular, two iron ions coordinate with three bis(bidentate) deprotonated ligands $(L^1)^{2-}$ in distorted octahedral coordination modes with facial arrangement of the donor atoms. The Fe–O and Fe–S bond lengths are in the same ranges as those recently reported for an Fe(III) complex of the simple bidentate benzoyl-N,N-diethylthiourea ligand.[19] Despite considerable deviation of the six-membered chelate rings from the planarity, as pointed out from the O–C–N–C and C–N–C–S torsion angles (Table 3.1), the typical extended π-systems for chelating aroylthiourea moieties are indicated by the double bond character of the C–O, C–N and C–S bonds.[21, 35] Additionally, slightly longer C(S)–N_{amide} bonds in comparison with the adjacent C(O)–N_{amide} bonds illustrate that electron density of the S,O chelates locates less on the soft S donors than on the hard O donors, which are in favor of the hard acceptor Fe^{3+}. With their empty voids, the isostructural, cryptand-like metallacycles $[Fe_2(L^1)_3]$ and $[In_2(L^1)_3]$ could be suitable as hosts for metal ions. However, all attempts to produce such an inclusion complex with small cations, even with Li^+, have failed. These results could be due to the fact that the coordination capacity of the central voids is insufficient for cation binding, and more seriously, the direction of three inner hydrogen atoms of the phenylene spacers towards the cavities remarkably reduces their effective sizes. These complications will be overcome, when the internal phenylene C–H group of H_2L^1 is replaced by a pyridine N atom as has been done with the synthesis of H_2L^2.
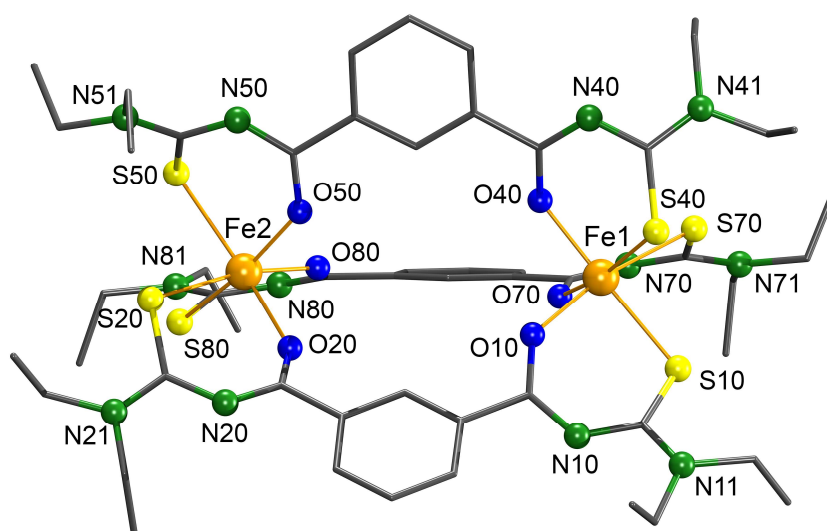
Figure 3.2 Molecular structure of $[Fe_2(L^1)_3]$. Hydrogen atoms are omitted for clarity.

Table 3.1 Selected bond lengths (Å) and torsion angles (°) in $[Fe_2(L^1)_3]$

Bond lengths (Å)							
Fe1–S10	2.427(4)	C10-O10	1.275(3)	C40–O40	1.274(3)	C70–O70	1.270(3)
Fe1–S40	2.453(2)	C10–N10	1.315(3)	C40–N40	1.318(3)	C70–N70	1.322(3)
Fe1–S70	2.465(2)	C11–N10	1.351(3)	C41–N40	1.340(3)	C71–N70	1.343(3)
Fe1–O10	1.989(9)	C11–N11	1.334(3)	C41–N41	1.330(3)	C71–N71	1.342(3)
Fe1–O40	1.987(7)	C11–S10	1.733(2)	C41–S40	1.742(2)	C71–S70	1.737(2)
Fe1–O70	1.993 (8)						
Fe2–S20	2.456(2)	C20–O20	1.269(3)	C50–O50	1.272(3)	C80–O80	1.271(3)
Fe2–S50	2.461(6)	C20–N20	1.325(3)	C50–N50	1.317(3)	C80–N80	1.320(3)
Fe2–S80	2.424 (7)	C21–N20	1.345(3)	C51–N50	1.339(3)	C81–N80	1.339(3)
Fe2–O20	1.999(1)	C21–N21	1.340(3)	C51–N51	1.335(3)	C81–N81	1.341(3)
Fe2–O50	2.007(7)	C21–S20	1.735(2)	C51–S50	1.743(2)	C81–S80	1.739(2)
Fe2–O80	1.983(9)						

Torsion angles (°)			
O10–C10–N10–C11	-5.20(9)	O20–C20–N20–C21	-9.66(7)
C10–N10–C11–S10	-22.38(4)	C20–N20–C21–S20	-22.10(5)
O40–C40–N40–C41	-14.79(2)	O50–C50–N50–C51	-21.11(6)
C40–N40–C41–S40	-34.89(1)	C50–N50–C51–S50	-30.42(9)
O70–C70–N70–C71	-12.44(9)	O80–C80–N80–C81	-9.69(3)
C70–N70–C71–S70	-26.81(6)	C80–N80–C81–S80	-20.21(3)

3.2. Metallacryptates derived from the ligand H_2L^2

3.2.1 The iron(III) metallacryptates $\{M \subset [Fe_2(L^2)_3]\}(PF_6)$ (M = Rb$^+$, K$^+$, Na$^+$, Tl$^+$, NH$_4^+$) and related compounds

Assuming that the *S,O* coordination mode of the ligand remains after the modification of the spacer, a neutral {2}-metallacryptand with the composition of $[Fe_2(L^2)_3]$ should result from the reaction of iron(III) ions and H_2L^2 under the same condition used for the synthesis of the previous complexes. Nonetheless, the product does not directly deposit from the reaction mixture as expected from the proposed composition. The good solubility in MeOH is a strong evidence for the formation of an ionic compound. After efforts to precipitate such species with different counterions, a product was isolated with Tl(I) ions with a yield of 62%. The IR

spectrum of the compound exhibits a strong $\nu_{C=O}$ band at 1601 cm^{-1}, which corresponds to a bathochromic shift of approximately 70 cm^{-1} with respect to the uncoordinated ligand. Compared with the standard value of approximately 200 cm^{-1} reported for benzoylthioureato chelates,[21, 35-36] the shift is quite modest and might be caused by a smaller degree of electron delocalization within the aroylthiourea moieties. The absence of a ν_{NH} band in the region above 3100 cm^{-1} indicates the expected deprotonation of the ligand. Slow evaporation of the solution of the product in a CH$_2$Cl$_2$/MeOH mixture gave single crystals of good quality. An X-ray diffraction analysis exhibits an unexpected structure of the composition of [TlFe(L^2)$_2$]. It is supported by elemental analysis and the presence of a peak associated with the fragment [Fe(L^2)$_2$]$^-$ in the ESI$^-$ MS spectrum. Figure 3.3a illustrates the structure of the mixed-metal complex [TlFe(L^2)$_2$]. Selected bond lengths are summarized in Table 3.2. The Fe^{3+} ion is six-coordinate with a distorted octahedral environment formed by two planar donor atom sets, (*N,N,N*) and (*O,N,N*). Each of them belongs to one deprotonated ligand (L^2)$^{2-}$. The former consists of the pyridine N atom and two amide N atoms of the first and second aroyl thiourea arms, while the latter comprises the pyridine N atom of the other ligand, the carbonyl O atom of its first arm and the amide N atom of the second arm. The fact that the C–O and C–S bonds in the amide-coordinated arms are shorter than those in the chelate rings of [Fe$_2$(L^1)$_3$] implies the greater double bond character of these bonds and, thus, the location of the negative charge of the arms on the amide N atoms, which directly bond with the Fe^{3+} ion. A similar charge location on the O40 atom can be deduced from the remarkably elongated C40–O40 bond and the shortened C40–N40 bond. The resulting hard Lewis base O40$^-$ acts as bridging ligand for the hard Lewis acids Fe^{3+} and Tl$^+$.

(a)   (b)
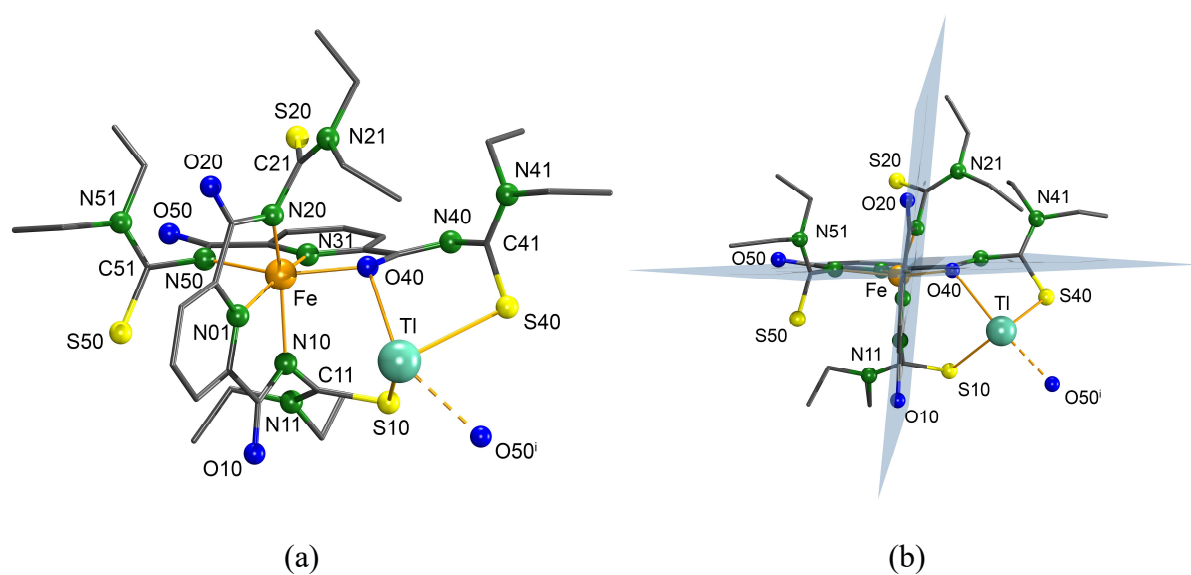
Figure 3.3 (a) Molecular structure of [TlFe(L^2)$_2$] (b) View along the N01–Fe–N31 connecting line. Hydrogen atoms are omitted for clarity.

Table 3.2 Selected bond lengths (Å) in [TlFe(L^2)$_2$]

Fe–N01	2.117(5)	O10–C10	1.228(9)	O40–C40	1.302(7)
Fe–N10	2.139(5)	C10–N10	1.356(8)	C40–N40	1.292(8)
Fe–N20	2.064(6)	N10–C11	1.413(8)	N40–C41	1.384(9)
Fe–N31	2.074(5)	C11–N11	1.308(9)	C41–N41	1.323(1)
Fe–O40	2.048(4)	C11–S10	1.701(7)	C41–S40	1.698(8)
Fe–N50	2.132(5)	O20–C20	1.245(8)	O50–C50	1.236(8)
Tl–S10	3.004(2)	C20–N20	1.341(8)	C50–N50	1.344(8)
Tl–S40	2.967(2)	N20–C21	1.415(9)	N50–C51	1.417(8)
Tl–O40	2.799(4)	C21–N21	1.315(9)	C51–N51	1.320(9)
Tl–O50^i	2.599(5)	C21–S20	1.682(7)	C51–S50	1.659(8)

Symmetry operation used to generate equivalent atoms: ^{i}x, 3/2-y, z-1/2

It is interesting that the Tl$^+$ ion acts not only as charge compensator for the anionic complex [Fe(L^2)$_2$]$^-$, but also as metal center for complexation. Indeed, Tl$^+$ is four-coordinate with a *S,S,O,O*-coordination sphere, which is formed by three donor atoms of one Fe chelate and an O atom of an adjacent unit. The resulting coordination polyhedra can be best described as square pyramids or distorted pseudo-triangular bipyramids taking into account a stereochemically active 6s lone pair of the Tl$^+$ ion as a fifth ligand. An analogous coordination geometry has been recently reported for Pb^{2+} ions in a polymeric complex with the ligand H$_2$L^1.[35]
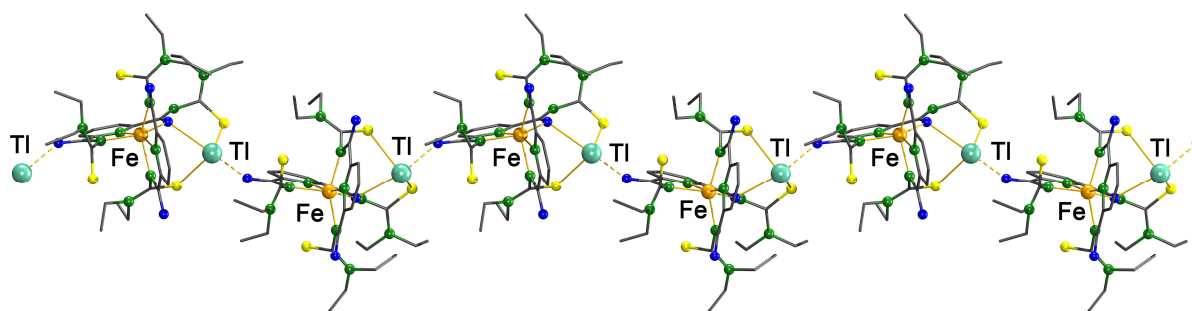
Figure 3.4 Structure of the 1D polymeric chain [TlFe(L^2)$_2$]$_\infty$. Hydrogen atoms are omitted for clarity.

The intermolecular Tl–O interaction is responsible for the formation of the 1D polymeric chain [TlFe(L^2)$_2$]$_\infty$ in the solid state (Figure 3.4), which can be considered as driving force for the separation of the anionic species [Fe(L^2)$_2$]$^-$ from the reaction mixture by using the large cation Tl$^+$. Another striking feature of the complex is the great deviation of the –C(S)–NEt$_2$ parts from the ligands planes (Figure 3.3b). Such deviation prevents electron delocalization within

aroylthiourea moieties, even within the *S,O* chelate ring surrounding Tl^+. This is in agreement with the modest bathochromic shift of the $\nu_{C=O}$ band observed in the IR spectrum and provides an explanation for the lesser double bond character of the $C(S)–N_{amide}$ bonds compared to the adjacent C–N bonds.

The failed synthesis of the {2}-metallacryptand $[Fe(L^2)_3]$ indicates that the 'hard acid' Fe^{3+} favours a mixture of 'borderline' and 'hard' base donor sets (*N,N,N* and *O,N,N*) over a mixture of 'soft' and 'hard' base chelators (*S,O*). In order to direct Fe^{3+} to the *S,O*-chelating aroylthiourea unit for coordination, reactions of H_2L^2 with mixtures of Fe^{3+} and 'harder' metal ions were carried out. In the above-mentioned reaction, Tl^+ was added as a second metal ion even after the addition of the base NEt_3 and finally only acted as a 'counterion'. When Tl^+ is added together with the Fe^{3+} ions to H_2L^2 before the supporting base, the reaction gives also an ionic complex, which is well soluble in MeOH. But this product was separated as PF_6^- salt upon addition of (*n*-Bu_4N)(PF_6) with a yield of 56%. The presence of the counter anion is verified by a strong band in the IR spectrum of the isolated solid at 839 cm^{-1}, which is characteristic of the $\nu_{P–F}$ vibrations.[45] The disappearance of the ν_{NH} band in the region above 3100 cm^{-1} and the strong bathochromic shift of the $\nu_{C=O}$ band by about 170 cm^{-1} prove the deprotonation of the ligand and the formation of *S,O* chelates with extended π-systems. This information is a positive sign of the successful synthesis of the expected {2}-ironcryptand $[Fe_2(L^2)_3]$. An X-ray structure analysis of the resulting complex confirms these conclusions by revealing a host-guest compound with the composition of $\{Tl \subset [Fe_2(L^2)_3]\}(PF_6)$. The cationic {2}-ironcryptate presented in Figure 3.5a is generated by the capture of the guest Tl^+ ion in the void of the {2}-ironcryptand $[Fe_2(L^2)_3]$ composed of two Fe^{3+} ions and three pentadentate deprotonated ligands $(L^2)^{2-}$. Each Fe atom is coordinated in a distorted octahedral environment with a facial arrangement of the sulfur atoms as found before for the tris-complexes of In(III) and Fe(III) with the ligand H_2L^1. The Fe–S bond lengths are in the range of 2.368(4) – 2.451(9) Å. They are in good agreement with those in $[Fe_2(L^1)_3]$, while the Fe–O bonds range between 2.003(3) Å and 2.045(3) Å, and are slightly longer than the corresponding bonds in $[Fe_2(L^1)_3]$. The elongation of the Fe–O bonds provides more space and more electron density for the central void to host the Tl^+ ion, which is nearly aligned with the two Fe^{3+} ions. The requirement of a negative charge to capture the guest cation causes a partial location of π-electron density on oxygen atoms and a less degree of delocalization in the chelate rings, which is pointed out by the clear distinction between the adjacent $C(O)–N_{amide}$ and $C(S)–N_{amide}$ bonds (Table 3.3). Adopting an axially truncated trigonal bipyramidal geometry, the guest cation is nine-coordinate with six oxygen donors and three pyridine nitrogen donors forming the mutual

base of the two truncated triangular pyramids (Figure 3.5b).

(a)   (b)
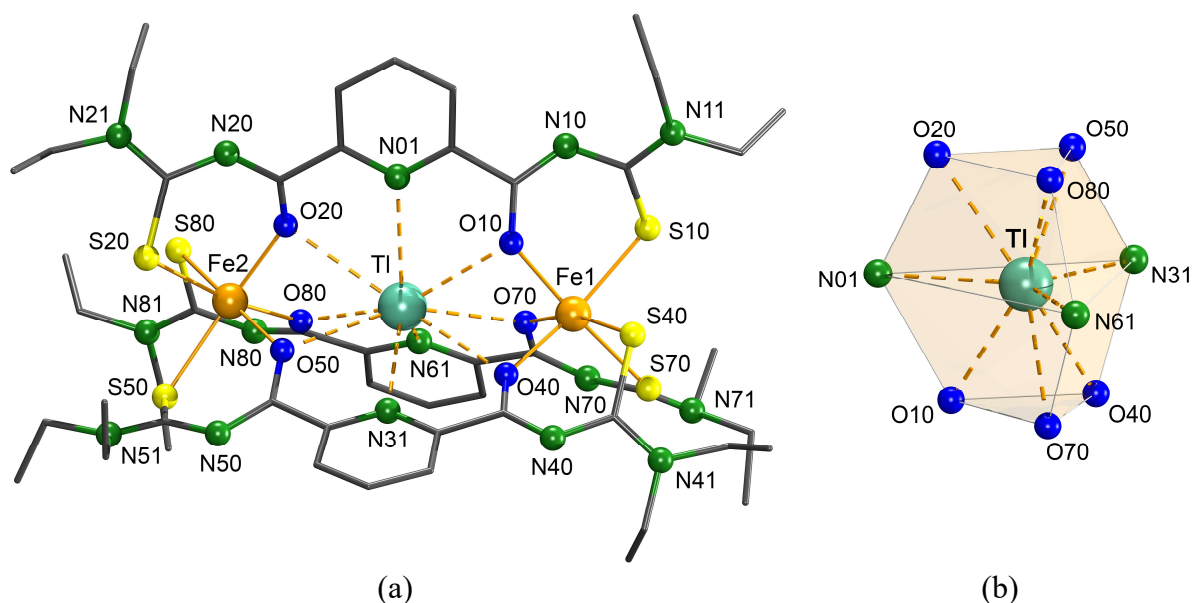
Figure 3.5 (a) Structure of the cationic {2}-ironcryptate $\{Tl \subset [Fe_2(L^2)_3]\}^+$. Hydrogen atoms are omitted for clarity (b) Axially truncated trigonal bipyramidal coordination sphere surrounding the guest cation Tl^+.

Table 3.3 Selected bond lengths (Å) in $\{Tl \subset [Fe_2(L^2)_3]\}(PF_6)$

Fe1–O10	2.021(3)	Fe1–S10	2.406(2)	Fe2–O20	2.020(3)	Fe2–S20	2.407(4)
Fe1–O40	2.027(3)	Fe1–S40	2.451(9)	Fe2–O50	2.044(3)	Fe2–S50	2.412(3)
Fe1–O70	2.045(3)	Fe1–S70	2.368(4)	Fe2–O80	2.003(3)	Fe2–S80	2.416(5)
Tl–O10	2.792(3)	C10–O10	1.276(5)	C40–O40	1.273(5)	C70–O70	1.271(5)
Tl–O40	2.857(3)	C10–N10	1.312(6)	C40–N40	1.321(5)	C70–N70	1.317(6)
Tl–O70	2.885(3)	C11–N11	1.343(6)	C41–N41	1.331(5)	C71–N71	1.327(6)
Tl–N01	2.909(3)	C11–N10	1.353(6)	C41–N40	1.360(6)	C71–N70	1.355(6)
Tl–N31	2.962(4)	C11–S10	1.730(4)	C41–S40	1.741(4)	C71–S70	1.731(4)
Tl–N61	2.965(4)	C20–O20	1.275(5)	C50–O50	1.274(5)	C80–O80	1.275(5)
Tl–O20	2.949(3)	C20–N20	1.314(6)	C50–N50	1.317(6)	C80–N80	1.309(6)
Tl–O50	2.805(3)	C21–N21	1.332(6)	C51–N51	1.327(6)	C81–N81	1.324(6)
Tl–O80	2.788(3)	C21–N20	1.353(6)	C51–N50	1.353(6)	C81–N80	1.354(6)
		C21–S20	1.739(4)	C51–S50	1.742(5)	C81–S80	1.747(4)

This coordination mode is hitherto unknown for Tl^+ and very rare for other hard monovalent metal ions such as alkali metal ions, where only a few examples with structurally well-characterized potassium-containing compounds have been reported.[46-48] This lack of information motivated ongoing experiments with the alkali metal ions Li^+, Na^+, K^+, Rb^+ and

Cs^+, or NH_4^+ instead of Tl^+.

When the same synthetic route was applied for the reactions of H_2L^2 and a mixture of Fe^{3+} with such monovalent cations, pure products directly precipitated as PF_6^- salts from the reaction mixtures, with the exception of the smallest (Li^+) and the largest (Cs^+) ions. This exception could be explained by the assumption that the radii of both cations do not fit into the cavity of the expected Fe(III) {2}-metallacryptand, thus, cannot stabilize such systems. The proposed compositions $\{M \subset [Fe_2(L^2)_3]\}(PF_6)$ (M = Rb^+, K^+, Na^+ or NH_4^+) of the isolated solids are supported by elemental analyses, IR spectroscopy as well as X-ray structural analyses. No unusual features were found in the IR spectra or in the molecular structures of the products (Table 3.4). Analogous with the bonding situation of the Tl^+ ion in the previous inclusion complex, the coordination polyhedra around the guest alkali metal ions Na^+, K^+ and Rb^+ are best described by axially truncated triangular bipyramids, which consist of three pyridine nitrogen atoms being located at the vertices of the mutual triangular base and six carbonyl oxygen atoms occupying the remaining vertices of the two truncated triangular pyramids. Such a coordination fashion is also believed to play an important role in capturing the ammonium cation in the central void by an intramolecular hydrogen bonding network. Unfortunately, there is no clear illustration for the proposed hydrogen bonds due to difficulties in the determination of the positions of the ammonium hydrogen atoms (Figure 3.6). However, in the solid state, the guest ammonium ion can be detected by the additional weak broad band at 3244 cm^{-1} in IR spectrum, which is assigned to ν_{NH} stretches.[45]
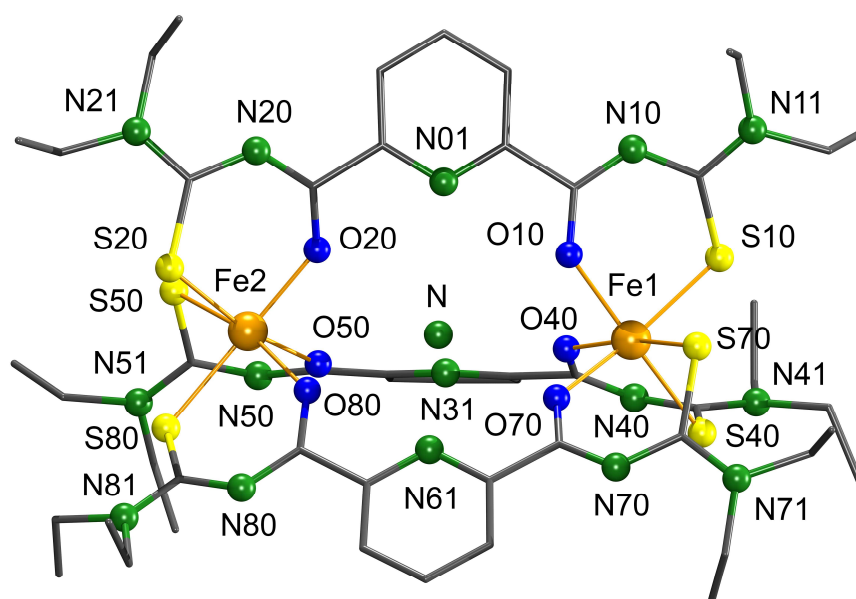
Figure 3.6 Structure of the cationic {2}-ironcryptate $\{NH_4 \subset [Fe_2(L^2)_3]\}^+$. Hydrogen atoms are omitted for clarity.

Table 3.4 Selected bond lengths (Å) in $\{M \subset [Fe_2(L^2)_3]\}(PF_6)$ complexes

M	Fe–O	Fe–S	M–O	M–N
Rb$^+$	2.007(7) – 2.053(7)	2.376(2) – 2.447(3)	2.767(7) – 2.912(7)	2.911(6) – 2.989(8)
K$^+$	2.001(6) – 2.046(5)	2.377(2) – 2.442(2)	2.736(5) – 2.881(6)	2.904(7) – 2.953(6)
Na$^+$	2.001(2) – 2.035(2)	2.368(4) – 2.445(2)	2.614(3) – 2.943(3)	2.822(3) – 2.978(3)
Tl$^+$	2.003(3) – 2.045(3)	2.368(4) – 2.451(9)	2.788(3) – 2.949(3)	2.909(3) – 2.965(4)
NH$_4^+$	2.012(3) – 2.046(3)	2.371(5) – 2.454(5)	2.765(4) – 2.939(4)	2.908(4) – 2.963(4)

The ESI$^+$ mass spectra of the inclusion compounds with alkali metal ions strongly support the existence of the cationic complex species by the presence of peaks of the fragments $[\{M \subset [Fe_2(L^2)_3]\}]^+$ (M = Na$^+$, K$^+$ or Rb$^+$). Meanwhile, only base peaks of the fragment $[\{K \subset [Fe_2(L^2)_3]\}]^+$, which result from exchange of the guest cations, appear in the mass spectra of the Tl$^+$- and NH$_4^+$-inclusion complexes.

3.2.2 The indium(III) metallacryptates $\{M \subset [In_2(L^2)_3]\}(PF_6)$ (M = Rb$^+$, K$^+$, Na$^+$, NH$_4^+$)

With the aim of facilitating NMR characterization of the complexes of the composition $\{M^I \subset [M^{III}_2(L^2)_3]\}^+$, the diamagnetic In^{3+} ion was used instead of the Fe^{3+} ion. Applying the same synthetic procedure as described for Fe^{3+} for experiments with InCl$_3$, similar $\{2\}$-metallacryptates of the composition $\{M \subset [In_2(L^2)_3]\}(PF_6)$ (M = Rb$^+$, K$^+$, Na$^+$ or NH$_4^+$) were obtained. They were characterized by elemental analyses, IR and NMR spectroscopy, and X-ray crystallography. Similar to the Fe(III) assemblies, the species $[In_2(L^2)_3]$, which is formed by the distorted octahedral coordination of two In^{3+} ions with three deprotonated ligands $(L^2)^{2-}$, accommodates one hard monocation in its central cavity by interactions with six oxygen and three pyridine nitrogen donor atoms. Depended on the nature of the guest cation, the directional interactions are coordination or hydrogen bonds (Figure 3.7 and 3.8). Interestingly, in case of the NH$_4^+$-inclusion complex, the consideration of the residual electron density peaks around the central N atom in the difference Fourier map allows the determination of the potential positions of ammonium hydrogen atoms. The assumption that the NH hydrogen atoms occupy the positions of the detected electron density peaks enables a revelation about the

intramolecular hydrogen bonding network between the guest NH_4^+ ion and the set of nine electron donors arranging in an axially truncated trigonal bipyramidal fashion (Figure 3.8).
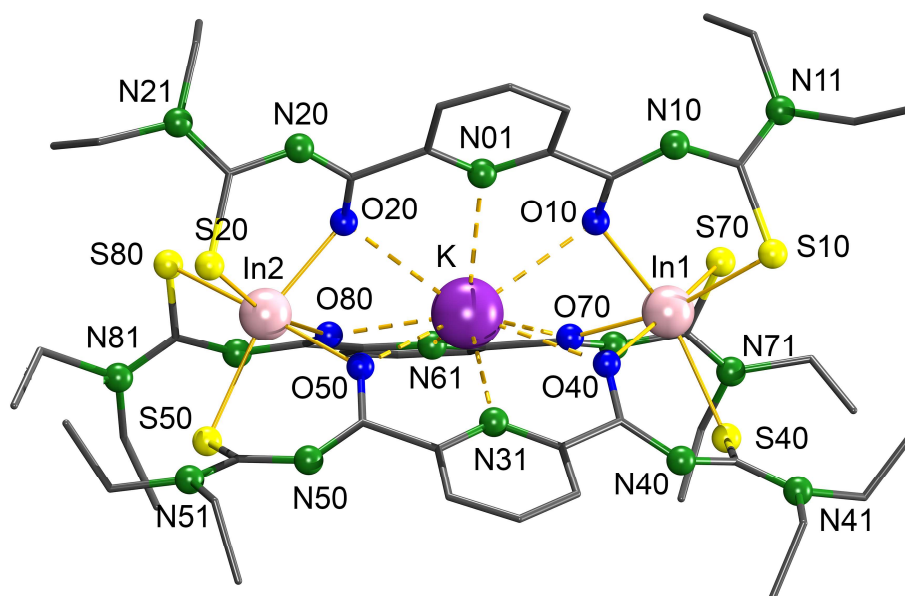
Figure 3.7 Structure of the cationic {2}-indiumcryptate $\{K \subset [In_2(L^2)_3]\}^+$. Hydrogen atoms are omitted for clarity.
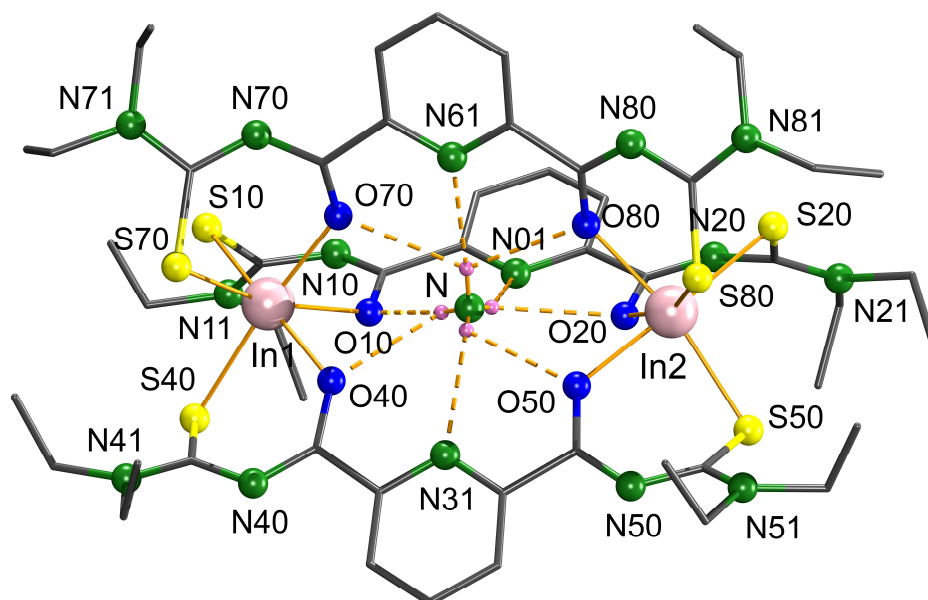
Figure 3.8 Structure of the cationic {2}-indiumcryptate $\{NH_4 \subset [In_2(L^2)_3]\}^+$. Hydrogen atoms bonded to carbon atoms are omitted for clarity. The small pink spheres represent residual electron density peaks around the central N atom in the difference Fourier map. The dashed bonds present the hydrogen bonds assuming that hydrogen atoms adopt positions of the electron density peaks.

Table 3.5 Selected bond lengths (Å) in $\{M \subset [In_2(L^2)_3]\}(PF_6)$ complexes

M	In–O	In–S	M–O	M–N
Rb^+	2.181(3) – 2.213(3)	2.529(4) – 2.549(9)	2.774(3) – 2.953(3)	2.937(4) – 3.002(4)
K^+	2.178(3) – 2.206(3)	2.527(5) – 2.551(7)	2.736(3) – 2.931(3)	2.907(3) – 2.969(3)
NH_4^+	2.185(3) – 2.214(3)	2.532(1) – 2.552(4)	2.779(4) – 2.947(4)	2.926(5) – 3.007(5)

In all structurally characterized complexes, the values of In–O bond lengths range between 2.178(3) Å and 2.214(3) Å, and are slightly larger than those found in the complex $[In_2(L^1)_3]$,[35] while In–S bond lengths are in the range of 2.527(5) – 2.552(4) Å and are consistent with those in $[In_2(L^1)_3]$ (Table 3.5). The partial double bond character of the C–O, C–N and C–S bonds of the aroylthiourea moieties strongly suggests the typical formation of π-delocalized systems, which are also visible in the IR spectra by the significant bathochromic shifts of the $v_{C=O}$ bands from 1674 cm^{-1} for the uncoordinated H_2L^2 to around 1540 cm^{-1} for the products.

The diamagnetism of the In(III) metallacryptates enables the use of NMR spectroscopy for the investigation of their structures in solution. The absence of broad singlet signals of NH protons in the ^1H NMR spectra as well as of medium broad v_{NH} bands in the IR spectra strongly suggests the deprotonation of the ligand during the complexation. The ethyl residues of the ligands show each two signals in the ^1H and ^{13}C NMR spectra for the methylene and methyl groups, which reflects hindered rotation around the $C(S)$–NEt$_2$ bonds. Such a behavior is derived from the partial multiple-bond character of the $C(S)$–NR^{1}R^2 bonds and is frequently observed for benzoylthioureas and their metal complexes.[21, 49-50] It is noteworthy that the existence of an inclusion complex with ammonium cations can be detected in the ^1H and ^{15}N NMR spectra of the labelled compounds $\{^{14}NH_4/^{15}NH_4 \subset [In_2(L^2)_3]\}(PF_6)$. The latter can be prepared following the same procedure using ^{15}N-enriched ammonium chloride. Due to the different properties of the two magnetically active nuclei, ^{14}N (I = 1) and ^{15}N (I = 1/2), spin-coupling between ^1H (I = 1/2) and each of the nuclei gives rise to distinct splitting patterns with different coupling constants. In the ^1H NMR spectra of the complexes measured in DMSO-d_6, the signal corresponding to the $^{14}NH_4^+$ protons is found as a 1:1:1 triplet at 9.56 ppm with $^1J(^{14}N-^1H) = 50.8$ Hz, while the sharp doublet at the same position with J = 72.8 Hz can be assigned to $^{15}NH_4^+$ protons (Figures 3.9 a and b). Compared with the "free" ammonium ion in the same solvent, the ^1H NMR chemical shifts of the captured ion are downfield by 2.11 ppm.

The measured coupling constants, however, are in the same regions with those previously reported for NH_4^+.[51] More details about dynamic properties of the inclusion species in solution can be acquired from the ^{15}N NMR data of the ^{15}N-labelled complex. The $^{15}N\{^1H\}$ NMR spectrum of the compound in DMSO-d_6 invokes one resonance at -345.6 ppm and a less intense resonance at -357.5 ppm (Figure 3.9 b), whereas only one signal at -345.6 ppm appears when $CDCl_3$ is used as solvent. The assignment of these signals is undertaken with respect to the ^{15}N DEPT NMR spectra measured in DMSO-d_6 and $CDCl_3$. It is interesting that both of the DEPT spectra are identical and exhibit an unique quintet at -345.6 ppm with a coupling constant $^1J(^{15}N\text{-}^1H)$ of 72.8 Hz (Figure 3.9 c). The found independence of the chemical shift from the solvent, splitting pattern and coupling constant reveals that the resonance at -345.6 ppm corresponds to the encapsulated $^{15}NH_4^+$ ions and, the remaining signal at -357.5 ppm is assigned to the free $^{15}NH_4^+$ ions, which could result from the slow (with respect to the NMR time scale) host–guest equilibrium in DMSO.
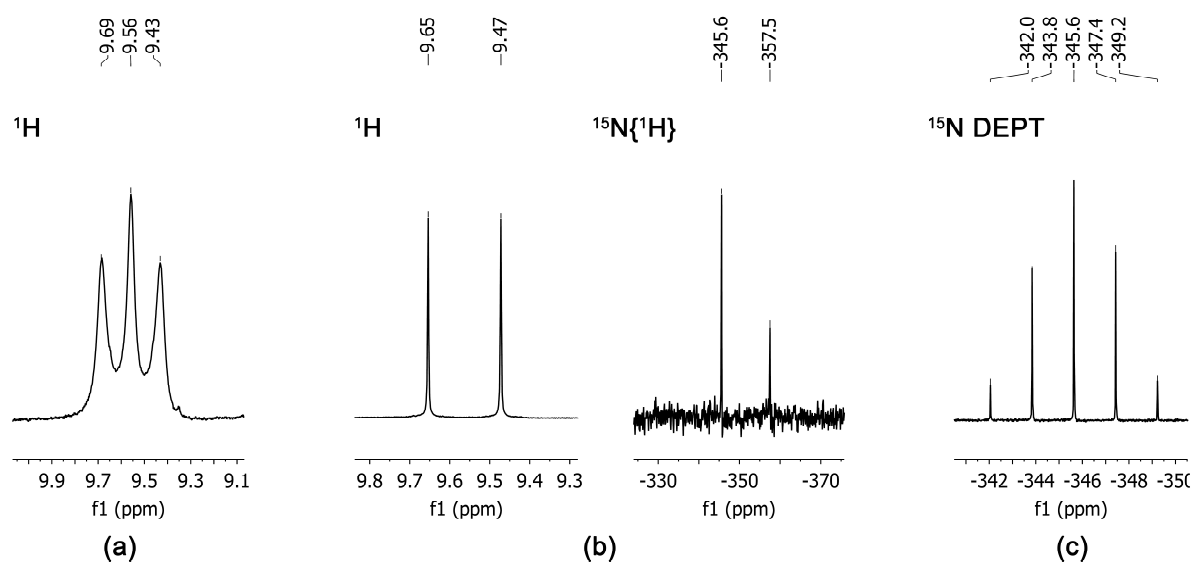
Figure 3.9 Selected NMR regions showing spin-coupling between ^1H and $^{14}N/^{15}N$: (a) ^1H NMR spectrum of $\{^{14}NH_4 \subset [In_2(L^2)_3]\}(PF_6)$ (b) ^1H NMR and $^{15}N\{^1H\}$ NMR and (c) ^{15}N DEPT NMR spectrum of $\{^{15}NH_4 \subset [In_2(L^2)_3]\}(PF_6)$ in DMSO-d_6.

The failed synthesis of the metallacryptand $[Fe_2(L^2)_3]$ from the reaction of H_2L^2 and Fe^{3+} ions and the ready formation of {2}-metallacryptates $\{M^I \subset [M^{III}_2(L^2)_3]\}$ ($M^I = Rb^+$, K^+, Na^+, Tl^+ or NH_4^+; $M^{III} = Fe^{3+}$ or In^{3+}) during reactions of H_2L^2 with mixtures of M^I and M^{III} ions demonstrate the template effect of the monocations M^I during the construction of the metallamacrocyclic systems. Directional interactions between the hard template ions M^I and hard donor atoms of the ligand system follow Pearson acid base concept directing the M^{III} ions

towards the aroylthiourea moieties and drive the formation of {2}-metallacryptates. In order to verify the assumption, the same synthetic approach is exploited in creation of heteronuclear complexes based on the novel catechol-spacered ligand H_2L^3.

3.3. Metallacryptates derived from the ligand H_2L^3

3.3.1 The iron(III) metallacryptates $\{M \subset [Fe_2(L^3)_3]\}(PF_6)$ (M = Cs$^+$, Rb$^+$, K$^+$, Tl$^+$, NH$_4^+$)

One-pot reactions of the ligand H_2L^3 with mixtures of FeCl$_3$ and MCl (M = Cs$^+$, Rb$^+$, K$^+$, NH$_4^+$) or Fe(NO$_3$)$_3$ and TlNO$_3$ in MeOH result in dark-red solutions. The addition of Et$_3$N and subsequent workup with (n-Bu$_4$N)(PF$_6$) give dark-red solids, which are readily soluble in organic solvents such as CH$_2$Cl$_2$ or chloroform. In the IR spectra of products, there are no absorptions in the region above 3100 cm^{-1} corresponding to v_{NH} stretches, which can be found in the spectrum of the uncoordinated ligand. This is a strong hint for the existence of the doubly deprotonated form (L^3)$^{2-}$ of the ligand. The formation of chelate rings after the coordination, which is normally accompanied with a large delocalization of π-electrons, is proved by bathochromic shifts of the $v_{C=O}$ bands from 1660 cm^{-1} in H_2L^3 to the region around 1560 cm^{-1}. These shifts are remarkable, however not as high as observed in other benzoylthiourea chelates, where these bands usually appear between 1400 cm^{-1} and 1500 cm^{-1}. The additional strong absorption bands around 840 cm^{-1} are assigned to the $v_{P–F}$ stretches. The existence of $\{M \subset [Fe_2(L^3)_3]\}^+$ species (M = Cs$^+$, Rb$^+$, K$^+$, Tl$^+$ or NH$_4^+$) can be detected by the presence of corresponding fragments in the ESI$^+$ mass spectra of the complexes. These observations and the elemental analyses strongly suggest a general composition of $\{M \subset [Fe_2(L^3)_3]\}(PF_6)$ (M = Cs$^+$, Rb$^+$, K$^+$, Tl$^+$ or NH$_4^+$) of the metal-ligand assemblies. Single crystals suitable for X-ray crystallography were produced from slow evaporation of solutions of the complexes in CH$_2$Cl$_2$/MeOH mixtures. The representative structure of the cationic host-guest complex $\{K \subset [Fe_2(L^3)_3]\}^+$ is shown in Figure 3.10a and selected bond lengths are given in Table 3.6. The structural analyses represent C_3-symmetric {2}-metallacryptates, in which all metal cations lie perfectly on crystallographic threefold axes (Figure 3.10b). As expected, the metallacryptand [Fe$_2$(L^3)$_3$] is composed of two Fe(III) ions linked through three doubly deprotonated ligands (L^3)$^{2-}$. As a consequence, each Fe^{3+} ion is octahedrally coordinated to three *S,O*-chelating aroylthioureato moieties with facial arrangement of the sulfur atoms.
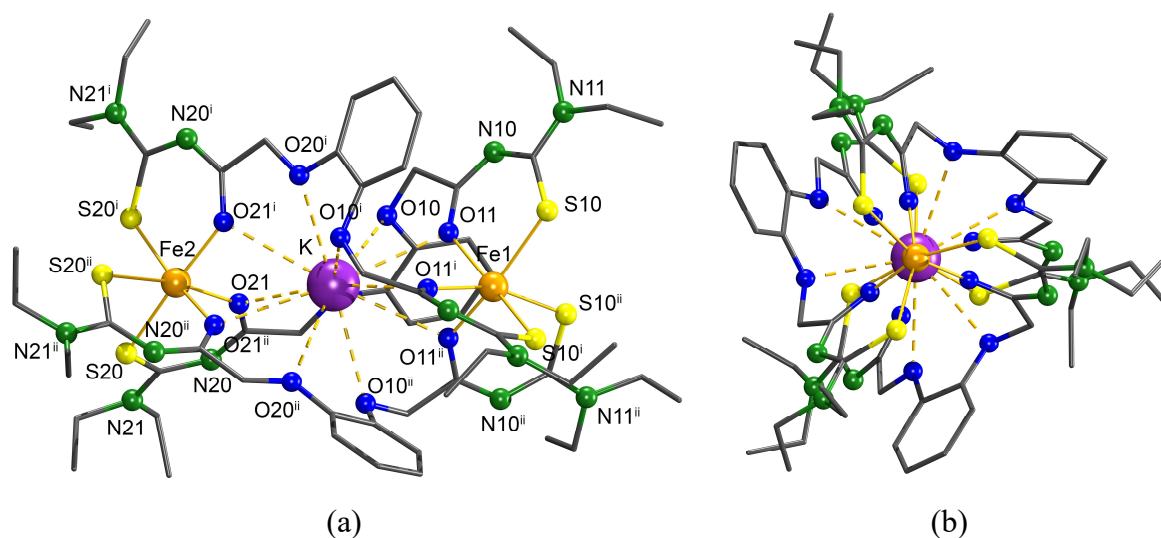
Figure 3.10 (a) Structure of the cationic {2}-ironcryptate {K ⊂ [Fe$_2$(L^3)$_3$]}$^+$. Hydrogen atoms are omitted for clarity. Symmetry operations used to generate equivalent atoms: ^{i} –y, x–y, z and ^{ii} –x+y, –x, z (b) View along the crystallographic threefold axis.

Table 3.6 Selected bond lengths (Å) in {K ⊂ [Fe$_2$(L^3)$_3$]}(PF$_6$)

K–O10	3.037(4)	Fe1–O11	2.006(4)	C11–O11	1.242(6)	C21–O21	1.257(6)
K–O11	3.138(4)	Fe1–S10	2.415(8)	C11–N10	1.304(7)	C21–N20	1.320(7)
K–O20	3.030(4)	Fe2–O21	2.007(4)	C12–N11	1.343(7)	C22–N21	1.341(6)
K–O21	3.155(4)	Fe2–S20	2.402(4)	C12–N10	1.359(7)	C22–N20	1.351(7)
				C12–S10	1.723(6)	C22–S20	1.736(5)

In analogy to the Fe(III) and In(III) metallacryptands derived from H$_2$L^2, the resulting {2}-ironcryptand is capable to encapsulate a hard monovalent cation in the central cavity. Alkaline metal ions like K$^+$, Rb$^+$ and Cs$^+$ or Tl$^+$ ions are twelve-coordinate by six carbonyl and six catecholate oxygen donors. Interestingly, also ammonium ions can be accommodated as guest cations in the intramolecular void. They are bonded by hydrogen bonds, which are established between the hydrogen atoms of the ammonium ions and each three oxygen atoms of the organic framework. The resulting bonding situation is presented in Figure 3.11, and bonding parameters of hydrogen bonds around NH$_4^+$ are summarized in Table 3.7.

Despite the fact that the Fe–O and Fe–S bond lengths (Table 3.8) are in the same ranges for those in Fe(III) tris-complexes discussed in the preceding parts, the observed planarity of chelate rings containing (L^3)$^{2-}$ ligands is in direct contrast to the considerable distortions observed in the former cases. This significant difference arises from the higher flexibility of the backbone of the ligand H$_2$L^3. In (L^3)$^{2-}$, free rotation of two aroylthiourea arms around the

24

O–CH$_2$ bonds, which is reflected by the torsion angles, C$_{ar}$–O–CH$_2$–C(O), (Table 3.8) is responsible for providing an optimal coordination environment for metal ions. On the other hand, in (L^1)$^{2-}$ and (L^2)$^{2-}$, conjugation of two aroyl thiourea moieties with the aromatic spacers benzene or pyridine prevents from such a free rotation. Thus, the adaptation of ligand skeletons to metal binding is exclusively done by deviation of atom(s) from the chelate planes, in other words by the distortion of chelate rings.
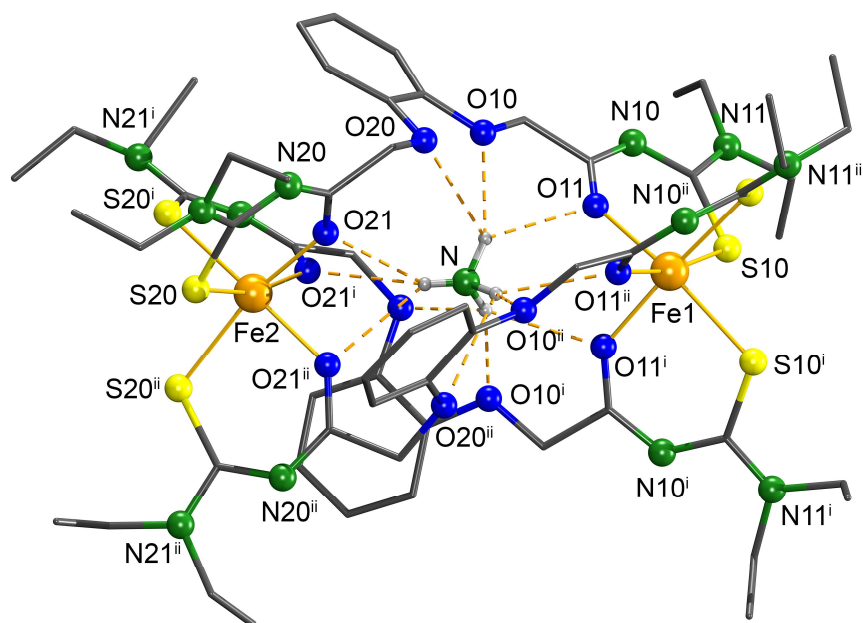
Figure 3.11 Structure of the cationic {2}-ironcryptate {NH$_4$ ⊂ [Fe$_2$(L^3)$_3$]}$^+$. Hydrogen atoms bonded to carbon atoms are omitted for clarity. Symmetry operations used to generate equivalent atoms: ^{i} –x+y, –x+1, z and ^{ii} –y+1, x–y+1, z.

Table 3.7 Geometrical parameters of hydrogen bonds in {NH$_4$ ⊂ [Fe$_2$(L^3)$_3$]}(PF$_6$)

D–H⋯A	d(D–H) (Å)	d(H⋯A) (Å)	d(D⋯A) (Å)	<(DHA) (°)
N–H1⋯O10	0.942(6)	2.213(7)	3.095(4)	155.23(8)
N–H1⋯O11	0.942(7)	2.430(5)	3.149(8)	132.92(7)
N–H1⋯O20	0.942(7)	2.681(3)	3.111(9)	108.52(7)
N–H2⋯O21	0.804(2)	2.541(1)	3.222(8)	143.38(1)
N–H2⋯O21^i	0.804(2)	2.541(1)	3.222(8)	143.38(1)
N–H2⋯O21^{ii}	0.804(2)	2.541(1)	3.222(8)	143.38(1)

Symmetry operations used to generate equivalent atoms: ^{i} -x+y, -x+1, z and ^{ii} -y+1, x-y+1, z

Table 3.8 Selected bond lengths (Å) and torsion angles (°) in $\{M \subset [Fe_2(L^3)_3]\}(PF_6)$ complexes

M	Fe–O	Fe–S	M–O	Angle[#]
Cs^+	1.998(3)/ 2.011(3)	2.405(5)/ 2.413(6)	3.182(3) – 3.251(3)	-179.00(5)/ -73.44(9)
NH_4^+	2.003(3)/ 2.008(3)	2.405(6)/ 2.415(1)	3.095(4) – 3.222(8)	175.73(8)/ 71.65(3)
Rb^+	2.009(4)/ 2.014(4)	2.404(2)/ 2.415(8)	3.097(4) – 3.185(4)	-175.22(6)/ -72.64(2)
Tl^+	2.008(4)/ 2.012(4)	2.405(7)/ 2.416(5)	3.105(4) – 3.219(4)	176.75(2)/ 71.90(1)
K^+	2.006(4)/ 2.007(4)	2.402(4)/ 2.415(8)	3.030(4) – 3.155(4)	-173.10(2)/ -72.28(7)

[#] torsion angle $< [C_{ar}–O–CH_2–C(O)]$

3.3.2 The cobalt(III) metallacryptates $\{M \subset [Co_2(L^3)_3]\}(PF_6)$ (M = Cs^+, Rb^+, K^+, Tl^+, NH_4^+)

When analogous reactions as described for the Fe(III) complexes are performed with Co^{2+}, another well-known 6-coordinate metal ion, the ions are oxidized during the complex formation and the corresponding, more inert Co(III) complexes are formed. Identical oxidation has been reported during the preparation of mononuclear Co(III) tris-complexes with benzoylthiourea ligands.[20, 52-56] The identity of the isolated {2}-metallacryptates of the composition $\{M \subset [Co_2(L^3)_3]\}(PF_6)$ (M = Cs^+, Rb^+, K^+, Tl^+, NH_4^+) was confirmed by elemental analyses, spectroscopic methods, including IR, NMR and MS, and X-ray crystallography. The IR spectra of the products containing the M^I ions exhibit no absorptions in the region above 3100 cm^{-1} and, hence, indicate the deprotonation of the ligands during complexation. An extra weak, broad band at 3238 cm^{-1} in the IR spectrum of the complex with the ammonium ion results from the v_{NH} stretches of NH_4^+. The intense absorption at 1659 cm^{-1} corresponding to the $v_{C=O}$ vibrations in H_2L^3 shifts to 1560 cm^{-1}. In spite of the bathochromic shifts of only about 100 cm^{-1}, there is reliable evidence for chelate formation with π-electron delocalization within the chelate rings. Intense bands at 841 cm^{-1} are assigned to the $v_{P–F}$ stretches. The formal oxidation state '+3' of the cobalt ions is confirmed by the diamagnetism of the isolated compounds. Expectedly, the ^1H NMR spectra of the products in $CDCl_3$ show no signals of NH protons, which confirms the deprotonation of the ligand as already concluded from the IR spectra. The resonances of the methylene protons of OCH_2 appear as two doublets with typical geminal spin coupling constants (J = 16.0 – 16.2 Hz). In comparison with the broad singlet resonance of the same protons in the uncoordinated ligand, this observation means that the energy barrier of the rotation around the $O–CH_2$ bond significantly increases after coordination. A similar increase of the rotational barrier occurs for the methylene groups of the $C(S)–NEt_2$ residues. The rigid arrangement around the tertiary nitrogen atoms results in four magnetically nonequivalent

protons with four well-resolved sextets. They appear in the range of 3.2 – 4.2 ppm with an ABX$_3$ splitting pattern, where J$_{AB}$ (~14 Hz) is approximately twice of J$_{AX}$ (~7 Hz). The ^{1}H NMR spectra of complexes with either unlabeled and ^{15}N-enriched ammonium cations in CDCl$_3$ reveal additional signals relating to the NH$_4^+$ protons. A triplet (J = 53.8 Hz) at 6.70 ppm or a doublet (J = 75.2 Hz) at 6.69 ppm arises from spin coupling of ^{1}H (I = 1/2) with ^{14}N (I = 1) and ^{15}N (I = 1/2) respectively. Only broad and less-resolved signals in the same regions are observed in the ^{1}H NMR spectra of the complexes measured in DMSO-d_6. It is remarkable that in the case of the NH$_4^+$ host-guest complex, the ^{1}H NMR chemical shifts of the captured ammonium ion are upfield by 0.9 ppm in comparison with the "free" ion in the same solvent. In contrast to the complicated ^{1}H NMR spectra, the corresponding ^{13}C NMR spectra are simple since they are exclusively influenced by hindered rotation around the C(S)–NEt$_2$ bonds. Consequently, two separated signals for each CH$_2$ and CH$_3$ carbon atom of the NEt$_2$ groups appear. The signal assigned to the OCH$_2$ carbon atom locates around 69 ppm, while the chemical shifts of the aromatic carbon atoms are in the range from 110 ppm to 150 ppm. The low intense resonances of the C=O and C=S carbon atoms are found close to 175 ppm and 173 ppm respectively. Analogous to the In(III) complexes, the use of ^{15}N-enriched ammonium enables the ^{15}N NMR spectroscopy to study the NH$_4^+$ inclusion in the Co(III) complex in solution (Figure 3.12).
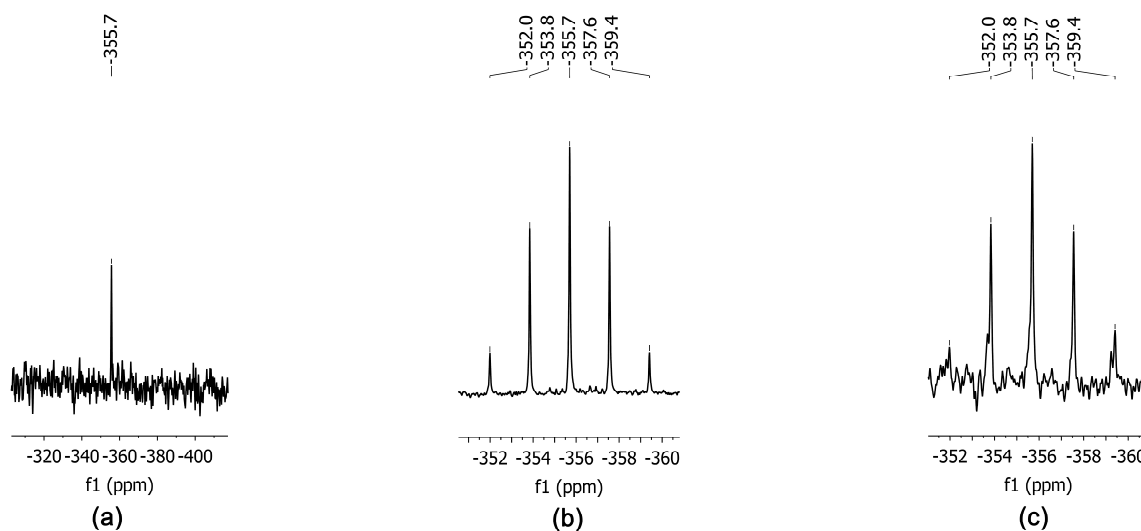
Figure 3.12 (a) ^{15}N{^{1}H} NMR spectrum in DMSO-d_6 (b) ^{15}N DEPT NMR spectrum in CDCl$_3$ and (c) ^{15}N NMR spectrum in DMSO-d_6 of {^{15}NH$_4$ ⊂ [Co$_2$(L^3)$_3$]}(PF$_6$).

The ^{15}N{^{1}H} NMR spectra obtained from the solutions of the ^{15}N-labelled complex in CDCl$_3$ as well as in DMSO-d_6 are indistinguishable and show an unique resonance at -355.7 ppm (Figure 3.12a). The proximity of this signal to the one of the free ^{15}NH$_4^+$ at -351.6 ppm is a

challenge to the assignment of the observed signal to the guest ammonium cation. Nevertheless, the ambiguity is resolved by the quintet split of the signal at -355.7 ppm with the coupling constant of 75.5 Hz in the NMR spectra, in which the coupling between ^{15}N and ^{1}H nuclei is remained (Figure 3.12b and c).

High resolution ESI^+ mass spectra of the complexes display the base peaks of the expected cationic {2}-metallacryptates $\{M \subset [Co_2(L^3)_3]\}^+$. Match between observed isotopic patterns and simulated ones strongly supports the assigned compositions, thereby providing further proof of the existence of host–guest complexes, including labelled ammonium inclusion complexes (Figure 3.13), in solution. Furthermore, compared with the preceding series of oligonuclear assemblies, the fragments of the composition $\{K \subset [Co_2(L^3)_3]\}^+$ are absent or have a low intensity. Since they result from typical cation exchange reactions with the ESI matrix, these results can be interpreted in terms of a higher inertness of the cobalt complexes towards cation exchange reactions.

(a)   (b)
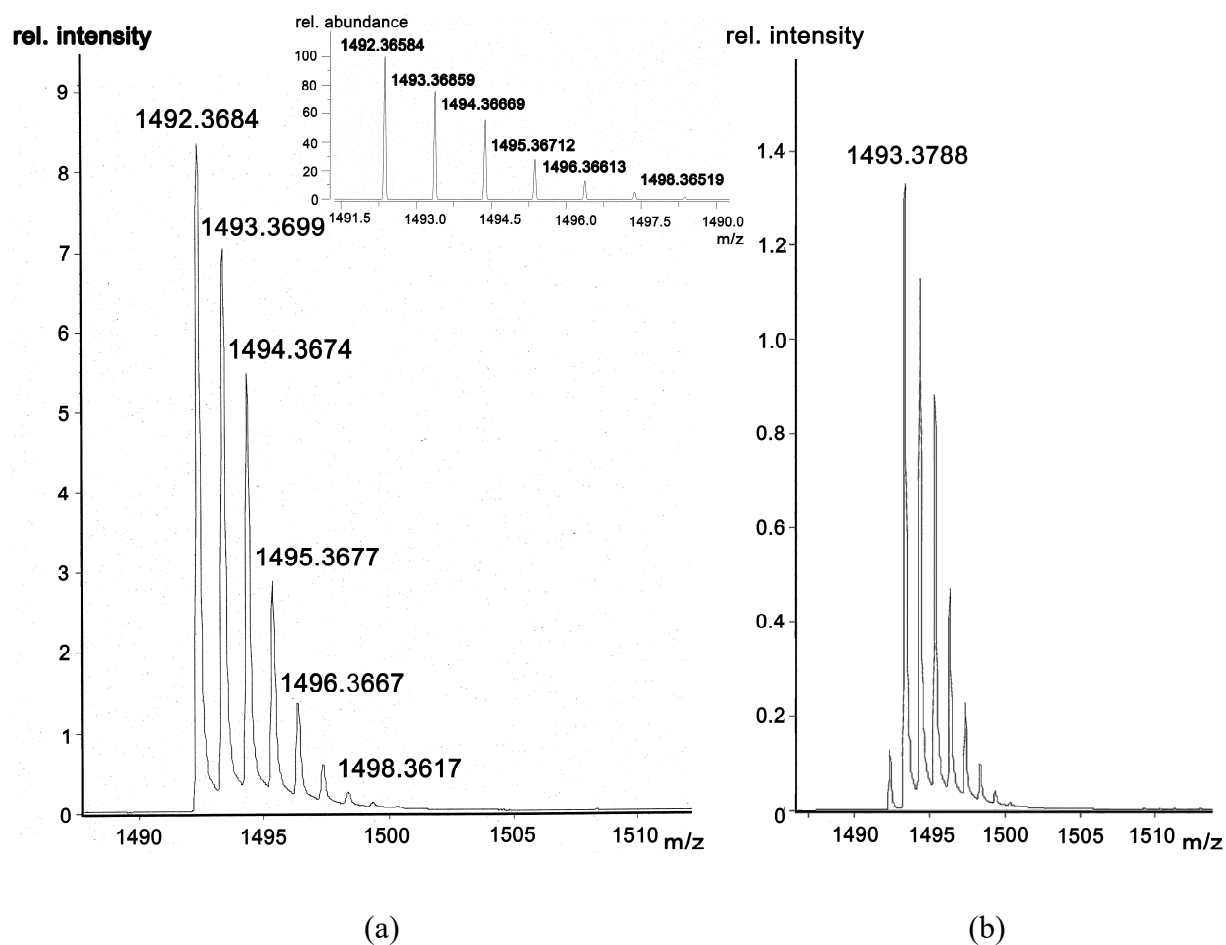
Figure 3.13 Base peaks in high resolution ESI^+ mass spectra (a) observed and simulated patterns of $\{^{14}NH_4 \subset [Co_2(L^3)_3]\}(PF_6)$ and (b) observed pattern of $\{^{15}NH_4 \subset [Co_2(L^3)_3]\}(PF_6)$.

The solid-state structures of the {2}-metallacryptates are studied by single crystal X-ray diffraction. As a representative for the series of cobalt compounds, the cation of $\{K \subset [Co_2(L^3)_3]\}(PF_6)$ is shown in Figure 3.14.
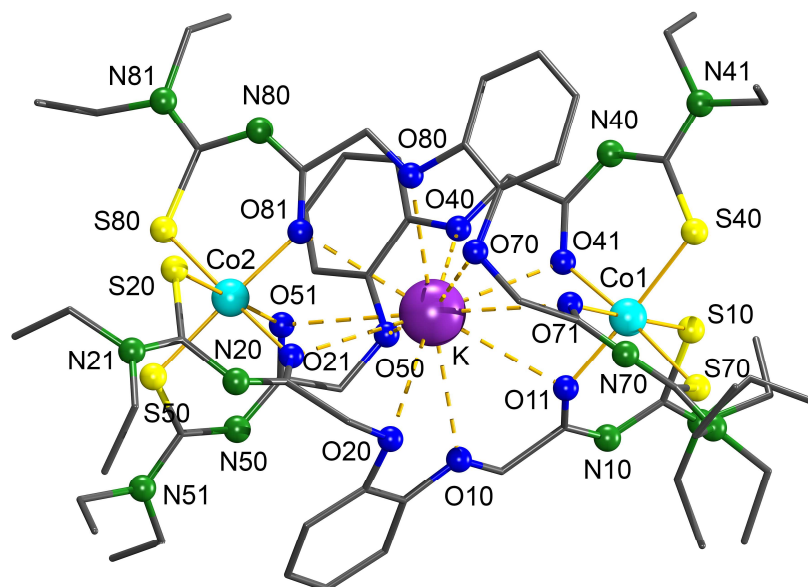
Figure 3.14 Structure of the cationic {2}-cobaltcryptate $\{K \subset [Co_2(L^3)_3]\}^+$. Hydrogen atoms are omitted for clarity.

Table 3.9 (a) Selected bond lengths (Å) in $\{K \subset [Co_2(L^3)_3]\}(PF_6)$

Bond lengths (Å)							
K–O10	2.952(5)	Co1–O11	1.912(4)	Co1–O41	1.912(4)	Co1–O71	1.911(4)
K–O11	2.950(4)	Co1–S10	2.211(4)	Co1–S40	2.209(9)	Co1–S70	2.212(5)
K–O20	3.087(5)	Co2–O21	1.914(4)	Co2–O51	1.916(4)	Co2–O81	1.914(4)
K–O21	3.273(5)	Co2–S20	2.195(4)	Co2–S50	2.221(2)	Co2–S80	2.212(1)
K–O40	2.995(4)	C11–O11	1.240(7)	C41–O41	1.255(7)	C71–O71	1.254(7)
K–O41	3.075(4)	C11–N10	1.323(8)	C41–N40	1.304(8)	C71–N70	1.313(8)
K–O50	3.082(5)	C12–N11	1.332(9)	C42–N41	1.349(8)	C72–N71	1.336(8)
K–O51	3.120(4)	C12–N10	1.352(9)	C42–N40	1.329(8)	C72–N70	1.352(7)
K–O70	3.235(5)	C12–S10	1.724(7)	C42–S40	1.731(6)	C72–S70	1.732(7)
K–O71	3.046(4)	C21–O21	1.262(7)	C51–O51	1.250(7)	C81–O81	1.249(7)
K–O80	3.005(4)	C21–N20	1.312(8)	C51–N50	1.326(8)	C81–N80	1.312(8)
K–O81	3.083(4)	C22–N21	1.340(8)	C52–N51	1.331(8)	C82–N81	1.320(8)
		C22–N20	1.351(8)	C52–N50	1.363(8)	C82–N80	1.356(8)
		C22–S20	1.725(6)	C52–S50	1.730(7)	C82–S80	1.730(7)

Table 3.9 (b) Selected angles (°) in $\{K \subset [Co_2(L^3)_3]\}(PF_6)$

Angle (°)					
O11–Co1–S10	94.84(1)	O41–Co1–S40	95.46(1)	O71–Co1–S70	94.29(1)
O71–Co1–S40	177.35(1)	O41–Co1–S10	176.44(1)	O11–Co1–S70	175.10(1)
O71–Co1–O11	84.79(2)	O71–Co1–O41	83.80(2)	O11–Co1–O41	83.31(2)
S40–Co1–S10	87.65(7)	S40–Co1–S70	88.28(7)	S10–Co1–S70	90.01(7)
O21–Co2–S20	94.12(1)	O51–Co2–S50	92.64(1)	O81–Co2–S80	94.62(1)
O81–Co2–S20	177.58(1)	O51–Co2–S80	177.65(2)	O21–Co2–S50	177.13(2)
O81–Co2–O21	85.28(2)	O81–Co2–O51	83.96(2)	O21–Co2–O51	84.49(2)
S20–Co2–S80	87.75(7)	S20–Co2–S50	86.20(7)	S80–Co2–S50	89.33(8)

Similarly to the Fe(III) complexes, the slightly distorted octahedral coordination spheres of the two Co^{3+} ions, which are reflected by the bond lengths and angles around the transition metal ions (Table 3.9), are occupied by the donor atoms of three doubly deprotonated ligands $(L^3)^{2-}$. This leads to a cryptand-like species of the composition $[Co_2(L^3)_3]$, which captures one hard monocation in its central cavity by weak interactions with twelve oxygen donors. The Co–O and Co–S bond lengths are in the same range with the values observed in the mononuclear tris-complexes of Co(III) with bidentate benzoylthioureato ligands.[20, 52-56]

3.4 Möβbauer spectroscopy and cyclic voltammetry of iron(III) metallamacrocycles

Möβbauer measurements were performed with the representative complexes, $[Fe_2(L^1)_3]$, $\{K \subset [Fe_2(L^2)_3]\}(PF_6)$ and $\{K \subset [Fe_2(L^3)_3]\}(PF_6)$, at 13 K without an external magnetic field applied to the γ-beam. All the spectra exhibit a weak and broad absorption (Figure 3.15) with the isomer shift in the expected range for Fe(III) compounds.[57] However, owing to magnetic relaxation effects,[57] the absorption pattern is unresolved, and therefore, it is a challenge to the simulation of the spectra as well as the interpretation of electronic properties of iron centers.

(a)　　　　　　　　　(b)　　　　　　　　　(c)
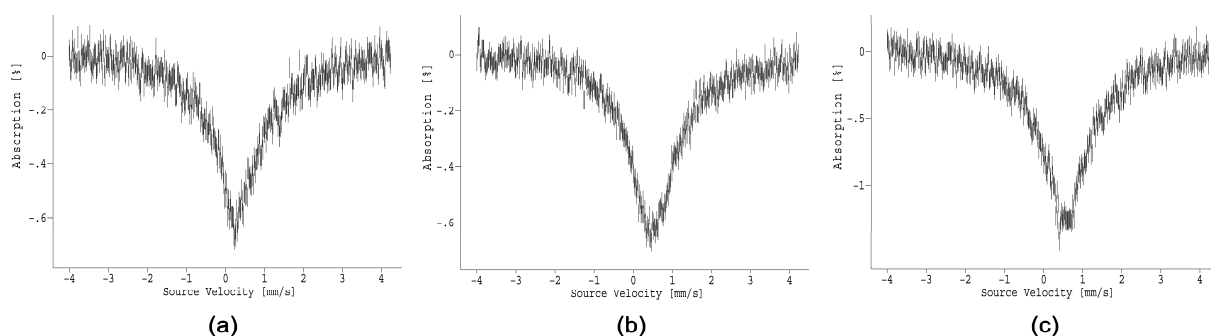
Figure 3.15 Zero-field Möβbauer spectra of (a) $[Fe_2(L^1)_3]$ (b) $\{K \subset [Fe_2(L^2)_3]\}(PF_6)$ and (c) $\{K \subset [Fe_2(L^3)_3]\}(PF_6)$ recorded at 13 K.

The utilization of Fe^{3+} ions in the metallamacrocycles produced compounds with a redox behavior, which makes them interesting for electrochemical studies. Thus, cyclic voltammetry measurements of the representative compounds, $[Fe_2(L^1)_3]$, $\{K \subset [Fe_2(L^2)_3]\}(PF_6)$ and $\{K \subset [Fe_2(L^3)_3]\}(PF_6)$, were undertaken in dry DMF under Ar atmosphere. The voltammograms display two consecutive one-electron transfer processes corresponding to the quasi-reversible stepwise reductions of the two iron centers (Scheme 3.1).

$$\mathrm{[Fe^{III} \ldots Fe^{III}]^n} \quad \underset{-e}{\overset{E^o_1{}' \; +e}{\rightleftharpoons}} \quad \mathrm{[Fe^{II} \ldots Fe^{III}]^{(n-1)}} \quad \underset{-e}{\overset{E^o_2{}' \; +e}{\rightleftharpoons}} \quad \mathrm{[Fe^{II} \ldots Fe^{II}]^{(n-2)}}$$
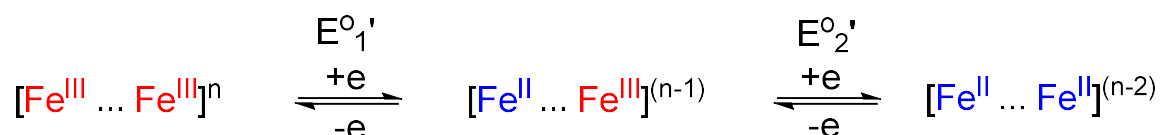
(n = 0 for $[Fe_2(L^1)_3]$ and n = 1 for $\{K \subset [Fe_2(L^2)_3]\}(PF_6)$ and $\{K \subset [Fe_2(L^3)_3]\}(PF_6)$)

Scheme 3.1 Stepwise reduction of Fe(III) centers in Fe(III) metallamacrocycles. Guest cations and ligands are excluded for simplification.

Because the difference between the standard potential of the two consecutive processes ($\Delta E^{o'} = E^o_1{}' - E^o_2{}'$), which determines of the separation of the two redox potentials, strongly depends on the degree of interaction between the two redox centers of the intermediate mixed-valent compounds,[58-59] the partially separated features of signals in voltammograms recorded for the complexes of H_2L^1 and H_2L^2 (Figure 3.16a and b) indicate slight delocalization of charge between the two iron ions. This can be caused by the conjugation of the chelating aroylthioureas with the aromatic spacers (benzene or pyridine). In contrast, the aliphatic O–CH$_2$ bonds prevent a potential conjugation in the backbone of $(L^3)^{2-}$ ligands and, hence, produce electronic isolation of two iron ions, which is responsible for the poor resolution of the redox waves (Figure 3.16c).

In fact, the degree of charge delocalization in mixed-valent compounds can be evaluated through a calculation of the equilibrium constant, K_{com}, of the comproportionation reaction,[58-59] which, in the present case, is given as:

$$\mathrm{[Fe^{III} \ldots Fe^{III}]^n} + \mathrm{[Fe^{II} \ldots Fe^{II}]^{(n-2)}} \rightleftharpoons 2\mathrm{[Fe^{II} \ldots Fe^{III}]^{(n-1)}} \quad K_{com} = exp\left(\frac{\Delta E^{o'}}{RT}\right)$$
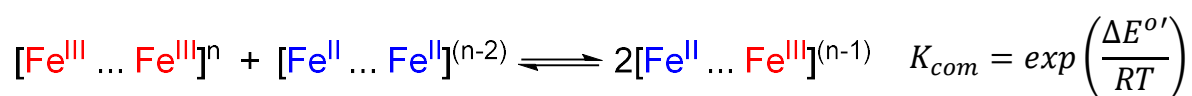
Because of the low resolution of the two-peak systems, especially in case of $\{K \subset [Fe_2(L^3)_3]\}(PF_6)$, it is difficult to determine the exact values of $E^o_1{}'$ and $E^o_2{}'$. However, the peak separation, $\Delta E^{o'}$, as a function of the difference (ΔE_p) between the potential of the

most cathodic (E_{pc}) and the most anodic (E_{pa}) peaks, has been calculated theoretically.[60] The use of this result enables an immediate evaluation of $\Delta E^{0'}$ through the measurement of $\Delta E_p'$. Table 3.9 summarizes voltammetric parameters and the calculated comproportionation constants, K_{com}, for the representative iron(III) metallamacrocycles.

$E(V)$ *vs.* Fc$^+$/Fc

(a)

$E(V)$ *vs.* Fc$^+$/Fc

(b)

$E(V)$ *vs.* Fc$^+$/Fc

(c)
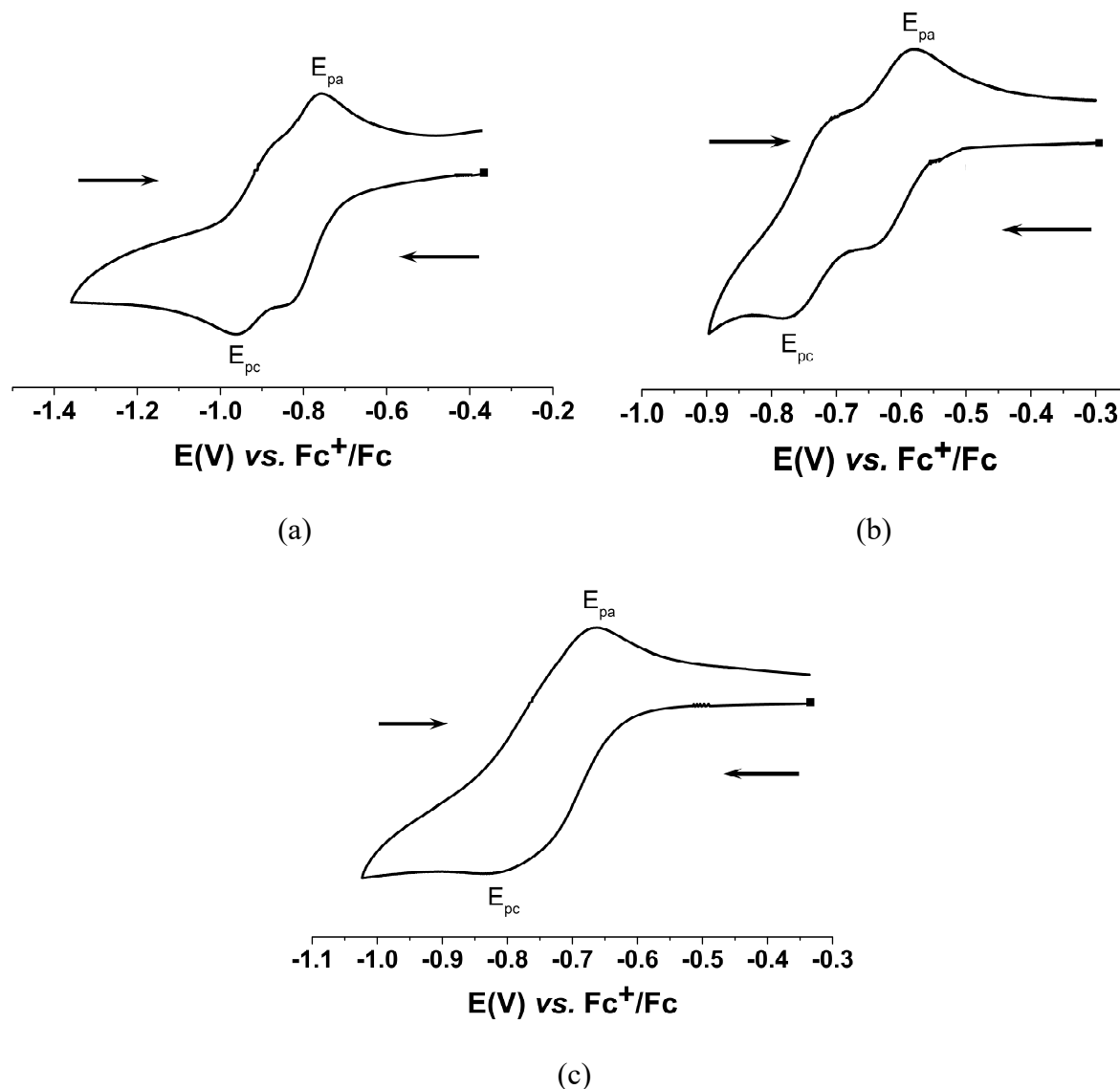
Figure 3.16 Cyclic voltammograms of the complexes (2 mM) in 0.15 M (n-Bu$_4$N)(PF$_6$) – DMF at a scan rate of 150 mV/s (a) [Fe$_2$(L^1)$_3$] (b) {K $\subset$ [Fe$_2$(L^2)$_3$]}(PF$_6$) and (c) {K $\subset$ [Fe$_2$(L^3)$_3$]}(PF$_6$)

Table 3.9 Cyclic voltammetric parameters of consecutive one-electron transfer processes and comproportionation constants, K_{com}, for iron(III) metallamacrocycles

Complex	E_{pc} (V)	E_{pa} (V)	$\Delta E_p'$ (V)	$\Delta E^{0'}$ (V)	K_{com} (298 K)
[Fe$_2$(L^1)$_3$]	-0.965	-0.756	0.209	0.160	5.1×10^2
{K $\subset$ [Fe$_2$(L^2)$_3$]}(PF$_6$)	-0.782	-0.579	0.203	0.150	3.4×10^2
{K $\subset$ [Fe$_2$(L^3)$_3$]}(PF$_6$)	-0.832	-0.663	0.169	0.127	1.4×10^2

Although all K_{com} values are in the range of $10^2 - 10^6$, which is, according to the Robin-Day classification,[61] typical for mixed-valent compounds with slight charge delocalization between redox centers, the K_{com} constant calculated for the complex of the novel ligand H_2L^3 is at the border between the class of compounds containing isolated and partially interacting redox centers. This information is in good agreement with the conclusion drawn from the features of the voltammograms.

3.5 Summary and conclusion

Series of oligonuclear assemblies have been successfully synthesized by one-pot reactions of H_2L^2 or H_2L^3 with mixtures of octahedral, trivalent metal ions M^{III} ($M^{III} = Fe^{3+}$, Co^{3+}, In^{3+}) and hard monovalent ions M^I ($M^I = Cs^+$, Rb^+, K^+, Na^+, Tl^+ and NH_4^+). The resulting {2}-metallacryptates are afforded by the encapsulation of one guest monocation M^I in the central void of the {2}-metallacryptands $[M^{III}_2(L)_3]$, which are formed by distorted octahedral coordination of two trivalent metal ions M^{III} with three aroylbis(thioureato) dianions $(L^2)^{2-}$ or $(L^3)^{2-}$. The failure of all attempts to prepare the {2}-metallacryptand $[Fe_2(L^2)_3]$ in the absence of guest cations apparently demonstrates that the metal-ligand self-assembly is driven by the template effect of the guest monocations. The use of trivalent metal ions with different electronic properties allows the design of target structures with particular functionality. While diamagnetic Co^{3+} and In^{3+} ions facilitate NMR characterization of assemblies, Fe^{3+} ions lead to interesting electrochemical properties studied by cyclic voltammetry. Furthermore, the coordination capacity and flexibility of the ligand systems exert considerable influences on the structural characteristics and redox properties of the obtained coordination assemblies.

The next Chapters will exclusively focus on coordination assemblies constructed from the novel ligand H_2L^3 using a similar synthetic approach.

Chapter 4

Assemblies with four–coordinate metal ions

As being presented in the previous Chapter, the self-assembly of the bis(bidentate) ligand H_2L^3 with mixtures of the six-coordinate transition metal ions, Fe(III) or Co(III), and hard monocationic ions yields {2}-metallacryptates with defined compositions and structures. Since the favored octahedral coordination mode of the transition metal ions is considered to be the driving force for the formation of the discrete systems, the use of metal ions with preference to other coordination geometry might produce metal-ligand assemblies with other topologies. Suitable candidates for such experiments are Cu(II) ions, which prefer coordination numbers between four and six due to a significant Jahn-Teller effect. A survey of the published literature reveals that Cu(II) ions in most of complexes with aroyl mono- or bis-thiourea(s) are four-coordinate and adopt square-planar geometry with *cis* configuration.[18-19, 34-35, 62-64] There are very few of structurally characterized complexes, in which Cu^{2+} ions are coordinated in *trans* square-planar or square-pyramidal fashions.[31, 65]

4.1 The copper(II) metallacoronates

Reactions of the ligand H_2L^3 with mixtures of Cu^{2+} ions and monovalent cations M^+ (M = Cs, Rb, K or Tl) were done with the addition of Et_3N as a supporting base. The subsequent workup with (n-Bu_4N)(PF_6) allows the precipitation of the products from the reaction mixtures and their isolation as PF_6^- salts in solid form. Strong absorption bands around 840 cm^{-1} in the IR spectra confirm the presence of PF_6^- anions in the products, thereby implying the existence of cationic complexes. In addition, the absence of medium absorptions in the region above 3100 cm^{-1} and a remarkable bathochromic shift of the intense $v_{C=O}$ stretch to 1540 cm^{-1} obviously reflect the complete deprotonation of the ligand H_2L^3 and the formation of *S,O* chelates with a high degree of π-electron delocalization. These observations propose the composition of {M ⊂ [$Cu_2(L^3)_2$]}(PF_6) for the resulting complexes. The spectroscopic findings are strongly supported by the elemental analyses of the products, with the exception of the Cs$^+$ complex. X-ray structural studies on single crystals obtained from slow evaporation of solutions of the complexes in CH_2Cl_2/MeOH shed light on this ambiguity. According to these analyses, each copper atom is four-coordinate with two aroylthioureato moieties. The linkage of the bis(bidentate) catechol-spacered dianions (L^3)$^{2-}$ by Cu(II) ions generates 2D metallacoronands, which possess topologies analogous to the conventional organic crown ethers. The central

cavities of the host compounds can accommodate one hard monocation. Two different types of metallacoronands are induced depending on the size of the guest cations.

The inclusion of ions such as Rb^+, Tl^+ or K^+ leads to {2}-metallacoronates with the expected composition of $\{M \subset [Cu_2(L^3)_2]\}(PF_6)$ (M = Rb^+, K^+ or Tl^+). A representative structure of these compounds is presented in Figure 4.1.
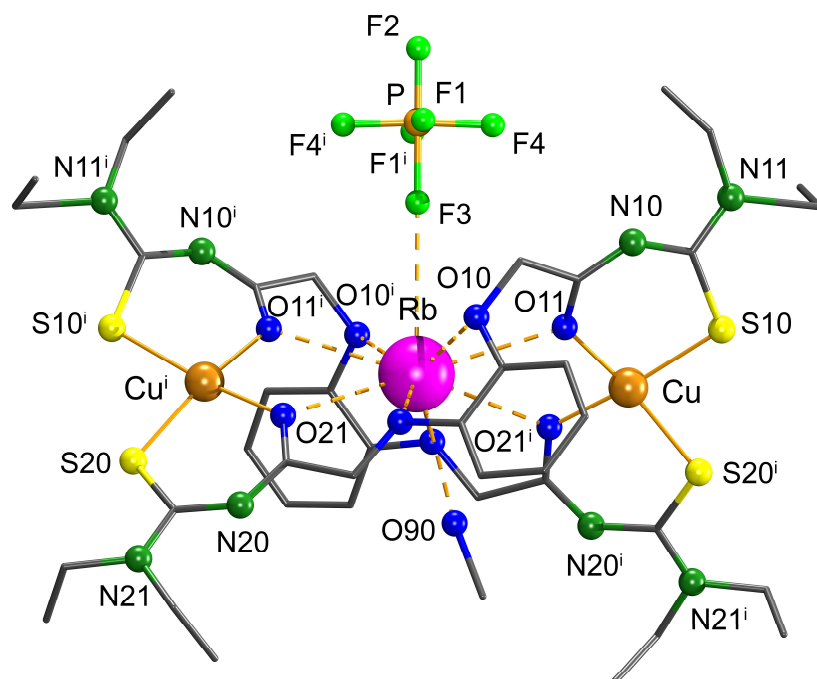
Figure 4.1 Structure of the {2}-coppercoronate $\{(MeOH)Rb \subset [Cu_2(L^3)_2]\}(PF_6)$. Hydrogen atoms are omitted for clarity. Symmetry transformation used to generate equivalent atoms: [i] –x, y, 1/2–z.

The copper(II) {2}-metallacoronates crystallize in the monoclinic space group C2/c. The molecules have a C_2 axis, which is through the M···P connecting line and parallel to the crystallographic *b* axis. Three metal centers are virtually aligned. Each Cu^{2+} ion binds with two *S,O*-bidentate aroylthioureato moieties. One of the resulting chelate rings is almost planar, while a significant deviation from planarity is found for the remaining ring. The values of the dihedral angles between the two mean least-square chelate planes (Table 4.1) are a clear sign of a strongly distorted tetrahedral ligand environment surrounding the Cu(II) ions. The values of the Cu–O, Cu–S bond lengths (Table 4.1) are similar to those found in binuclear copper(II) complexes with isophthaloylbis(thioureas), which have been previously reported.[34-35] Beside the coordinative bonds with eight oxygen donors from the ligand backbones, the coordination sphere of the encapsulated cations M^+ is saturated by weak interactions with a solvent molecule

and the counter anion PF_6^-. The strength of the interactions between the guest cations and the counterion reduces from Rb^+ to Tl^+ and becomes negligible in the case of K^+. This decrease in bond strength adheres to elongation of the $M\cdots F$ distances from Rb^+ to K^+ (Table 4.1).

Table 4.1 Selected distances, bond lengths (Å) and dihedral angle (°) in $\{M \subset [Cu_2(L^3)_2]\}(PF_6)$ complexes

M	Radius (Å)[*]	Cu⋯Cu	Cu⋯M	Cu–O	Cu–S	M–O	M⋯F	Angle[#]
Tl^+	1.59	8.360(8)	4.183(9)	1.927(7)/ 1.945(7)	2.258(9)/ 2.225(9)	2.939(3) – 3.105(3)	3.788(3)	17.37(3)
Rb^+	1.61	8.355(2)	4.182(7)	1.934(9)/ 1.942(2)	2.256(5)/ 2.221(2)	2.959(5) – 3.110(4)	3.367(9)	18.61(5)
K^+	1.51	8.271(9)	4.136(3)	1.934(3)/ 1.927(2)	2.230(5)/ 2.260(1)	2.808(5) – 3.072(4)	4.194(6)	13.35(5)

[*] for coordination number 8 [66]
[#] dihedral angle between two mean least-square chelate planes

The powder EPR spectrum of the magnetically diluted 2-metallacoronate system $\{K \subset [(Cu/Ni)_2(L^3)_2]\}(PF_6)$ demonstrates the virtually square-planar coordination environment of the Cu(II) ions. The powdered solid sample comprises of the Cu(II) complex (0.5 %) and the isostructural diamagnetic host Ni(II) compound (99.5 %), which is discussed in the next Chapter. Figure 4.2 depicts a comparison of the experimental and simulated spectra.
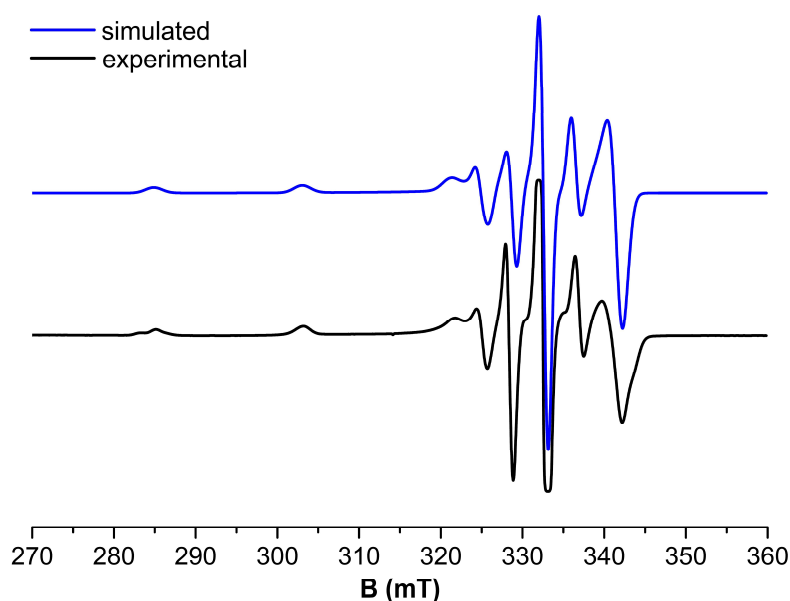
Figure 4.2 Experimental and simulated X-band powder EPR spectrum of the diamagnetically diluted system $\{K \subset [(Cu/Ni)_2(L^3)_2]\}(PF_6)$.

The EPR parameters obtained are given in Table 4.2. The splitting pattern is typical for the magnetic dilution related (S = 1/2) Cu^{II}-species and analogous to the pattern previously reported for the Cu(II) dinuclear complex with the ligand H_2L^1.[34] The tensors g and A^{Cu} reflect the slightly rhombic symmetry of the effective ligand field at Cu(II) centers, which is consistent with the deviation from the square-planar coordination mode of the transition metal ions.

Table 4.2 EPR-parameters of the diamagnetically diluted system $\{K \subset [(Cu/Ni)_2(L^3)_2]\}(PF_6)$. All hyperfine interaction parameters A_i are given in the unit of 10^{-4} cm^{-1}.

Complex	g_x	g_y	g_z	A_x	A_y	A_z
$\{K \subset [(Cu/Ni)_2(L^3)_2]\}(PF_6)$	2.031	2.029	2.152	37.2	31.5	182.6
$[(Cu/Ni)_2(L^1)_2]$ [34]		2.036	2.157		33.4	175.8

It is surprising that the encapsulation of the larger cation Cs^+ introduces a dramatic change in the composition and the structure of the resulting complex with three Cu(II) ions, the structure of which is exhibited in Figure 4.3.
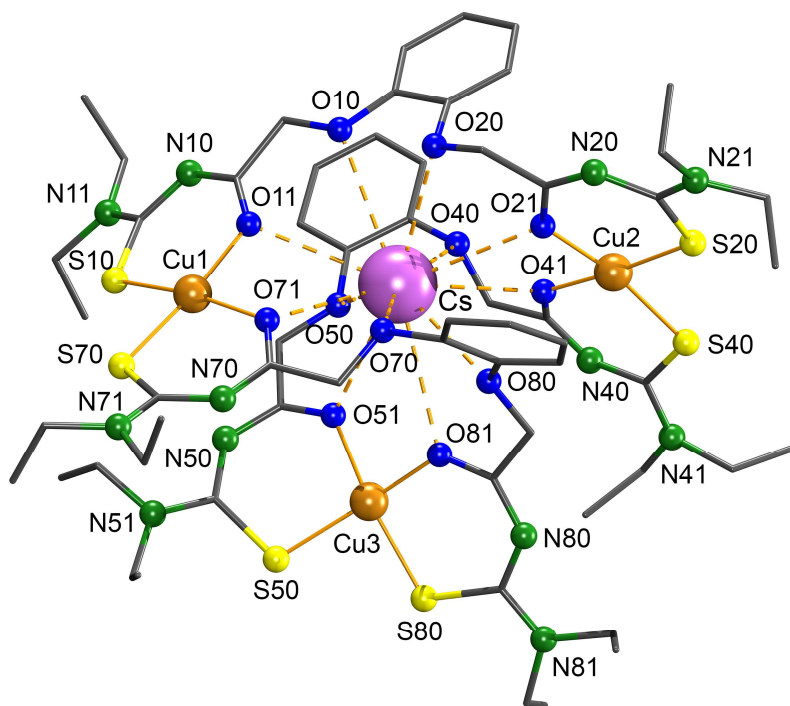
Figure 4.3 Structure of the cationic {3}-coppercoronate $\{Cs \subset [Cu_3(L^3)_3]\}^+$. Hydrogen atoms are omitted for clarity.

Hitherto, copper(II) trinuclear complexes with aroylthioureas have been exclusively supposed with paraphthaloylbis(thioureas).[28, 31, 67] The {3}-metallacoronate with the composition of $\{Cs \subset [Cu_3(L^3)_3]\}(PF_6)$ crystallizes in the triclinic space group $P\bar{1}$. The nearly square-planar

coordination geometry of the Cu(II) ions is illustrated by dihedral angles between the mean least-square planes of chelate rings of 8.67°, 10.31° and 28.84° for atoms Cu1, Cu2 and Cu3 respectively. Compared with the {2}-coppercoronates, no unusual bond lengths are detected for this structure (Table 4.3). In analogy to the bonding situation in the $(L^3)^{2-}$ complexes described in the previous Chapter, almost all chelate rings are nearly planar, except the ring formed by the atoms Cu3, O51, C51, N50, C52, S50 with a maximum deviation from the mean least-square plane of 0.241 Å for atom C52. This planarity is due to the flexible methylene bridges between aroylthiourea moieties and the spacer. The higher double-bond character of the $C(O)–N_{amide}$ bonds compared to $C(S)–N_{amine}$ bonds indicates that the negative charges of the chelate rings partially locate on the oxygen donors, which directly interact with the captured cation.

Table 4.3 Selected distances and bond lengths (Å) in $\{Cs \subset [Cu_3(L^3)_3\}(PF_6)$

Cs···Cu1	4.149(2)	Cs···Cu2	4.333(6)	Cs···Cu3	4.553(3)	Cu1···Cu2	8.458(6)
Cs–O10	3.320(6)	Cs–O40	3.115(9)	Cs–O70	3.143(3)	Cu1–O11	1.933(5)
Cs–O11	3.320(3)	Cs–O41	3.146(1)	Cs–O71	3.172(6)	Cu1–S10	2.240(2)
Cs–O20	3.174(1)	Cs–O50	3.243(7)	Cs–O80	3.148(8)	Cu1–O71	1.948(5)
Cs–O21	3.308(7)	Cs–O51	3.354(6)	Cs–O81	3.533(4)	Cu1–S70	2.221(2)
Cu2···Cu3	6.846(1)	Cu3···Cu1	5.715(1)	C11–O11	1.267(8)	C21–O21	1.279(9)
Cu2–O21	1.931(5)	Cu3–O51	1.941(5)	C11–N10	1.312(9)	C21–N20	1.307(9)
Cu2–S20	2.230(2)	Cu3–S50	2.225(2)	C12–N11	1.335(9)	C22–N21	1.315(1)
Cu2–O41	1.926(5)	Cu3–O81	1.929(5)	C12–N10	1.364(9)	C22–N20	1.366(1)
Cu2–S40	2.246(2)	Cu3–S80	2.232(2)	C12–S10	1.724(7)	C22–S20	1.700(8)
C41–O41	1.254(9)	C51–O51	1.270(8)	C71–O71	1.270(9)	C81–O81	1.273(8)
C41–N40	1.322(1)	C51–N50	1.294(8)	C71–N70	1.320(1)	C81–N80	1.318(9)
C42–N41	1.332(9)	C52–N51	1.319(9)	C72–N71	1.319(1)	C82–N81	1.330(9)
C42–N40	1.371(9)	C52–N50	1.367(9)	C72–N70	1.341(9)	C82–N80	1.355(9)
C42–S40	1.722(7)	C52–S50	1.738(7)	C72–S70	1.720(8)	C82–S80	1.723(7)

ESI^+ mass spectrometry provides useful information about dynamic properties of the complexes. The detection of fragments belonging to the free guest cations M^+, the {3}-coppercoronates $\{M \subset [Cu_3(L^3)_3]\}^+$ and the {2}-coppercoronates $\{M \subset [Cu_2(L^3)_2]\}^+$, in the mass spectra supports an assumption of an equilibrium between these two types of metallacoronates (Scheme 4.1). Structural conversion between the {3}- and {2}-metallacoronands, $[Cu_3(L^3)_3]$ and $[Cu_2(L^3)_2]$, can occur owing to lability of the metal ions,

which is a critical parameter for the self-assembling processes. The direction of the equilibrium shift and, thus, the separation of the particular structure type in the solid state is determined by the thermodynamic stability of the corresponding host-guest complex. Similar guest-induced equilibrium shift in supramolecular dynamic systems has been extensively studied for Pd(II)-based coordination assemblies.[68-69]

$\{M \subset [Cu_2(L^3)_2]\}^+$ $\{M \subset [Cu_3(L^3)_3]\}^+$
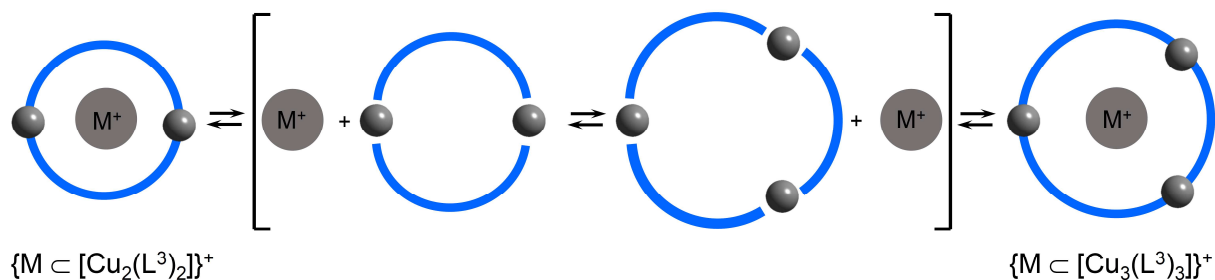
Scheme 4.1 Proposed equilibrium between {2}- and {3}-coppercoronate species in solution. Blue curves represent the bis-bidentate chelating ligands $(L^3)^{2-}$ ($M^+ = Cs^+, Rb^+, K^+$ or Tl^+).

The EPR spectroscopic studies on the Cu(II) metallocoronates support the proposed equilibrium in solution. For each of the compounds, the EPR experiments were carried out with the frozen solution and diamagnetically diluted powder samples at the temperature of liquid nitrogen (77 K). The appearance of the additional signals (Figure 4.4) in the solution spectra is a clear evidence for the presence of further components, which are generated from the equilibrium process in solution.
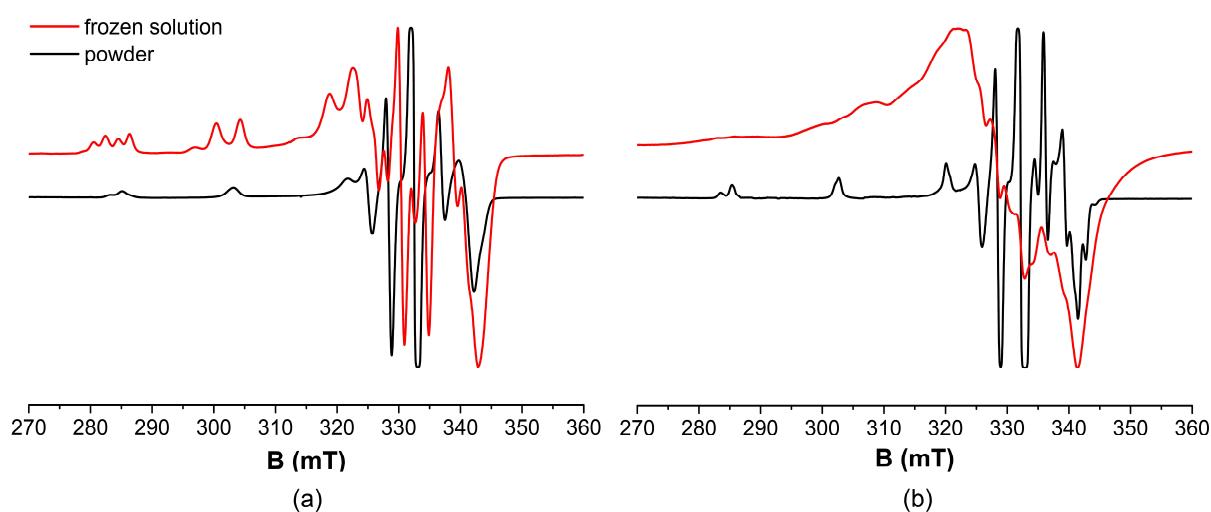
Figure 4.4 X-band EPR spectra of frozen CHCl$_3$/toluene-solution and powder samples in Ni(II) hosts at 77 K of (a) $\{K \subset [Cu_2(L^3)_2]\}(PF_6)$ and (b) $\{Cs \subset [Cu_3(L^3)_3]\}(PF_6)$.

4.2 Summary and conclusion

As a result of square-planar coordination, self-assembly of the Cu^{2+} ions with the novel ligand H_2L^3 in the presence of hard monovalent metal ions M^+ ($M^+ = Cs^+$, Rb^+, K^+ or Tl^+) produces 2D metallamacrocycles. They are topologically equivalent to classical organic coronates. Compositions and structures of such metallacoronates strongly depend on the size of the guest cations. The large size and the preferred coordination number of twelve of Cs^+ ions play an essential role in the construction of {3}-metallacoronates, $\{Cs \subset [Cu_3(L^3)_3]\}(PF_6)$, whereas smaller guest cations enable the assembly of {2}-metallacoronates, $\{M \subset [Cu_2(L^3)_2]\}(PF_6)$ ($M = Rb^+$, K^+ or Tl^+). Mass spectrometric and EPR spectroscopic data reveal dynamic processes of the resulting assemblies in solution and propose a guest-induced mechanism for the formation of particular type of structures.

Chapter 5

Assemblies with four– or six–coordinate metal ions

In this Chapter, Ni^{2+} ions, which form stable complexes with the coordination numbers four and six, are employed in a rational design of self-assembled oligonuclear systems. Despite the fact that in all structurally well-characterized complexes with aroylthioureas, Ni(II) ions exclusively adopt the square-planar geometry, the template effect of guest cations and the strict control of stoichiometry of the reactions allow access to the octahedral coordination mode of the transition metal ion.

5.1 The nickel(II) metallacoronates

Carefully following the procedure described for the synthesis of the Cu(II) complexes, the combination of equivalent amounts of H_2L^3, Ni^{2+} ions and one hard monocation such as, Cs^+, Rb^+ or K^+, results in the formation of metallacoronates. X-ray diffraction analyses of the resulting self-assembled structures expose structural analogies with the Cu(II) complexes. Particularly, the cores of the metallacoronands $[Ni_2(L^3)_2]$ and $[Ni_3(L^3)_3]$ show nearly square-planar coordination of the Ni(II) centers with the aroylbis(thioureato) dianions $(L^3)^{2-}$, and the central void of the {2}-metallacoronand $[Ni_2(L^3)_2]$ accommodates a monovalent ion such as Rb^+ and K^+, whereas the larger ion Cs^+ is located in the center of the {3}-metallacoronand $[Ni_3(L^3)_3]$. In case of the Cs^+-containing inclusion compound, single crystals for X-ray crystallography were obtained from slow evaporation of a solution of the solid product in a mixture of $CH_2Cl_2/MeOH$. On the other hand, the slow evaporation of a reaction mixture without the addition of PF_6^- salts produced suitable crystals for structure determination of the Rb^+-containing host-guest complex. Figures 5.1 and 5.2 depict the structures of these compounds. According to X-ray diffraction analyses, in both compounds, each Ni atom is four-coordinate with two aroylthioureato moieties. The Ni–O and Ni–S bond lengths (Tables 5.1 and 5.2) are in the expected ranges for square-planar Ni(II) complexes with aroylbis(thioureas).[31, 70] Similar to the Cu(II) complex containing Rb^+, the isostructural Ni(II) {2}-metallacoronate crystallizes in the monoclinic space group C2/c with a molecular two-fold axis through the Rb···Cl connecting line (Figure 5.1). The coordination sphere of the guest cation Rb^+ comprises eight oxygen atoms from the ligand backbones, one oxygen from a solvent molecule and one chlorido co-ligand, which also compensates the charge. The low value of 8.63° of the dihedral angle between the two mean chelate planes surrounding the Ni(II) atoms

reflects their nearly square-planar coordination modes. Compared with the corresponding Cu(II) complex, the degree of deviation from the planarity significantly decreases. This observation is expected from the change of the electronic configuration of transition metal ions from a d^9 system in the case of Cu^{2+} to a d^8 system, which favors the square-planar geometry, in the case of Ni^{2+}.
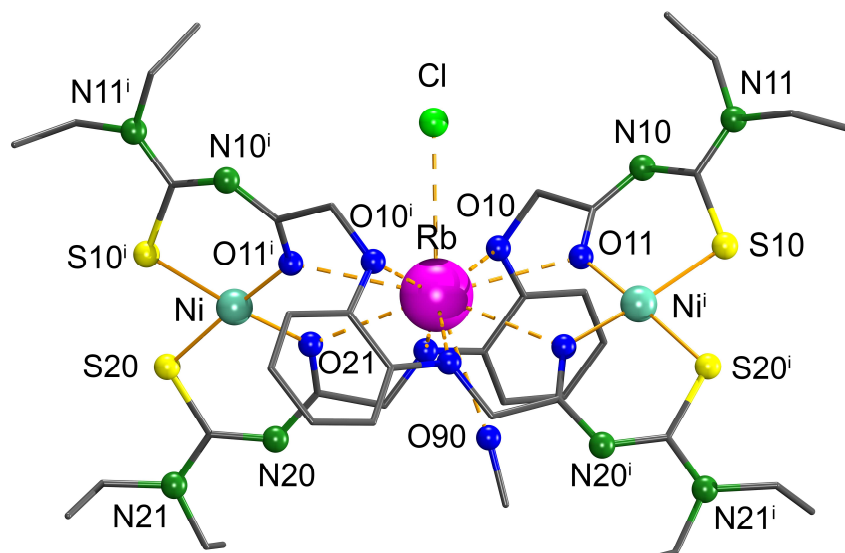
Figure 5.1 Structure of the complex {2}-nickelcoronate {(MeOH)ClRb ⊂ [Ni₂(L³)₂]}. Hydrogen atoms are omitted for clarity. Symmetry operation used to generate equivalent atoms: ⁱ 2–x, y, 1/2–z.

Table 5.1 Selected bond lengths and distances (Å) in {(MeOH)ClRb ⊂ [Ni₂(L³)₂]}

Rb–O10	2.929(5)	Ni–O11	1.874(4)	C11–O11	1.275(7)	C21–O21	1.264(7)
Rb–O11	3.062(4)	Ni–S10	2.166(3)	C11–N10	1.310(8)	C21–N20	1.322(8)
Rb–O20	2.984(5)	Ni–O21	1.876(4)	C12–N11	1.336(8)	C22–N21	1.336(8)
Rb–O21	3.131(4)	Ni–S20	2.143(4)	C12–N10	1.335(8)	C22–N20	1.347(8)
Rb–O90	3.138(2)	Ni⋯Ni	8.359(1)	C12–S10	1.728(6)	C22–S20	1.733(6)
Rb–Cl	3.490(4)	Rb⋯Ni	4.184(9)				

A comparison of the structures of the nickel(II) and copper(II) {3}-metallacoronates draws an analogy between their bonding situations. The Ni1 and Ni2 ions are coordinated in practically square-planar geometry with dihedral angles between two mean least-square chelate planes of 3.14° and 3.42° respectively, while the value of 29.27° of the dihedral angle exhibits a strongly distorted tetrahedral coordination mode for the remaining ion Ni3. Except the considerable deviation of 0.263 Å for the atom C52 from the mean chelate plane surrounding the atom Ni3, only minor deviations from planarity in the other chelate rings are observed.
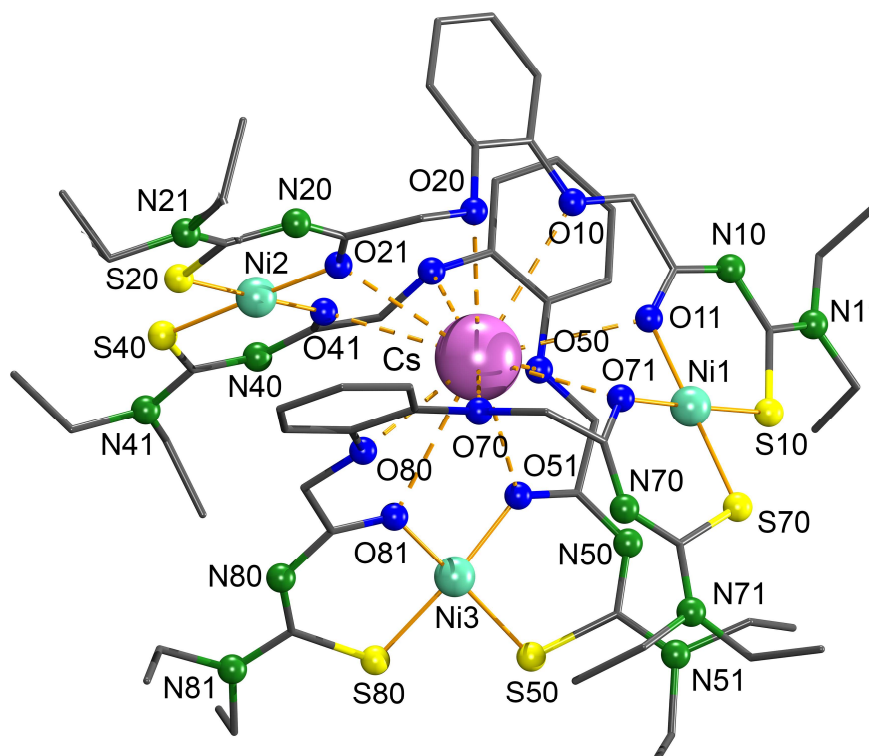
Figure 5.2 Structure of the cationic {3}-nickelcoronate $\{Cs \subset [Ni_3(L^3)_3]\}^+$. Hydrogen atoms are omitted for clarity.

Table 5.2 Selected distances and bond lengths (Å) in $\{Cs \subset [Ni_3(L^3)_3]\}(PF_6)$

Cs⋯Ni1	3.987(4)	Cs⋯Ni2	4.201(8)	Cs⋯Ni3	4.391(1)	Ni1⋯Ni2	8.159(2)
Cs–O10	3.310(9)	Cs–O40	3.134(7)	Cs–O70	3.078(5)	Ni1–O11	1.865(3)
Cs–O11	3.194(1)	Cs–O41	3.137(3)	Cs–O71	3.226(2)	Ni1–S10	2.149(3)
Cs–O20	3.200(2)	Cs–O50	3.193(6)	Cs–O80	3.155(1)	Ni1–O71	1.874(3)
Cs–O21	3.289(8)	Cs–O51	3.224(1)	Cs–O81	3.352(5)	Ni1–S70	2.149(6)
Ni2⋯Ni3	6.571(2)	Ni3⋯Ni1	5.727(3)	C11–O11	1.271(5)	C21–O21	1.264(5)
Ni2–O21	1.866(3)	Ni3–O51	1.885(3)	C11–N10	1.305(5)	C21–N20	1.317(5)
Ni2–S20	2.145(4)	Ni3–S50	2.154(4)	C12–N11	1.335(5)	C22–N21	1.329(6)
Ni2–O41	1.873(3)	Ni3–O81	1.887(3)	C12–N10	1.358(6)	C22–N20	1.352(6)
Ni2–S40	2.146(8)	Ni3–S80	2.135(7)	C12–S10	1.730(5)	C22–S20	1.735(5)
C41–O41	1.273(5)	C51–O51	1.276(5)	C71–O71	1.276(9)	C81–O81	1.261(5)
C41–N40	1.307(5)	C51–N50	1.312(5)	C71–N70	1.311(5)	C81–N80	1.322(5)
C42–N41	1.327(6)	C52–N51	1.321(5)	C72–N71	1.330(5)	C82–N81	1.333(5)
C42–N40	1.346(5)	C52–N50	1.346(5)	C72–N70	1.355(6)	C82–N80	1.344(5)
C42–S40	1.740(5)	C52–S50	1.748(5)	C72–S70	1.738(5)	C82–S80	1.733(4)

The shorter distances between the metal ions in the oligonuclear Ni(II) complex (Table 5.2) in comparison with those in the corresponding Cu(II) complex are in good agreement with the effective sizes of Ni^{2+} and Cu^{2+} ions when they are in the same ligand field. In contrast, such distances in the isostructural Ni(II) and Cu(II) {2}-metallacoronates are almost equal and appear to be independent of the two transition metal ions. This interesting feature can be explained by the fact that {2}-metallacoronands are more rigid than {3}-metallacoronands in providing optimal voids to accommodate guest cations.

Spectroscopic data of the complexes are consistent with the results of the X-ray structural analyses. Double deprotonation of the organic ligands and their existence as dianions $(L^3)^{2-}$ with typical delocalization of π-electron density within the aroylthioureato moieties are validated by the absence of ν_{NH} bands in the region above 3100 cm^{-1} and the bathochromic shift of the $\nu_{C=O}$ bands in IR spectra of about 115 cm^{-1}. In addition, the presence of a PF_6^- anion can be detected by strong absorptions around 840 cm^{-1}. The well-resolved NMR spectra are clear manifestations of the diamagnetism of the Ni(II) metallacoronates and, therefore, square-planar coordination geometry of the Ni(II) ions. ^{1}H NMR spectra show disappearance of the NH signals of the H_2L^3 ligand, which is a clear evidence for the deprotonation of the ligand. Aromatic protons appear as two multiplets in the range of 6.7 – 7.0 ppm, whereas broad singlets at approximately 4.6 ppm are assigned to the OCH_2 protons. As a consequence of hindered rotation around the C–NEt$_2$ bonds, two sets of signals, each including one triplet and one quartet, are observed for the ethyl groups in the ^{1}H NMR spectra. Due to the same reason, ^{13}C NMR spectra of the complexes exhibit two separated signals for each methylene and methyl carbon atom of the NEt$_2$ groups. The bridging methylene OCH_2 resonance appears at about 71 ppm, while chemical shifts of aromatic carbons are in the lower field from 110 ppm to 150 ppm. Peaks with low intensities at 171 ppm and 175 ppm are associated with the resonances of the C=S and C=O groups, respectively.

ESI$^+$ mass spectra of the nickel compounds suggest the presence of equilibria between different complexes in solution. They show peaks associated with the free guest cations M$^+$, the {3}-nickelcoronates {M ⊂ [Ni$_3$(L^3)$_3$]}$^+$ and the {2}-nickelcoronates {M ⊂ [Ni$_2$(L^3)$_2$]}$^+$ (M = Cs$^+$, Rb$^+$ or K$^+$). This finding is very similar to that with the analogous Cu(II) complexes.

5.2 The nickel(II) metallacryptates

On the basis of the results with the six-coordinate trivalent ions Fe^{3+} and Co^{3+}, which have been discussed in Chapter 3, a strategy was derived for the synthesis of analogous complexes with

the divalent metal ion Ni^{2+}. They should be able to form anionic $\{2\}$-metallacryptates of the composition $\{M \subset [Ni_2(L^3)_3]\}^-$ ($M = Cs^+$, Rb^+ or K^+), which might be separated as ion pairs with large counter cations. Thus, three equivalents of the ligand H_2L^3 were allowed to react with two equivalents of $Ni(OAc)_2$ in MeOH in the presence of a tenfold excess of alkali metal ions such as Cs^+, Rb^+ or K^+. The pure green solids were isolated and analyzed. No unusual absorption bands are found in the IR spectra of the resulting products. ESI^- mass spectra present peaks corresponding to the expected fragments $\{M \subset [Ni_2(L^3)_3]\}^-$. These observations and the elemental analyses indicate that the obtained solids represent the supposed complexes $M\{M \subset [Ni_2(L^3)_3]\}$. Unfortunately, all attempts to produce single crystals for structure determination have failed up to now.

In order to provide more convincing evidence for the formation of $\{2\}$-metallacryptates based on Ni(II), similar reactions utilizing alkali earth metal ions M^{2+} ($M^{2+} = Ba^{2+}$, Sr^{2+} or Ca^{2+}) instead of monovalent ions were performed. Treatment of equivalent amounts of the ligand H_2L^3 with $BaCl_2$ and $Ni(OAc)_2$ in MeOH produces a yellow-green solid, which rapidly deposits from the reaction mixture. Close resemblance between the IR spectrum of the product and those of the above alkali metal-containing complexes is a strong hint for structural similarity of these compounds. Slow evaporation of a solution of the product in a CH_2Cl_2/n-hexane mixture leads to single crystals suitable for X-ray crystallography. The diffraction analyses reveal a neutral triple-stranded structure of $\{Ba \subset [Ni_2(L^3)_3]\}$ with a C_2 axis through the Ba atom and the center of one phenylene ring. The structure of the product is shown in Figure 5.3. Similar to the situation in the Fe(III) and Co(III) tris-complexes, the core metallacryptand, $[Ni_2(L^3)_3]^{2-}$, is afforded by the hitherto unknown distorted octahedral coordination of two Ni^{2+} ions by three bis(aroylthioureato) dianions $(L^3)^{2-}$. An increase of the effective radius of the Ni^{2+} ions with respect to the change of coordination number from four to six would account for the fact that all Ni–O and Ni–S bonds are longer than those in preceding square-planar Ni(II) complexes. The void of the resulting cryptand is occupied by a Ba^{2+} ion binding with twelve oxygen donors. It is remarkable that all Ba–$O_{carbonyl}$ distances are shorter than the corresponding Ba–O_{ether} ones (Table 3.5). Such a bonding feature has been not perceived in any of the previous complexes, where the guest cations interact with the neutral host exclusively through coordinative bonds. In this case of the Ni/Ba-compound, the bonding situation reflects additional electrostatic interactions between the Ba^{2+} cation and the negatively-charged metallacryptand, $[Ni_2(L^3)_3]^{2-}$, especially through its carbonyl oxygen atoms. This electrostatic interaction is also responsible for the bend angle of $146.01°$ between three metal centers Ni$\cdots$Ba$\cdots$Ni and a significantly shorter Ni$\cdots$Ni distance of $6.960(2)$ Å compared with the distances Fe$\cdots$Fe or Co$\cdots$Co in their

metallacryptates derived from H_2L^3, which are in the ranges of 8.081(4) – 8.190(4) Å and 7.839(1) – 8.092(0) Å, respectively. The marked difference between C(O)–N_{amide} and C(S)–N_{amide} bond lengths is indicative of the less extent of π-electron delocalization within the chelates formed by the aroylthioureas and, hence, well corresponds to the low bathochromic shifts of 65 cm^{-1} of the $\nu_{C=O}$ frequency in the IR spectra.
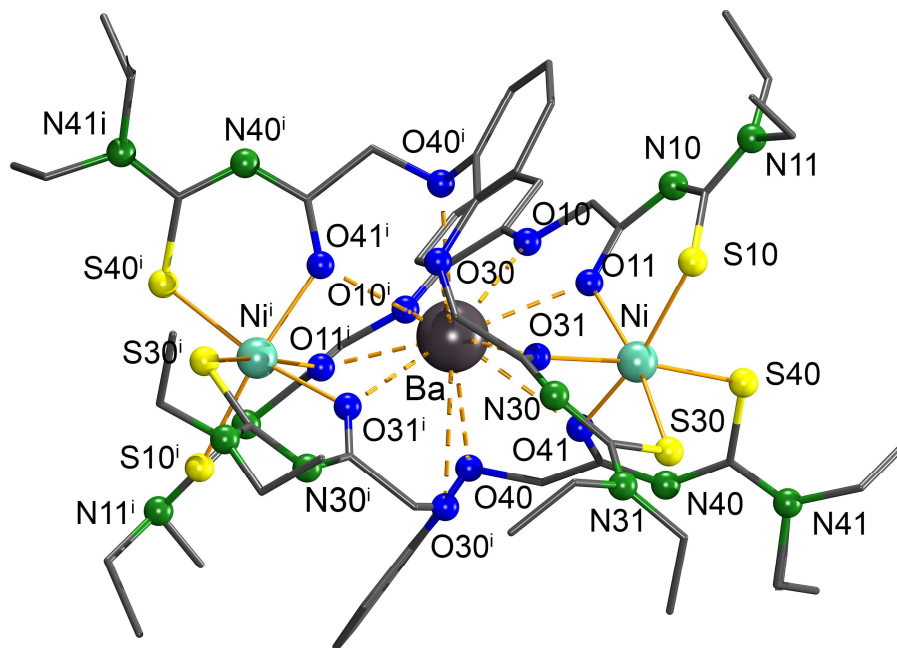
Figure 5.3 Molecular structure of the complex {2}-nickelcryptate {Ba ⊂ [Ni$_2$(L^3)$_3$]}. Hydrogen atoms are omitted for clarity. Symmetry transformation used to generate equivalent atoms: ^{i} –x, y, 1/2–z.

Table 5.3 Selected bond lengths and distances (Å) in {Ba ⊂ [Ni$_2$(L^3)$_3$]}

Ni–O11	2.061(3)	C11–O11	1.247(5)	C31–O31	1.243(5)	C41–O41	1.246(5)
Ni–O31	2.065(3)	C11–N10	1.320(5)	C31–N30	1.319(6)	C41–N40	1.311(6)
Ni–O41	2.057(3)	C12–N11	1.336(5)	C32–N31	1.338(6)	C42–N41	1.344(6)
Ni–S10	2.378(4)	C12–N10	1.370(5)	C32–N30	1.360(6)	C42–N40	1.351(7)
Ni–S30	2.361(9)	C12–S10	1.708(5)	C32–S30	1.688(5)	C42–S40	1.722(6)
Ni–S40	2.364(8)	Ba–O10	3.043(3)	Ba–O30	2.875(3)	Ba⋯O40	3.263(3)
Ni⋯Ni	6.960(2)	Ba–O11	2.679(3)	Ba–O31	2.856(3)	Ba–O41	2.736(3)
Ba⋯Ni	3.639(3)						

5.3 The nickel(II) metallalariate-ethers

Reactions of H_2L^3 with mixtures of $SrCl_2$ or $CaCl_2$ and $Ni(OAc)_2$ under the same conditions described before yield unexpected products with moderate yields (~ 40%). After the structures of the products had been determined, the procedure was optimized by using the correct stoichiometric amounts of the precursors. Figure 5.4 illustrates the structure of the resulting host-guest systems with the guest cations Sr^{2+}.
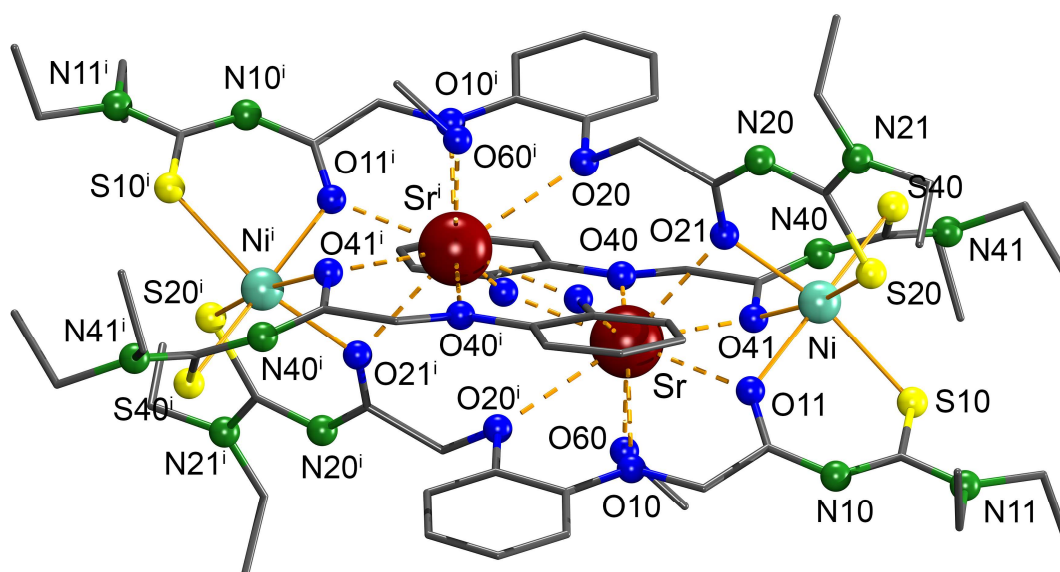
Figure 5.4 Molecular structure of the metallalariate-ether $\{(MeOH)_2Sr_2 \subset [Ni_2(L^3)_2(L^{3'})_2]\}$. Hydrogen atoms are omitted for clarity. Symmetry operation used to generate equivalent atoms: ^{i} −x, −y, −z.

The tetranuclear assemblies are generated from the capture of two M^{2+} ions in the central void of the lariate-ether metallamacrocycle $[Ni_2(L^3)_2(L^{3'})_2]^{4-}$. The structure is composed of two octahedrally coordinated Ni(II) ions linked through two bipodal bis(thioureato) dianions $(L^3)^{2-}$ and two bidentate thioureato dianions $(L^{3'})^{2-}$ resulting from the cleavage one O–CH$_2$ bond of the anions $(L^3)^{2-}$ (Scheme 5.1).
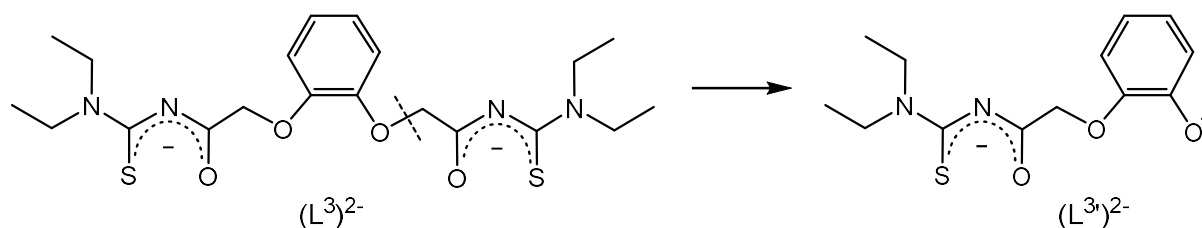
Scheme 5.1 The formation of the bis-bidentate thioureato dianion $(L^{3'})^{2-}$

The coordination of the resulting dianions $(L^{3'})^{2-}$ with Ni^{2+} ions gives rise to two sidearms of the metallalariate-ether $[Ni_2(L^3)_2(L^{3'})_2]^{4-}$, which provide a sufficient amount of donor atoms for the encapsulation of two guest cations. Each of them interacts with nine oxygen donors, eight of them from the ligand backbones, while the last originates from a coordinated solvent molecule. The midpoint of connecting line between guest cations is a molecular inversion center.

When the same procedure is applied for rare earth metal ions M^{3+} ($M^{3+} = La^{3+}$, Ce^{3+}, Pr^{3+}), which have radii in the range of Ca^{2+} and Sr^{2+}, isostructural complexes are produced. Because the charge of the guest cations changes to 3+, the obtained host-guest systems are positively charged. Charge compensation is done by the small acetate co-ligands, which finally give the neutral metallamacrocyclic systems $\{(AcO)_2M_2 \subset [Ni_2(L^3)_2(L^{3'})_2]\}$. A representative structure is shown in Figure 5.5.
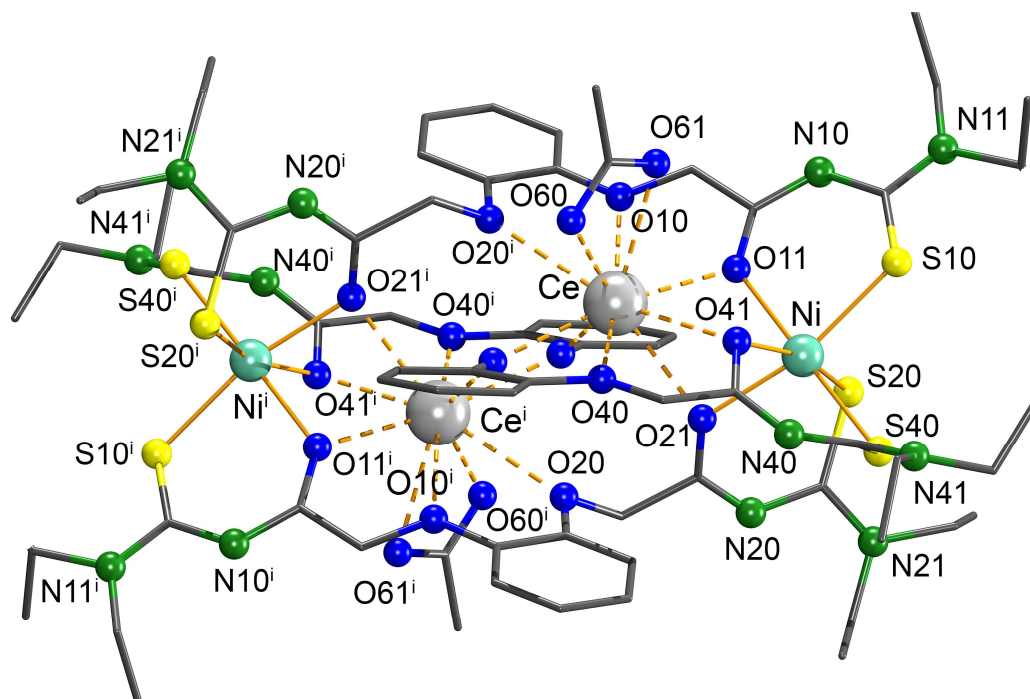
Figure 5.5 Molecular structure of the metallalariate-ether $\{(AcO)_2Ce_2 \subset [Ni_2(L^3)_2(L^{3'})_2]\}$. Hydrogen atoms are omitted for clarity. Symmetry operation used to generate equivalent atoms: ^{i} 1–x, 2–y, –z.

Due to the additional interaction with the acetato co-ligands, each lanthanide cation has a coordination number of ten. The Ni–O and Ni–S bonds are slightly longer than the corresponding bonds in the Ni(II) metallacryptates. The small elongation of these bonds enables the formation of metallamacrocycles with more inner space suitable for the capture of two guest

cations. Table 5.4 shows the considerable influence of the charge of the guest ions on the distances between the metal ions. The higher is the cationic charge, the greater is the electrostatic repulsion between the metal ions, and consequently the more they move away from each other. On the other hand, in each series of the studied compounds (alkali earth metal ion or lanthanide ion inclusion compounds), the relation between the ionic radii and the metal-metal distances, especially the Ni⋯Ni ones, appears to be irregular. This irregularity is the consequence of the distortion of the host metallamacrocycle $[Ni_2(L^3)_2(L^{3'})_2]^{4-}$ along the Ni⋯Ni axis, which generates an optimal coordination environment for the guest cations.

Table 5.4 Selected distances and bond lengths (Å) in Ni(II) metallalariate-ethers

M	Radius (Å)*	Ni⋯Ni	Ni⋯M	M⋯M	Ni–O	Ni–S	M–O
					2.064(3)	2.336(3)	2.441(3)
Sr^{2+}	1.31	9.711(6)	3.432(8)	3.677(6)	–	–	–
					2.077(3)	2.410(9)	2.860(3)
					2.049(2)	2.349(5)	2.327(5)
Ca^{2+}	1.18	9.738(4)	3.350(6)	3.617(9)	–	–	–
					2.086(2)	2.425(2)	3.063(4)
					2.048(5)	2.338(2)	2.450(4)
La^{3+}	1.27	9.788(7)	3.451(5)	4.001(5)	–	–	–
					2.120(4)	2.393(2)	2.778(4)
					2.046(5)	2.345(2)	2.442(4)
Ce^{3+}	1.25	9.770(4)	3.442(6)	3.984(4)	–	–	–
					2.125(4)	2.391(2)	2.734(4)
					2.052(4)	2.374(5)	2.440(3)
Pr^{3+}	–	9.777(4)	3.452(5)	3.987(3)	–	–	–
					2.136(3)	2.400(6)	2.724(3)

* coordination number 9 for alkali-earth metal ions and 10 for lanthanide ions [66]

The ESI$^+$ MS data confirm the existence of Ni(II) metallalariate-ethers in solution and in the gas phase. In case of the alkali-earth-metal complexes, the base peaks correspond to the protonated molecular ions $[M+H]^+$, while the most intense peaks associate with the fragments $[M-AcO]^+$ in the mass spectra of the lanthanide complexes. Additionally, high resolution ESI$^+$ MS data matching the simulated patterns of the major peaks confirms the assigned compositions (Figure 5.6).
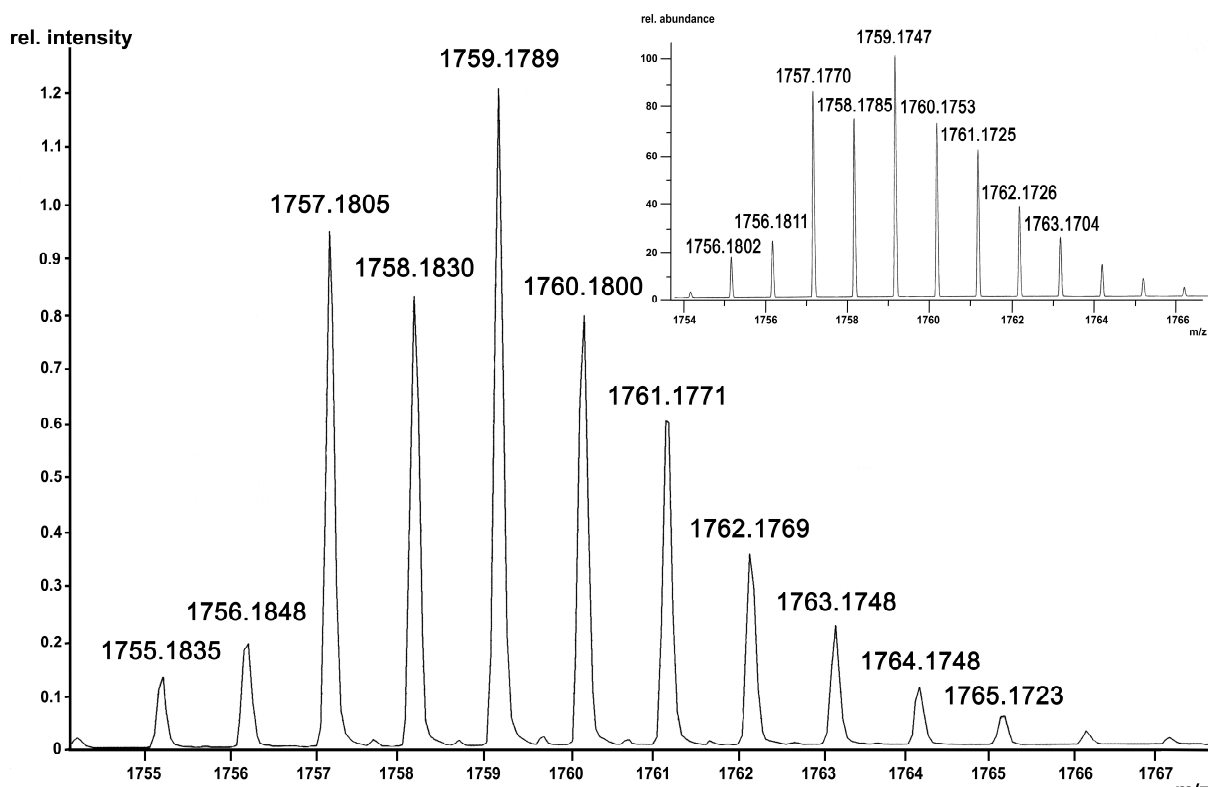
(a)
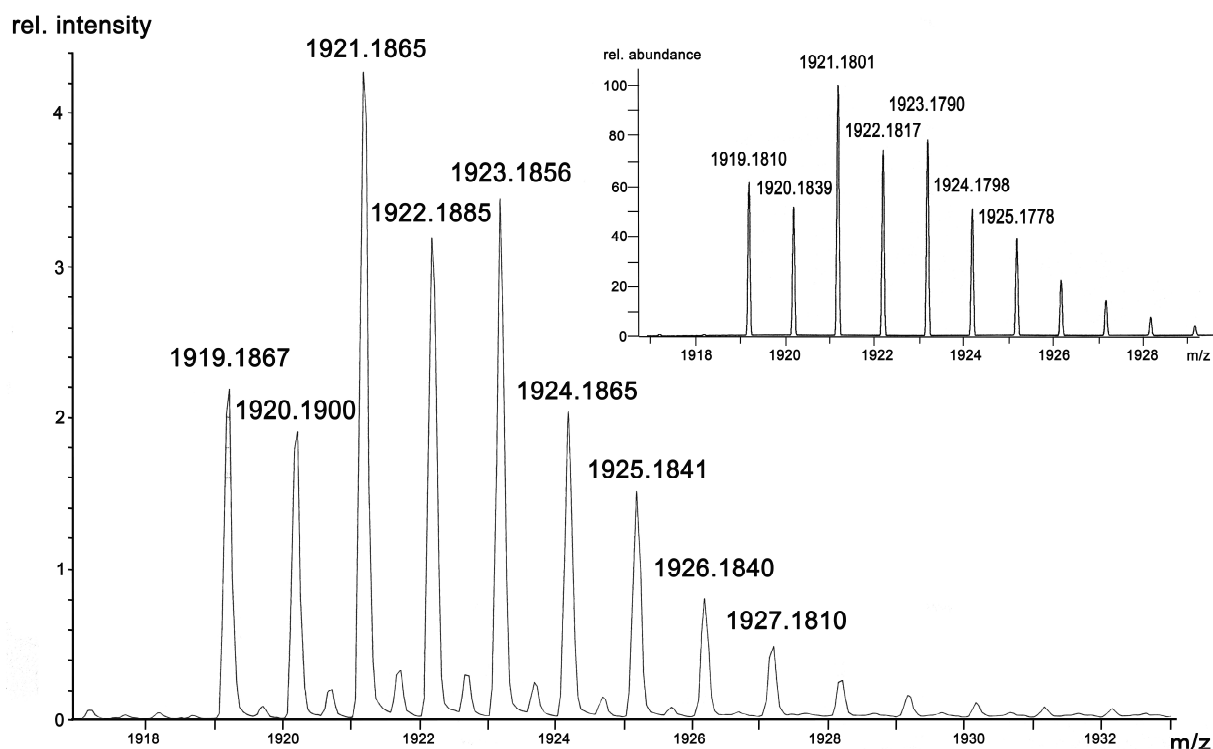
(b)

Figure 5.6 Observed and simulated isotopic patterns of base peaks in high resolution ESI$^+$ mass spectra of (a) {Sr$_2$ ⊂ [Ni$_2$(L^3)$_2$(L^3')$_2$]} and (b) {(AcO)$_2$Ce$_2$ ⊂ [Ni$_2$(L^3)$_2$(L^3')$_2$]}

5.4 Summary and conclusion

Exploiting different stoichiometries of one-pot reactions between the ligand H_2L^3 and mixtures of Ni^{2+} ions and hard cations enables both coordination numbers of four and six of the transition metal ion, thereby facilitating the formation of assemblies with different compositions and topologies. Metallacoronates are developed from the square-planar, four-coordinate mode of Ni^{2+} ions, while their octahedral six-coordinate fashion induces either metallacryptates or hitherto unprecedented metallalariate-ethers depending on the size of guest cations.

Chapter 6

Assemblies with thiophilic metal ions

Despite the fact that aroylthioureas should possess a high affinity to thiophilic metal ions, surprisingly less is known about this area of their coordination chemistry. A survey of literature reveals only a few reports of aroylthiourea complexes with ions such as Ag(I),[25, 39, 71-73] Au(I),[26, 35] or Hg(II).[74-76] Nevertheless, some of these complexes have notable structures. For example, one is a discrete 26-membered bimetallamacrocycle of Hg(II) with paraphthaloylbis(N,N-diethylthioureas), where mercury atoms are almost linear coordinated by the sulfur donor atoms.[76] Another interesting example is a cationic coordination polymer with Ag(I), in which the metal ions are exclusively S-bonded to the ligand H_2L^2.[39] In this context, the following Chapter focuses on assemblies based on the thiophilic metal ions Ag(I) and Hg(II).

6.1 The silver(I) metallacoronates

Starting with the doubly deprotonated ligand $(L^3)^{2-}$ and taking into account the preferred linear coordination mode of Ag^+ ions, the formation of a negatively charged {2}-metallacoronand $[Ag_2(L^3)_2]^{2-}$ might be expected. For charge compensation, which was identified as an important driving force in the previous experiments, guest alkaline earth metal ions M^{2+} ($M^{2+} = Ca^{2+}$, Sr^{2+} or Ba^{2+}) were used as one of molecular components. Elemental analyses of the resulting colorless solids match the proposed composition $\{M \subset [Ag_2(L^3)_2]\}$ ($M = Ca^{2+}$, Sr^{2+} or Ba^{2+}) of neutral {2}-metallacoronates. X-ray diffraction analyses of single crystals obtained from slow evaporation of CH_2Cl_2/MeOH solutions of the complexes show their structures.

The complex with central Ca^{2+} ions crystallizes in the monoclinic space group $P2_1/c$ with two crystallographically independent molecules in the asymmetric unit (Figure 6.1 a). In each molecule, two Ag^+ ions exclusively bind the soft sulfur atoms of two $(L^3)^{2-}$ ligands. Such a behavior is not unexpected with regard to the well-known high thiophilicity of Ag(I). On the other hand, all hard oxygen atoms from the ligand skeletons orientate towards the cationic guest located in the central void of the {2}-metallacoronand $[Ag_2(L^3)_2]^{2-}$. Hence, the Ca^{2+} ion is eight-coordinate with a triangulated-dodecahedral arrangement of donor atoms.[77] The Ag–S bond lengths vary from 2.371(3) to 2.461(2) Å, which are shorter than the sum of covalent radii of Ag (1.45(5)Å) and S (1.05(3)Å) and in the same range for those observed in the Ag(I) complexes with deprotonated aroylmonothioureas.[71, 73, 78]
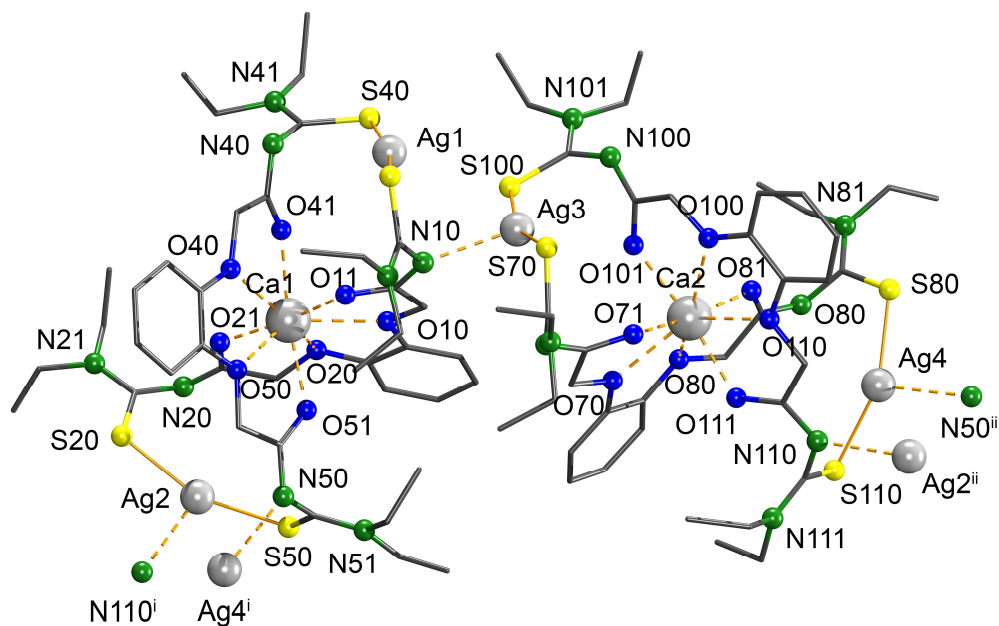
(a)
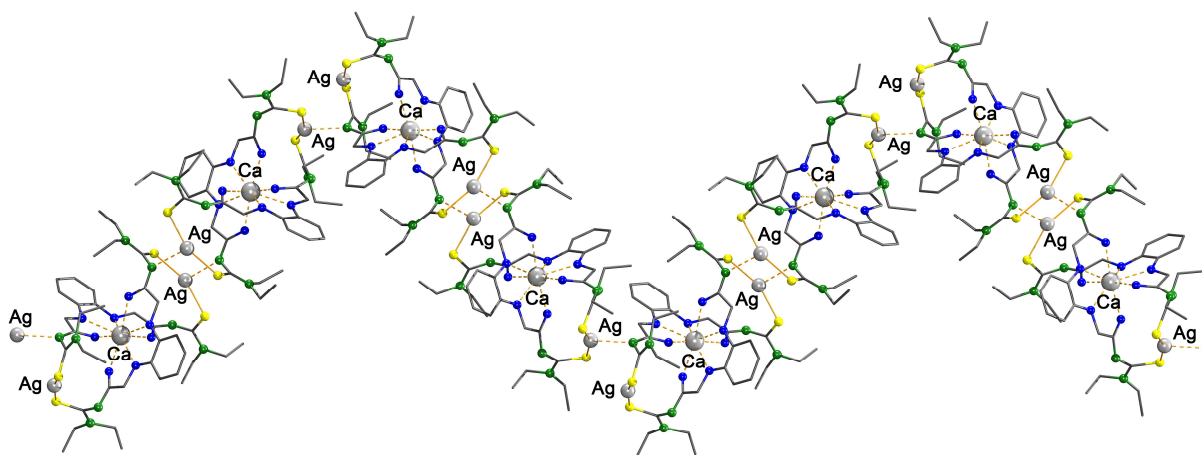
(b)

Figure 6.1 Molecular structure of (a) the asymmetric unit $\{Ca \subset [Ag_2(L^3)_2]\}_2$ and (b) the resulting 1D polymeric zig–zag chain $\{\{Ca \subset [Ag_2(L^3)_2]\}_2\}_\infty$. Hydrogen atoms are omitted for clarity.

The significant deviation of the S–Ag–S angles from linearity (Table 6.1) may result from distortions due to the optimal accommodation of the guest cations. In addition, interactions between the Ag(I) ions with amide N atoms of the adjacent units, namely Ag3···N10, Ag2···N110[i] and Ag4···N50[ii], may also contribute to the deviation. These intermolecular interactions are also responsible for the aggregation of the obtained subunits and the formation of 1D polymeric zig-zag chains in the solid state (Figure 6.1b).

Table 6.1 Selected bond lengths, distances (Å) and angles (º) in $\{Ca \subset [Ag_2(L^3)_2]\}_2$

Bond lengths and distances (Å)							
Ca1–O10	2.552(5)	Ag1–S10	2.371(3)	C11–O11	1.263(1)	C21–O21	1.242(1)
Ca1–O11	2.318(6)	Ag1–S40	2.377(3)	C11–N10	1.293(1)	C21–N20	1.280(1)
Ca1–O20	2.571(6)	Ag2–S20	2.437(2)	C12–N11	1.323(1)	C22–N21	1.358(1)
Ca1–O21	2.282(6)	Ag2–S50	2.461(2)	C12–N10	1.336(1)	C22–N20	1.352(1)
Ca1–O40	2.514(6)	Ag1⋯Ca1	5.132(9)	C12–S10	1.716(1)	C22–S20	1.704(1)
Ca1–O41	2.311(6)	Ag2⋯Ca1	5.162(8)	C41–O41	1.231(1)	C51–O51	1.241(9)
Ca1–O50	2.538(6)	Ag1⋯Ag2	10.289(7)	C41–N40	1.334(1)	C51–N50	1.311(1)
Ca1–O51	2.316(6)	Ag3–S70	2.397(3)	C42–N41	1.338(1)	C52–N51	1.343(1)
Ca2–O70	2.525(6)	Ag3–S100	2.409(3)	C42–N40	1.338(1)	C52–N50	1.362(1)
Ca2–O71	2.366(6)	Ag4–S80	2.440(2)	C42–S40	1.705(1)	C52–S50	1.694(1)
Ca2–O80	2.546(6)	Ag4–S110	2.452(2)	C71–O71	1.256(1)	C81–O81	1.236(9)
Ca2–O81	2.304(6)	Ag3⋯Ca2	5.070(7)	C71–N70	1.296(1)	C81–N80	1.315(1)
Ca2–O100	2.502(5)	Ag4⋯Ca2	5.369(9)	C72–N71	1.296(1)	C82–N81	1.318(9)
Ca2–O101	2.335(6)	Ag3⋯Ag4	10.414(3)	C72–N70	1.337(1)	C82–N80	1.381(1)
Ca2–O110	2.503(5)	Ag3⋯N10	2.497(7)	C72–S70	1.726(1)	C82–S80	1.702(8)
Ca2–O111	2.333(6)	Ag4–N50[ii]	2.493(7)	C101–O101	1.267(1)	C111–O111	1.245(9)
Ag2⋯Ag4[i]	3.447(7)	Ag2–N110[i]	2.484(6)	C101–N100	1.302(1)	C111–N110	1.324(1)
C102–S100	1.707(9)	C112–S110	1.707(9)	C102–N101	1.321(1)	C112–N111	1.310(1)
				C102–N100	1.355(1)	C112–N110	1.388(1)

Angles (º)			
S10–Ag1–S40	166.15(1)	S70–Ag3–S100	160.20(9)
S20–Ag2–S50	156.24(9)	S80–Ag4–S110	154.80(8)

Symmetry operations used to generate equivalent atoms: [i] -x+2,y-1/2,-z+1/2 and [ii] -x+2,y+1/2, -z+1/2

The Ba^{2+}- and Sr^{2+}-capturing complexes crystallize in form of $\{(MeOH)M \subset [Ag_2(L^3)_2]\}$ units in the triclinic space group $P\bar{1}$. Similarly to the preceding assembly, they comprise metallacoronands, $[Ag_2(L^3)_2]$, which are composed of two Ag(I) ions linked through two doubly deprotonated ligands $(L^3)^{2-}$. The divalent cations are located in the molecular cavity of the metallamacrocycles. Due to the large radii of Ba^{2+} and Sr^{2+}, the coordination spheres of the guest cations M^{2+} are saturated by solvent molecules (Figure 6.2a and 6.3a). Therefore, the Ba^{2+} ion is nine coordinate, whereas the coordination number of the Sr^{2+} ion is eight. The atom O51 with a Sr–O distance of 3.388(5) Å is not incorporated in the coordination sphere. The bonding

situation of the Ag(I) ions is similar to that observed in the Ca^{2+}-capturing complex (Table 6.2 and 6.3). The smallest Ag···Ag contact in the solid state is longer than the Ag···Ag distance of 2.889 Å in metallic silver.[79] This means that no metal-metal bonds are established. The intermolecular Ag···N_{amide} interactions play a vital role in the assembly of the structural units in the 1D polymeric chains in the solid state structure of the Ba^{2+} complex (Figure 6.3b). In case of the Sr^{2+}-complex, dimeric units, instead of a coordination polymer, are formed (Figure 6.2b). The center of the Sr···Sr connecting line of the dimer represents the inversion center.

(a)

(b)
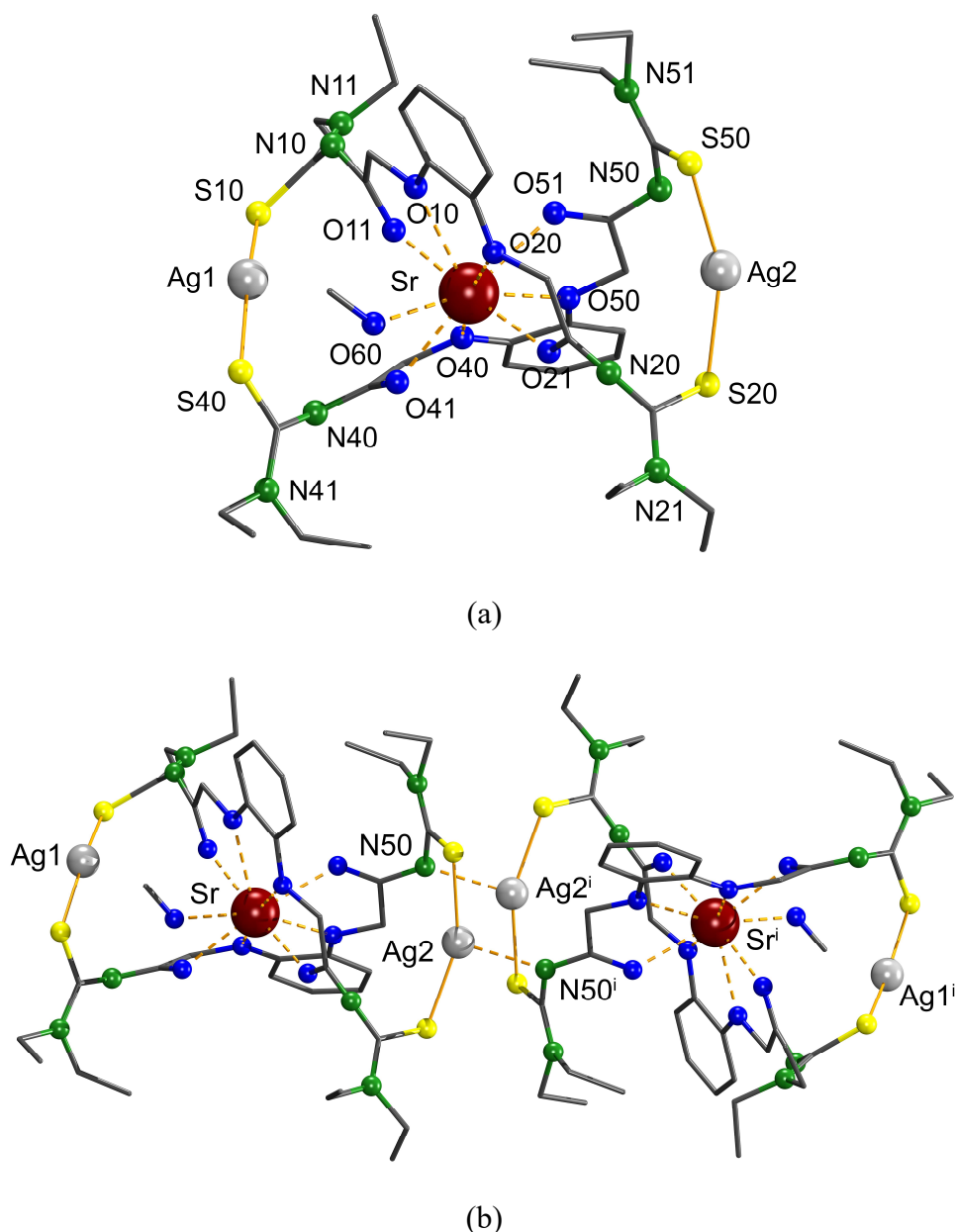
Figure 6.2 Molecular structure (a) of the {2}-metallacoronate $\{(MeOH)Sr \subset [Ag_2(L^3)_2]\}$ and (b) of the dimer $\{(MeOH)Sr \subset [Ag_2(L^3)_2]\}_2$. Hydrogen atoms are omitted for clarity.

Table 6.2 Selected bond lengths, distances (Å) and angles (°) in {(MeOH)Sr ⊂ [Ag$_2$(L^3)$_2$]}

Bond lengths and distances (Å)

Sr–O10	2.756(3)	Ag1–S10	2.420(4)	C11–O11	1.228(6)	C21–O21	1.250(5)
Sr–O11	2.462(4)	Ag1–S40	2.428(4)	C11–N10	1.285(7)	C21–N20	1.327(6)
Sr–O20	2.770(3)	Ag2–S20	2.445(1)	C12–N11	1.315(6)	C22–N21	1.332(6)
Sr–O21	2.499(4)	Ag2–S50	2.460(4)	C12–N10	1.368(6)	C22–N20	1.355(6)
Sr–O40	2.827(3)	Ag1···Sr	4.957(4)	C12–S10	1.709(6)	C22–S20	1.722(5)
Sr–O41	2.513(3)	Ag2···Sr	5.717(7)	C41–O41	1.266(6)	C51–O51	1.238(5)
Sr–O50	2.788(3)	Ag1···Ag2	10.647(8)	C41–N40	1.317(6)	C51–N50	1.316(6)
Sr–O60	2.682(3)	Ag2···N50^i	2.506(4)	C42–N41	1.335(7)	C52–N51	1.301(7)
Sr···O51	3.388(5)	Ag2···Ag2^i	3.169(7)	C42–N40	1.358(6)	C52–N50	1.385(5)
				C42–S40	1.714(5)	C52–S50	1.716(5)

Angles (°)

S10–Ag1–S40	162.40(5)	S20–Ag2–S50	156.04(5)

Symmetry operation used to generate equivalent atoms: ^{i} -x+1,-y+1,-z+1

(a)

(b)
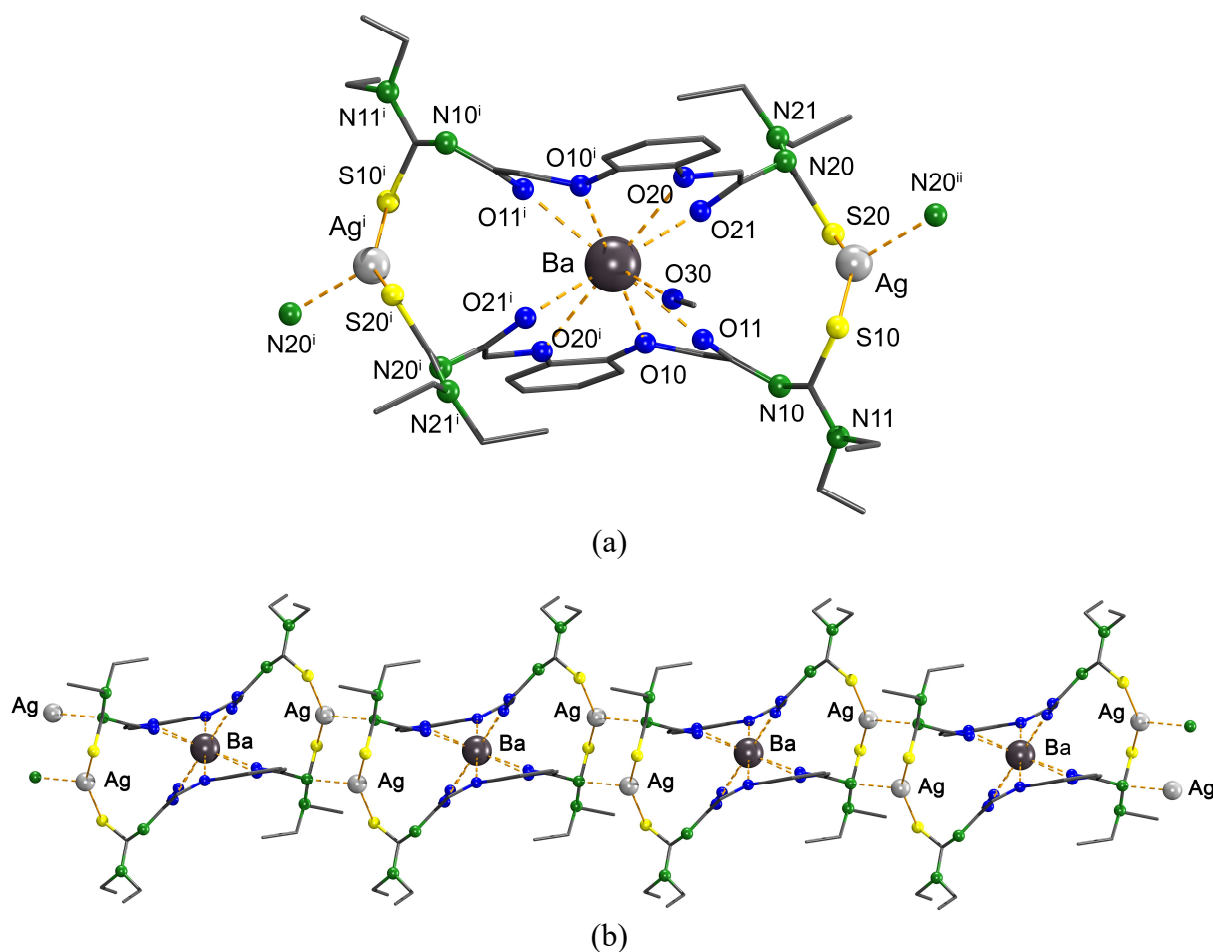
Figure 6.3 Molecular structure of (a) the {2}-metallacoronate {(MeOH) Ba ⊂ [Ag$_2$(L^3)$_2$]} and (b) the 1D polymeric chain {(MeOH) Ba ⊂ [Ag$_2$(L^3)$_2$]}$_\infty$. Hydrogen atoms are omitted for clarity.

Table 6.3 Selected bond lengths, distances (Å) and angle (º) in $\{(MeOH)Ba \subset [Ag_2(L^3)_2]\}$

Bond lengths and distances (Å)							
Ba–O10	2.854(5)	Ag–S10	2.439(7)	C11–O11	1.264(9)	C21–O21	1.250(8)
Ba–O11	2.738(6)	Ag–S20	2.450(2)	C11–N10	1.297(1)	C21–N20	1.319(9)
Ba–O20	2.916(5)	Ag···Ag	11.357(1)	C12–N11	1.399(14)	C22–N21	1.344(9)
Ba–O21	2.689(5)	Ag···Ba	5.678(5)	C12–N10	1.369(1)	C22–N20	1.369(9)
Ba–O30	2.896(1)	Ag···N20[i]	2.448(6)	C12–S10	1.679(8)	C22–S20	1.694(7)
Ag[i]···Ag[iii]	3.564(4)	Ag[iii]···N20	2.448(6)				

Angle (º)	
S10–Ag–S20[ii]	150.01(7)

Symmetry operations used to generate equivalent atoms: [i] x+1, y+1, z; [ii] -x, -y+1, -z+1 and [iii] x-1, y-1, z

A comparison of the structures of the three coordination assemblies gives further evidence for the flexibility of the ligand system. Specifically, the deprotonated ligand can exist in either twisted or untwisted conformation depending on the guest cation. The former is the result of a virtually perpendicular deviation of the C(S)–NEt$_2$ moieties in opposite directions from the mean plane of the ligand and brings about helical topologies for the inclusion complexes with Ca^{2+} and Sr^{2+}. A comparable deviation of the moieties in the same direction results in the formation of the latter structure without helicity, which serves as organic framework in the assembly with Ba^{2+}. Within the thiourea moieties, there is only a partial delocalization of π-electrons, which is reflected by the significant difference of C(O)–N$_{amide}$ and C(S)–N$_{amide}$ bond lengths, even though all C–S, C–O and C–N bond lengths lie between the values for corresponding single and double bonds.

Besides the X-ray diffraction analysis, the compounds were characterized by spectroscopic methods. The modest bathochromic shifts of approximately 80 cm^{-1} of the $\nu_{C=O}$ bands in the IR spectra strongly suggest a low degree of polarization of the carbonyl groups, which is consistent with the *S*-monodentate coordination mode of the ligand with Ag(I). The existence of the ligand in its deprotonated form is confirmed by the absence of the NH stretching vibration in the region above 3100 cm^{-1} in the IR spectra and the disappearance of NH resonances in the ^{1}H NMR spectra. Two separated sets of signals for the peripheral ethyl groups in the ^{1}H NMR as well as the ^{13}C NMR spectra show the typical hindered rotation around the C(S)–NEt$_2$ bonds, which is caused by their partial double bond character. While significant downfield shifts are observed for the C=S resonances (from 165.2 ppm in the uncoordinated ligand to the region of 176 – 190 ppm), the C=O resonances are shifted to higher field by about 10 ppm. The C=O and

C=S signals in the ^{13}C NMR spectra are assigned with regard to the covalent character of the Ag–S bonds as well as the ionic properties of the M–O bonds/interactions.

6.2 The mercury(II) metallacryptates

With the aim of constructing oligonuclear systems with Hg(II), reactions of three equivalents of the ligand H_2L^3 with mixtures of two equivalents of Hg(NO$_3$)$_2$ and one equivalent of an alkali earth metal salt M(NO$_3$)$_2$ (M = Ca^{2+}, Sr^{2+} or Ba^{2+}) were performed in MeOH. Addition of a supporting base like Et$_3$N facilitates deprotonation of the ligand and accelerates the formation and deposition of the products. The procedure only worked in the cases of Sr^{2+} and Ba^{2+}. All IR, ^{1}H NMR and ^{13}C NMR spectroscopic features of the resulting complexes are similar to the facts discussed for the previously discussed Ag(I) compounds and shall not be repeated in detail. Solid state structures reveal isostructural Hg(II) {2}-metallacryptates with the compositions of {M $\subset$ [Hg$_2$(L^3)$_3$]} as were also verified by elemental analyses. Figure 6.4a depicts the representative structure of the Sr^{2+}-containing assembly with a molecular C_2 axis through the Sr^{2+} cation. Selected bond lengths and distances in the Sr^{2+} and Ba^{2+} compounds are given in Table 6.4. The {2}-metallacryptates are formed by the encapsulation of the cationic guests in the molecular holes of the {2}-metallacryptand established by the linkage between two Hg(II) ions and three aroylthioureato ligands (L^3)$^{2-}$. The mercury atoms mainly coordinate to the ligands through the soft sulfur donors. Nonetheless, the Hg–S bond lengths are longer than those in previously reported Hg(II) complexes with aroylthioureas and, surprisingly, are also longer than the sum of covalent radii of Hg (1.32(5)Å) and S (1.05(3)Å).[74-76, 78] With regard to the expected covalent character of these bonds, this fact is entirely unexpected. Such an elongation of Hg–S bonds can be caused by the further weak interaction of mercury atoms with oxygen donors. Specifically, the distances Hg–O41 and Hg–O21 are shorter than the sum of Van der Waals radii (3.02Å) of the corresponding atoms.[80] Considering the bond lengths and distances surrounding the Hg(II) ions, an effective coordination number of five with distorted trigonal bipyramidal coordination geometry (Figure 4.6b) can be assumed. On the other hand, it is remarkable that the M–O$_{ether}$ separations are much longer than the M–O$_{carbonyl}$ ones. They are also longer than those observed in the inclusion complexes with M^{2+} ions based on Ni(II) (see Chapter 5.3) and Ag(I). These observations allow the conclusion that weak M$\cdots$O$_{ether}$ interactions play only a minor role in capturing guest cations, and the strong ionic M–O$_{carbonyl}$ bonds dominate for this effect. Hence, primarily six carbonyl oxygen atoms

coordinate to the guest cation, the coordination polyhedron of which is an octahedron with a high degree of distortion.
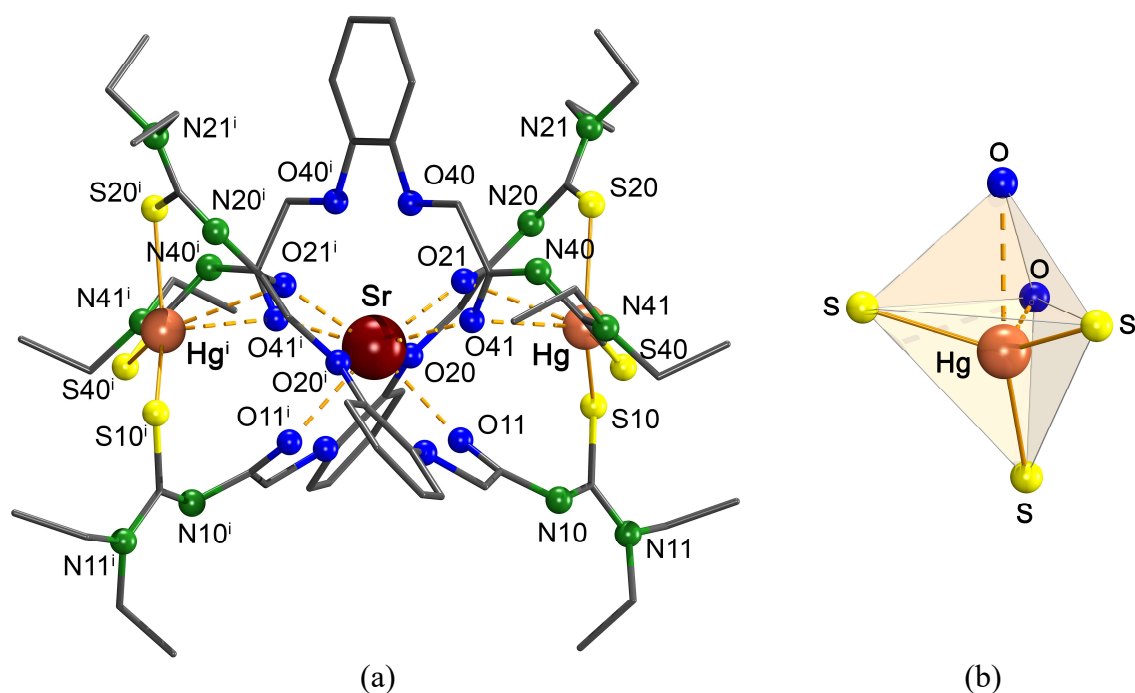
Figure 6.4 (a) Molecular structure of {Sr ⊂ [Hg₂(L³)₃]}. Hydrogen atoms are omitted for clarity. Symmetry operation used to generate equivalent atoms: ^{i} 1–x, y, 1/2–z. (b) Distorted trigonal bipyramidal coordination sphere surrounding Hg(II) ions.

Table 6.4 Selected bond lengths and distances (Å) in {M ⊂ [Hg₂(L³)₃]} (M = Sr²⁺ or Ba²⁺)

	M = Sr²⁺	M = Ba²⁺		M = Sr²⁺	M = Ba²⁺
Hg–S10	2.438(2)	2.427(5)	C11–O11	1.230(9)	1.231(4)
Hg–S20	2.447(2)	2.442(3)	C11–N10	1.349(1)	1.347(4)
Hg–S40	2.500(2)	2.495(1)	C12–N11	1.333(1)	1.331(4)
Hg⋯O41	2.783(6)	2.767(5)	C12–N10	1.334(1)	1.329(4)
Hg⋯O21	2.826(6)	2.882(1)	C12–S10	1.749(9)	1.757(3)
Hg⋯O11	3.359(9)	3.532(7)	C21–O21	1.242(1)	1.234(3)
Hg⋯Hg	8.395(6)	8.679(1)	C21–N20	1.344(1)	1.341(4)
Hg⋯M	4.213(8)	4.349(2)	C22–N21	1.326(1)	1.335(4)
M–O11	2.546(1)	2.697(3)	C22–N20	1.345(1)	1.340(4)
M–O21	2.503(7)	2.669(1)	C22–S20	1.757(9)	1.754(3)
M–O41	2.577(3)	2.717(1)	C41–O41	1.241(1)	1.233(4)
M⋯O20	3.147(8)	3.162(3)	C41–N40	1.339(1)	1.336(4)
M⋯O40	3.163(1)	3.155(4)	C42–N41	1.364(1)	1.345(4)
M⋯O10	3.202(1)	3.190(2)	C42–N40	1.343(1)	1.335(4)
			C42–S40	1.721(9)	1.742(3)

Another interesting structural feature is the high degree of electron delocalization within the aroylthioureato ligands, which is demonstrated by a partial double bond character of all C–S, C–O, and C–N bonds including endocyclic C–N bonds. This is remarkable since there are no chelate rings formed or the formed one shows a highly distorted conformation.

6.3 Summary and conclusion

Stoichiometric self-assembly of the ligand H_2L^3 with mixtures of alkali earth metal ions and thiophilic metal ions such as Ag(I) or Hg(II) produces coordination assemblies of rational compositions and structures. Due to the high thiophilicity of the transition metal ions, their coordination spheres are mainly created by sulfur atoms. The two-coordinate Ag(I) ions enable the formation of the {2}-metallacoronates {M $\subset$ [Ag$_2$(L^3)$_2$]} (M = Ca^{2+}, Sr^{2+} or Ba^{2+}). Aggregation of such assemblies particularly by intermolecular Ag$\cdots$N$_{amide}$ interactions results in dimeric or polymeric entities in the solid state. Discrete {2}-metallacryptate species {M $\subset$ [Hg$_2$(L^3)$_3$]} (M = Sr^{2+} or Ba^{2+}) evolve from metal ions with uncommon coordination numbers, namely five-coordinate Hg(II) ions and six-coordinate guest alkali earth metal ions.

Chapter 7
Experimental section

7.1. Starting materials

All chemicals and reagents were purchased from commercial sources (Acros Organics, Fluka, Sigma–Aldrich, Alfa Aesar, Cambridge Isotope Laboratories).

All solvents were used as received (pure for synthesis) unless otherwise stated.

7.2. Analytical methods

Elemental analyses of carbon, hydrogen, nitrogen and sulfur were determined using a *Heraeus vario EL* elemental analyzer.

IR spectra were measured from KBr pellets on a *Shimadzu – FTIR 8300* spectrometer.

The ^{1}H, ^{13}C, ^{15}N NMR spectra were recorded on a *JEOL 400MHz* spectrometer.

The EPR spectra were measured on a Magnettech *Miniscope* MS400 spectrometer with the rectangular resonator TE102. The diamagnetically diluted Cu(II)/Ni(II) systems of the ligand H_2L^3 were prepared by dissolving both components of the desired powder system in proportion 0.5 % Cu(II) complex and 99.5 % Ni(II) complex in CH_2Cl_2 and then evaporating the organic solvent at room temperature. The spectral simulations were performed with Bruker's WinEPR *SimFonia* Version 1.25 program.[81]

The Mößbauer spectra were recorded on a SeeCo MS6 spectrometer. The spectrometer comprises the following instruments: A Janis CCS-850 cryostat with vibration damping sample holder stand, including a CTI-Cryogenics closed cycle 10K refrigerator and a CTI-Cryogenics 8200 helium compressor. The cold head and sample mount are equipped with calibrated DT-670-Cu-1.4L silicon diode temperature probes and heaters. Temperature is controlled by a LakeShore 335 temperature controller in the range of 12 K – 300 K. Spectra are recorded using a LND-45431 Kr gas proportional counter with beryllium window connected to the SeeCo W204 gamma-ray spectrometer. The W204 includes high voltage supply, a 10 bit and 5 µs ADC and two single channel analyzers. Motor control and recording of spectra is taken care of by the W304 resonant gamma ray spectrometer. For the reported spectra a Rivertec MCo7.114 source (^{57}Co in Rh matrix) with an activity of about 1.4 GBq was used.

Cyclic voltammetry at a platinum electrode was performed in DMF solutions containing (n–Bu$_4$N)(PF$_6$) (0.15 M) and the complex (0.2 mM) at room temperature, under an atmosphere

of argon using a three/electrode setup with a *Gamry PCI4 – 300* potentiostat board and the *PHE200* software. Redox potentials were internally referenced against ferrocenium/ferrocence (Fc^+/Fc).

The ESI–TOF mass spectra were measured on an *Agilent 6210 ESI–TOF*, Agilent Technologies, Santa Clara, CA, USA. Solvent flow rate was adjusted to 4 µL/min. Spray voltage was set to 4 kV. Drying gas flow rate was set to 15 psi (1 bar). All other parameters were adjusted for a maximum abundance of the relative $[M+H]^+$ peaks.

7.3. Syntheses

7.3.1 Isophthaloylbis(*N,N*–diethylthiourea), H_2L^1

The ligand H_2L^1 was synthesized according to the method outlined by Douglas and Dains.[13, 67] Yield: 70%.

Elemental analysis

Calcd. for $C_{18}H_{26}N_4O_2S_2$: C, 54.80; H, 6.64; N, 14.20; S, 16.25%. Found: C, 55.64; H, 6.52; N, 14.28; S, 15.76%.
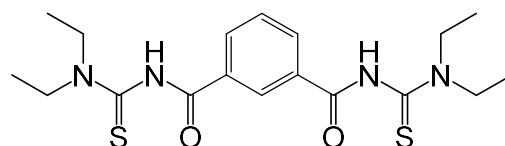
IR (KBr, cm^{-1}): 3119 (m), 2974 (m), 2938 (m), 2875 (m), 1690 (s), 1537 (s), 1447 (s), 1449 (s), 1431 (s), 1281 (m), 1215 (s), 1130 (s), 1101 (w), 1076 (m), 887 (w), 725 (m).

^{1}H NMR (400 MHz, $CDCl_3$, ppm): 9.03 (s, 2H, NH); 8.25 (s, 1H, Ph), 7.97 (d, J = 8.0 Hz, 2H, Ph), 7.53 (t, J = 8.0 Hz, 1H, Ph); 4.01 (q, J = 8.0 Hz, 4H, CH_2); 3.59 (q, J = 8.0 Hz, 4H, CH_2), 1.35 (t, J = 8.0 Hz, 6H, CH_3); 1.30 (t, J = 8.0 Hz, 6H, CH_3).

^{13}C{^{1}H} NMR ($CDCl_3$, ppm): 179.5 (C=O); 163.7 (C=S); 133.0, 132.8, 129.46, 126.8 (Ph); 47.9, 47.6 (CH_2); 13.4, 11.5 (CH_3).

ESI^+ MS (*m/z*): 811.2903 (calcd. 811.2892), 81% $[2M + Na]^+$; 433.1138 (calcd. 433.1134), 52% $[M + K]^+$; 417.1401 (calcd. 417.1395), 100% $[M + Na]^+$.

7.3.2 Binuclear iron(III) complex, [Fe₂(L¹)₃]

H_2L^1 (59.2 mg, 0.15 mmol) was added to a solution of $FeCl_3 \cdot 6H_2O$ (27.0 mg, 0.1 mmol) in 1 mL MeOH. The ligand dissolved quickly and a dark red precipitate deposited immediately from the solution after the addition of 2 drops of Et_3N. After stirring for 2 h at 50⁰C, the product was filtered off, washed with a small amount of MeOH and dried in vacuum. Single crystals

suitable for X–ray analysis were obtained by slow evaporation of a solution of the complex in DMF. Yield: 82% (53 mg).

Elemental analysis

Calcd. for $C_{54}H_{72}O_6N_{12}S_6Fe_2$: C, 50.30; H, 5.63; N, 13.04; S, 14.92%. Found: C, 50.15; H, 5.54; N, 13.09; S, 14.60%.

IR (KBr, cm^{-1}): 3429 (w), 2976 (w), 2932 (w), 2870 (w), 1504 (s), 1422 (vs), 1354 (m), 1256 (w), 1076 (w), 725 (w).

ESI$^+$ MS (*m/z*): 1327.23, 12% [M + K]$^+$; 1311.2590 (calcd. 1311.2619), 33% [M + Na]$^+$; 1289.2771 (calcd. 1289.2799), 30% [M + H]$^+$.
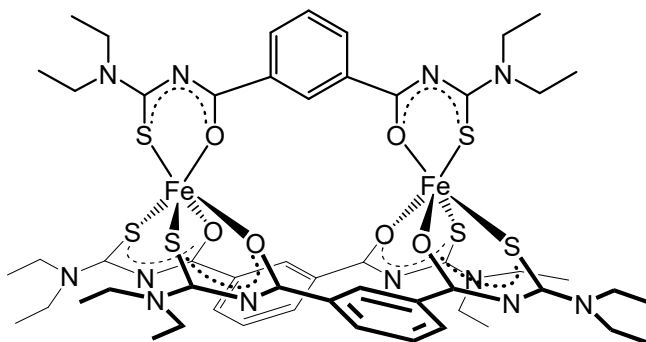
7.3.3 Dipicolinoylbis(*N,N*–diethylthiourea), H₂L²

N,N–Diethylthiourea (I)

The synthesis of the compound **I** was performed following the procedure reported by Yokoyama *et al.*[41] with some modifications. Ethyl chloroformate (9.5 mL, 0.1 mol) was added dropwise to a suspension of KSCN (9.70 g, 0.1 mol) in dry acetone (80 mL). The mixture was heated on reflux under Ar atmosphere for 2 h. Diethyl amine (12.5 mL, 0.12 mol) in dry acetone (80 mL) was added dropwise to the reaction mixture before it had been cooled to 5^{0}C. After being stirred at room temperature overnight, the mixture was treated with 6M HCl (200 mL) and then extracted with ethyl acetate. After evaporation of the extract, *N'*–ethoxycarbonyl *N,N*–diethylthiourea was obtained as a yellow oil. A mixture of this intermediate (0.1 mol) and conc. HCl (30 mL) was heated on reflux for 3 days. The obtained solution was kept in an ice bath and was neutralized with $(NH_4)_2CO_3$ and then extracted with ethyl acetate. Evaporation of the extract gave an analytically pure product, which deposited as a colorless crystalline solid. It was collected by filtration and washed with diethyl ether. Yield: 50% (6.60 g).

Elemental analysis

Calcd. for $C_5H_{12}N_2S$: C, 45.42; H, 9.15; N, 21.19; S, 24.25%. Found: C, 45.33; H, 8.90; N, 21.52; S, 24.15%.

IR (KBr, cm^{-1}): 3375 (m), 3296 (m), 3190 (s), 3101 (w), 2974 (m), 2934 (w), 2895 (w), 1628 (s), 1518 (s), 1435 (m), 1360 (s), 1207 (w), 1074 (m), 843 (m), 667 (w), 527 (m).
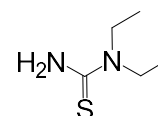
^{1}H NMR (400 MHz, CDCl$_3$, ppm): 5.62 (br, 2H, NH$_2$); 3.63 (br, 4H, CH$_2$), 1.24 (t, J = 8.0 Hz, 6H, CH$_3$).

^{13}C{^{1}H} NMR (CDCl$_3$, ppm): 180.6 (C=S); 45.9 (CH$_2$); 12.6 (CH$_3$).

Dipicolinoylbis(*N*,*N*–diethylthiourea), H$_2$L^2

A mixture of previously dried dipicolinic acid (3.34 g, 0.02 mol), SOCl$_2$ (30 mL, 0.4 mol) and a few drops of DMF was heated on reflux under Ar atmosphere until a clear solution was obtained. Subsequently, the reaction mixture was stirred for 2 more hours and the residual SOCl$_2$ was removed under reduced pressure. This gives a colorless solid of dipicolinoyl chloride. This solid was dissolved in dry THF (60 mL) and added dropwise at 0°C (ice bath) to a mixture of **I** (5.28 g, 0.04 mol) and Et$_3$N (8.5 mL, 0.06 mol) in dry THF (30 ml) under an atmosphere of dry Ar. The resulting mixture was warmed up to 40 – 50^{0}C and stirred for 2 h. After cooling to room temperature, the formed colorless precipitate of (Et$_3$NH)Cl was filtered off and the THF was removed under reduced pressure. The resulting solid was washed thoroughly with MeOH, which finally gave the ligand H$_2$L^2 as a colorless solid. Yield: 92% (7.27 g).

Elemental analysis

Calcd. for C$_{17}$H$_{25}$N$_5$O$_2$S$_2$: C, 51.62; H, 6.37; N, 17.71; S, 16.21%. Found: C, 51.70; H, 6.29; N, 17.79; S, 15.81%.
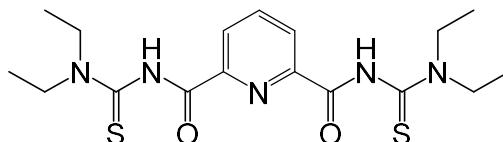
IR (KBr, cm^{-1}): 3267 (m), 2974 (w), 2934 (w), 2874 (w), 1674 (s), 1520 (s), 1447 (s), 1418 (s), 1277 (m), 1225 (s), 1101 (w), 997 (w), 752 (m).

^{1}H NMR (400 MHz, CDCl$_3$, ppm): 9.40 (s, 2H, NH); 8.42 (d, J = 8.0 Hz, 2H, *m*–Py), 8.11 (dd, J = 8.0 Hz, 1H, *p*–Py), 4.04 (q, J = 6.4 Hz, 4H, CH$_2$); 3.68 (q, J = 6.4 Hz, 4H, CH$_2$); 1.34 (t, J = 6.4 Hz, 6H, CH$_3$); 1.31 (t, J = 6.8 Hz, 6H, CH$_3$).

^{13}C{^{1}H} NMR (CDCl$_3$, ppm): 177.3 (C=O); 159.3 (C=S); 148.0, 139.8, 126.9 (Py); 47.8, (CH$_2$); 13.6, 11.5 (CH$_3$).

ESI$^+$ MS (*m/z*): 813.2796 (calcd. 813.2797), 85% [2M + Na]$^+$; 434.11, 10% [M + K]$^+$; 418.1349 (calcd. 418.1347), 100% [M + Na]$^+$.

7.3.4 Mononuclear iron(III) complex, Tl[Fe(L^2)$_2$]

H$_2$L^2 (79.0 mg, 0.2 mmol) was added to a solution of Fe(NO$_3$)$_3$ · 9 H$_2$O (40.4 mg, 0.1 mmol) in 1.5 mL MeOH. The color of the solution changed immediately to dark red. After stirring for

30 min at room temperature, 2 drops of Et$_3$N and then TlNO$_3$ (26.6 mg, 0.1 mmol) dissolved in H$_2$O (0.5 mL) were added to the reaction mixture. The temperature was increased to 50^{0}C and kept for 2 h. Slow evaporation of the solvent at room temperature resulted in precipitation of dark-red crystals, which were suitable for X–ray analysis. The product was filtered off, washed with cold MeOH and dried in vacuum. Yield: 62% (65 mg).
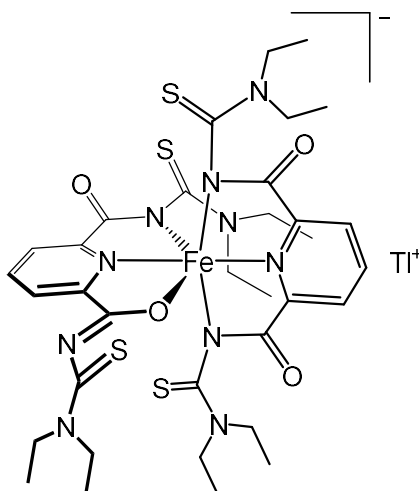
Elemental analysis

Calcd. for Tl[Fe(L^2)$_2$] · H$_2$O, C$_{34}$H$_{48}$O$_5$N$_{10}$S$_4$FeTl: C, 38.33; H, 4.54; N, 13.15; S, 12.04%. Found: C, 38.12; H, 4.42; N, 12.93; S, 11.80%.

IR (KBr, cm^{-1}): 3422 (w), 2972 (w), 2932 (w), 2872 (w), 1601 (vs), 1499 (m), 1427 (m), 1360 (s), 1250 (m), 1099 (w), 957 (w), 756 (w).

ESI$^-$ MS (*m/z*): 842.1966 (calcd. 842.1936), 6% [Fe(L^2)$_2$]$^-$, 416.1231 (calcd. 416.1191), 25% [Na(L^2)]$^-$.

7.3.5 Iron(III) {2}–metallacryptates, {M ⊂ [Fe$_2$(L^2)$_3$]}(PF$_6$) (M = Rb$^+$, K$^+$, Na$^+$, Tl$^+$, NH$_4$$^+$)

H$_2$L^2 (59.3 mg, 0.15 mmol) was added to a solution of FeCl$_3$ · 6 H$_2$O (27.0 mg, 0.1 mmol) and 0.05 mmol MCl (M = Rb$^+$, K$^+$, Na$^+$ and NH$_4$$^+$) in 1 mL MeOH and a few drops of H$_2$O. Due to the low solubility of TlCl in H$_2$O and MeOH in case of Tl$^+$, the nitrate salts, Fe(NO$_3$)$_3$ · 9 H$_2$O and TlNO$_3$, were used. The ligand dissolved rapidly and the color of the solution changed immediately to dark. The mixture was stirred for 30 min at room temperature and 3 drops of Et$_3$N were added. After stirring for additional 30 min, (*n*–Bu$_4$N)(PF$_6$) (19.4 mg, 0.05 mmol) was added, the temperature was increased to 50^{0}C and kept for 2 h. During this time, a dark precipitate deposited. The product was filtered off, washed with a small amount of MeOH and

dried in vacuum. Single crystals suitable for X–ray analysis were obtained by slow evaporation of solutions of the complexes in CH_2Cl_2/MeOH mixtures.

$$M = Rb^+, K^+, Na^+, Tl^+, NH_4^+$$

{Rb ⊂ [Fe₂(L²)₃]}(PF₆)
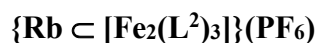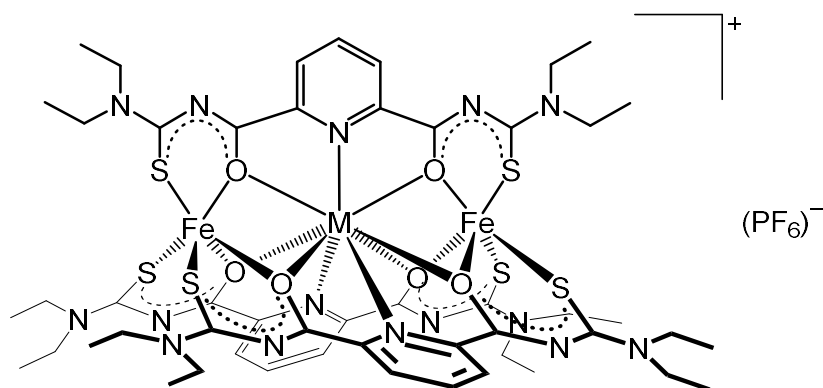
Yield: 67% (49 mg).

Elemental analysis

Calcd. for $C_{51}H_{69}O_6N_{15}S_6PF_6Fe_2Rb$: C, 40.23; H, 4.57; N, 13.80; S, 12.63%. Found: C, 40.54; H, 4.62; N, 13.37; S, 12.87%.

IR (KBr, cm^{-1}): 3427 (w), 2976 (w), 2934 (w), 1510 (s), 1433 (s), 1412 (s), 1356 (m), 1252 (m), 1150 (w), 839 (s), 746 (w), 557 (w).

ESI⁺ MS (*m/z*): 1376.1625 (calcd. 1376.1696), 39% {Rb ⊂ [Fe₂(L²)₃]}⁺; 1330.2156 (calcd. 1330.2215), 100% {K ⊂ [Fe₂(L²)₃]}⁺.

{K ⊂ [Fe₂(L²)₃]}(PF₆)
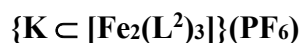
Yield: 75% (65 mg).

Elemental analysis

Calcd. for $C_{51}H_{69}O_6N_{15}S_6PF_6Fe_2K$: C, 41.49; H, 4.71; N, 14.23; S, 13.03%. Found: C, 41.52; H, 4.65; N, 14.25; S, 13.18 %.

IR (KBr, cm^{-1}): 3441 (w), 2974 (w), 2934 (w), 1506 (s), 1435 (s), 1355 (m), 1254 (m), 1196 (w), 1076 (w), 841 (m).

ESI⁺ MS (*m/z*): 1330.2180 (calcd. 1330.2215), 100% {K ⊂ [Fe₂(L²)₃]}⁺.

{Na ⊂ [Fe₂(L²)₃]}(PF₆)
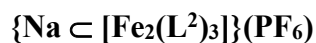
Yield: 90% (67 mg).

Elemental analysis

Calcd. for $C_{51}H_{69}O_6N_{15}S_6PF_6Fe_2Na$: C, 41.95; H, 4.76; N, 14.39; S, 13.18%. Found: C, 41.58; H, 4.46; N, 14.05; S, 13.64 %.

IR (KBr, cm^{-1}): 2974 (w), 2936 (w), 1541 (m), 1506 (s), 1437 (s), 1417 (s), 1355 (m), 1256 (m), 1152 (w), 1076 (w), 839 (m).

ESI$^+$ MS (m/z): 1330.2172 (calcd. 1330.2215), 100% {K $\subset$ [Fe$_2$(L^2)$_3$]}$^+$.; 1314.24, 13% {Na $\subset$ [Fe$_2$(L^2)$_3$]}$^+$.

{Tl $\subset$ [Fe$_2$(L^2)$_3$]}(PF$_6$)

Yield: 56% (46 mg).

Elemental analysis

Calcd. for {Tl $\subset$ [Fe$_2$(L^2)$_3$]}(PF$_6$) $\cdot$ 3H$_2$O, $C_{51}H_{75}O_9N_{15}S_6PF_6Fe_2Tl$: C, 36.13; H, 4.46; N, 12.39; S, 11.34%. Found: C, 35.88; H, 4.10; N, 12.12; S, 10.87%.

IR (KBr, cm^{-1}): 3431 (w), 2976 (w), 2935 (w), 2872 (w), 1508 (s), 1431 (s), 1410 (s), 1356 (m), 1252 (m), 1150 (w), 839 (s), 746 (w), 557 (w).

ESI$^+$ MS (m/z): 1330.2259 (calcd. 1330.2215), 100% {K $\subset$ [Fe$_2$(L^2)$_3$]}$^+$.

{NH$_4$ $\subset$ [Fe$_2$(L^2)$_3$]}(PF$_6$)

Yield: 60% (44 mg).

Elemental analysis

Calcd. for $C_{51}H_{73}O_6N_{16}S_6PF_6Fe_2$: C, 42.09; H, 5.06; N, 15.40; S, 13.22%. Found: C, 42.27; H, 5.45; N, 15.46; S, 13.11 %.

IR (KBr, cm^{-1}): 3244 (w), 2966 (w), 2934 (w), 1508 (s), 1431 (s), 1416 (s), 1354 (m), 1261 (m), 1149 (w), 1093 (m), 841 (s).

ESI$^+$ MS (m/z): 1330.2317 (calcd. 1330.2215), 100% {K $\subset$ [Fe$_2$(L^2)$_3$]}$^+$.

7.3.6 Indium(III) {2}–metallacryptates, {M $\subset$ [In$_2$(L^2)$_3$]}(PF$_6$) (M = Rb$^+$, K$^+$, Na$^+$, NH$_4^+$)

The complexes were synthesized following the procedure outlined for the Fe(III) complexes, except that InCl$_3$ was used instead of FeCl$_3$ $\cdot$ 6 H$_2$O. The isotope–labeled compound {^{15}NH$_4$ $\subset$ [In$_2$(L^2)$_3$]}(PF$_6$) was prepared using ^{15}NH$_4$Cl. After the addition of H$_2$L^2 to the solutions of the salts in MeOH, the ligand dissolved completely within 5 min and the color of the solutions changed gradually to slightly yellow. The products deposited as colorless precipitates, which were filtered off, washed with MeOH and dried in vacuum. Single crystals

suitable for X–ray analyses were obtained by slow evaporation of CH_2Cl_2/MeOH/toluene solutions of the complexes.

M = Rb⁺, K⁺, Na⁺, NH₄⁺
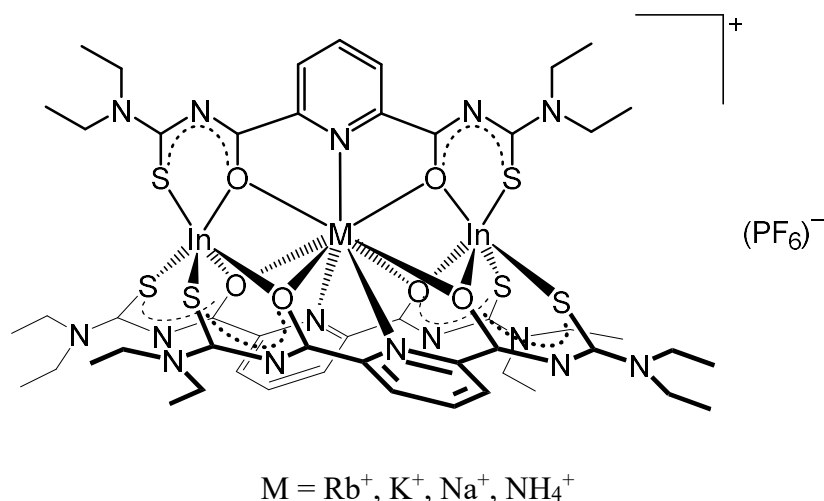
{Rb ⊂ [In₂(L²)₃]}(PF₆)

Yield: 83% (68 mg).

Elemental analysis

Calcd. for {Rb ⊂ [In₂(L²)₃]}(PF₆) · 2 MeOH, $C_{53}H_{77}O_8N_{15}S_6PF_6In_2Rb$: C, 37.34; H, 4.55; N, 12.32; S, 11.29%. Found: C, 37.25; H, 4.46; N, 12.14; S, 11.16 %.

IR (KBr, cm^{-1}): 3460 (w), 2980 (w), 2936 (w), 1553 (s), 1516 (vs), 1435 (vs), 1416 (vs), 1356 (m), 1254 (m), 1076 (m), 841 (s), 741 (w), 745 (m).

¹H NMR (400 MHz, $CDCl_3$, ppm): 8.30 (d, J = 7.6 Hz, 6H, *m*–Py); 7.82 (t, J = 7.6 Hz, 3H, *p*–Py); 4.03 (q, J = 7.2 Hz, 12H, CH_2); 3.88 (q, J = 7.2 Hz, 12H, CH_2); 1.41 (t, J = 7.2 Hz, 18H, CH_3); 1.28 (t, J = 7.2 Hz, 18H, CH_3).

¹³C{¹H} NMR ($CDCl_3$, ppm): 176.4 (C=O); 168.5 (C=S); 154.6, 137.3, 127.0 (Py); 47.1, 46.6 (CH_2); 13.4, 13.1 (CH_3).

ESI⁺ MS (*m/z*): 1494.1027 (calcd. 1494.1075), 100% {Rb ⊂ [In₂(L²)₃]}⁺; 1448.1547 (calcd. 1448.1594), 80% {K ⊂ [In₂(L²)₃]}⁺; 1432.18, 12% {Na ⊂ [In₂(L²)₃]}⁺.

{K ⊂ [In₂(L²)₃]}(PF₆)

Yield: 75% (60 mg).

Elemental analysis

Calcd. for {K ⊂ [In₂(L²)₃]}(PF₆) · 2 MeOH $C_{53}H_{77}O_8N_{15}S_6PF_6In_2K$: C, 38.39; H, 4.68; N, 12.67; S, 11.60%. Found: C, 38.23; H, 4.51; N, 12.39; S, 11.36 %.

IR (KBr, cm^{-1}): 3445 (w), 2978 (w), 2936 (w), 1557 (s), 1516 (vs), 1435 (vs), 1418 (vs), 1356 (m), 1254 (m), 1076 (m), 841 (s), 745 (m).

^{1}H NMR (400 MHz, CDCl$_3$, ppm): 8.31 (d, J = 7.6 Hz, 6H, *m*–Py); 7.82 (t, J = 7.6 Hz, 3H, *p*–Py); 4.02 (q, J = 7.2 Hz, 12H, CH$_2$); 3.87 (q, J = 7.2 Hz, 12H, CH$_2$); 1.43 (t, J = 7.2 Hz, 18H, CH$_3$); 1.28 (t, J = 7.2 Hz, 18H, CH$_3$).

^{13}C{^{1}H} NMR (CDCl$_3$, ppm): 176.1 (C=O); 168.2 (C=S); 154.2, 137.4, 126.9 (Py); 47.2, 46.6 (CH$_2$); 13.4, 13.2 (CH$_3$).

ESI$^+$ MS (*m/z*): 1448.1555 (calcd. 1448.1594), 100% {K $\subset$ [In$_2$(L^2)$_3$]}$^+$.

{Na $\subset$ [In$_2$(L^2)$_3$]}(PF$_6$)

Yield: 62% (49 mg).

Elemental analysis

Calcd. for C$_{51}$H$_{69}$O$_6$N$_{15}$S$_6$PF$_6$In$_2$Na: C, 38.81; H, 4.41; N, 13.31; S, 12.19 %. Found: C, 38.20; H, 4.89; N, 12.96; S, 12.78 %.

IR (KBr, cm^{-1}): 3445 (w), 2978 (w), 2936 (w), 1558 (s), 1520 (vs), 1435 (vs), 1418 (vs), 1356 (m), 1256 (m), 1078 (m), 841 (s), 745 (m).

^{1}H NMR (400 MHz, CDCl$_3$, ppm): 8.33 (d, J = 8.0 Hz, 6H, *m*–Py); 7.83 (t, J = 8.0 Hz, 3H, *p*–Py); 4.01 (q, J = 7.2 Hz, 12H, CH$_2$); 3.87 (q, J = 7.2 Hz, 12H, CH$_2$); 1.41 (t, J = 7.2 Hz, 18H, CH$_3$); 1.28 (t, J = 7.2 Hz, 18H, CH$_3$).

^{13}C{^{1}H} NMR (CDCl$_3$, ppm): 175.7 (C=O); 167.9 (C=S); 153.7, 137.5, 126.8 (Py); 47.1, 46.5 (CH$_2$); 13.4, 13.2 (CH$_3$).

ESI$^+$ MS (*m/z*): 1448.1564 (calcd. 1448.1594), 100% {K $\subset$ [In$_2$(L^2)$_3$]}$^+$.

{^{14}NH$_4$/^{15}NH$_4$ $\subset$ [In$_2$(L^2)$_3$]}(PF$_6$)

Yield: 89% (70 mg).

Elemental analysis

Calcd. for {NH$_4$ $\subset$ [In$_2$(L^2)$_3$]}(PF$_6$) · 2 MeOH, C$_{53}$H$_{81}$O$_8$N$_{16}$S$_6$PF$_6$In$_2$: C, 38.88; H, 4.99; N, 13.69; S, 11.75%. Found: C, 39.03; H, 4.92; N, 13.41; S, 11.64%.

IR (KBr, cm^{-1}): 3429 (w), 3224 (w), 2976 (w), 2934 (w), 1520 (s), 1422 (vs), 1356 (m), 1254 (m), 1078 (w), 843, 744 (w), 557 (w).

^{1}H NMR (400 MHz, CDCl$_3$, ppm):

{^{14}NH$_4$ $\subset$ [In$_2$(L^2)$_3$]}(PF$_6$) 9.72 (t, ^{1}J(^{14}N–^{1}H) = 52.2 Hz, 4H, ^{14}NH$_4$); 8.31 (d, J = 8.0 Hz, 6H, *m*–Py); 7.84 (t, J = 8.0 Hz, 3H, *p*–Py); 4.03 (q, J = 7.2 Hz, 12H, CH$_2$); 3.87 (q, J = 7.2 Hz, 12H, CH$_2$); 1.41 (t, J = 7.2 Hz, 18H, CH$_3$); 1.27 (t, J = 7.2 Hz, 18H, CH$_3$).

{^{15}NH$_4$ ⊂ [In$_2$(L^2)$_3$]}(PF$_6$) 9.72 (d, ^{1}J(^{15}N–^{1}H) = 72.8 Hz, 4H, ^{15}NH$_4$); 8.31 (d, J = 8.0 Hz, 6H, *m*–Py); 7.84 (t, J = 8.0 Hz, 3H, *p*–Py); 4.03 (q, J = 7.2 Hz, 12H, CH$_2$); 3.87 (q, J = 7.2 Hz, 12H, CH$_2$); 1.41 (t, J = 7.2 Hz, 18H, CH$_3$); 1.27 (t, J = 7.2 Hz, 18H, CH$_3$).

^{13}C{^{1}H} NMR (CDCl$_3$, ppm): 176.6 (C=O); 168.0 (C=S); 154.3, 137.6, 127.1 (Py); 47.2, 46.7 (CH$_2$); 13.4, 13.1 (CH$_3$).

^{15}N{^{1}H} NMR (CDCl$_3$, ppm, standard MeNO$_2$): **{^{15}NH$_4$ ⊂ [In$_2$(L^2)$_3$]}(PF$_6$)** -345.6.

^{15}N DEPT NMR (CDCl$_3$, ppm, standard MeNO$_2$): **{^{15}NH$_4$ ⊂ [In$_2$(L^2)$_3$]}(PF$_6$)** -345.6 (quintet, ^{1}J(^{15}N–^{1}H) = 73.0 Hz).

^{1}H NMR (400 MHz, DMSO-*d$_6$*, ppm):

{^{14}NH$_4$ ⊂ [In$_2$(L^2)$_3$]}(PF$_6$) 9.56 (t, ^{1}J(^{14}N–^{1}H) = 50.8 Hz, 4H, ^{14}NH$_4$); 8.41 (d, J = 8.0 Hz, 6H, *m*–Py); 8.11 (t, J = 8.0 Hz, 3H, *p*–Py); 3.97 (q, J = 6.8 Hz, 12H, CH$_2$); 3.88 (q, J = 6.8 Hz, 12H, CH$_2$); 1.32 (t, J = 6.8 Hz, 18H, CH$_3$); 1.15 (t, J = 6.8 Hz, 18H, CH$_3$).

{^{15}NH$_4$ ⊂ [In$_2$(L^2)$_3$]}(PF$_6$) 9.56 (d, ^{1}J(^{15}N–^{1}H) = 72.8 Hz, 4H, ^{15}NH$_4$); 8.41 (d, J = 8.0 Hz, 6H, *m*–Py); 8.10 (t, J = 8.0 Hz, 3H, *p*–Py); 3.97 (q, J = 6.8 Hz, 12H, CH$_2$); 3.87 (q, J = 6.8 Hz, 12H, CH$_2$); 1.32 (t, J = 6.8 Hz, 18H, CH$_3$); 1.14 (t, J = 6.8 Hz, 18H, CH$_3$). **NH$_4$Cl** 7.45 (s, br).

^{13}C{^{1}H} NMR (DMSO-*d$_6$*, ppm): 175.7 (C=O); 167.0 (C=S); 153.7, 139.8, 128.1 (Py); 47.4, 46.9 (CH$_2$); 13.7, 13.2 (CH$_3$).

^{15}N{^{1}H} NMR (DMSO-*d$_6$*, ppm, standard MeNO$_2$): **{^{15}NH$_4$ ⊂ [In$_2$(L^2)$_3$]}(PF$_6$)** -345.6, -357.6. **^{15}NH$_4$Cl** -351.6 (br).

^{15}N DEPT NMR (DMSO-*d$_6$*, ppm, standard MeNO$_2$): **{^{15}NH$_4$ ⊂ [In$_2$(L^2)$_3$]}(PF$_6$)** -345.6 (quintet, ^{1}J(^{15}N–^{1}H) = 72.8 Hz). **^{15}NH$_4$Cl** no signal.

ESI$^+$ MS (*m/z*): 1448.1553 (calcd. 1448.1594), 100% {K ⊂ [In$_2$(L^2)$_3$]}$^+$; 1427.22, 3% {NH$_4$ ⊂ [In$_2$(L^2)$_3$]}$^+$.

7.3.7 2,2'–[1,2–Phenylenebis(oxy)]diacetoylbis(*N,N*–diethylthiourea), H$_2$L^3

2,2'–[1,2–Phenylenebis(oxy)]diacetic acid (II)

The preparation of the compound **II** was adopted from the literature.[42] A solution of NaOH (40.0 g) in 90 mL H$_2$O was added dropwise to a mixture of catechol (11.0 g, 0.1 mol) and chloroacetic acid (28.4 g, 0.3 mol). The mixture was stirred at 90°C in an oil bath for 2 h and after cooling to room temperature, the solution was kept in an ice bath. Then, concentrated HCl was dropped into the solution with stirring until the pH value of 2. The solution was filtered and the tan precipitate was thoroughly washed with cold water. Recrystallization of the obtained solid from hot water afforded **II** as a colorless microcrystalline solid. Yield: 90% (20.3 g).

Elemental analysis

Calcd. for $2C_{10}H_{10}O_6 \cdot H_2O$: C, 51.07; H, 4.71%. Found: C, 51.27; H, 4.44%.

IR (KBr, cm^{-1}): 3462 (br, w), 2914 (br, m), 2687 (w), 2646 (w), 2534 (w), 1742 (m), 1670 (s), 1508 (s), 1427 (m), 1251 (s), 1205 (s), 1132 (m), 1057 (m), 918 (w), 752 (m), 662 (w).

^{1}H NMR (400 MHz, DMSO–d_6, ppm): 6.84 (br, 4H, Ph); 4.56 (s, 4H, OCH$_2$).

^{13}C{^{1}H} NMR (DMSO–d_6, ppm): 171.0 (C=O); 147.9, 121.9, 114.5 (Ph); 65.8 (CH$_2$).
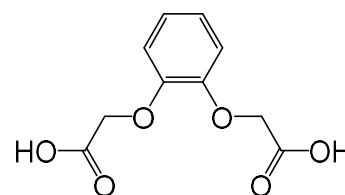
2,2'–[1,2–Phenylenebis(oxy)]diacetoylbis(*N,N*–diethylthiourea), H$_2$L^3

The ligand H$_2$L^3 was prepared by a similar procedure as described for H$_2$L^2. A mixture of dry dicarboxylic acid **II** (4.52 g, 0.02 mol) and an excess of SOCl$_2$ (30 mL, 0.4 mol) was heated to reflux under an Ar atmosphere for 3 h until a clear solution was obtained. The resulting reaction mixture was stirred for 2 more hours and the residual SOCl$_2$ was removed under reduced pressure. The remaining solid was dissolved in dry THF (60 mL) and added at 0°C (ice bath) dropwise under an Ar atmosphere to a mixture of **I** (5.28 g, 0.04 mol) and Et$_3$N (12.8 mL, 0.04 mol) in dry THF (30 ml). After warming to 40 – 50°C and stirring for 2 h, the mixture was cooled to room temperature. A colorless precipitate of (Et$_3$NH)Cl was filtered off and THF was removed under reduced pressure. The resulting solid was washed thoroughly with MeOH to give the ligand H$_2$L^3 as a colorless solid. Yield: 70% (6.36 g).

Elemental analysis

Calcd. for $C_{20}H_{30}N_4O_4S_2$: C, 52.84; H, 6.65; N, 12.32; S, 14.11%. Found: C, 52.20; H, 6.07; N, 11.93; S, 13.77%.

IR (KBr, cm^{-1}): 3163 (m), 2986 (w), 2932 (w), 1659 (s), 1531 (s), 1454 (m), 1427 (m), 1277 (w), 1234 (m), 1200 (s), 1138 (m), 1060 (w), 960 (w), 756 (m).

^{1}H NMR (400 MHz, CDCl$_3$, ppm): 8.92 (s, 2H, NH); 7.06 – 7.01 (m, 2H, Ph); 6.98 – 6.93 (m, 2H, Ph); 4.66 (s, 4H, OCH$_2$); 3.95 (q, J = 6.4 Hz, 4H, NCH$_2$); 3.55 (q, J = 6.4 Hz, 4H, NCH$_2$); 1.31 (t, J = 6.4 Hz, 6H, CH$_3$), 1.23 (t, J = 6.4 Hz, 6H, CH$_3$).

^{13}C{^{1}H} NMR (CDCl$_3$, ppm): 177.8 (C=O); 165.1 (C=S); 147.5, 123.7, 115.5 (Ph); 69.4 (OCH$_2$); 48.0, 47.8 (NCH$_2$); 13.4, 11.5 (CH$_3$).
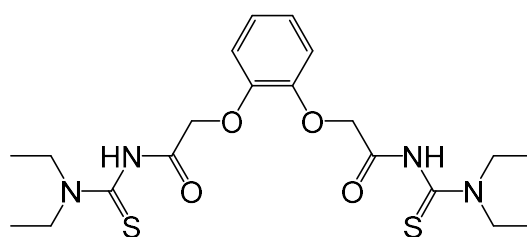
^{1}H NMR (400 MHz, CD$_2$Cl$_2$, ppm): 8.85 (s, 2H, NH); 7.04 – 7.01 (m, 2H, Ph); 6.99 – 6.96 (m, 2H, Ph); 5.30 (s, 4H, OCH$_2$); 3.91 (q, J = 6.8 Hz, 4H, NCH$_2$); 3.50 (q, J = 6.8 Hz, 4H, NCH$_2$); 1.26 (t, J = 6.4 Hz, 6H, CH$_3$), 1.19 (t, J = 6.4 Hz, 6H, CH$_3$).

^{13}C{^{1}H} NMR (CD$_2$Cl$_2$, ppm): 178.0 (C=O); 165.2 (C=S); 147.6, 123.4, 115.5 (Ph); 69.5 (OCH$_2$); 47.8, 47,6 (NCH$_2$); 13.1, 11.1 (CH$_3$).

ESI$^+$ MS (*m/z*): 931.3332 (calcd. 931.3315), 85% [2M + Na]$^+$; 493.13, 10% [M + K]$^+$; 477.1617 (calcd. 477.1606), 100% [M + Na]$^+$; 455.18, 5% [M + H]$^+$.

7.3.8 Iron(III) {2}−metallacryptates, {M ⊂ [Fe$_2$(L^3)$_3$]}(PF$_6$) (M = Cs$^+$, Rb$^+$, K$^+$, Tl$^+$, NH$_4$$^+$)

H$_2$L^3 (68.2 mg, 0.15 mmol) was added to solutions of FeCl$_3$ · 6 H$_2$O (27.0 mg, 0.1 mmol) and 0.05 mmol MCl (M = Cs$^+$, Rb$^+$, K$^+$, and NH$_4$$^+$) in 1 mL MeOH and a few drops of water. In case of the Tl$^+$ complex, Fe(NO$_3$)$_3$ · 9 H$_2$O and TlNO$_3$ were used as starting materials. The ligand dissolved quickly and the color of the solutions changed immediately to dark red. The mixtures were stirred at room temperature for 30 min and 3 drops of Et$_3$N were added. After stirring at room temperature for more 30 min, (*n*–Bu$_4$N)(PF$_6$) (19.4 mg, 0.05 mmol) was added and the temperature was increased to 50^{0}C and kept for 2 h. During this process, dark red precipitates deposited. The products were filtered off, washed with a small amount of MeOH and dried in vacuum. Single crystals suitable for X–ray analysis were obtained by slow evaporation of solutions of the complexes in CH$_2$Cl$_2$/MeOH mixtures.
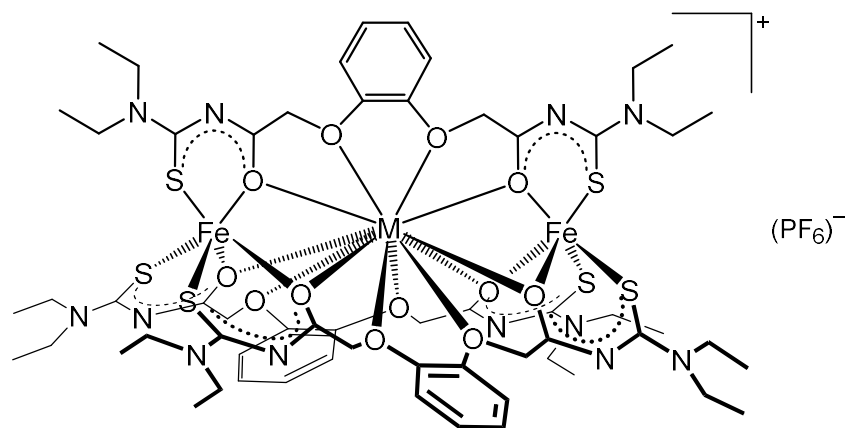
M = Cs$^+$, Rb$^+$, K$^+$, Tl$^+$, NH$_4$$^+$

{Cs ⊂ [Fe$_2$(L^3)$_3$]}(PF$_6$)
Yield: 85% (74 mg).

Elemental analysis

Calcd. for $C_{60}H_{84}O_{12}N_{12}S_6PF_6Fe_2Cs$: C, 41.24; H, 4.85; N, 9.62; S, 11.01%. Found: C, 40.94; H, 4.62; N, 9.37; S, 10.87%.

IR (KBr, cm^{-1}): 3427 (w), 2980 (w), 2936 (w), 1560 (m), 1533 (m), 1506 (vs), 1425 (vs), 1344 (m), 1248 (m), 1200 (m), 1126 (m), 841 (s), 745 (w), 557 (w).

ESI$^+$ MS (*m/z*): 1601.2424 (calcd. 1601.2409), 100% $\{Cs \subset [Fe_2(L^3)_3]\}^+$; 1507.30, 16% $\{K \subset [Fe_2(L^3)_3]\}^+$.

$\{Rb \subset [Fe_2(L^3)_3]\}(PF_6)$

Yield: 88% (75 mg).

Elemental analysis

Calcd. for $C_{60}H_{84}O_{12}N_{12}S_6PF_6Fe_2Rb$: C, 42.39; H, 4.98; N, 9.89; S, 11.32%. Found: C, 42.42; H, 4.97; N, 9.75; S, 11.46 %.

IR (KBr, cm^{-1}): 3441 (w), 2978 (w), 2932 (w), 1558 (m), 1539 (m), 1504 (vs), 1427 (vs), 1346 (m), 1254 (m), 1200 (w), 1126 (m), 841 (s), 744 (w), 559 (w).

ESI$^+$ MS (*m/z*): 1553.2511 (calcd. 1553.2473), 100% $\{Rb \subset [Fe_2(L^3)_3]\}^+$; 1507.30, 13% $\{K \subset [Fe_2(L^3)_3]\}^+$.

$\{K \subset [Fe_2(L^3)_3]\}(PF_6)$

Yield: 81% (65 mg).

Elemental analysis

Calcd. for $C_{60}H_{84}O_{12}N_{12}S_6PF_6Fe_2K$: C, 43.58; H, 5.12; N, 10.17; S, 11.64%. Found: C, 43.58; H, 5.46; N, 10.05; S, 11.64 %.

IR (KBr, cm^{-1}): 3429 (w), 2978 (w), 2932 (w), 1558 (m), 1539 (m), 1504 (vs), 1427 (vs), 1346 (m), 1254 (m), 1196 (w), 1126 (m), 841 (s), 741 (w), 559 (w).

ESI$^+$ MS (*m/z*): 1507.3000 (calcd. 1507.2992), 100% $\{K \subset [Fe_2(L^3)_3]\}^+$.

$\{Tl \subset [Fe_2(L^3)_3]\}(PF_6)$

Yield: 59% (54 mg).

Elemental analysis

Calcd. for $C_{60}H_{84}O_{12}N_{12}S_6PF_6Fe_2Tl$: C, 39.62; H, 4.66; N, 9.24; S, 10.58%. Found: C, 39.82; H, 4.73; N, 9.28; S, 10.17%.

IR (KBr, cm^{-1}): 3427 (w), 2980 (w), 2934 (w), 1557 (s), 1506, 1427 (s), 1344 (m), 1255 (m), 1200 (m), 1124 (m), 843 (s), 745 (w), 557 (w).

ESI$^+$ MS (*m/z*): 1673.3220 (calcd. 1673.3100), 84% {Tl ⊂ [Fe$_2$(L^3)$_3$]}$^+$; 1507.3108 (calcd. 1507.2992), 100% {K ⊂ [Fe$_2$(L^3)$_3$]}$^+$.

{NH$_4$ ⊂ [Fe$_2$(L^3)$_3$]}(PF$_6$)

Yield: 78% (64 mg).

Elemental analysis

Calcd. for {NH$_4$ ⊂ [Fe$_2$(L^3)$_3$]}(PF$_6$) · 4H$_2$O, C$_{60}$H$_{96}$O$_{16}$N$_{13}$S$_6$PF$_6$Fe$_2$: C, 42.28; H, 5.68; N, 10.68; S, 11.29%. Found: C, 42.27; H, 5.45; N, 10.46; S, 11.11 %.

IR (KBr, cm^{-1}): 3437 (w), 3242 (w), 2980 (w), 2935 (w), 1537 (m), 1504 (vs), 1427 (vs), 1344 (m), 1256 (m), 1198 (m), 1124 (m), 1053 (w), 843 (s), 744 (m), 557 (w).

ESI$^+$ MS (*m/z*): 1507.3020 (calcd. 1507.2992), 100% {K ⊂ [Fe$_2$(L^3)$_3$]}$^+$; 1486.37, 15% {NH$_4$ ⊂ [Fe$_2$(L^3)$_3$]}$^+$.

7.3.9 Cobalt(III) {2}–metallacryptates, {M ⊂ [Co$_2$(L^3)$_3$]}(PF$_6$) (M = Cs$^+$, Rb$^+$, K$^+$, Tl$^+$, NH$_4^+$)

The complexes were synthesized following the same procedure given for the Fe(III) complexes, except that CoCl$_2$ · 6 H$_2$O or Co(NO$_3$)$_2$ · 6 H$_2$O in the case of Tl$^+$, were used instead of FeCl$_3$· 6 H$_2$O. The labeled compound {^{15}NH$_4$ ⊂ [Co$_2$(L^3)$_3$]}(PF$_6$) was prepared using ^{15}NH$_4$Cl. After adding the ligand to the solutions of the metal salts, it dissolved within 5 min and the color of the solutions changed gradually to green. The products deposited as green precipitates. They were filtered off, washed with MeOH and dried in vacuum. Except for the Cs$^+$-capturing complex, single crystals suitable for X–ray analysis were obtained by slow evaporation of solutions of the complexes in CH$_2$Cl$_2$/MeOH/toluene mixtures (or in DMF in case of the rubidium-containing complex).
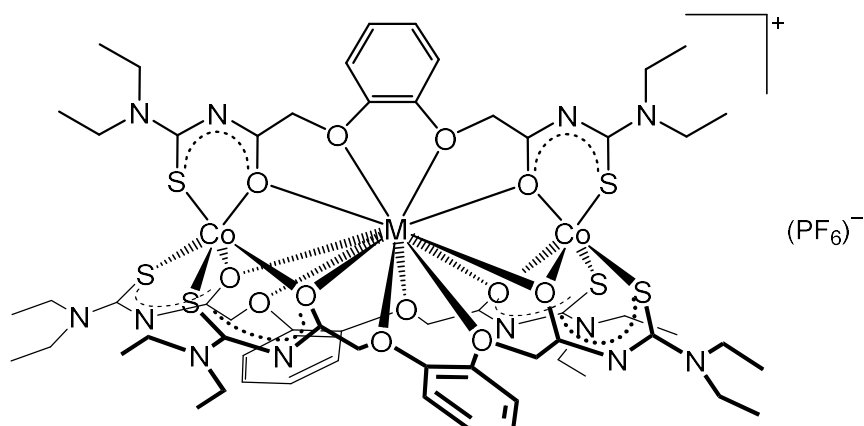

M = Cs$^+$, Rb$^+$, K$^+$, Tl$^+$, NH$_4^+$

{Cs ⊂ [Co$_2$(L^3)$_3$]}(PF$_6$)

Yield: 41% (36 mg).

Elemental analysis

Calcd. for C$_{60}$H$_{84}$O$_{12}$N$_{12}$S$_6$PF$_6$Co$_2$Cs: C, 41.10; H, 4.83; N, 9.59; S, 10.97%. Found: C, 40.90; H, 4.90; N, 9.75; S, 11.08 %.

IR (KBr, cm^{-1}): 3472 (w), 2978 (w), 2932 (w), 1551 (vs), 1501 (vs), 1427 (vs), 1346 (m), 1250 (m), 1204 (w), 1126 (m), 841 (s), 741 (w), 559 (w).

^{1}H NMR (400 MHz, CDCl$_3$, ppm): 6.78 – 6.70 (m, 12H, Ph); 4.49 (d, J = 16.0 Hz, 6H, OCH$_2$); 4.38 (d, J = 16.0 Hz, 6H, OCH$_2$); 4.08 (dq, J = 14.4 Hz, 7.2 Hz, 6H, NCH$_2$); 3.82 (dq, J = 14.4 Hz, 7.2 Hz, 6H, NCH$_2$); 3.68 (dq, J = 14.4 Hz, 7.2 Hz, 6H, NCH$_2$); 3.48 (dq, J = 14.4 Hz, 7.2 Hz, 6H, NCH$_2$); 1.32 (t, J = 7.2 Hz, 18H, CH$_3$); 1.16 (t, J = 7.2 Hz, 18H, CH$_3$).

^{13}C{^{1}H} NMR (CDCl$_3$, ppm): 175.8 (C=O); 172.8 (C=S); 145.6, 121.4, 111.8 (Ph); 68.9 (OCH$_2$); 45.7, 45.5 (NCH$_2$); 13.4, 12.9 (CH$_3$).

ESI$^+$ MS (*m/z*): 1607.2478 (calcd. 1607.2374), 100% {Cs ⊂ [Co$_2$(L^3)$_3$]}$^+$.

{Rb ⊂ [Co$_2$(L^3)$_3$]}(PF$_6$)

Yield: 47% (40 mg).

Elemental analysis

Calcd. for C$_{60}$H$_{84}$O$_{12}$N$_{12}$S$_6$PF$_6$Co$_2$Rb: C, 42.24; H, 4.96; N, 9.85; S, 11.28%. Found: C, 42.21; H, 4.97; N, 9.64; S, 11.47 %.

IR (KBr, cm^{-1}): 3441 (w), 2978 (w), 2932 (w), 1558 (vs), 1504 (vs), 1423 (vs), 1342 (m), 1250 (m), 1196 (w), 1126 (m), 841 (s), 741 (w), 556 (w).

^{1}H NMR (400 MHz, CDCl$_3$, ppm): 6.77 – 6.71 (m, 12H, Ph); 4.54 (d, J = 16.0 Hz, 6H, OCH$_2$); 4.45 (d, J = 16.0 Hz, 6H, OCH$_2$); 4.03 (dq, J = 14.4 Hz, 7.2 Hz, 6H, NCH$_2$); 3.82 (dq, J = 13.6 Hz, 6.8 Hz, 6H, NCH$_2$); 3.65 (dq, J = 14.4 Hz, 7.2 Hz, 6H, NCH$_2$); 3.44 (dq, J = 13.6 Hz, 6.8 Hz, 6H, NCH$_2$); 1.29 (t, J = 7.0 Hz, 18H, CH$_3$); 1.14 (t, J = 7.0 Hz, 18H, CH$_3$).

^{13}C{^{1}H} NMR (CDCl$_3$, ppm): 175.6 (C=O); 172.9 (C=S); 146.1, 121.4, 111.9 (Ph); 68.9 (OCH$_2$); 45.7, 45.5 (NCH$_2$); 13.4, 12.8 (CH$_3$).

ESI$^+$ MS (*m/z*): 1559.2426 (calcd. 1559.2438), 100% {Rb ⊂ [Co$_2$(L^3)$_3$]}$^+$; 1513.29, 17% {K ⊂ [Co$_2$(L^3)$_3$]}$^+$.

{K ⊂ [Co$_2$(L^3)$_3$]}(PF$_6$)

Yield: 55% (46 mg).

Elemental analysis

Calcd. for $C_{60}H_{84}O_{12}N_{12}S_6PF_6Co_2K$: C, 43.42; H, 5.10; N, 10.13; S, 11.59%. Found: C, 43.18; H, 5.17; N, 9.89; S, 11.83 %.

IR (KBr, cm^{-1}): 3468 (w), 2978 (w), 2932 (w), 1558 (vs), 1504 (vs), 1427 (vs), 1346 (m), 1250 (m), 1196 (w), 1126 (m), 841 (s), 741 (w), 559 (w).

^{1}H NMR (400 MHz, CDCl$_3$, ppm): 6.98 – 6.86 (m, 12H, Ph); 4.58 (d, J = 16.0 Hz, 6H, OCH$_2$); 4.52 (d, J = 16.0 Hz, 6H, OCH$_2$); 4.01 (dq, J = 12.8 Hz, 6.4 Hz, 6H, NCH$_2$); 3.81 (dq, J = 13.6 Hz, 6.8 Hz, 6H, NCH$_2$); 3.63 (dq, J = 14.4 Hz, 7.2 Hz, 6H, NCH$_2$); 3.43 (dq, J = 13.6 Hz, 6.8 Hz, 6H, NCH$_2$); 1.27 (t, J = 7.2 Hz, 18H, CH$_3$); 1.13 (t, J = 7.0 Hz, 18H, CH$_3$).

^{13}C{^{1}H} NMR (CDCl$_3$, ppm): 175.6 (C=O); 172.9 (C=S); 146.7, 121.5, 112.4 (Ph); 69.3 (OCH$_2$); 45.7, 45.5 (NCH$_2$); 13.3, 12.8 (CH$_3$).

ESI$^+$ MS (*m/z*): 1513.3010 (calcd. 1513.2957), 100% $\{K \subset [Co_2(L^3)_3]\}^+$.

$\{Tl \subset [Co_2(L^3)_3]\}(PF_6)$

Yield: 42% (38 mg).

Elemental analysis

Calcd. for $C_{60}H_{84}O_{12}N_{12}S_6PF_6Co_2Tl$: C, 39.49; H, 4.64; N, 9.21; S, 10.54%. Found: C, 39.30; H, 5.04; N, 8.97; S, 10.17 %.

IR (KBr, cm^{-1}):): 3317 (w), 2974 (w), 2936 (w), 1557 (vs), 1504 (vs), 1418 (s), 1339 (m), 1248 (m), 1200 (w), 1126 (m), 843 (s), 739 (w), 557 (w).

^{1}H NMR (400 MHz, CDCl$_3$, ppm): 6.77 – 6.70 (m, 12H, Ph); 4.61 (d, J = 16.2 Hz, 6H, OCH$_2$); 4.46 (d, J = 16.2 Hz, 6H, OCH$_2$); 4.05 (dq, J = 14.4 Hz, 7.2 Hz, 6H, NCH$_2$); 3.83 (dq, J = 13.6 Hz, 6.8 Hz, 6H, NCH$_2$); 3.65 (dq, J = 14.4 Hz, 7.2 Hz, 6H, NCH$_2$); 3.44 (dq, J = 13.6 Hz, 6.8 Hz, 6H, NCH$_2$); 1.30 (t, J = 7.2 Hz, 18H, CH$_3$); 1.15 (t, J = 7.0 Hz, 18H, CH$_3$).

^{13}C{^{1}H} NMR (CDCl$_3$, ppm): 175.4 (C=O); 172.8 (C=S); 146.0, 121.4, 111.9 (Ph); 68.9 (OCH$_2$); 45.7, 45.5 (NCH$_2$); 13.4, 12.8 (CH$_3$).

ESI$^+$ MS (*m/z*): 1679.3155 (calcd. 1679.3064), 100% $\{Tl \subset [Co_2(L^3)_3]\}^+$; 1513.30, 17% $\{K \subset [Co_2(L^3)_3]\}^+$.

$\{^{14}NH_4/^{15}NH_4 \subset [Co_2(L^3)_3]\}(PF_6)$

Yield: 63% (52 mg).

Elemental analysis

Calcd. for $C_{60}H_{88}O_{12}N_{13}S_6PF_6Co_2$: C, 43.98; H, 5.41; N, 11.11; S, 11.74%. Found: C, 43.81; H, 5.98; N, 10.67; S, 11.31%.

IR (KBr, cm^{-1}): 3444 (w), 3238 (w), 2978 (w), 2936 (w), 1556 (s), 1504 (vs), 1427 (vs), 1346 (m), 1246 (m), 1126 (m), 1055 (w), 843 (s), 737 (w), 557 (w).

^{1}H NMR (400 MHz, CDCl$_3$, ppm):

{^{14}NH$_4$ ⊂ [Co$_2$(L^3)$_3$]}(PF$_6$) 6.70 (t, ^{1}J(^{14}N–^{1}H) = 53.8 Hz, 4H, ^{14}NH$_4$); 6.74 – 6.72 (m, br, 12H, Ph); 4.55 (d, J = 16.0 Hz, 6H, OCH$_2$); 4.44 (d, J = 16.0 Hz, 6H, OCH$_2$); 4.04 (dq, J = 13.6 Hz, 6.8 Hz, 6H, NCH$_2$); 3.80 (dq, J = 14.4 Hz, 7.2 Hz, 6H, NCH$_2$); 3.64 (dq, J = 14.4 Hz, 7.2 Hz, 6H, NCH$_2$); 3.43 (dq, J = 13.6 Hz, 6.8 Hz, 6H, NCH$_2$); 1.29 (t, J = 7.0 Hz, 18H, CH$_3$); 1.13 (t, J = 7.0 Hz, 18H, CH$_3$).

{^{15}NH$_4$ ⊂ [Co$_2$(L^3)$_3$]}(PF$_6$) 6.69 (d, ^{1}J(^{15}N–^{1}H) = 75.2 Hz, 4H, ^{15}NH$_4$); 6.76 – 6.70 (m, br, 12H, Ph); 4.54 (d, J = 15.6 Hz, 6H, OCH$_2$); 4.43 (d, J = 16.0 Hz, 6H, OCH$_2$); 4.04 (dq, J = 14.4 Hz, 7.2 Hz, 6H, NCH$_2$); 3.81 (dq, J = 13.6 Hz, 6.8 Hz, 6H, NCH$_2$); 3.64 (dq, J = 14.4 Hz, 7.2 Hz, 6H, NCH$_2$); 3.43 (dq, J = 13.6 Hz, 6.8 Hz, 6H, NCH$_2$); 1.29 (t, J = 7.0 Hz, 18H, CH$_3$); 1.13 (t, J = 7.0 Hz, 18H, CH$_3$).

^{13}C{^{1}H} NMR (CDCl$_3$, ppm): 175.5 (C=O); 172.8 (C=S); 146.1, 121.4, 111.7 (Ph); 68.9 (OCH$_2$); 45.7, 45.5 (NCH$_2$); 13.4, 12.8 (CH$_3$).

^{15}N{^{1}H} NMR (CDCl$_3$, ppm, standard MeNO$_2$): **{^{15}NH$_4$ ⊂ [Co$_2$(L^3)$_3$]}(PF$_6$)** -355.7.

^{15}N DEPT NMR (CDCl$_3$, ppm, standard MeNO$_2$): **{^{15}NH$_4$ ⊂ [Co$_2$(L^3)$_3$]}(PF$_6$)** -355.7 (quintet, ^{1}J(^{15}N–^{1}H) = 75.3 Hz).

^{1}H NMR (400 MHz, DMSO-d_6, ppm): 6.78 – 6.46 (br, 16H, Ph + NH$_4$); 4.56 (br, 12H, OCH$_2$); 3.88 (br, 6H, NCH$_2$); 3.73 (br, 6H, NCH$_2$); 3.61 (br, 6H, NCH$_2$); 3.46 (estimated, br, 6H, NCH$_2$, overlaps with broad signal of H$_2$O at 3.32 ppm); 1.74 (br, 18H, CH$_3$); 1.06 (br, 18H, CH$_3$). **^{15}NH$_4$Cl** 7.45 (s, br).

^{13}C{^{1}H} NMR (DMSO-d_6, ppm): 175.9 (C=O); 171.9 (C=S); 145.7, 121.5, 112.2 (Ph); 68.8 (OCH$_2$); 45.6, 45.5 (NCH$_2$); 13.6, 12.9 (CH$_3$).

^{15}N{^{1}H} NMR (DMSO-d_6, ppm, standard MeNO$_2$): **{^{15}NH$_4$ ⊂ [Co$_2$(L^3)$_3$]}(PF$_6$)** -355.7. **^{15}NH$_4$Cl** -351.6.

^{15}N DEPT NMR (DMSO-d_6, ppm, standard MeNO$_2$): **{^{15}NH$_4$ ⊂ [Co$_2$(L^3)$_3$]}(PF$_6$)** no signal. **^{15}NH$_4$Cl** no signal.

^{15}N NMR (DMSO-d_6, ppm, standard MeNO$_2$): **{^{15}NH$_4$ ⊂ [Co$_2$(L^3)$_3$]}(PF$_6$)** -355.7 (quintet, ^{1}J(^{15}N–^{1}H) = 75.2 Hz). **^{15}NH$_4$Cl** -351.7 (s, br).

ESI$^+$ MS (*m/z*): **{^{14}NH$_4$ ⊂ [Co$_2$(L^3)$_3$]}(PF$_6$)** 1513.30, 16% {K ⊂ [Co$_2$(L^3)$_3$]}$^+$; 1492.3684 (calcd. 1492.3664), 100% {^{14}NH$_4$ ⊂ [Co$_2$(L^3)$_3$]}$^+$. **{^{15}NH$_4$ ⊂ [Co$_2$(L^3)$_3$]}(PF$_6$)** 1513.31, 19% {K ⊂ [Co$_2$(L^3)$_3$]}$^+$; 1493.3788 (calcd. 1493.3664), 100% {^{15}NH$_4$ ⊂ [Co$_2$(L^3)$_3$]}$^+$.

7.3.10 Copper(II) metallacoronates

H_2L^3 (45.6 mg, 0.1 mmol) was added to solutions containing $Cu(OAc)_2 \cdot H_2O$ (20.0 mg, 0.1 mmol) and 0.05 mmol MCl (M = Cs^+, Rb^+ and K^+) and few drops of H_2O in 1 mL MeOH. In the case of Tl^+, $Cu(NO_3)_2 \cdot 3 H_2O$ and $TlNO_3$ were used. The ligand dissolved gradually within 5 min. After the addition of 2 drops of Et_3N and stirring for more 30 min at room temperature, $(n–Bu_4N)(PF_6)$ (19.4 mg, 0.05 mmol) was added and the temperature was increased to 50^0C and kept for 2h. During this process, brown precipitates deposited. The products were filtered off, washed with a small amount of MeOH and dried in vacuum. Single crystals suitable for X–ray analysis were obtained by slow evaporation of solutions of the complexes in CH_2Cl_2/MeOH mixtures.

{Cs ⊂ [Cu₃(L³)₃]}(PF₆)
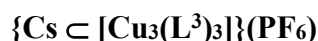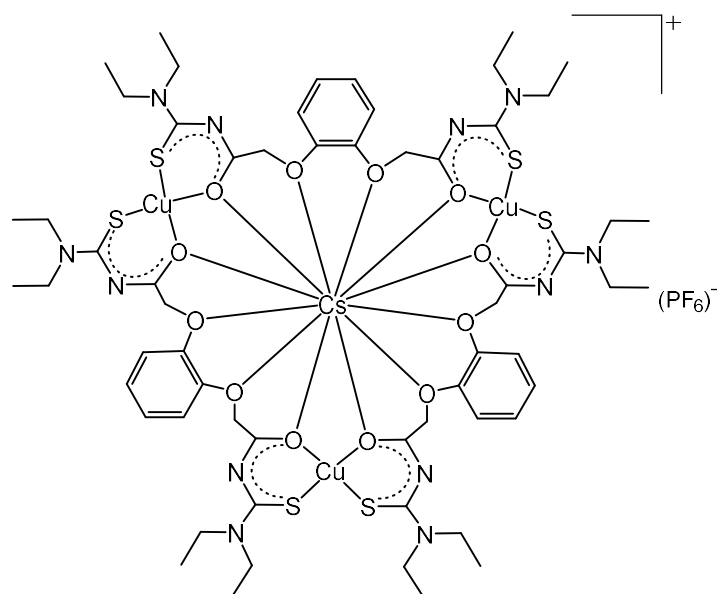
Yield: 79% (48 mg).

Elemental analysis

Calcd. for $C_{60}H_{84}O_{12}N_{12}S_6PF_6Cu_3Cs$: C, 39.46; H, 4.64; N, 9.20; S, 10.53%. Found: C, 38.87; H, 4.63; N, 9.03; S, 10.74%.

IR (KBr, cm^{-1}): 3437 (w), 2976 (w), 2933 (w), 1544 (s), 1502 (s), 1429 (s), 1348 (s), 1257 (m), 1203 (w), 1128 (m), 843 (s), 557 (w).

ESI⁺ MS (*m/z*): 1680.1626 (calcd. 1680.1580), 25% {Cs ⊂ [Cu₃(L³)₃]}⁺; 1165.08, 18% {Cs ⊂ [Cu₂(L³)₂]}⁺; 1055.1613 (calcd. 1055.1576), 32% {Na ⊂ [Cu₂(L³)₂]}⁺; 132.9058 (calcd. 132.9055), 100% Cs^+.

M = Rb⁺, K⁺, Tl⁺
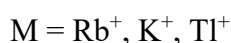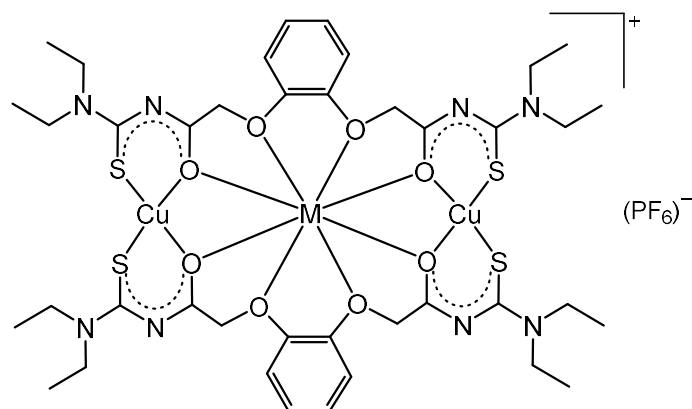
{Rb ⊂ [Cu₂(L³)₂]}(PF₆)

Yield: 67% (42 mg).

Elemental analysis

Calcd. for $C_{40}H_{56}O_8N_8S_4PF_6Cu_2Rb$: C, 38.05; H, 4.47; N, 8.87; S, 10.16%. Found: C, 38.49; H, 4.15; N, 8.90; S, 10.54%.

IR (KBr, cm⁻¹): 3423 (w), 2978 (w), 2933 (w), 1541 (s), 1504 (s), 1429 (s), 1348 (s), 1244 (m), 1202 (w), 1126 (m), 845 (s), 557 (w).

ESI⁺ MS (*m/z*): 1632.1695, (calcd. 1632.1644) 51% {Rb ⊂ [Cu₃(L³)₃]}⁺; 1117.0830 (calcd. 1117.0794), 49% {Rb ⊂ [Cu₂(L³)₂]}⁺; 1055.16, 16% {Na ⊂ [Cu₂(L³)₂]}⁺; 84.9119 (calcd. 84.9118), 100% Rb⁺.

{K ⊂ [Cu₂(L³)₂]}(PF₆)

Yield: 71% (43 mg).

Elemental analysis

Calcd. for $C_{40}H_{56}O_8N_8S_4PF_6Cu_2K$: C, 39.50; H, 4.64; N, 9.21; S, 10.54%. Found: C, 39.94; H, 4.47; N, 9.40; S, 10.22%.

IR (KBr, cm⁻¹): 3443 (w), 2976 (w), 2934 (w), 1541 (s), 1504 (s), 1429 (s), 1350 (m), 1244 (m), 1202 (w), 1128 (m), 845 (s), 557 (w).

ESI⁺ MS (*m/z*): 1586.2193 (calcd. 1586.2163), 67% {K ⊂ [Cu₃(L³)₃]}⁺; 1071.1362 (calcd. 1071.1315) , 100% {K ⊂ [Cu₂(L³)₂]}⁺; 1055.1594 (calcd. 1055.1576), 23% {Na ⊂ [Cu₂(L³)₂]}⁺.

{Tl ⊂ [Cu₂(L³)₂]}(PF₆)

Yield: 40% (28 mg).

Elemental analysis

Calcd. for $C_{40}H_{56}O_8N_8S_4PF_6Cu_2Tl$: C, 34.77; H, 4.09; N, 8.11; S, 9.28%. Found: C, 33.96; H, 3.76; N, 8.98; S, 8.89%.

IR (KBr, cm^{-1}): 3408 (w), 2974 (w), 2934 (w), 1541 (m), 1503 (s), 1429 (s), 1348 (m), 1238 (m), 1126 (m), 845 (s), 745 (w), 557 (w).

ESI$^+$ MS (m/z): 1752.24, 10% $\{Tl \subset [Cu_3(L^3)_3]\}^+$; 1235.1518 (calcd. 1235.1440), 21% $\{Tl \subset [Cu_2(L^3)_2]\}^+$; 204.9747 (calcd. 204.9744), 100% Tl^+.

7.3.11 Nickel(II) metallacoronates

The complexes were synthesized following the procedure described for the Cu(II) complexes, except that Ni(OAc)$_2$ · 4 H$_2$O was used instead of Cu(OAc)$_2$ · H$_2$O. After addition of the salt mixtures, the ligand dissolved quickly and the color of the solution changed to purple. The products deposited as purple precipitates, which were filtered off, washed with MeOH and dried in vacuum.

$\{Cs \subset [Ni_3(L^3)_3]\}(PF_6)$
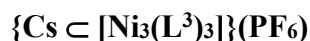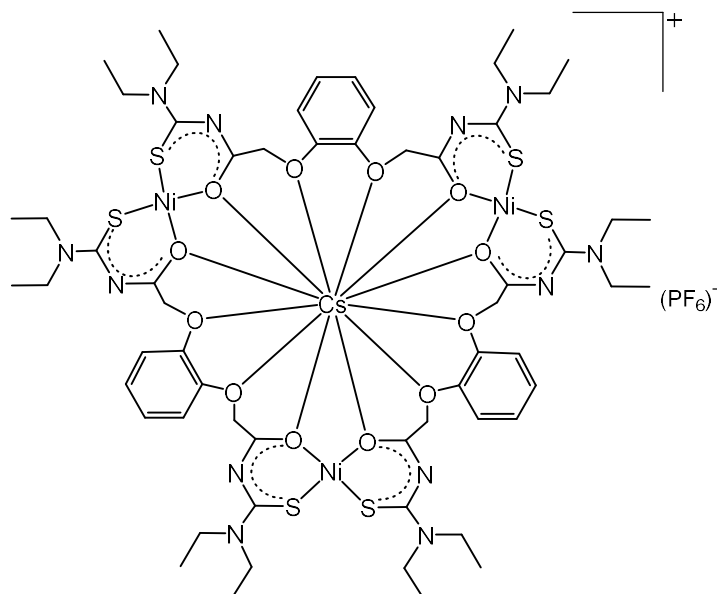
Yield: 98% (59 mg).

Elemental analysis

Calcd. for $C_{60}H_{84}O_{12}N_{12}S_6PF_6Ni_3Cs$: C, 39.78; H, 4.67; N, 9.28; S, 10.62%. Found: C, 40.12; H, 4.76; N, 9.05; S, 10.30%.

IR (KBr, cm^{-1}): 3435 (w), 2974 (w), 2938 (w), 1545 (s), 1508 (vs), 1429 (s), 1352 (m), 1260 (m), 847 (s).

¹H NMR (400 MHz, CD₂Cl₂, ppm): 6.91 – 6.89 (m, 6H, Ph); 6.77 – 6.74 (m, 6H, Ph); 4.58 (br, 12H, OCH₂); 3.64 (q, J = 6.8 Hz, 12H, NCH₂); 3.62 (q, J = 6.8 Hz, 12H, NCH₂); 1.22 (t, J = 7.0 Hz, 18H, CH₃); 1.14 (t, J = 7.2 Hz, 18H, CH₃).

¹³C{¹H} NMR (CD₂Cl₂, ppm): 175.2 (C=O); 171.1 (C=S); 146.9, 122.5, 114.9 (Ph); 70.9 (OCH₂); 46.2, 45.7 (NCH₂); 13.0, 12.1 (CH₃).

ESI⁺ MS (*m/z*): 1665.19, 11% {Cs ⊂ [Ni₃(L³)₃]}⁺; 1155.0977 (calcd. 1155.0820), 24% {Cs ⊂ [Ni₂(L³)₂]}⁺; 1061.16, 15% {K ⊂ [Ni₂(L³)₂]}⁺; 1045.1815 (calcd. 1045.1663) , 35% {Na ⊂ [Ni₂(L³)₂]}⁺; 132.9060 (calcd. 132.9055), 100% Cs⁺.

Single crystals suitable for X–ray analysis were obtained by slow evaporation of a solution of the complex in a CH₂Cl₂/MeOH mixture.

M = Rb⁺, K⁺
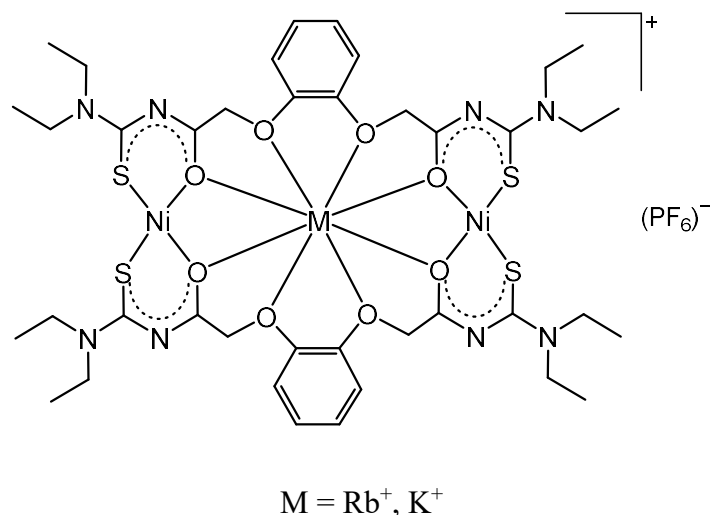
{Rb ⊂ [Ni₂(L³)₂]}(PF₆)

Yield: 93% (58 mg).

Elemental analysis Calcd. for C₄₀H₅₆O₈N₈S₄Ni₂PF₆Rb: C, 38.34; H, 4.50; N, 8.94; S, 10.24%. Found: C, 38.75; H, 4.21; N, 9.06; S, 10.30%.

IR (KBr, cm⁻¹): 3445 (w), 2980 (w), 2936 (w), 1557 (s), 1508 (vs), 1433 (s), 1356 (m), 1250 (m), 843 (s).

¹H NMR (400 MHz, CD₂Cl₂, ppm): 6.94 – 6.91 (m, 4H, Ph); 6.83 – 6.81 (m, 4H, Ph); 4.60 (br, 8H, OCH₂); 3.62 (q, J = 6.8 Hz, 8H, NCH₂); 3.60 (q, J = 6.8 Hz, 8H, NCH₂); 1.21 (t, J = 7.0 Hz, 12H, CH₃); 1.12 (t, J = 7.2 Hz, 12H, CH₃).

¹³C{¹H} NMR (CD₂Cl₂, ppm): 175.4 (C=O); 171.0 (C=S); 147.7, 123.0, 116.1 (Ph); 71.7 (OCH₂); 46.2, 45.7 (NCH₂); 13.0, 12.1 (CH₃).

ESI⁺ MS (*m/z*): 1617.18, 15% {Rb ⊂ [Ni₃(L³)₃]}⁺; 1107.0842, (calcd. 1107.0884) 25% {Rb ⊂ [Ni₂(L³)₂]}⁺; 1061.16, 20% {K ⊂ [Ni₂(L³)₂]}⁺; 1045.1619, (calcd. 1045.1663) 35% {Na ⊂ [Ni₂(L³)₂]}⁺; 84.9102 (calcd. 84.9118), 88% Rb⁺.

{K ⊂ [Ni₂(L³)₂]}(PF₆)

Yield: 80% (48 mg).

Elemental analysis Calcd. for C₄₀H₅₆O₈N₈S₄PF₆Ni₂K: C, 39.82; H, 4.68; N, 9.29; S, 10.63%. Found: C, 40.33; H, 4.98; N, 9.27; S, 10.64%.

IR (KBr, cm⁻¹): 3445 (w), 2976 (w), 2940 (w), 1543 (s), 1508 (vs), 1429 (s), 1352 (m), 1246 (m), 847 (s).

¹H NMR (400 MHz, CD₂Cl₂, ppm): 6.95 – 6.93 (m, 4H, Ph); 6.91 – 6.88 (m, 4H, Ph); 4.55 (br, 8H, OCH₂); 3.61 (q, J = 7.2 Hz, 8H, NCH₂); 3.59 (q, J = 7.2 Hz, 8H, NCH₂); 1.20 (t, J = 7.2 Hz, 12H, CH₃); 1.10 (t, J = 7.2 Hz, 12H, CH₃).

¹³C{¹H} NMR (CD₂Cl₂, ppm): 175.3 (C=O); 171.1 (C=S); 148.1, 123.2, 116.6 (Ph); 72.2 (OCH₂); 46.2, 45.6 (NCH₂); 12.9, 12.1 (CH₃).

ESI⁺ MS (*m/z*): 1571.25, 7% {K ⊂ [Ni₃(L³)₃]}⁺; 1061.1558, (calcd. 1061.1403) 79% {K ⊂ [Ni₂(L³)₂]}⁺; 1045.1818, (calcd. 1045.1663) 92% {Na ⊂ [Ni₂(L³)₂]}⁺.

7.3.12 Nickel(II) {2}–metallacryptates

H₂L³ (68.2 mg, 0.15 mmol) was added to solutions of Ni(OAc)₂ · 4 H₂O (25.0 mg, 0.1 mmol) and BaCl₂ (10.4 mg, 0.05 mmol) or a tenfold excess of MCl (M = Cs⁺, Rb⁺ and K⁺) in 1 mL MeOH and a few drops of H₂O. The ligand dissolved within 5 min and the mixture was stirred at room temperature for 30 min. Addition of 3 drops of Et₃N caused an immediate change of color of the solution from violet to yellow- green and the separation of yellow-green solids from the reaction mixture. The products were filtered off, washed with MeOH and dried in vacuum.

M/Mⁿ⁺ = Cs⁺, Rb⁺, K⁺, Ba²⁺
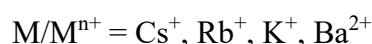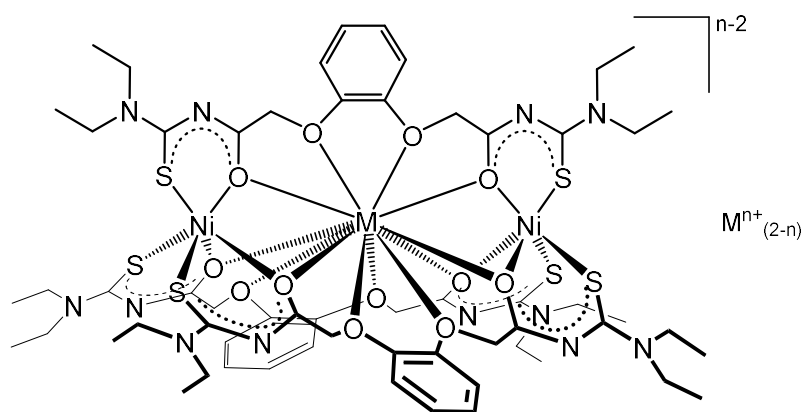
Cs {Cs ⊂ [Ni$_2$(L^3)$_3$]}

Yield: 55% (48 mg).

Elemental analysis

Calcd. for C$_{60}$H$_{84}$O$_{12}$N$_{12}$S$_6$Ni$_2$Cs$_2$: C, 41.39; H, 4.86; N, 9.65; S, 11.05%. Found: C, 41.07; H, 5.32; N, 9.55; S, 10.91%.

IR (KBr, cm^{-1}): 3435 (w), 2974 (w), 2930 (w), 1582 (m), 1557 (m), 1502 (s), 1420 (vs), 1342 (m), 1246 (m), 1200 (w), 1125 (m), 1009 (w), 737 (w).

ESI$^-$ MS (*m/z*): 453.1758 (calcd. 453.1630), 100% [HL^3]$^-$; 1607.2366 (calcd. 1607.2373), 11% {Cs ⊂ [Ni$_2$(L^3)$_3$]}$^-$.

Rb {Rb ⊂ [Ni$_2$(L^3)$_3$]}

Yield: 47% (39 mg).

Elemental analysis

Calcd. for C$_{60}$H$_{84}$O$_{12}$N$_{12}$S$_6$Ni$_2$Rb$_2$: C, 43.78; H, 5.14; N, 10.21; S, 11.69%. Found: C, 43.49; H, 5.15; N, 10.90; S, 11.54%.

IR (KBr, cm^{-1}): 3439 (w), 2976 (w), 2930 (w), 1585 (m), 1557 (m), 1504 (s), 1423 (vs), 1341 (m), 1252 (s), 1202 (w), 1125 (m), 1009 (w), 737 (w).

ESI$^-$ MS (*m/z*): 453.1621 (calcd. 453.1630), 75% [HL^3]$^-$; 1559.2459 (calcd. 1559.2462), 8% {Rb ⊂ [Ni$_2$(L^3)$_3$]}$^-$.

K {K ⊂ [Ni$_2$(L^3)$_3$]}

Yield: 53% (41 mg).

Elemental analysis

Calcd. for C$_{60}$H$_{84}$O$_{12}$N$_{12}$S$_6$Ni$_2$K$_2$: C, 46.39; H, 5.45; N, 10.82; S, 12.39%. Found: C, 46.40; H, 5.46; N, 10.86; S, 12.45%.

IR (KBr, cm^{-1}): 3441 (w), 2974 (w), 2930 (w), 1584 (m), 1557 (m), 1504 (s), 1418 (vs), 1339 (m), 1248 (m), 1200 (w), 1125 (m), 1009 (w), 735 (w).

ESI$^-$ MS (*m/z*): 453.1736 (calcd. 453.1630), 100% [HL^3]$^-$; 1513.2961 (calcd. 1513.2955), 11% {K ⊂ [Ni$_2$(L^3)$_3$]}$^-$.

{Ba ⊂ [Ni$_2$(L^3)$_3$]}

Yield: 70% (56 mg).

Elemental analysis

Calcd. for C$_{60}$H$_{84}$O$_{12}$N$_{12}$S$_6$Ni$_2$Ba: C, 44.69; H, 5.25; N, 10.42; S, 11.93%. Found: C, 44.70; H, 5.32; N, 10.44; S, 11.96%.

IR (KBr, cm^{-1}): 3495 (w), 2972 (w), 2930 (w), 1584 (s), 1557 (s), 1503 (s), 1420 (vs), 1339 (m), 1250 (s), 1202 (w), 1123 (m), 1010 (w), 739 (w).

Single crystals were obtained by slow evaporation of a solution of the complex in a CH$_2$Cl$_2$/ *n*–hexane mixture.

7.3.13 Nickel(II) metallalariate-ether type complexes

H$_2$L^3 (68.2 mg, 0.2 mmol) was added to solutions of Ni(OAc)$_2$ · 4 H$_2$O (25.0 mg, 0.1 mmol) and 0.1 mmol M^{II}Cl$_2$ or M^{III}(NO$_3$)$_3$ (M^{II} = Sr^{2+}, Ca^{2+}; M^{III} = La^{3+}, Ce^{3+}, Pr^{3+}) in 1 mL MeOH and few drops of H$_2$O. The resulting solutions were treated as described for the nickel(II) metallacryptates. The green products were filtered off, washed with MeOH and dried in vacuum. Single crystals were obtained by slow evaporation of solutions of the complexes in CH$_2$Cl$_2$/MeOH mixtures.

M^{II} = Sr^{2+}, Ca^{2+} M^{III} = La^{3+}, Ce^{3+}, Pr^{3+}; X = AcO$^-$

{Sr$_2$ ⊂ [Ni$_2$(L^3)$_2$(L^3')$_2$]}
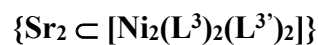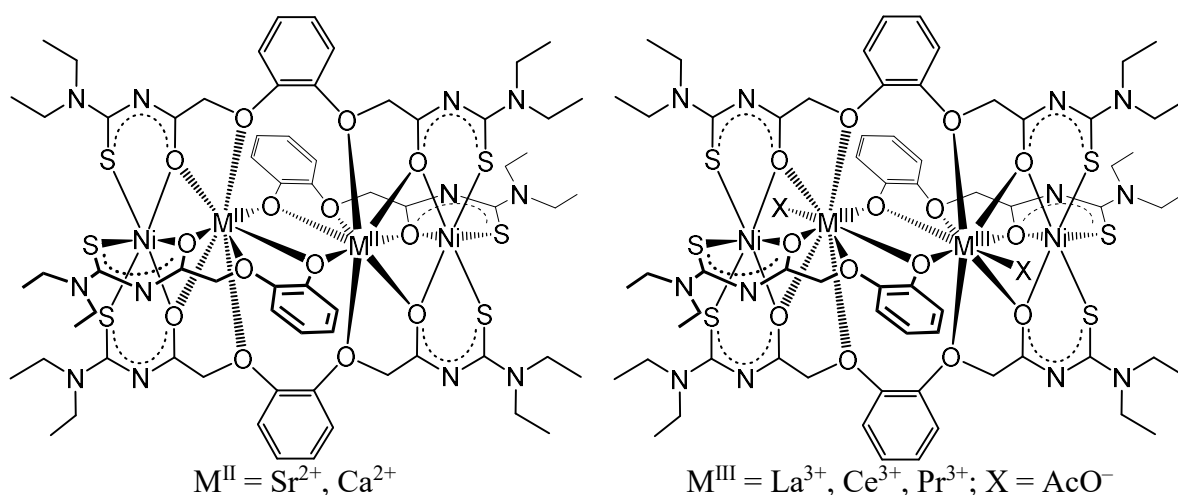
Yield: 68% (60 mg).

Elemental analysis

Calcd. for C$_{66}$H$_{88}$O$_{14}$N$_{12}$S$_6$Ni$_2$Sr$_2$: C, 45.08; H, 5.04; N, 9.56; S, 10.94%. Found: C, 44.82; H, 5.36; N, 9.28; S, 10.52%.

IR (KBr, cm^{-1}): 3429 (w), 2974 (w), 2931 (w), 1607 (vs), 1557 (m), 1504 (s), 1429 (s), 1346 (w), 1252 (m), 1209 (m), 1125 (m), 1037 (w), 735 (w).

ESI$^+$ MS (*m/z*): 1759.1789 (calcd. 1759.1746), 100% [M + H]$^+$.

{Ca$_2$ ⊂ [Ni$_2$(L^3)$_2$(L^3')$_2$]}
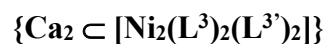
Yield: 60% (50 mg).

Elemental analysis

Calcd. for $C_{66}H_{88}O_{14}N_{12}S_6Ni_2Ca_2$: C, 47.66; H, 5.33; N, 10.10; S, 11.57%. Found: C, 47.16; H, 4.95; N, 9.77; S, 11.24%.

IR (KBr, cm^{-1}): 3425 (w), 2970 (w), 2924 (w), 1585 (s), 1551 (s), 1497 (s), 1423 (s), 1350 (m), 1245 (m), 1207 (w), 1122 (w), 733 (w).

ESI$^+$ MS (*m/z*): 1663.3014 (calcd. 1663.2860), 100% [M + H]$^+$.

{(AcO)$_2$La$_2 \subset$ [Ni$_2$(L^3)$_2$(L$^{3'}$)$_2$]}

Yield: 81% (80 mg).

Elemental analysis

Calcd. for $C_{70}H_{94}O_{18}N_{12}S_6Ni_2La_2$: C, 42.48; H, 4.79; N, 8.49; S, 9.72%. Found: C, 42.87; H, 4.96; N, 8.19; S, 9.62%.

IR (KBr, cm^{-1}): 3445 (w), 2978 (w), 2932 (w), 1593 (s), 1551 (s), 1497 (s), 1420 (s), 1354 (m), 1246 (m), 1192 (w), 1122 (w), 741 (w).

ESI$^+$ MS (*m/z*): 1919.1831 (calcd. 1919.1810), 100% [M − AcO]$^+$; 2001.19, 17% [M + Na]$^+$.

{(AcO)$_2$Ce$_2 \subset$ [Ni$_2$(L^3)$_2$(L$^{3'}$)$_2$]}

Yield: 85% (84 mg).

Elemental analysis

Calcd. for $C_{70}H_{94}O_{18}N_{12}S_6Ni_2Ce_2$: C, 42.43; H, 4.78; N, 8.48; S, 9.71%. Found: C, 42.65; H, 4.64; N, 8.67; S, 9.78%.

IR (KBr, cm^{-1}): 3482 (w), 2978 (w), 2933 (w), 1595 (s), 1558 (s), 1495 (s), 1418 (s), 1354 (m), 1283 (s), 1190 (w), 1117 (w), 743 (w).

ESI$^+$ MS (*m/z*): 1921,1865 (calcd. 1921.1801), 77% [M − AcO]$^+$.

{(AcO)$_2$Pr$_2 \subset$ [Ni$_2$(L^3)$_2$(L$^{3'}$)$_2$]}

Yield: 83% (82 mg).

Elemental analysis

Calcd. for $C_{70}H_{94}O_{18}N_{12}S_6Ni_2Pr_2$: C, 42.43; H, 4.78; N, 8.48; S, 9.71%. Found: C, 42.12; H, 4.68; N, 8.30; S, 9.73%.

IR (KBr, cm^{-1}): 3429 (w), 2976 (w), 2934 (w), 1595 (s), 1557 (s), 1495 (vs), 1418 (s), 1354 (m), 1280 (m), 1254 (m), 1190 (w), 1123 (w), 741 (w).

ESI$^+$ MS (*m/z*): 1923.1902 (calcd. 1923.1836), 100% [M − AcO]$^+$; 2005.19, 13% [M + Na]$^+$.

7.3.14 Silver(I) {2}−metallacoronates, {M $\subset$ [Ag$_2$(L^3)$_2$]} (M = Ba^{2+}, Sr^{2+}, Ca^{2+})

H$_2$L^3 (45.5 mg, 0.1 mmol) was added to solutions of AgNO$_3$ (17.0 mg, 0.1 mmol) and 0.05 mmol M(NO$_3$)$_2$ (M = Ba^{2+}, Sr^{2+} and Ca^{2+}) in 1 mL MeOH and a few drops of H$_2$O. The ligand dissolved quickly and the mixtures were stirred at room temperature for 30 min. Two drops of Et$_3$N were added, which resulted in an immediate deposition of the complexes from the reaction mixtures as colorless solids. They were filtered off, washed with a small amount of MeOH and dried in vacuum. Single crystals suitable for X–ray analysis were obtained by slow evaporation of solutions of the complexes in CH$_2$Cl$_2$/MeOH mixtures.

M = Ba^{2+}, Sr^{2+}, Ca^{2+}
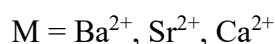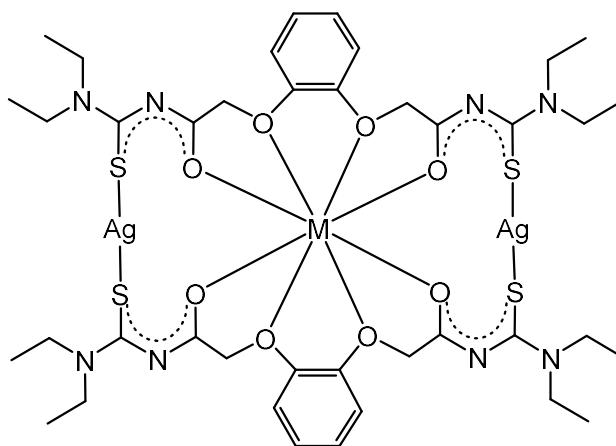
{Ba ⊂ [Ag$_2$(L^3)$_2$]}

Yield: 84% (53 mg).

Elemental analysis

Calcd. for {Ba ⊂ [Ag$_2$(L^3)$_2$]} · 2 H$_2$O, C$_{40}$H$_{60}$O$_{10}$N$_8$S$_4$Ag$_2$Ba: C, 37.12; H, 4.67; N, 8.66; S, 9.91%. Found: C, 37.00; H, 5.10; N, 8.26; S, 9.97%.

IR (KBr, cm^{-1}): 3425 (w), 2970 (w), 2924 (w), 1570 (vs), 1508 (vs), 1423 (s), 1346 (w), 1250 (s), 1126 (m), 1030 (w), 748 (w).

^{1}H NMR (400 MHz, CDCl$_3$, ppm): 6.87 (br, 8H, Ph); 4.46 (br, 4H, OCH$_2$); 4.15 (br, 4H, OCH$_2$); 3.79 (br, 8H, NCH$_2$); 3.41 (br, 8H, NCH$_2$); 1.03 (t, J = 7.0 Hz, 24H, CH$_3$).

^{13}C{^{1}H} NMR (CDCl$_3$, ppm): 176.4 (C=S); 168.6 (C=O); 146.7, 121.8, 112.9 (Ph); 71.5 (OCH$_2$); 46.6, 45.2 (NCH$_2$); 13.0, 12.7 (CH$_3$).

{Sr ⊂ [Ag$_2$(L^3)$_2$]}

Yield: 86% (52 mg).

Elemental analysis

Calcd. for $C_{40}H_{56}O_8N_8S_4Ag_2Sr$: C, 39.75; H, 4.67; N, 9.27; S, 10.61%. Found: C, 39.57; H, 4.84; N, 9.25; S, 10.71%.

IR (KBr, cm^{-1}): 3437 (w), 3238 (w), 2974 (w), 2932 (w), 1578 (vs), 1504 (vs), 1427 (s), 1350 (m), 1246 (s), 1123 (m), 1038 (w), 872 (w), 745 (w).

^{1}H NMR (400 MHz, CDCl$_3$, ppm): 6.99 (br, 8H, Ph); 4.79 (br, 8H, OCH$_2$); 3.74 (q, J = 6.9 Hz, 8H, NCH$_2$); 3.41 (q, J = 6.9 Hz, 8H, NCH$_2$); 1.15 (t, J = 7.0 Hz, 12H, CH$_3$); 1.04 (t, J = 7.2 Hz, 12H, CH$_3$).

^{13}C{^{1}H} NMR (CDCl$_3$, ppm): 187.8 (C=S); 166.3 (C=O); 146.3, 121.0, 112.3 (Ph); 71.1 (OCH$_2$); 47.6, 45.9 (NCH$_2$); 12.9, 12.1 (CH$_3$).

{Ca ⊂ [Ag$_2$(L^3)$_2$]}

Yield: 67% (39 mg).

Elemental analysis

Calcd. for $C_{40}H_{56}O_8N_8S_4Ag_2Ca$: C, 41.38; H, 4.86; N, 9.65; S, 11.05%. Found: C, 41.18; H, 5.06; N, 9.50; S, 10.35%.

IR (KBr, cm^{-1}): 3425 (w), 2970 (w), 2932 (w), 1582 (s), 1504 (s), 1431 (s), 1346 (m), 1246 (s), 1126 (m), 1042 (w), 829 (w), 741 (w).

^{1}H NMR (400 MHz, CDCl$_3$, ppm): 6.97 (br, 8H, Ph); 4.78 (br, 4H, OCH$_2$); 4.72 (br, 4H, OCH$_2$); 3.57 (br, 8H, NCH$_2$); 3.19 (br, 8H, NCH$_2$); 1.04 (t, J = 7.2 Hz, 12H, CH$_3$), 1.03 (t, J = 6.8 Hz, 12H, CH$_3$)

^{13}C{^{1}H} NMR (CDCl$_3$, ppm): 188.6 (C=S); 165.9 (C=O); 146.1, 121.9, 112.1 (Ph); 70.7 (OCH$_2$); 47.7, 46.2 (NCH$_2$); 12.7, 12.0 (CH$_3$).

7.3.15 Mercury(II) {2−metallacryptates, {M ⊂ [Hg$_2$(L^3)$_3$]} (M = Ba^{2+}, Sr^{2+})

H$_2$L^3 (68.3 mg, 0.15 mmol) was added to solutions of Hg(NO$_3$)$_2$ · H$_2$O (34.3 mg, 0.1 mmol) and 0.05 mmol M(NO$_3$)$_2$ (M = Ba^{2+}, Sr^{2+}) in 1 mL MeOH and a few drops of H$_2$O. The ligand dissolved rapidly and the mixtures were stirred at room temperature for 30 min. Addition of 3 drops of Et$_3$N resulted in the deposition of colorless solids, which were filtered off, washed with a small amount of MeOH and dried in vacuum. Single crystals suitable for X–ray analysis were obtained by slow evaporation of solutions of the complexes in CH$_2$Cl$_2$/MeOH mixtures.

$$M = Ba^{2+}, Sr^{2+}$$
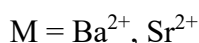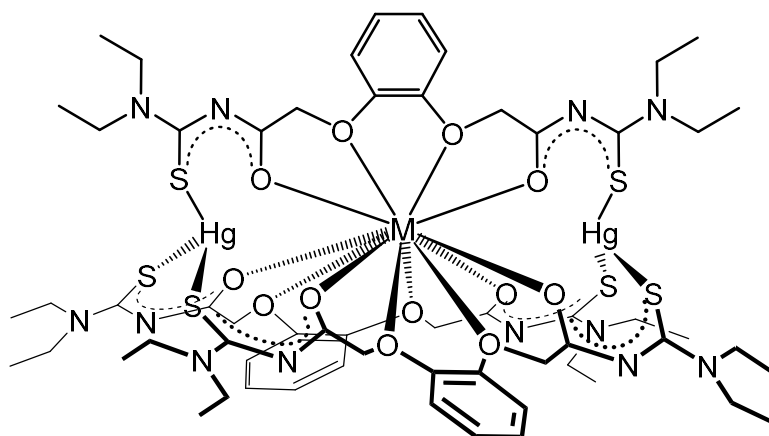
{Ba ⊂ [Hg₂(L³)₃]}

Yield: 95% (90 mg).

Elemental analysis

Calcd. for {Ba ⊂ [Hg₂(L³)₃]} · 3 H₂O, $C_{60}H_{90}O_{15}N_{12}S_6Hg_2Ba$: C, 36.95; H, 4.65; N, 8.62; S, 9.86%. Found: C, 36.83; H, 4.53; N, 8.80; S, 9.57%.

IR (KBr, cm⁻¹): 3445 (w), 2974 (w), 2932 (w), 1599 (s), 1574 (s), 1504 (s), 1423 (s), 1348 (m), 1250 (m), 1121 (m), 1042 (w), 961 (w), 737 (w).

¹H NMR (400 MHz, CDCl₃, ppm): 6.79 – 6.76 (m, 6H, Ph), 6.72 – 6.69 (m, 6H, Ph); 4.62 (br, 12H, OCH₂); 3.71 (q, J = 6.4 Hz, 12H, NCH₂); 3.47 (q, J = 6.4 Hz, 12H, NCH₂); 1.16 (t, J = 6.0 Hz, 18H, CH₃); 0.97 (t, J = 6.0 Hz, 18H, CH₃)

¹³C{¹H} NMR (CDCl₃, ppm): 178.8 (C=S); 173.2 (C=O); 147.5, 120.8, 113.1 (Ph); 71.2 (OCH₂); 46.1, 45.4 (NCH₂); 13.2, 12.8 (CH₃).

{Sr ⊂ [Hg₂(L³)₃]}

Yield: 88% (81 mg).

Elemental analysis

Calcd. for {Sr ⊂ [Hg₂(L³)₃]} · 2 H₂O, $C_{60}H_{88}O_{14}N_{12}S_6Hg_2Sr$: C, 38.28; H, 4.71; N, 8.93; S, 10.22%. Found: C, 38.39; H, 4.45; N, 9.03; S, 9.75%.

IR (KBr, cm⁻¹): 3442 (w), 2972 (w), 2932 (w), 2870 (w), 1603 (s), 1506 (s), 1423 (s), 1350 (s), 1256 (s), 1121 (s), 1053 (m), 962 (m), 739 (w), 598 (w).

¹H NMR (400 MHz, CDCl₃, ppm): 6.91 – 6.88 (m, 6H, Ph), 6.85 – 6.83 (m, 6H, Ph); 4.78 (br, 12H, OCH₂); 3.72 (q, J = 6.8 Hz, 12H, NCH₂); 3.47 (q, J = 6.8 Hz, 12H, NCH₂); 1.22 (t, J = 6.8 Hz, 18H, CH₃); 1.02 (t, J = 6.8 Hz, 18H, CH₃).

^{13}C{^{1}H} NMR (CDCl$_3$, ppm): 181.4 (C=S); 172.3 (C=O); 148.2, 119.6, 111.6 (Ph); 69.8 (OCH$_2$); 46.4, 46.0 (NCH$_2$); 12.9, 12.7 (CH$_3$).

7.4. Crystal structure determination

The intensities for the X–ray determinations were collected on *STOE* IPDS 2T or *Bruker* D8 Venture instruments with Mo/Kα radiation. The space groups were determined using *CHECK–HKL*.[82] Semi-empirical or numerical absorption corrections were carried out by the *SADABS* or *X–RED32* programs.[83-84] Structure solution and refinement were performed with the *SHELXS 97*,[85] *SHELXS 86,*[85] and *SHELXL 2014/7* programs included in the *WinGX* program package.[86-87] Hydrogen atoms were calculated for idealized positions and treated with the 'riding model' option of *SHELXL*. In case of the ammonium-containing inclusion complexes {NH$_4 \subset$ [Fe$_2$(L^3)$_3$]}(PF$_6$) and {NH$_4 \subset$ [Co$_2$(L^3)$_3$]}(PF$_6$), hydrogen atoms of the guest ammonium cations were calculated based on the electron density of the Fourier map difference and refined. Tables containing more information about crystal data, refinement, positional parameters and *ORTEP–3* [87] ellipsoid drawings are given as Supplementary material. A full set of crystallographic data including anisotropic thermal parameters, complete lists of bond lengths and angles, cif files and structure validation results are contained in the enclosed CD ROM.

Summary

This thesis describes the synthesis and characterization of well-ordered and multinuclear complexes developed from three aroylbis(N,N-dialkylthiourea) ligands.
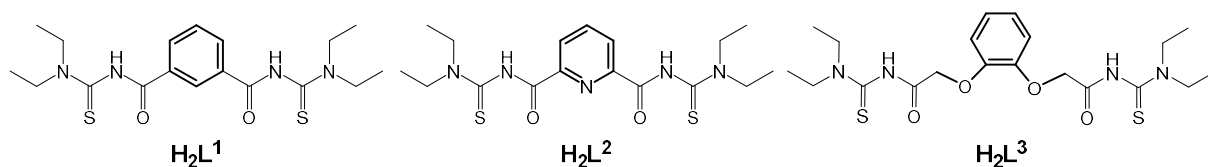
First reactions were carried out with the ligands H_2L^1 and H_2L^2 in order to establish an effective route for the synthesis of oligometallic complexes based on aroylbis(N,N-dialkylthioureas). The reaction of the ligand H_2L^1 with the octahedral Fe^{3+} ions results in the formation of the dinuclear Fe(III) complex $[Fe_2(L^1)_3]$ possessing a cryptand-like structure, however, with an empty molecular hole (Scheme 1).
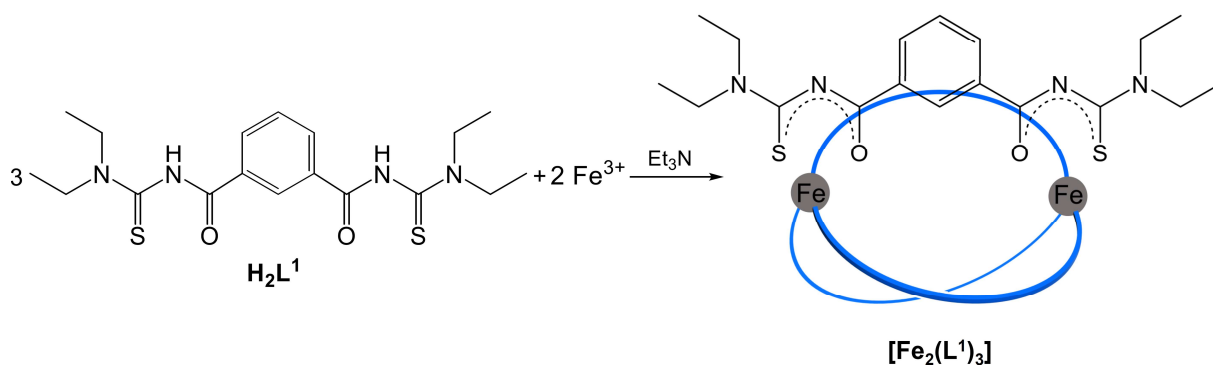
Scheme 1 Synthesis and structure of a dinuclear complex derived from H_2L^1.

Applying the same conditions for the reaction with H_2L^2, the anionic mononuclear Fe(III) complex $[Fe(L^2)_2]^-$ was formed and isolated with the large counter cation Tl^+. It is remarkable that when the counterion Tl^+ is added together with the Fe^{3+} ions to H_2L^2, the reaction gives rise to a cationic species, which can be separated as PF_6^- salt (Scheme 2). The resulting trinuclear complex with the composition of $\{Tl \subset [Fe_2(L^2)_3]\}(PF_6)$ was characterized by elemental analysis, IR spectroscopy and X-ray structure analysis. Such a simple procedure was also successfully exploited in the synthesis of other multinuclear systems derived from the aroylbis(N,N-dialkylthioureas), H_2L^2 and H_2L^3.
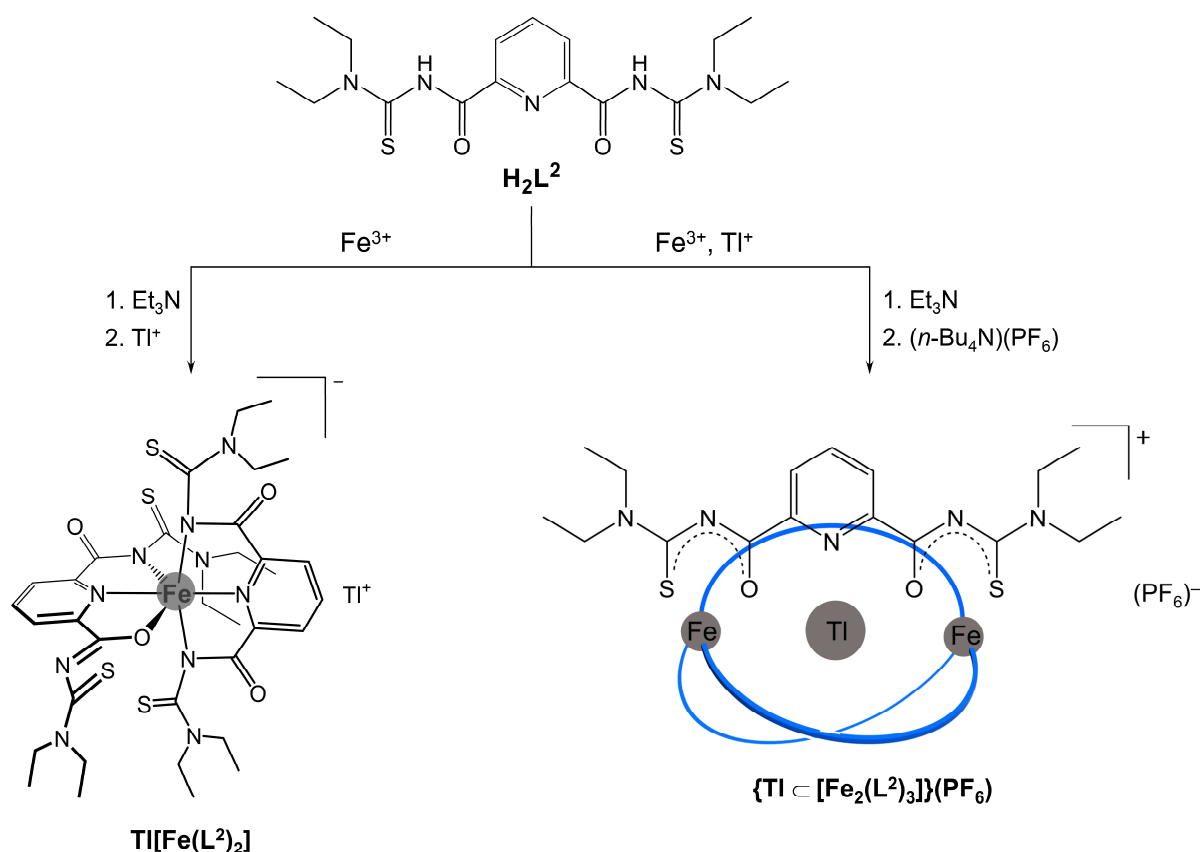
Scheme 2 Reactions of the ligand H$_2$L^2 with metal ions.

Various oligonuclear complexes with well-defined compositions and molecular structures (Schemes 3 and 4) were prepared in good yields by stoichiometric one-pot reactions of the ligands H$_2$L^2 or H$_2$L^3 and mixtures of a 'hard cation' and a 'softer metal ion' in the presence of a supporting base. The used 'hard cations' can be varied over a wide range including main group, transition metal, rare earth metal ions and even non-metal ions like NH$_4^+$. In the effective synthetic approach, the hard ions play an essential role as templates for the construction of the ligand-metal assemblies, which could be perceived as host–guest systems. By means of directional interactions, namely coordination or hydrogen bonds, with hard (and borderline) donor atoms from the ligand backbones, the hard cations are encapsulated in the central voids of the metallamacrocycles constructed from the coordination of the softer metal ions and the thiourea moieties of the deprotonated ligands. From the point of view of host-guest chemistry, the multinuclear systems are structurally classified according to topologically equivalent organic macrocyclic systems, such as crown ethers, lariate-ethers and cryptands.
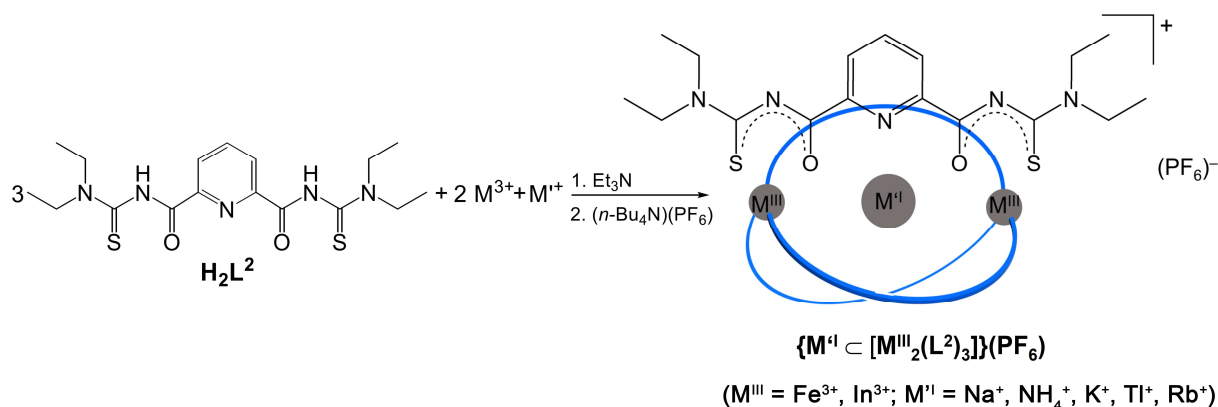
Scheme 3 Synthesis and structural topology of the trinuclear complexes derived from H_2L^2.

In case of the novel ligand H_2L^3, the systematic variation of metal ions used reveals the compositional and structural dependence of the resulting assemblies on the transition metal ions and guest cations, which can be effectively used in rational design of mixed-metal systems. Transition metal ions control the topology of the coordination assemblies using their well-defined coordination geometry. Specifically, the six-coordinate octahedral Fe^{3+}, Co^{3+} ions and five-coordinate Hg^{2+} ions facilitate the three-dimensional metallacryptates, whereas the four-coordinate pseudo square-planar Cu^{2+} ions and two-coordinate Ag^+ ions lead to two-dimensional metallacoronate architectures. When the transition metal ions enable complexes with the coordination numbers of four or six like Ni^{2+} ions, the strict control of stoichiometry of the reactants allows the selective formation of the corresponding structure types. In each multinuclear complex series, the size of the guest cations exerts influence on structural features of the coordination assemblies, such as metal–metal distances, conformations of ligand backbones and the planarity of chelate rings. In some cases, the change of the size of the guest cations brings about dramatic changes in the structural design of the products, for example, the formation of guest-induced {3}-metallacoronate $\{Cs \subset [M^{II}_3(L^3)_3]\}(PF_6)$ *vs.* {2}-metallacoronates $\{M^I \subset [M^{II}_2(L^3)_2]\}(PF_6)$ (M^I = Rb^+, K^+, Tl^+; M^{II} = Cu(II), Ni(II)), or the conversion of the {2}-metallacryptate $\{Ba \subset [Ni_2(L^3)_3]\}$ into the hitherto unprecedented metallalariate-ethers $\{(MeOH)_2M_2 \subset [Ni_2(L^3)_2(L^{3'})_2]\}$ (M = Sr^{2+}, Ca^{2+}). Beyond the metal ion properties, the structures of the ligands determine the overall architecture. Compared with the rigid ligand H_2L^2, the $O–CH_2$ bonds between the chelating groups and the central phenylene ring are responsible for the higher order of size, denticity and flexibility of the ligand H_2L^3. This structural feature is a good explanation for the successful adaption, even the partial decomposition, of the ligand H_2L^3 in order to provide optimal components for assembly with metal ions.
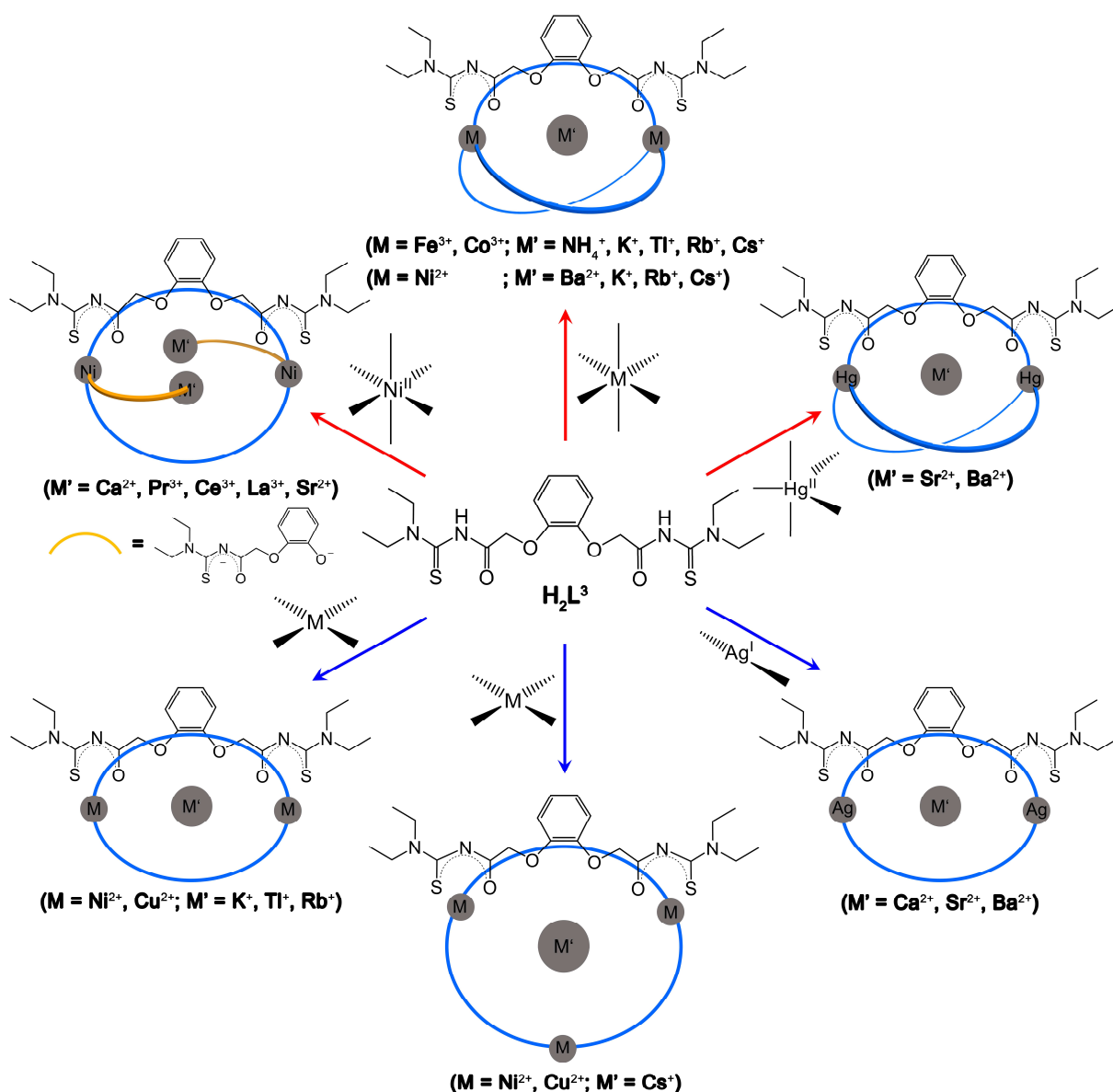
Scheme 4 Structural topologies of the oligonuclear complexes derived from H_2L^3.

In addition to the structural characterization, studies on dynamic properties in solution as well as physiochemical properties of some representative multinuclear systems were performed. The initial results are in agreement with the basic information deduced from the compositions and structures of the systems.

Zusammenfassung

Diese Arbeit befasst sich mit der Synthese und Charakterisierung definierter mehrkerniger Koordinationsverbindungen, die sich von drei unterschiedlichen Aroylbis(*N,N*-dialkyl-thioharnstoff)-Liganden ableiten.
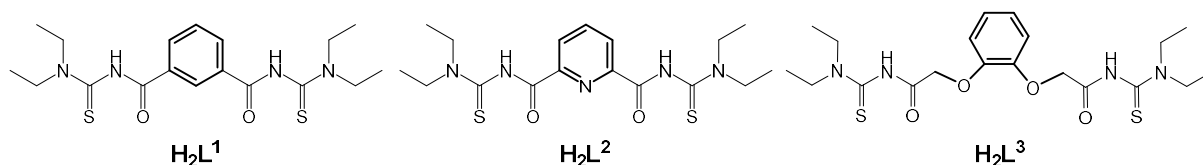
Erste orientierende Reaktionen wurden mit den Liganden H_2L^1 und H_2L^2 unternommen, um eine effektive Syntheseroute für oligometallische Komplexe mit Aroylbis(*N,N*-dialkyl-thioharnstoffen) zu erarbeiten. Die Reaktion des Liganden H_2L^1 mit oktaedrisch koordinierten Fe^{3+} Ionen ergab einen zweikernigen Fe(III)-Komplex, $[Fe_2(L^1)_3]$, der eine kryptandähnliche Struktur, jedoch mit einem unbesetzten Hohlraum, besitzt (Schema 1).
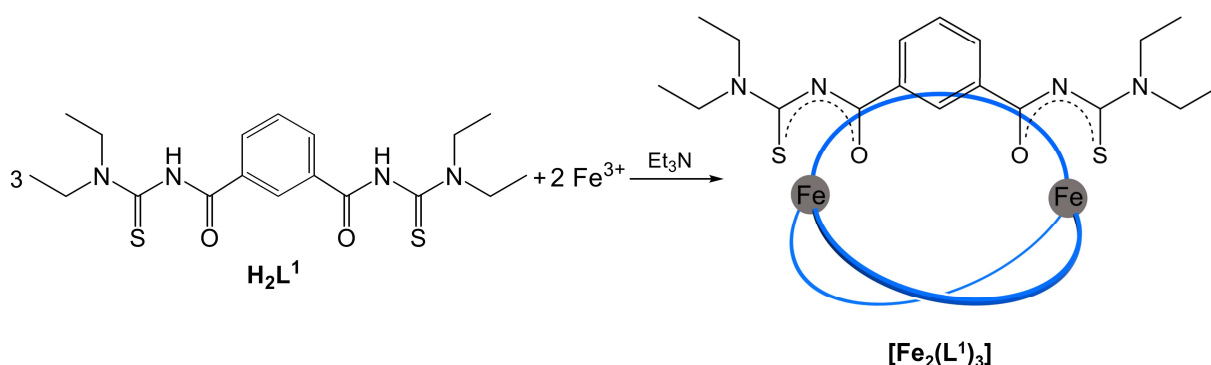
Schema 1 Synthese und Struktur eines zweikernigen Komplexes mit H_2L^1.

Eine Reaktion mit H_2L^2 liefert unter gleichen Reaktionbedingungen den anionischen mononuklearen Fe(III)-Komplex $[Fe(L^2)_2]^-$, der mit dem großen Kation Tl^+ isoliert werden kann. Es ist bemerkenswert, dass bei einer Reaktion, bei der Tl^+-Ionen zusammen mit den Fe^{3+}-Ionen zu H_2L^2 gegeben werden, eine kationische Spezies entsteht, die als PF_6^--Salz isoliert werden kann (Schema 2). Die Zusammensetzung $\{Tl \subset [Fe_2(L^2)_3]\}(PF_6)$ des resultierenden dreikernigen Komplexes wurde durch Elementaranalyse, IR-Spektroskopie und Röntgenstrukturanalyse bestimmt. Danach wurde dieses einfache Verfahren für die Synthese mehrkerniger Systeme aus den Aroylbis(*N,N*-dialkylthioharnstoffen) H_2L^2 und H_2L^3 erfolgreich auf die Synthese weiterer Verbindungen angewendet.
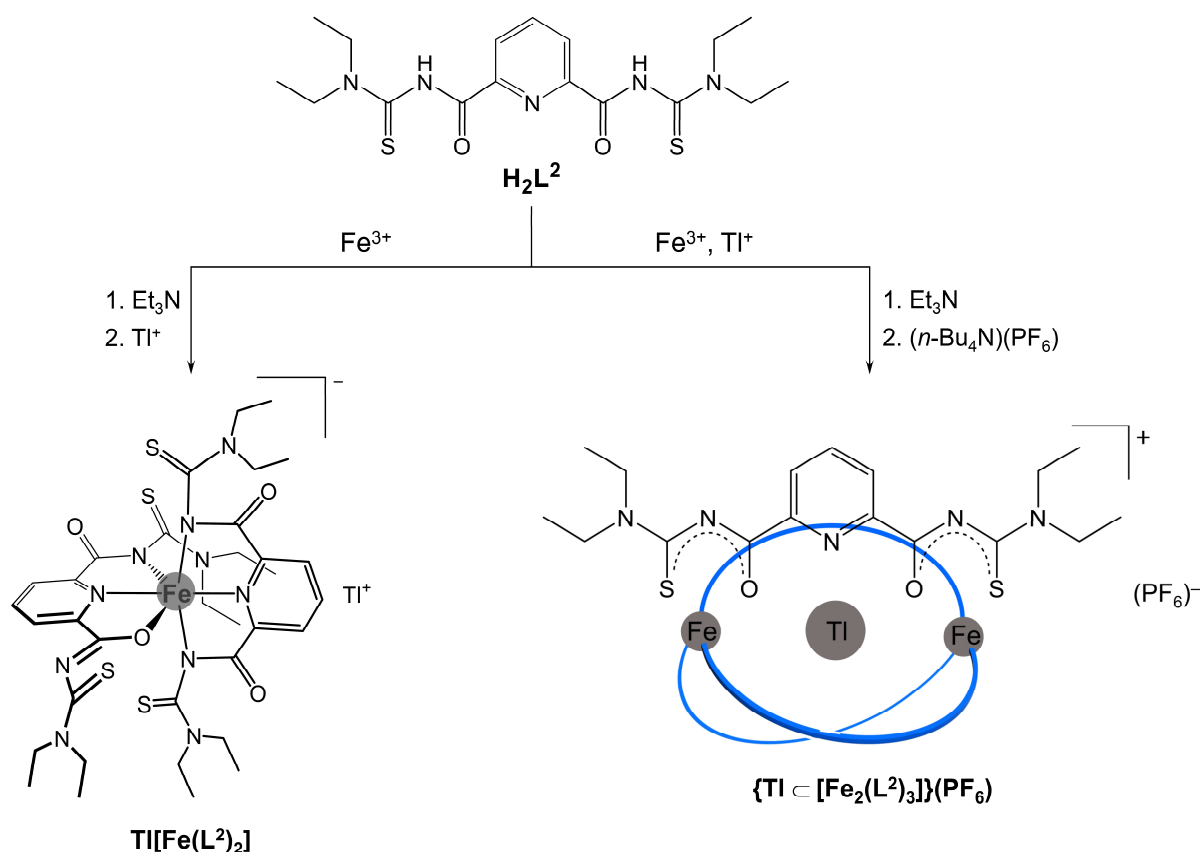
Schema 2 Reaktionen des Ligandes H_2L^2 mit Metallionen.

Eine Vielzahl mehrkerniger Komplexe mit definierten Zusammensetzungen und Strukturen (Schemas 3 und 4) wurden in guten Ausbeuten durch stöchiometrische Eintopfreaktionen der Liganden H_2L^2 und H_2L^3 und Mischungen aus einem "harten Kation" und einem "weicheren Metallion" in Gegenwart einer Hilfsbase dargestellt. Die verwendeten Kationen können in einem weiten Bereich, einschließlich Hauptgruppenmetall-, Übergangsmetall-, Lanthanoid- und sogar Nichtmetall-Ionen wie NH_4^+ variiert werden. Die verwendeten "harten Ionen" spielen eine wesentliche Rolle als Templates beim Aufbau der Ligand-Metall-Baugruppen, die als Wirt-Gast-Systeme betrachtet werden können. Durch gerichtete Wechselwirkungen, wie koordinative Bindungen oder Wasserstoffbrückenbindungen, mit harten Donoratomen der Liganden nehmen die harten Kationen definierte Positionen in den zentralen Hohlräumen der Metallamakrozyclen ein, die durch die Koordination der "weicheren Metallionen" mit den deprotonierten Aroylthioharnstoff-Einheiten aufgebaut werden. Vom Standpunkt der Wirt-Gast-Chemie könnten die mehrkernige Systeme entsprechend ihrer Topologie in Kronenether-, Kryptanden- und Lariatether-Systeme klassifiziert werden.
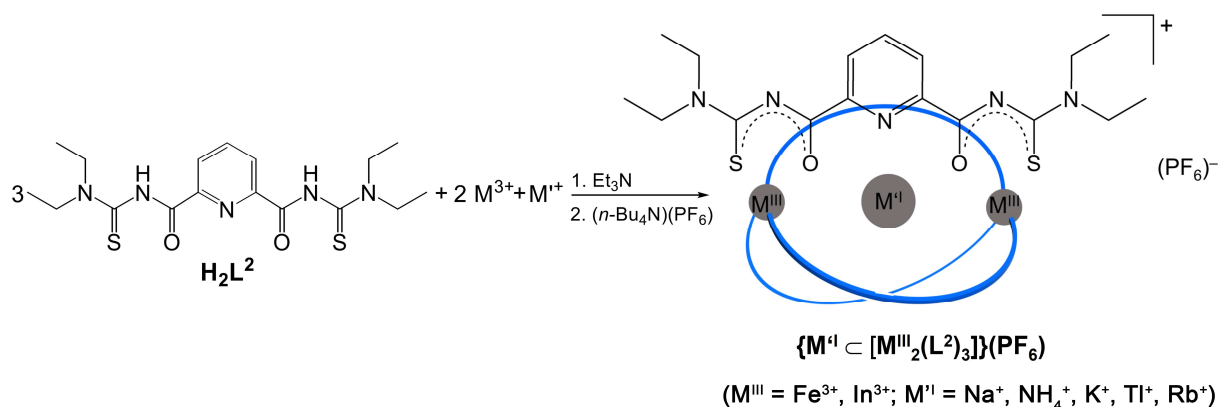
Schema 3 Synthese der dreikernigen H_2L^2-Komplexe.

Im Falle des neuartigen Ligandes H_2L^3 zeigen die erhaltenen Strukturen eine starke Abhängigkeit von den verwendeten Metallionen. Das gilt sowohl für die Übergangsmetallionen als auch für die Gastkationen. Diese Abhängigkeit kann als Basis für ein rationales Design der mehrkernigen Systeme verwendet werden. Übergangsmetallionen steuern die Topologie der Komplexe durch ihre bevorzugte Koordinationsgeometrie. Insbesondere erleichtern die oktaedrisch koordinierten Fe^{3+}, Co^{3+}-Ionen und die fünffach koordinierten Hg^{2+}-Ionen den Aufbau dreidimensionaler Metallakryptate, während die vierfach pseudo-quadratisch-planar koordinierten Cu^{2+}-Ionen und linear koordinierten Ag^{+}-Ionen zu zweidimensionalen kronenetherartigen Architekturen führen. Bei Übergangsmetallionen wie Ni^{2+}, das sowohl vierfach als auch sechsfach koordinieren kann, erlaubt die strenge Kontrolle der Stöchiometrie der Reaktionspartner die selektive Bildung entsprechender Strukturtypen. Die Gastkationen üben bei allen Strukturtypen einen großen Einfluss auf die Metall-Metall-Abstände, die Konformationen der Ligand-Rückgrate und die Planarität der Chelatringe aus. In einigen Fällen führt die Größenänderung der Gastkationen dramatische Veränderungen im Strukturtyp der Produkte herbei, z. B. bei der gastinduzierte Umwandlung der {3}-Metallakoronate $\{Cs \subset [M^{II}_3(L^3)_3]\}(PF_6)$ in {2}-Metallakoronate $\{M^{I} \subset [M^{II}_2(L^3)_2]\}(PF_6)$ (M^{I} = Rb^{+}, K^{+}, Tl^{+}; M^{II} = Cu(II), Ni (II)), oder bei der Umwandlung von {2}-Metallakryptaten $\{Ba \subset [Ni_2(L^3)_3]\}$ zu den neuartigen Metallalariatethern $\{(MeOH)_2M_2 \subset [Ni_2(L^3)_2(L^{3'})_2]\}$ (M = Sr^{2+}, Ca^{2+}). Jenseits der Eigenschaften der Metallionen bestimmen auch die Strukturen der Liganden die Gesamtarchitektur. Im Vergleich mit dem starren Liganden H_2L^2 sind die O–CH_2 Bindungen zwischen den chelatbildenden Gruppen und dem zentralen Phenylenring verantwortlich für die größere Flexibilität des Liganden H_2L^3. Dieses Strukturmerkmal ist eine gute Erklärung für die erfolgreiche Anpassung dieses Ligandes H_2L^3 an die koordinationschemischen Anforderungen der verwendeten Metallionen.
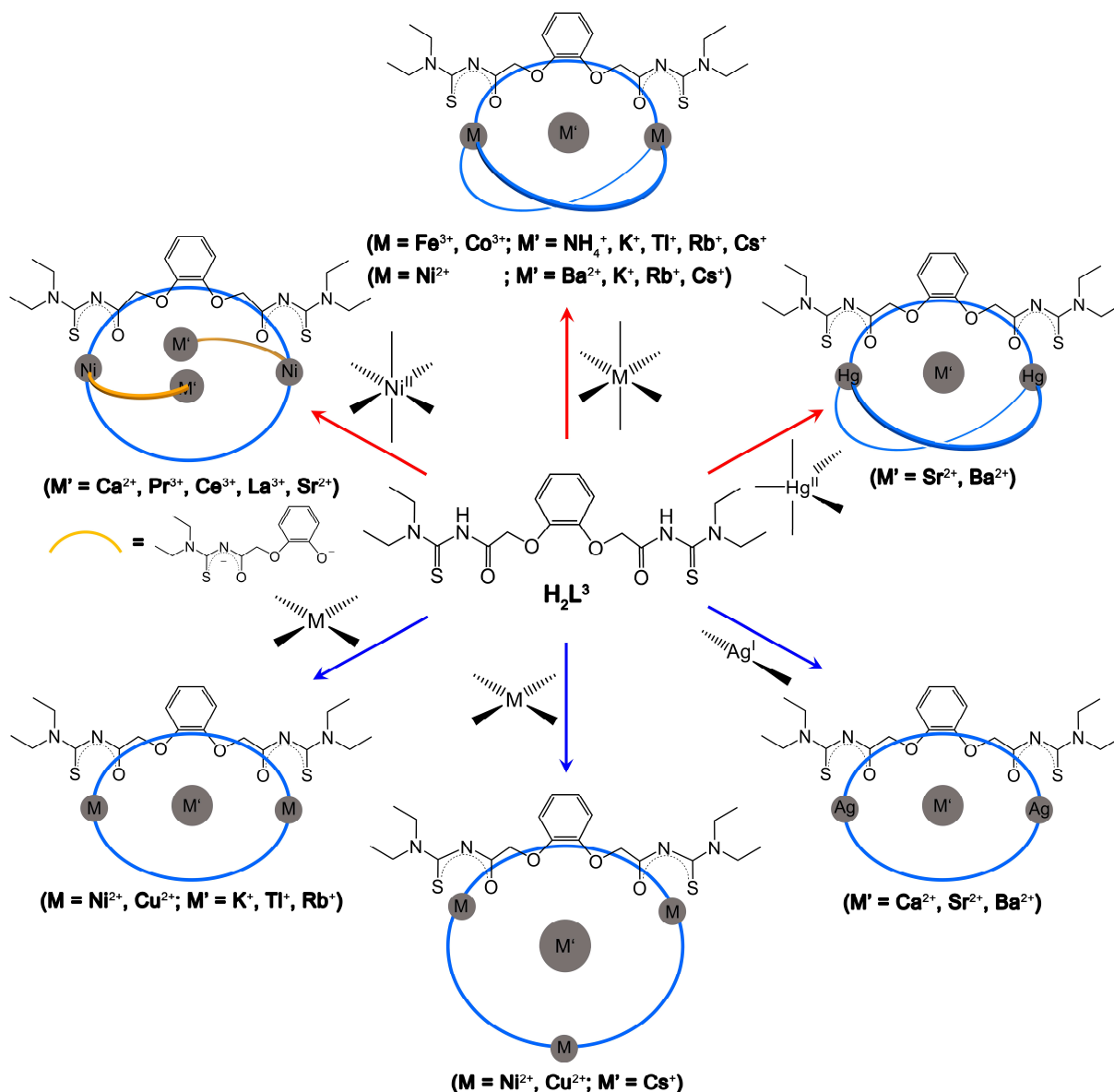
Schema 4 Strukturelle Topologie der mehrkernigen H_2L^3-Komplexe.

Zusätzlich zur strukturellen Charakterisierung der erhaltenen Mehrkernkomplexe wurden Untersuchungen zu dynamischen Eigenschaften in Lösung, und zu physikochemischen Parametern einiger repräsentativer Systeme durchgeführt. Die erhalten Ergebnisse sind in Übereinstimmung mit den grundlegenden Informationen, die aus den Strukturen der Systeme abgeleitet werden konnten.

References

1. Cook, T. R.; Zheng, Y.-R.; Stang, P. J., *Chem. Rev.* **2013,** *113*, 734.

2. Kryschenko, Y. K.; Seidel, S. R.; Arif, A. M.; Stang, P. J., *J. Am. Chem. Soc.* **2003,** *125*, 5193.

3. Cotton, F. A.; Lin, C.; Murillo, C. A., *Inorg. Chem.* **2001,** *40*, 478.

4. Caulder, D. L.; Powers, R. E.; Parac, T. N.; Raymond, K. N., *Angew. Chem. Int. Ed.* **1998,** *37*, 1840.

5. Fujita, M.; Oguro, D.; Miyazawa, M.; Oka, H.; Yamaguchi, K.; Ogura, K., *Nature* **1995,** *378*, 469.

6. Leininger, S.; Olenyuk, B.; Stang, P. J., *Chem. Rev.* **2000,** *100,* 853.

7. Fujita, M.; Umemoto, K.; Yoshizawa, M.; Fujita, N.; Kusukawa, T.; Biradha, K., *Chem. Commun.* **2001**, 509.

8. L. Caulder, D.; N. Raymond, K., *J. Chem. Soc., Dalton Trans.* **1999**, 1185.

9. Cotton, F. A.; Lin, C.; Murillo, C. A., *Acc. Chem. Res.* **2001,** *34*, 759.

10. Gianneschi, N. C.; Masar, M. S.; Mirkin, C. A., *Acc. Chem. Res.* **2005,** *38*, 825.

11. Nencki, M., *Ber. Dtsch. Chem. Ges.* **1873,** *6*, 598.

12. Dixon, A. E.; Taylor, J., *J. Chem. Soc., Trans.* **1908,** *93*, 18.

13. Douglass, I. B.; Dains, F. B., *J. Am. Chem. Soc.* **1934,** *56*, 719.

14. Beyer, L.; Hoyer, E.; Hennig, H.; Kirmse, R.; Hartmann, H.; Liebscher, J., *J. Prakt. Chem.* **1975,** *317*, 829.

15. Knuuttila, P.; Knuuttila, H.; Hennig, H.; Beyer, L., *Acta Chem. Scand.* **1982,** *36(A)*, 541.

16. Fitzl, G.; Beyer, L.; Sieler, J.; Richter, R.; Kaiser, J.; Hoyer, E., *Z. Anorg. Allg. Chem.* **1977,** *433*, 237.

17. Sacht, C.; Datt, M. S.; Otto, S.; Roodt, A., *J. Chem. Soc., Dalton Trans.* **2000**, 727.

18.   Richter, R.; Beyer, L.; Kaiser, J., *Z. Anorg. Allg. Chem.* **1980,** *461*, 67.

19.   Mandal, H.; Ray, D., *Inorg. Chim. Acta* **2014,** *414*, 127.

20.   Weiqun, Z.; Wen, Y.; Liqun, X.; Xianchen, C., *J. Inorg. Biochem.* **2005,** *99*, 1314.

21.   Huy, N. H.; Abram, U., *Inorg. Chem.* **2007,** *46*, 5310.

22.   Sieler, J.; Richter, R.; Hoyer, E.; Beyer, L.; Lindqvist, O.; Andersen, L., *Z. Anorg. Allg. Chem.* **1990,** *580*, 167.

23.   Bensch, W.; Schuster, M., *Z. Anorg. Allg. Chem.* **1992,** *615*, 93.

24.   Abram, U.; Abram, S.; Alberto, R.; Schibli, R., *Inorg. Chim. Acta* **1996,** *248*, 193.

25.   Braun, U.; Richter, R.; Sieler, J.; Yanovsky, A. I.; Struchkov, Y. T., *Z. Anorg. Allg. Chem.* **1985,** *529*, 201.

26.   Bensch, W.; Schuster, M., *Z. Anorg. Allg. Chem.* **1992,** *611*, 99.

27.   Koch, K. R.; Bourne, S., *J. Mol. Struct.* **1998,** *441*, 11.

28.   Köhler, R.; Kirmse, R.; Richter, R.; Sieler, J.; Hoyer, E.; Beyer, L., *Z. Anorg. Allg. Chem.* **1986,** *537*, 133.

29.   Richter, R.; Sieler, J.; Köhler, R.; Hoyer, E.; Beyer, L.; Hansen, L. K., *Z. Anorg. Allg. Chem.* **1989,** *578*, 191.

30.   R. Koch, K.; A. Bourne, S.; Coetzee, A.; Miller, J., *J. Chem. Soc., Dalton Trans.* **1999**, 3157.

31.   Selvakumaran, N.; Bhuvanesh, N. S. P.; Karvembu, R., *Dalton Trans.* **2014,** *43*, 16395.

32.   Koch, K. R.; Hallale, O.; Bourne, S. A.; Miller, J.; Bacsa, J., *J. Mol. Struct.* **2001,** *561*, 185.

33.   Bourne, S. A.; Hallale, O.; Koch, K. R., *Cryst. Growth Des.* **2005,** *5*, 307.

34.   Rodenstein, A.; Griebel, J.; Richter, R.; Kirmse, R., *Z. Anorg. Allg. Chem.* **2008,** *634*, 867.

35. Schwade, V. D.; Kirsten, L.; Hagenbach, A.; Lang, E. S.; Abram, U., *Polyhedron* **2013,** *55*, 155.

36. Nguyen, H. H.; Pham, C. T.; Rodenstein, A.; Kirmse, R.; Abram, U., *Inorg. Chem.* **2011,** *50*, 590.

37. Wioppiold, T. A.; Ackermann, J.; Lang, E. S.; Abram, U., *Polyhedron* **2015,** *87*, 202.

38. Jegathesh, J. J., Freie Universität Berlin, Berlin, **2013**.

39. Schröder, U.; Beyer, L.; Sieler, J., *Inorg. Chem. Commun.* **2000,** *3*, 630.

40. Dixon, A. E.; Taylor, J., *J. Chem. Soc., Trans.* **1912,** *101*, 558.

41. Yokoyama, M.; Ikuma, T.; Obara, N.; Togo, H., *J. Chem. Soc., Perkin Trans. 1* **1990**, 3243.

42. Sharghi, H.; Zare, A., *Synthesis* **2006,** *06*, 999.

43. Saalfrank, R. W.; Maid, H.; Scheurer, A., *Angew. Chem. Int. Ed.* **2008,** *47*, 8794.

44. Yeh, R. M.; Davis, A. V.; Raymond, K. N., Supramolecular Systems: Self-assembly. In *Comprehensive Coordination Chemistry II*, Second ed.; Fujita M. , P. A., Creutz C. , Ed. Elsevier Ltd.; **2003**; Vol. 7, pp 327.

45. Nakamoto, K., *Infrared and Raman Spectra of Inorganic and Coordination Compounds, Part A, Theory and Applications in Inorganic Chemistry, *. 6th ed.; Wiley; **2009**.

46. Saalfrank, R. W.; Seitz, V.; Heinemann, F. W.; Göbel, C.; Herbst-Irmer, R., *J. Chem. Soc., Dalton Trans.* **2001**, 599.

47. El Fallah, M. S.; Badyine, F.; Vicente, R.; Escuer, A.; Solans, X.; Font-Bardia, M., *Chem. Commun.* **2006**, 3113.

48. Albrecht, M.; Latorre, I.; Liu, Y.; Fröhlich, R., *Z. Naturforsch., B: Chem. Sci.* **2010,** *65*, 331.

49. Behrendt, S.; Beyer, L.; Dietze, F.; Kleinpeter, E.; Hoyer, E.; Ludwig, E.; Uhlemann, E., *Inorg. Chim. Acta* **1980,** *43*, 141.

50. Beyer, L.; Behrendt, S.; Kleinpeter, E.; Borsdorf, R.; Hoyer, E., *Z. Anorg. Allg. Chem.* **1977,** *437*, 282.

51. Sanders, J. K. M.; Hunter, B. K.; Jameson, C. J.; Romeo, G., *Chem. Phys. Lett.* **1988,** *143*, 471.

52. Bensch, W.; Schuster, M., *Zeitschrift für Kristallographie - Crystalline Materials* **1995,** *210*, 68.

53. Perez, H.; Mascarenhas, Y.; Plutin, A. M.; Souza Correa, R. d.; Duque, J., *Acta Crystallogr. Sect. E* **2008,** *64*, m503.

54. Gunasekaran, N.; Jerome, P.; Ng, S. W.; Tiekink, E. R. T.; Karvembu, R., *J. Mol. Catal. A: Chem.* **2012,** *353–354*, 156.

55. Yang, W.; Liu, H.; Li, M.; Wang, F.; Zhou, W.; Fan, J., *J. Inorg. Biochem.* **2012,** *116*, 97.

56. Tan, S. S.; Al-abbasi, A. A.; Mohamed Tahir, M. I.; Kassim, M. B., *Polyhedron* **2014,** *68*, 287.

57. Parish, R. V., Mössbauer spectroscopy In *NMR, NQR, EPR, and Mössbauer spectroscopy in inorganic chemistry*, Ellis Horwood Limited; **1990**.

58. Bott, A. W., *Current Separations* **1997,** *16*, 61.

59. Zanello, P., Consecutive Electron Transfer Processes. In *Inorganic Electrochemistry: Theory, Practice and Application*, The Royal Society of Chemistry; **2003**; p 99.

60. Richardson, D. E.; Taube, H., *Inorg. Chem.* **1981,** *20*, 1278.

61. Robin, M. B.; Day, P., Mixed Valence Chemistry-A Survey and Classification. In *Advances in Inorganic Chemistry and Radiochemistry*, Emeléus, H. J.; Sharpe, A. G., Eds. Academic Press; **1968**; Vol. 10, pp 247.

62. Ribeiro da Silva, M. A. V.; Ribeiro da Silva, M. D. M. C.; da Silva, L. s. C. M.; Gomes, J. R. B.; Damas, A. M.; Dietze, F.; Hoyer, E., *Inorg. Chim. Acta* **2003,** *356*, 95.

63. Pérez, H.; O'Reilly, B.; Plutín, A. M.; Martínez, R.; Durán, R.; Collado, I. G.; Mascarenhas, Y. P., *J. Coord. Chem.* **2011,** *64*, 2890.

64. Saeed, S.; Rashid, N.; Hussain, R.; Malik, M. A.; O'Brien, P.; Wong, W.-T., *New J. Chem.* **2013,** *37*, 3214.

65. Arslan, H.; Flörke, U.; Külcü, N.; Emen, M. F., *J. Coord. Chem.* **2006,** *59*, 223.

66. Shannon, R., *Acta Crystallogr. Sect. A* **1976,** *32*, 751.

67. Ugur, D.; Arslan, H.; Külcü, N., *Russ. J. Coor. Chem.* **2006,** *32*, 669.

68. Fujita, M.; Sasaki, O.; Mitsuhashi, T.; Fujita, T.; Yazaki, J.; Yamaguchi, K.; Ogura, K., *Chem. Commun.* **1996**, 1535.

69. Lee, S. B.; Hwang, S.; Chung, D. S.; Yun, H.; Hong, J.-I., *Tetrahedron Lett.* **1998,** *39*, 873.

70. Hallale, O.; Bourne, S. A.; Koch, K. R., *CrystEngComm* **2005,** *7*, 161.

71. Richter, R.; Dietze, F.; Schmidt, S.; Hoyer, E.; Poll, W.; Mootz, D., *Z. Anorg. Allg. Chem.* **1997,** *623*, 135.

72. Berhe, H. G.; Bourne, S. A.; Bredenkamp, M. W.; Esterhuysen, C.; Habtu, M. M.; Koch, K. R.; Luckay, R. C., *Inorg. Chem. Commun.* **2006,** *9*, 99.

73. Habtu, M. M.; Bourne, S. A.; Koch, K. R.; Luckay, R. C., *New J. Chem.* **2006,** *30*, 1155.

74. Richter, R.; Sieler, J.; Beyer, L.; Lindqvist, O.; Andersen, L., *Z. Anorg. Allg. Chem.* **1985,** *522*, 171.

75. Weiqun, Z.; Wen, Y.; Lihua, Q.; Yong, Z.; Zhengfeng, Y., *J. Mol. Struct.* **2005,** *749*, 89.

76. Richter, R.; Sieler, J.; Köhler, R.; Hoyer, E.; Beyer, L.; Leban, I.; Golič, L., *Z. Anorg. Allg. Chem.* **1989,** *578*, 198.

77. Wells, A. F., *Structural Inorganic Chemistry*. 4th ed.; Clarendon Press - Oxford; Oxford University Press, Ely House, London W1, **1975**; p 70.

78. Cordero, B.; Gomez, V.; Platero-Prats, A. E.; Reves, M.; Echeverria, J.; Cremades, E.; Barragan, F.; Alvarez, S., *Dalton Trans.* **2008**, 2832.

79. Singh, K.; Long, J. R.; Stavropoulos, P., *J. Am. Chem. Soc.* **1997,** *119*, 2942.

80. Bondi, A., *J. Phys. Chem.* **1964,** *68*, 441.

81. *WinEPR SimFonia*, Version 1.25; Bruker Instruments, Inc.: Billerica, MA USA, 1995.

82. Kretschmar, M. *CHECK-HKL*, Universität Tübingen, Germany, 1998.

83. Sheldrick, G. M. *SADABS*, Universität Göttingen, Germany, 2014.

84. *X-RED32*, STOE & Cie GmbH: Darmstadt, Germany, 2002.

85. Sheldrick, G., *Acta Crystallogr. Sect. A* **2008,** *64*, 112.

86. Sheldrick, G., *Acta Crystallogr. Sect. C* **2015,** *71*, 3.

87. Farrugia, L., *J. Appl. Crystallogr.* **2012,** *45*, 849.

Appendix

Crystallographic data

1. [Fe$_2$(L^1)$_3$]

Table 1. Crystal data and structure refinement for [Fe$_2$(L^1)$_3$].

Empirical formula	C$_{54}$H$_{72}$O$_6$N$_{12}$S$_5$Fe$_2$
Formula weight	1289.29
Instrument	Bruker D8 Venture
Temperature	100(2) K
Wavelength	0.71073 Å
Crystal system	Monoclinic
Space group	P 2$_1$/c
Unit cell dimensions	a = 11.729(1) Å α = 90°.
	b = 38.013(3) Å β = 95.90(1)°.
	c = 13.717(1) Å γ = 90°.
Volume	6083.4(8) Å^3
Z	4
Density (calculated)	1.408 g/cm^3
Absorption coefficient	0.741 mm^{-1}
F(000)	2704
Crystal size	0.25 x 0.20 x 0.17 mm^3
Theta range for data collection	2.373 to 24.999°.
Index ranges	-13<=h<=13, -45<=k<=45, -16<=l<=16
Reflections collected	130438
Independent reflections	10708 [R(int) = 0.0362]
Completeness to theta = 24.999°	99.9 %
Absorption correction	Semi-empirical from equivalents
Max. and min. transmission	0.7456 and 0.7040
Refinement method	Full-matrix least-squares on F^2
Data / restraints / parameters	10707 / 0 / 721
Goodness-of-fit on F^2	1.174
Final R indices [I>2sigma(I)]	R1 = 0.0346, wR2 = 0.0703
R indices (all data)	R1 = 0.0399, wR2 = 0.0720
Largest diff. peak and hole	0.286 and -0.307 e/Å^3

Table 2. Atomic coordinates (x 10^4) and equivalent isotropic displacement parameters (Å^2 x 10^3) for [Fe$_2$(L^1)$_3$]. U(eq) is defined as one third of the trace of the orthogonalized U^{ij} tensor.

	x	y	z	U(eq)
Fe(1)	7394(1)	1445(1)	2169(1)	13(1)
Fe(2)	3175(1)	1010(1)	-1952(1)	13(1)
C(01)	4002(2)	1850(1)	422(2)	14(1)
C(02)	4413(2)	2072(1)	1187(2)	14(1)
C(03)	3881(2)	2397(1)	1299(2)	20(1)
C(04)	2965(2)	2499(1)	654(2)	23(1)
C(05)	2557(2)	2281(1)	-109(2)	21(1)
C(06)	3071(2)	1954(1)	-233(2)	15(1)
C(10)	5434(2)	1973(1)	1884(2)	13(1)
C(11)	6370(2)	2112(1)	3452(2)	14(1)
C(12)	7366(2)	2403(1)	4911(2)	21(1)
C(13)	6972(2)	2260(1)	5855(2)	29(1)
C(14)	5638(2)	2672(1)	4008(2)	21(1)
C(15)	5926(2)	2958(1)	3307(2)	29(1)
N(10)	5537(2)	2155(1)	2705(1)	15(1)
N(11)	6473(2)	2381(1)	4081(1)	17(1)
O(10)	6105(1)	1742(1)	1582(1)	16(1)
S(10)	7200(1)	1740(1)	3713(1)	16(1)
C(20)	2637(2)	1721(1)	-1073(2)	14(1)
C(21)	1520(2)	1731(1)	-2612(2)	15(1)
C(22)	-13(2)	1768(1)	-3992(2)	19(1)
C(23)	365(2)	1950(1)	-4891(2)	26(1)
C(24)	139(2)	2215(1)	-2656(2)	22(1)
C(25)	-697(2)	2145(1)	-1910(2)	30(1)
N(20)	1930(2)	1878(1)	-1755(1)	17(1)
N(21)	600(2)	1892(1)	-3068(1)	18(1)
O(20)	2951(1)	1402(1)	-1020(1)	16(1)
S(20)	2122(1)	1383(1)	-3199(1)	18(1)
C(31)	7063(2)	1221(1)	-1155(2)	14(1)
C(32)	8207(2)	1259(1)	-775(2)	14(1)
C(33)	9072(2)	1235(1)	-1397(2)	18(1)
C(34)	8795(2)	1181(1)	-2386(2)	20(1)
C(35)	7659(2)	1159(1)	-2775(2)	19(1)
C(36)	6784(2)	1176(1)	-2157(2)	15(1)

C(40)	8489(2)	1334(1)	289(2)	15(1)
C(41)	9895(2)	1566(1)	1442(2)	16(1)
C(42)	11454(2)	1618(1)	2774(2)	27(1)
C(43)	12120(2)	1954(1)	2760(2)	36(1)
C(44)	11725(2)	1285(1)	1246(2)	26(1)
C(45)	11581(3)	898(1)	1463(3)	44(1)
N(40)	9555(2)	1430(1)	558(1)	19(1)
N(41)	10976(2)	1505(1)	1795(1)	19(1)
O(40)	7689(1)	1287(1)	837(1)	16(1)
S(40)	9038(1)	1839(1)	2080(1)	21(1)
C(50)	5555(2)	1139(1)	-2558(2)	15(1)
C(51)	4393(2)	955(1)	-3954(2)	16(1)
C(52)	3151(2)	901(1)	-5500(2)	26(1)
C(53)	3459(3)	597(1)	-6105(3)	63(1)
C(54)	4804(2)	1316(1)	-5337(2)	24(1)
C(55)	4364(2)	1679(1)	-5094(2)	35(1)
N(50)	5370(2)	1087(1)	-3510(1)	18(1)
N(51)	4144(2)	1041(1)	-4895(1)	19(1)
O(50)	4805(1)	1171(1)	-1957(1)	16(1)
S(50)	3526(1)	659(1)	-3400(1)	16(1)
C(61)	4882(2)	576(1)	1043(2)	14(1)
C(62)	5506(2)	479(1)	1921(2)	14(1)
C(63)	5344(2)	146(1)	2310(2)	17(1)
C(64)	4566(2)	-86(1)	1835(2)	19(1)
C(65)	3943(2)	11(1)	965(2)	18(1)
C(66)	4100(2)	342(1)	561(2)	14(1)
C(70)	6343(2)	728(1)	2446(2)	14(1)
C(71)	7931(2)	744(1)	3658(2)	15(1)
C(72)	9219(2)	740(1)	5200(2)	21(1)
C(73)	10354(2)	568(1)	5060(2)	27(1)
C(74)	7672(2)	291(1)	4880(2)	20(1)
C(75)	6625(2)	393(1)	5380(2)	32(1)
N(70)	7024(2)	585(1)	3167(1)	16(1)
N(71)	8267(2)	601(1)	4535(1)	16(1)
O(70)	6285(1)	1049(1)	2187(1)	16(1)
S(70)	8751(1)	1077(1)	3214(1)	16(1)
C(80)	3434(2)	442(1)	-386(2)	14(1)
C(81)	1809(2)	271(1)	-1444(2)	16(1)
C(82)	340(2)	-17(1)	-2584(2)	22(1)

C(83)	-857(2)	62(1)	-2311(2)	28(1)
C(84)	1449(2)	-355(1)	-1220(2)	20(1)
C(85)	926(2)	-370(1)	-255(2)	23(1)
N(80)	2602(2)	220(1)	-683(1)	16(1)
N(81)	1221(2)	-18(1)	-1747(1)	17(1)
O(80)	3748(1)	718(1)	-807(1)	16(1)
S(80)	1416(1)	673(1)	-1983(1)	18(1)
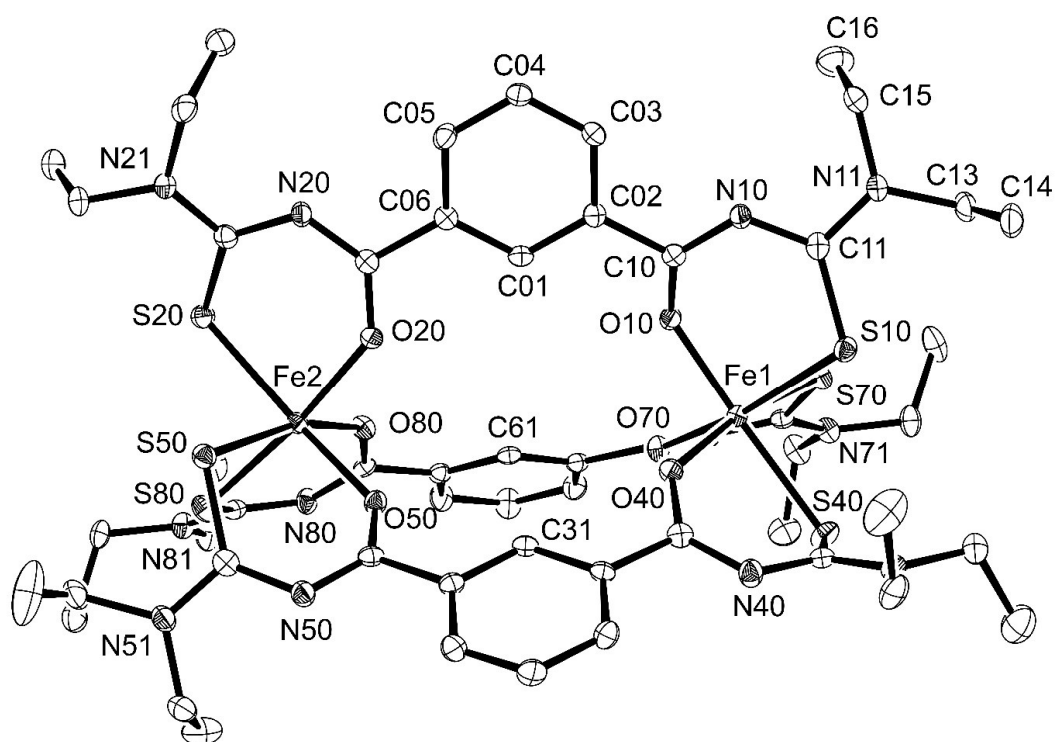
Figure 1: Ellipsoid plot (50% probability) of [Fe$_2$(L^1)$_3$].

114

2. [TlFe(L^2)$_2$] · 0.5 CH$_2$Cl$_2$

Table 3. Crystal data and structure refinement for [TlFe(L^2)$_2$] · 0.5 CH$_2$Cl$_2$.

Empirical formula	C$_{34.5}$H$_{47}$O$_4$N$_{10}$S$_4$ClFeTl
Formula weight	1089.73
Instrument	STOE IPDS 2T
Temperature	200(2) K
Wavelength	0.71073 Å
Crystal system	Monoclinic
Space group	P 2$_1$/c
Unit cell dimensions	a = 12.708(2) Å α = 90°.
	b = 22.616(5) Å β = 127.28(1)°.
	c = 19.602(3) Å γ = 90°.
Volume	4482.6(15) Å^3
Z	4
Density (calculated)	1.615 g/cm^3
Absorption coefficient	4.207 mm^{-1}
F(000)	2176
Crystal size	0.260 x 0.227 x 0.180 mm^3
Theta range for data collection	3.211 to 24.999°.
Index ranges	-14<=h<=15, -26<=k<=26, -23<=l<=23
Reflections collected	23516
Independent reflections	7768 [R(int) = 0.0902]
Completeness to theta = 24.999°	98.4 %
Absorption correction	Integration
Max. and min. transmission	0.5332 and 0.3174
Refinement method	Full-matrix least-squares on F^2
Data / restraints / parameters	7768 / 10 / 524
Goodness-of-fit on F^2	0.981
Final R indices [I>2sigma(I)]	R1 = 0.0455, wR2 = 0.1006
R indices (all data)	R1 = 0.0754, wR2 = 0.1100
Largest diff. peak and hole	1.078 and -1.484 e/Å^3

Table 4. Atomic coordinates (x 10^4) and equivalent isotropic displacement parameters (Å^2 x 10^3) for $[\text{TlFe}(\text{L}^2)_2] \cdot 0.5\ \text{CH}_2\text{Cl}_2$. U(eq) is defined as one third of the trace of the orthogonalized U^{ij} tensor.

	x	y	z	U(eq)
Tl	1452(1)	7727(1)	2509(1)	51(1)
Fe	1517(1)	8145(1)	4432(1)	36(1)
N(01)	3516(5)	7940(3)	5000(3)	40(1)
C(02)	3888(6)	7395(3)	5023(4)	43(2)
C(03)	5220(7)	7254(4)	5468(5)	59(2)
C(04)	6143(6)	7683(4)	5890(5)	61(2)
C(05)	5735(6)	8251(4)	5870(4)	53(2)
C(06)	4401(6)	8379(3)	5411(4)	43(2)
O(10)	2975(5)	6444(3)	4481(4)	68(2)
C(10)	2771(7)	6966(4)	4535(5)	51(2)
N(10)	1587(5)	7231(2)	4181(3)	37(1)
C(11)	479(6)	6859(3)	3647(4)	47(2)
S(10)	-301(2)	6875(1)	2572(1)	60(1)
N(11)	87(7)	6541(3)	4013(5)	75(2)
C(12)	-992(10)	6075(5)	3497(8)	99(3)
C(13)	-2136(12)	6374(6)	3244(8)	114(4)
C(14)	713(8)	6538(4)	4935(5)	62(2)
C(15)	1449(11)	5987(4)	5384(7)	91(3)
O(20)	4500(5)	9401(2)	5671(4)	66(2)
C(20)	3797(6)	8963(3)	5269(5)	46(2)
N(20)	2477(5)	8943(3)	4685(4)	42(1)
C(21)	1661(6)	9451(3)	4380(5)	45(2)
S(20)	408(2)	9437(1)	4452(2)	60(1)
N(21)	1867(6)	9870(3)	4007(4)	56(2)
C(22)	2716(8)	9822(4)	3745(6)	69(2)
C(23)	1954(12)	9553(5)	2846(8)	100(4)
C(24)	1013(9)	10410(4)	3689(6)	70(2)
C(25)	1528(11)	10872(4)	4370(7)	96(3)
N(31)	-392(4)	8066(2)	4059(3)	38(1)
C(32)	-1398(5)	8149(3)	3233(4)	40(2)
C(33)	-2690(6)	8094(3)	2966(4)	46(2)
C(34)	-2914(6)	7966(4)	3551(5)	50(2)
C(35)	-1848(6)	7899(3)	4415(4)	43(2)

C(36)	-588(6)	7962(3)	4650(4)	38(2)
O(40)	333(3)	8356(2)	3156(3)	38(1)
C(40)	-944(6)	8341(3)	2734(4)	41(2)
N(40)	-1828(5)	8519(3)	1958(3)	42(1)
C(41)	-1519(6)	8726(4)	1434(4)	48(2)
S(40)	-1051(2)	8240(1)	1003(1)	59(1)
N(41)	-1778(6)	9291(3)	1218(4)	58(2)
C(44)	-1598(9)	9549(4)	605(6)	75(3)
C(45)	-2834(10)	9522(6)	-294(6)	102(4)
C(42)	-2227(10)	9671(4)	1590(7)	84(3)
C(43)	-3763(12)	9605(8)	1109(8)	161(7)
O(50)	595(4)	7897(2)	6151(3)	48(1)
C(50)	651(6)	7954(3)	5546(4)	36(2)
N(52)	1744(4)	8022(2)	5593(3)	37(1)
C(51)	2963(6)	7943(3)	6417(4)	43(2)
S(50)	3657(2)	7279(1)	6700(1)	61(1)
N(55)	3480(5)	8412(3)	6919(4)	48(2)
C(55)	2856(9)	8988(4)	6675(6)	78(3)
C(54)	2459(12)	9181(6)	7168(9)	132(5)
C(52)	4799(7)	8381(4)	7764(5)	68(2)
C(53)	4765(8)	8134(5)	8482(5)	83(3)
C(60)	5529(18)	9376(7)	3517(11)	136(13)
Cl(1A)	4799(12)	9415(9)	2481(7)	104(5)
Cl(1B)	4637(14)	9859(17)	2679(16)	142(16)
Cl(2)	4960(7)	8796(4)	3787(5)	132(3)
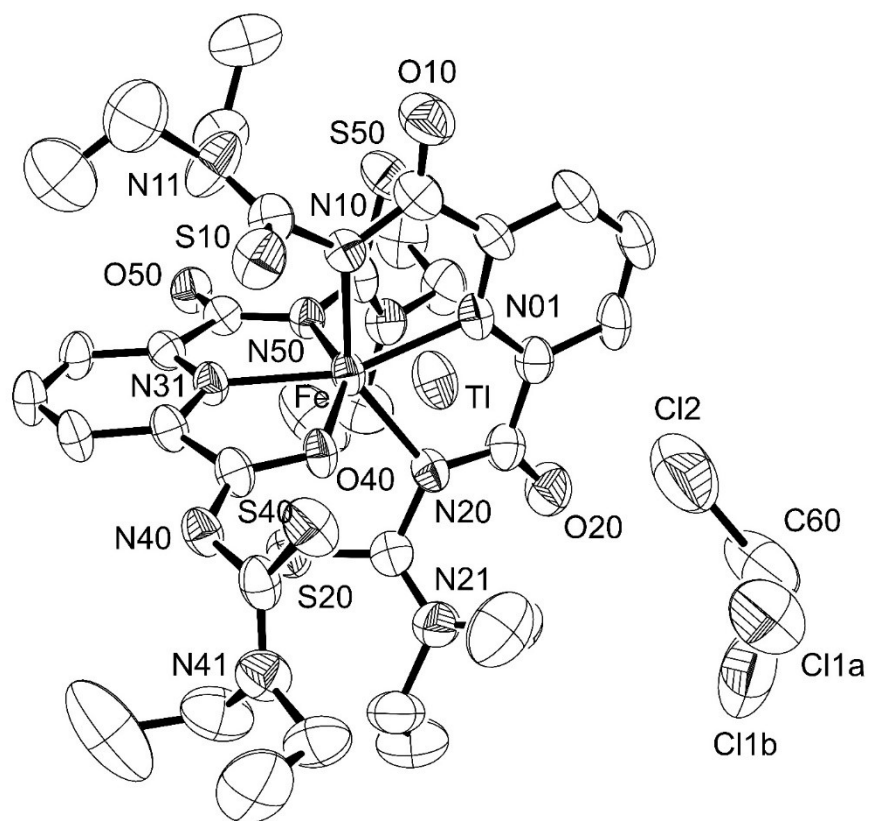
Figure 2: Ellipsoid plot (50% probability) of $[TlFe(L^2)_2] \cdot 0.5\ CH_2Cl_2$.

3. $\{Rb \subset [Fe_2(L^2)_3]\}(PF_6) \cdot 0.5\ CH_2Cl_2$

Table 5. Crystal data and structure refinement for $\{Rb \subset [Fe_2(L^2)_3]\}(PF_6) \cdot 0.5\ CH_2Cl_2$.

Empirical formula	$C_{51.5}H_{70}O_6N_{15}S_6PF_6ClFe_2Rb$
Formula weight	1565.19
Measurement instrument	STOE IPDS 2T
Temperature	200(2) K
Wavelength	0.71073 Å
Crystal system	Monoclinic
Space group	$P\ 2_1/c$
Unit cell dimensions	a = 15.864(2) Å $\qquad \alpha = 90°.$
	b = 12.369(1) Å $\qquad \beta = 101.41(1)°.$
	c = 35.400(3) Å $\qquad \gamma = 90°.$
Volume	$6809(1)\ Å^3$
Z	4
Density (calculated)	$1.527\ g/cm^3$
Absorption coefficient	$1.457\ mm^{-1}$
F(000)	3211
Crystal size	$0.23 \times 0.20 \times 0.17\ mm^3$
Theta range for data collection	3.153 to 25.000°.
Index ranges	-18<=h<=17, -14<=k<=13, -42<=l<=42
Reflections collected	28512
Independent reflections	11589 [R(int) = 0.1467]
Completeness to theta = 25.000°	96.6 %
Absorption correction	None
Refinement method	Full-matrix least-squares on F^2
Data / restraints / parameters	11589 / 0 / 794
Goodness-of-fit on F^2	0.908
Final R indices [I>2sigma(I)]	R1 = 0.0845, wR2 = 0.1976
R indices (all data)	R1 = 0.1689, wR2 = 0.2389
Largest diff. peak and hole	1.166 and -1.551 $e/Å^3$

Table 6. Atomic coordinates (x 10^4) and equivalent isotropic displacement parameters (Å^2 x 10^3) for {Rb $\subset$ [Fe$_2$(L^2)$_3$]}(PF$_6$) · 0.5 CH$_2$Cl$_2$. U(eq) is defined as one third of the trace of the orthogonalized U^{ij} tensor.

	x	y	z	U(eq)
Rb	8807(1)	5093(1)	1112(1)	51(1)
Fe(1)	10595(1)	3303(1)	1367(1)	47(1)
Fe(2)	7020(1)	6920(1)	868(1)	50(1)
N(01)	8717(5)	4685(7)	295(2)	49(2)
C(02)	9250(7)	3971(9)	181(2)	54(3)
C(03)	9306(7)	3785(8)	-206(2)	51(3)
C(04)	8780(7)	4415(9)	-484(2)	58(3)
C(05)	8238(7)	5135(9)	-374(2)	62(3)
C(06)	8207(6)	5260(8)	19(2)	50(3)
O(10)	9959(4)	3746(5)	836(1)	53(2)
C(10)	9845(7)	3352(9)	491(2)	53(3)
N(10)	10223(6)	2513(7)	377(2)	54(2)
C(11)	10731(7)	1815(9)	616(3)	57(3)
S(10)	10672(2)	1539(2)	1086(1)	63(1)
N(11)	11273(6)	1249(8)	447(2)	69(3)
C(14)	11319(9)	1431(11)	35(3)	79(4)
C(15)	10612(10)	872(11)	-238(3)	91(4)
C(12)	11965(10)	553(12)	675(4)	95(5)
C(13)	11771(12)	-619(14)	610(5)	122(6)
O(20)	7481(5)	5954(6)	497(1)	57(2)
C(20)	7577(7)	6026(9)	146(2)	53(3)
N(20)	7170(6)	6660(7)	-127(2)	55(2)
C(21)	6668(7)	7508(8)	-72(2)	50(3)
S(20)	6706(2)	8227(2)	354(1)	58(1)
N(21)	6137(6)	7865(7)	-391(2)	59(2)
C(24)	6154(8)	7370(10)	-768(3)	67(3)
C(25)	5594(11)	6415(12)	-841(3)	110(5)
C(22)	5499(8)	8703(11)	-387(3)	75(4)
C(23)	5787(10)	9836(11)	-472(4)	89(4)
N(31)	7894(5)	3926(6)	1638(2)	46(2)
C(32)	8305(6)	3168(8)	1882(2)	46(2)
C(33)	7954(7)	2776(9)	2184(3)	57(3)
C(34)	7166(7)	3138(9)	2239(3)	61(3)

C(35)	6736(7)	3913(9)	1986(2)	56(3)
C(36)	7127(6)	4280(8)	1689(2)	45(2)
O(40)	9443(4)	3193(5)	1532(1)	50(2)
C(40)	9167(6)	2825(8)	1830(2)	48(2)
N(40)	9571(6)	2154(7)	2100(2)	51(2)
C(41)	10410(7)	1927(8)	2161(2)	51(3)
S(40)	11207(2)	2568(2)	1980(1)	56(1)
N(41)	10674(6)	1122(7)	2417(2)	53(2)
C(44)	10046(7)	546(9)	2602(3)	64(3)
C(45)	9713(9)	-461(11)	2376(4)	84(4)
C(42)	11552(8)	836(9)	2546(3)	62(3)
C(43)	12011(9)	1594(11)	2870(3)	91(4)
O(50)	7199(4)	5670(6)	1237(2)	57(2)
C(50)	6697(7)	5175(8)	1429(2)	49(3)
N(50)	5905(6)	5387(7)	1437(2)	51(2)
C(51)	5407(7)	6099(8)	1193(3)	51(3)
S(50)	5532(2)	6358(3)	726(1)	60(1)
N(51)	4775(6)	6537(7)	1327(2)	57(2)
C(54)	4661(8)	6316(11)	1728(3)	79(4)
C(55)	5279(10)	6986(13)	2022(3)	104(5)
C(52)	4123(8)	7264(10)	1099(3)	70(3)
C(53)	3335(8)	6671(12)	918(4)	92(4)
N(61)	9950(6)	6936(7)	1427(2)	49(2)
C(62)	10801(7)	6784(8)	1549(2)	49(3)
C(63)	11367(7)	7658(9)	1630(3)	57(3)
C(64)	11052(8)	8688(10)	1583(3)	69(3)
C(65)	10183(8)	8821(9)	1458(3)	58(3)
C(66)	9657(7)	7951(9)	1385(2)	51(3)
O(70)	10548(4)	4895(5)	1493(2)	49(2)
C(70)	11114(7)	5634(9)	1583(2)	51(3)
N(70)	11953(6)	5514(8)	1721(2)	60(2)
C(71)	12331(6)	4539(9)	1719(2)	51(3)
S(70)	12096(2)	3642(2)	1329(1)	54(1)
N(71)	12990(6)	4307(7)	2012(2)	54(2)
C(74)	13215(8)	5089(10)	2341(3)	74(3)
C(75)	12637(9)	4842(11)	2634(3)	91(4)
C(72)	13446(7)	3281(9)	2057(3)	60(3)
C(73)	14362(9)	3400(11)	1983(4)	90(4)
O(80)	8296(4)	7267(6)	1070(2)	50(2)
C(80)	8679(7)	8066(9)	1247(2)	50(3)

N(80)	8380(6)	9024(7)	1313(2)	57(2)
C(81)	7541(7)	9238(9)	1243(2)	53(3)
S(80)	6724(2)	8339(2)	1293(1)	62(1)
N(81)	7328(6)	10272(9)	1170(2)	68(3)
C(84)	8002(9)	11096(11)	1149(4)	86(4)
C(85)	8187(11)	11148(13)	740(4)	111(5)
C(82)	6441(8)	10651(11)	1070(3)	72(3)
C(83)	6097(9)	11143(12)	1412(3)	95(5)
P	3745(3)	9914(3)	1837(1)	82(1)
F(2)	3763(9)	11011(11)	1609(4)	186(5)
F(4)	4482(7)	9473(9)	1644(3)	141(3)
F(5)	4470(14)	10403(16)	2134(5)	255(7)
F(6)	3118(13)	9442(16)	1475(5)	265(8)
Cl(91)	6749(7)	3480(7)	687(2)	121(2)
Cl(90)	6418(7)	2381(7)	-9(2)	121(2)
C(90)	6311(12)	3528(14)	214(4)	43(4)
F(1A)	3583(12)	8685(13)	1944(5)	109(8)
F(1B)	4044(19)	9080(20)	2185(8)	132(12)
F(3A)	2889(16)	10253(15)	1944(6)	144(10)
F(3B)	3478(18)	10451(19)	2184(7)	117(12)
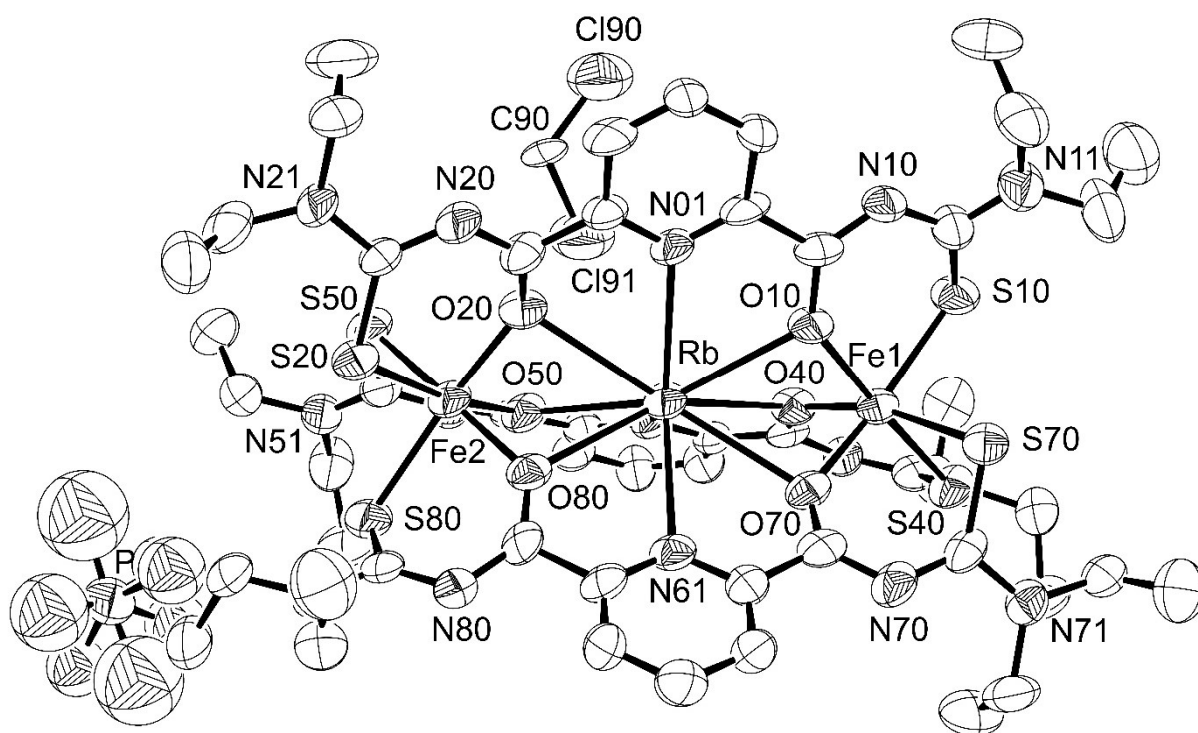
Figure 3: Ellipsoid plot (50% probability) of $\{Rb \subset [Fe_2(L^2)_3]\}(PF_6) \cdot 0.5\ CH_2Cl_2$.

4. {K ⊂ [Fe₂(L²)₃]}(PF₆) · 0.5 CH₂Cl₂

Table 7. Crystal data and structure refinement for {K ⊂ [Fe₂(L²)₃]}(PF₆) · 0.5 CH₂Cl₂.

Empirical formula	$C_{51.5}H_{70}O_6N_{15}S_6PF_6ClFe_2K$
Formula weight	1518.82
Measurement instrument	STOE IPDS 2T
Temperature	200(2) K
Wavelength	0.71073 Å
Crystal system	Monoclinic
Space group	P 2₁/c
Unit cell dimensions	a = 15.924(1) Å α = 90°.
	b = 12.326(1) Å β = 101.78(1)°.
	c = 35.501(3) Å γ = 90°.
Volume	6821.4(9) Å³
Z	4
Density (calculated)	1.479 g/cm³
Absorption coefficient	0.806 mm⁻¹
F(000)	3139
Crystal size	0.240 x 0.200 x 0.170 mm³
Theta range for data collection	3.245 to 24.999°.
Index ranges	-18<=h<=18, -14<=k<=14, -32<=l<=42
Reflections collected	31376
Independent reflections	11946 [R(int) = 0.1404]
Completeness to theta = 25.000°	99.5 %
Absorption correction	None
Refinement method	Full-matrix least-squares on F^2
Data / restraints / parameters	11946 / 1 / 794
Goodness-of-fit on F^2	0.837
Final R indices [I>2sigma(I)]	R1 = 0.0782, wR2 = 0.1866
R indices (all data)	R1 = 0.1622, wR2 = 0.2183
Largest diff. peak and hole	1.182 and -1.250 e/Å³

Table 8. Atomic coordinates (x 10^4) and equivalent isotropic displacement parameters ($\mathring{A}^2$ x 10^3) for {K $\subset$ [Fe$_2$(L^2)$_3$]}(PF$_6$) · 0.5 CH$_2$Cl$_2$. U(eq) is defined as one third of the trace of the orthogonalized U^{ij} tensor.

	x	y	z	U(eq)
Fe(1)	10579(1)	-1713(1)	1367(1)	39(1)
Fe(2)	7029(1)	1928(1)	863(1)	42(1)
K	8808(1)	98(1)	1110(1)	44(1)
N(01)	8711(4)	-311(5)	297(2)	44(2)
C(02)	9245(5)	-1035(6)	182(2)	42(2)
C(03)	9301(5)	-1188(7)	-200(3)	51(2)
C(04)	8773(5)	-582(7)	-483(3)	53(2)
C(05)	8223(5)	150(6)	-369(2)	49(2)
C(06)	8197(5)	259(6)	23(2)	43(2)
O(10)	9911(3)	-1268(4)	843(2)	46(1)
C(10)	9844(5)	-1645(6)	503(2)	41(2)
N(10)	10220(4)	-2479(5)	381(2)	45(2)
C(11)	10701(5)	-3180(6)	623(2)	46(2)
S(10)	10629(2)	-3483(2)	1088(1)	56(1)
N(11)	11270(4)	-3754(6)	462(2)	59(2)
C(12)	11927(7)	-4469(9)	687(4)	92(4)
C(13)	11734(9)	-5632(10)	626(5)	123(5)
C(14)	11312(7)	-3551(9)	48(3)	77(3)
C(15)	10620(8)	-4082(9)	-234(4)	97(4)
O(20)	7503(3)	970(4)	502(2)	48(1)
C(20)	7573(5)	1029(6)	152(3)	48(2)
N(20)	7161(4)	1672(5)	-123(2)	47(2)
C(21)	6662(5)	2519(6)	-71(2)	45(2)
S(20)	6733(1)	3252(2)	353(1)	52(1)
N(21)	6141(4)	2883(5)	-388(2)	50(2)
C(24)	6121(6)	2361(8)	-764(3)	67(3)
C(25)	5535(8)	1371(10)	-824(4)	103(4)
C(22)	5508(5)	3744(7)	-386(3)	65(3)
C(23)	5809(6)	4852(7)	-476(3)	78(3)
N(31)	7907(4)	-1067(5)	1632(2)	40(2)
C(32)	8292(4)	-1827(6)	1875(2)	37(2)
C(33)	7953(5)	-2243(6)	2171(3)	54(2)
C(34)	7151(5)	-1867(7)	2218(3)	58(2)

C(35)	6741(5)	-1122(7)	1971(3)	50(2)
C(36)	7124(5)	-715(6)	1672(2)	41(2)
O(40)	9435(3)	-1789(4)	1533(2)	43(1)
C(40)	9182(5)	-2179(6)	1827(2)	42(2)
N(40)	9566(4)	-2847(5)	2096(2)	44(2)
C(41)	10409(5)	-3088(6)	2166(2)	41(2)
S(40)	11203(1)	-2432(2)	1982(1)	49(1)
N(41)	10656(4)	-3883(5)	2415(2)	51(2)
C(42)	11563(5)	-4158(7)	2553(3)	56(2)
C(43)	11994(6)	-3427(8)	2877(3)	73(3)
C(44)	10036(6)	-4485(7)	2597(3)	61(3)
C(45)	9675(6)	-5447(8)	2371(3)	80(3)
O(50)	7207(3)	646(4)	1217(2)	47(1)
C(50)	6735(5)	156(6)	1420(2)	43(2)
N(50)	5927(4)	397(5)	1431(2)	48(2)
C(51)	5436(5)	1116(6)	1188(2)	43(2)
S(50)	5544(1)	1365(2)	717(1)	53(1)
N(51)	4803(4)	1570(5)	1318(2)	48(2)
C(54)	4709(6)	1357(8)	1722(3)	72(3)
C(55)	5316(7)	1996(10)	2010(3)	95(4)
C(52)	4157(5)	2295(7)	1094(3)	60(2)
C(53)	3358(6)	1677(9)	911(4)	97(4)
N(61)	9947(4)	1919(5)	1420(2)	40(2)
C(62)	10801(5)	1789(6)	1542(2)	38(2)
C(63)	11358(5)	2639(6)	1630(3)	49(2)
C(64)	11043(6)	3683(7)	1583(3)	61(3)
C(65)	10171(5)	3831(6)	1464(3)	53(2)
C(66)	9651(5)	2953(6)	1386(2)	44(2)
O(70)	10532(3)	-111(4)	1486(2)	42(1)
C(70)	11097(5)	629(6)	1577(2)	41(2)
N(70)	11935(4)	486(5)	1710(2)	48(2)
C(71)	12311(5)	-495(6)	1703(2)	44(2)
S(70)	12064(1)	-1381(2)	1317(1)	46(1)
N(71)	12970(4)	-712(5)	1993(2)	48(2)
C(72)	13444(5)	-1728(7)	2038(3)	56(2)
C(73)	14338(6)	-1626(9)	1960(4)	87(4)
C(74)	13208(6)	63(7)	2315(3)	61(2)
C(75)	12681(7)	-156(9)	2621(3)	83(3)
O(80)	8301(3)	2242(4)	1073(2)	46(1)
C(80)	8690(5)	3055(7)	1245(2)	45(2)

N(80)	8384(4)	4029(5)	1299(2)	53(2)
C(81)	7545(5)	4259(6)	1231(3)	49(2)
S(80)	6741(1)	3337(2)	1291(1)	56(1)
N(81)	7337(4)	5286(5)	1156(2)	55(2)
C(84)	7988(6)	6107(7)	1133(4)	84(4)
C(85)	8159(8)	6151(9)	717(5)	109(5)
C(82)	6438(5)	5668(7)	1061(3)	59(2)
C(83)	6132(6)	6117(9)	1405(3)	81(3)
C(90)	6381(11)	8522(11)	215(4)	55(5)
Cl(90)	6744(7)	8490(7)	663(3)	149(2)
Cl(91)	6371(7)	7391(7)	-10(3)	149(2)
P	3747(2)	4877(2)	1857(1)	87(1)
F(1)	4510(5)	4475(7)	1670(3)	135(3)
F(2)	3708(8)	5961(10)	1615(4)	201(4)
F(4)	4384(11)	5539(13)	2145(5)	267(7)
F(6)	3139(10)	4309(12)	1519(5)	242(6)
F(3)	2882(13)	5178(13)	1955(6)	173(8)
F(3B)	3410(20)	5460(20)	2196(10)	118(14)
F(5)	4138(12)	4083(14)	2240(6)	121(9)
F(5B)	3587(9)	3696(10)	1953(4)	108(6)
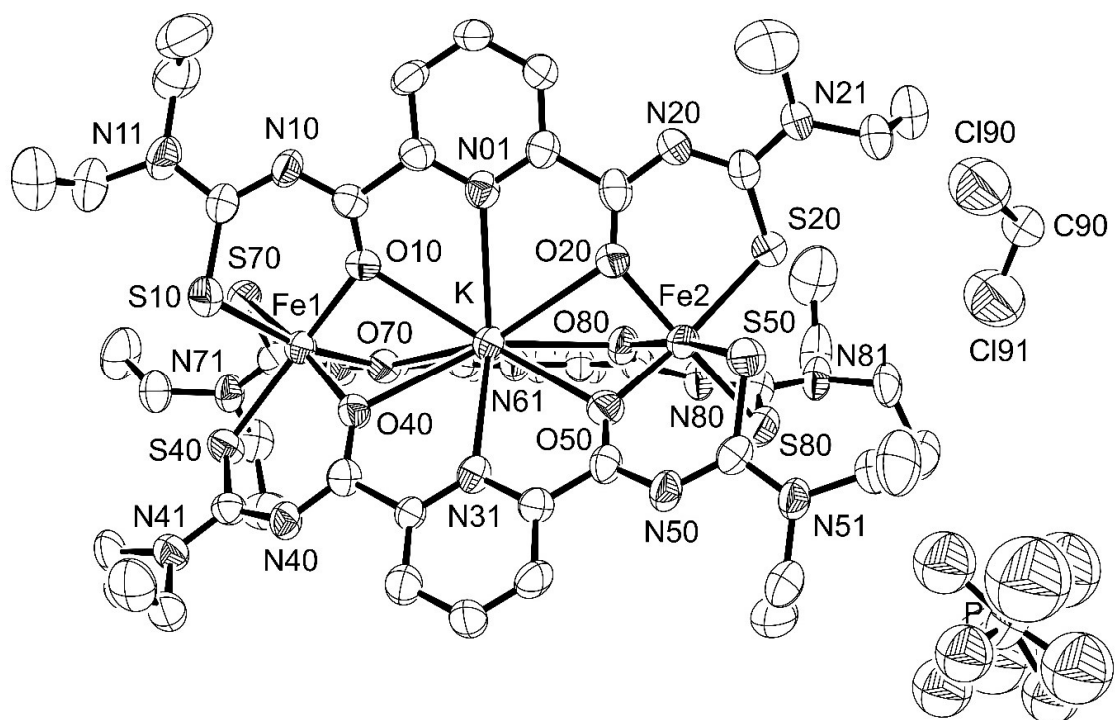
Figure 4: Ellipsoid plot (50% probability) of $\{K \subset [Fe_2(L^2)_3]\}(PF_6) \cdot 0.5\ CH_2Cl_2$.

5. $\{Na \subset [Fe_2(L^2)_3]\}(PF_6) \cdot CH_2Cl_2$

Table 9. Crystal data and structure refinement for $\{Na \subset [Fe_2(L^2)_3]\}(PF_6) \cdot CH_2Cl_2$.

Empirical formula	$C_{52}H_{71}O_6N_{15}S_6PF_6Cl_2Fe_2Na$
Formula weight	1545.15
Measurement instrument	Bruker D8 Venture
Temperature	100(2) K
Wavelength	0.71073 Å
Crystal system	Monoclinic
Space group	P 2_1/c
Unit cell dimensions	a = 15.658(1) Å $\qquad$ $\alpha = 90°$.
	b = 12.252(1) Å $\qquad$ $\beta = 101.42(2)°$.
	c = 35.108 (2) Å $\qquad$ $\gamma = 90°$.
Volume	6601.6(6) Å^3
Z	4
Density (calculated)	1.555 g/cm^3
Absorption coefficient	0.818 mm^{-1}
F(000)	3192
Crystal size	0.5 x 0.1 x 0.02 mm^3
Theta range for data collection	2.277 to 24.999°.
Index ranges	-16<=h<=18, -14<=k<=14, -41<=l<=41
Reflections collected	67549
Independent reflections	11632 [R(int) = 0.0297]
Completeness to theta = 24.999°	99.9 %
Absorption correction	Semi-empirical from equivalents
Max. and min. transmission	0.7455 and 0.7002
Refinement method	Full-matrix least-squares on F^2
Data / restraints / parameters	11631 / 26 / 837
Goodness-of-fit on F^2	1.028
Final R indices [I>2sigma(I)]	R1 = 0.0462, wR2 = 0.1250
R indices (all data)	R1 = 0.0551, wR2 = 0.1317
Largest diff. peak and hole	1.057 and -1.657 e/Å^3

Table 10. Atomic coordinates (x 10^4) and equivalent isotropic displacement parameters (Å^2 x 10^3) for {Na ⊂ [Fe$_2$(L^2)$_3$]}(PF$_6$) · CH$_2$Cl$_2$. U(eq) is defined as one third of the trace of the orthogonalized U^{ij} tensor.

	x	y	z	U(eq)
Na	3813(1)	5024(1)	1105(1)	25(1)
Fe(1)	5585(1)	3177(1)	1376(1)	10(1)
Fe(2)	1978(1)	6828(1)	864(1)	12(1)
N(01)	3700(2)	4657(2)	303(1)	11(1)
C(02)	4257(2)	3950(3)	193(1)	12(1)
C(03)	4354(2)	3817(3)	-189(1)	15(1)
C(04)	3863(2)	4463(3)	-474(1)	17(1)
C(05)	3283(2)	5197(3)	-369(1)	14(1)
C(06)	3212(2)	5258(3)	20(1)	11(1)
C(10)	4821(2)	3305(3)	513(1)	11(1)
C(11)	5731(2)	1753(3)	622(1)	14(1)
C(12)	6974(2)	485(3)	671(1)	26(1)
C(13)	6805(3)	-706(3)	588(1)	38(1)
C(14)	6332(2)	1413(3)	40(1)	23(1)
C(15)	5589(3)	914(3)	-245(1)	27(1)
N(10)	5233(2)	2487(2)	389(1)	14(1)
N(11)	6297(2)	1211(2)	452(1)	18(1)
O(10)	4865(1)	3656(2)	858(1)	13(1)
S(10)	5632(1)	1415(1)	1089(1)	17(1)
C(20)	2560(2)	6012(3)	144(1)	12(1)
C(21)	1655(2)	7529(3)	-68(1)	13(1)
C(22)	489(2)	8782(3)	-377(1)	20(1)
C(23)	799(2)	9914(3)	-459(1)	26(1)
C(24)	1151(2)	7451(3)	-773(1)	20(1)
C(25)	557(3)	6468(4)	-852(1)	37(1)
N(20)	2171(2)	6687(2)	-128(1)	13(1)
N(21)	1142(2)	7923(2)	-387(1)	14(1)
O(20)	2425(2)	5873(2)	485(1)	16(1)
S(20)	1696(1)	8211(1)	369(1)	17(1)
N(31)	4949(2)	6789(2)	1410(1)	12(1)
C(32)	5808(2)	6667(3)	1535(1)	12(1)
C(33)	6388(2)	7536(3)	1609(1)	17(1)
C(34)	6062(2)	8591(3)	1551(1)	20(1)

C(35)	5173(2)	8727(3)	1430(1)	19(1)
C(36)	4643(2)	7813(3)	1365(1)	13(1)
C(40)	6120(2)	5506(3)	1583(1)	11(1)
C(41)	7351(2)	4388(3)	1718(1)	12(1)
C(42)	8463(2)	3113(3)	2069(1)	18(1)
C(43)	9400(2)	3217(3)	2015(1)	24(1)
C(44)	8194(2)	4931(3)	2348(1)	19(1)
C(45)	7597(3)	4757(3)	2634(1)	26(1)
N(40)	6959(2)	5368(2)	1720(1)	14(1)
N(41)	7991(2)	4163(2)	2017(1)	15(1)
O(40)	5538(1)	4779(2)	1495(1)	13(1)
S(40)	7100(1)	3492(1)	1325(1)	13(1)
C(50)	3670(2)	7923(3)	1236(1)	15(1)
C(51)	2505(2)	9136(3)	1243(1)	19(1)
C(52)	1392(2)	10580(3)	1082(1)	23(1)
C(53)	1096(2)	11044(3)	1434(1)	27(1)
C(54)	2962(2)	10997(3)	1129(1)	28(1)
C(55)	3114(3)	11061(4)	720(1)	39(1)
N(50)	3364(2)	8895(2)	1290(1)	20(1)
N(51)	2298(2)	10176(3)	1170(1)	21(1)
S(50)	1700(1)	8216(1)	1309(1)	20(1)
O(50)	3268(1)	7087(2)	1078(1)	15(1)
N(61)	2883(2)	3821(2)	1637(1)	11(1)
C(62)	3281(2)	3065(3)	1888(1)	11(1)
C(63)	2927(2)	2664(3)	2195(1)	14(1)
C(64)	2128(2)	3061(3)	2246(1)	17(1)
C(65)	1704(2)	3826(3)	1986(1)	15(1)
C(66)	2104(2)	4181(3)	1686(1)	12(1)
C(70)	4166(2)	2707(3)	1833(1)	11(1)
C(71)	5409(2)	1764(3)	2168(1)	12(1)
C(72)	6589(2)	704(3)	2559(1)	18(1)
C(73)	6990(3)	1457(3)	2890(1)	26(1)
C(74)	5037(2)	327(3)	2592(1)	20(1)
C(75)	4720(2)	-652(3)	2341(1)	27(1)
N(70)	4549(2)	1999(2)	2095(1)	13(1)
N(71)	-286(2)	6427(2)	1325(1)	15(1)
S(70)	6216(1)	2464(1)	1995(1)	14(1)
O(70)	4429(1)	3109(2)	1544(1)	13(1)
C(80)	1694(2)	5064(3)	1412(1)	12(1)

C(81)	375(2)	6000(3)	1190(1)	14(1)
C(82)	-951(2)	7133(3)	1092(1)	20(1)
C(83)	-1733(2)	6481(3)	892(1)	33(1)
C(84)	-400(2)	6184(3)	1722(1)	23(1)
C(85)	218(3)	6823(3)	2028(1)	30(1)
N(80)	892(2)	5309(2)	1437(1)	13(1)
N(81)	5664(2)	969(2)	2421(1)	14(1)
S(80)	479(1)	6262(1)	715(1)	18(1)
O(80)	2184(1)	5497(2)	1207(1)	16(1)
P	8765(1)	9799(1)	1802(1)	23(1)
F(3)	8833(2)	10928(2)	1594(1)	61(1)
F(4)	8673(3)	8638(3)	1987(1)	84(1)
F(1A)	9529(2)	9317(2)	1607(1)	34(1)
F(2A)	8001(3)	10246(3)	1989(2)	83(2)
F(5A)	8082(3)	9360(3)	1433(1)	68(1)
F(6A)	9472(4)	10210(4)	2154(1)	93(2)
F(1B)	9642(14)	9426(18)	1817(8)	34(1)
F(2B)	7790(30)	10330(30)	1736(12)	83(2)
F(5B)	8594(19)	9600(20)	1354(9)	68(1)
F(6B)	8870(30)	10220(30)	2226(9)	93(2)
C(90)	8722(4)	6508(4)	9765(1)	50(1)
Cl(1)	8275(2)	6645(2)	9310(1)	108(1)
Cl(2A)	8490(5)	7518(5)	10035(1)	231(3)
Cl(2B)	7862(11)	5988(17)	9872(5)	231(3)
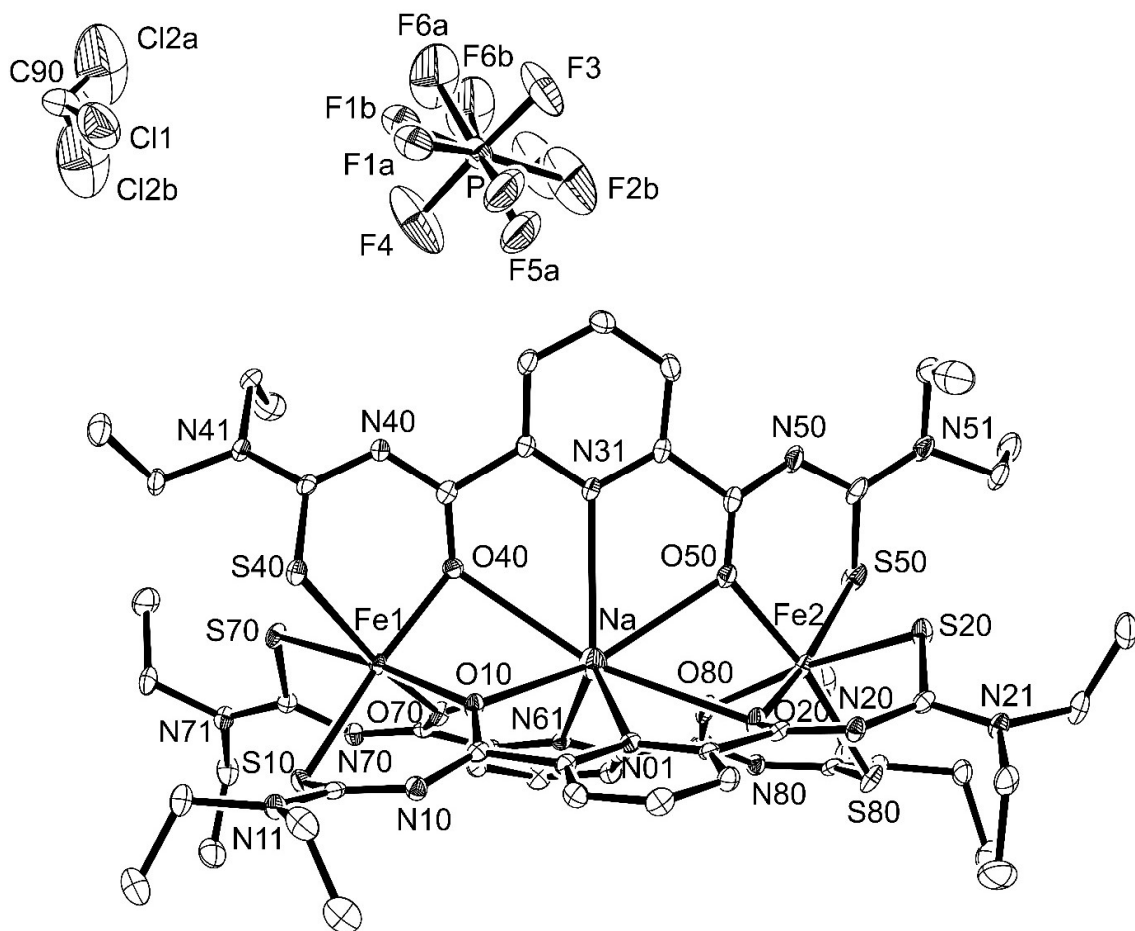
Figure 5: Ellipsoid plot (50% probability) of $\{Na \subset [Fe_2(L^2)_3]\}(PF_6) \cdot CH_2Cl_2$.

6. {Tl $\subset$ [Fe$_2$(L^2)$_3$]}(PF$_6$) $\cdot$ CH$_2$Cl$_2$

Table 11. Crystal data and structure refinement for {Tl $\subset$ [Fe$_2$(L^2)$_3$]}(PF$_6$) $\cdot$ CH$_2$Cl$_2$.

Empirical formula	C$_{52}$H$_{71}$O$_6$N$_{15}$S$_6$PF$_6$Cl$_2$Fe$_2$Tl
Formula weight	1726.53
Measurement instrument	Bruker D8 venture
Temperature	100(2) K
Wavelength	0.71073 Å
Crystal system	Monoclinic
Space group	P 2$_1$/c
Unit cell dimensions	a = 15.687(1) Å α = 90°.
	b = 12.244(1) Å β = 100.95(2)°.
	c = 35.028(2) Å γ = 90°.
Volume	6605.5(8) Å^3
Z	4
Density (calculated)	1.736 g/cm^3
Absorption coefficient	3.238 mm^{-1}
F(000)	3472
Crystal size	0.30 x 0.28 x 0.26 mm^3
Theta range for data collection	2.272 to 25.000°.
Index ranges	-18<=h<=18, -14<=k<=14, -41<=l<=41
Reflections collected	83389
Independent reflections	11639 [R(int) = 0.0385]
Completeness to theta = 25.000°	99.9 %
Absorption correction	Semi-empirical from equivalents
Max. and min. transmission	0.7455 and 0.5925
Refinement method	Full-matrix least-squares on F^2
Data / restraints / parameters	11639 / 30 / 837
Goodness-of-fit on F^2	1.047
Final R indices [I>2sigma(I)]	R1 = 0.0326, wR2 = 0.0807
R indices (all data)	R1 = 0.0394, wR2 = 0.0849
Largest diff. peak and hole	1.295 and -2.002 e/Å^3

Table 12. Atomic coordinates (x 10^4) and equivalent isotropic displacement parameters (Å^2 x 10^3) for {Tl $\subset$ [Fe$_2$(L^2)$_3$]}(PF$_6$) · CH$_2$Cl$_2$. U(eq) is defined as one third of the trace of the orthogonalized U^{ij} tensor.

	x	y	z	U(eq)
Fe(1)	4385(1)	3253(1)	3636(1)	8(1)
Fe(2)	8005(1)	6923(1)	4126(1)	10(1)
Tl	6187(1)	5077(1)	3886(1)	12(1)
N(01)	6287(2)	4670(3)	4711(1)	10(1)
C(02)	5736(3)	3963(3)	4825(1)	10(1)
C(03)	5669(3)	3816(4)	5215(1)	13(1)
C(04)	6185(3)	4455(4)	5491(1)	15(1)
C(05)	6754(3)	5191(4)	5378(1)	13(1)
C(06)	6798(3)	5269(3)	4986(1)	9(1)
C(10)	5140(3)	3331(4)	4513(1)	10(1)
C(11)	4237(3)	1787(4)	4409(1)	13(1)
C(12)	2989(3)	539(4)	4376(2)	23(1)
C(13)	3169(4)	-671(4)	4432(2)	35(1)
C(14)	3702(3)	1404(4)	5008(1)	20(1)
C(15)	4460(3)	872(4)	5275(1)	23(1)
N(10)	4771(2)	2481(3)	4642(1)	12(1)
N(11)	3687(2)	1237(3)	4589(1)	15(1)
O(10)	5019(2)	3718(2)	4169(1)	12(1)
S(10)	4268(1)	1494(1)	3928(1)	16(1)
C(20)	7432(3)	6046(4)	4855(1)	11(1)
C(21)	8356(3)	7540(4)	5070(1)	10(1)
C(22)	9547(3)	8745(4)	5386(1)	18(1)
C(23)	9264(3)	9888(4)	5473(2)	24(1)
C(24)	8850(3)	7421(4)	5775(1)	17(1)
C(25)	9420(4)	6417(4)	5850(2)	30(1)
N(20)	7825(2)	6708(3)	5127(1)	11(1)
N(21)	8877(2)	7906(3)	5390(1)	13(1)
O(20)	7556(2)	5942(3)	4507(1)	13(1)
S(20)	8334(1)	8253(1)	4639(1)	14(1)
N(31)	5033(2)	6907(3)	3567(1)	11(1)
C(32)	4174(3)	6768(3)	3450(1)	9(1)
C(33)	3598(3)	7640(4)	3379(1)	14(1)

C(34)	3919(3)	8697(4)	3434(1)	18(1)
C(35)	4805(3)	8844(4)	3548(1)	16(1)
C(36)	5342(3)	7936(4)	3613(1)	12(1)
C(40)	3860(3)	5606(4)	3405(1)	10(1)
C(41)	2631(3)	4490(4)	3266(1)	10(1)
C(42)	1533(3)	3214(4)	2911(1)	16(1)
C(43)	606(3)	3306(4)	2974(2)	21(1)
C(44)	1811(3)	5033(4)	2632(1)	17(1)
C(45)	2416(3)	4852(4)	2347(1)	24(1)
N(40)	3022(2)	5481(3)	3265(1)	12(1)
N(41)	2002(2)	4267(3)	2964(1)	13(1)
O(40)	4423(2)	4855(2)	3495(1)	11(1)
S(40)	2856(1)	3597(1)	3659(1)	12(1)
C(50)	6311(3)	8063(4)	3747(1)	13(1)
C(51)	7475(3)	9262(4)	3742(1)	18(1)
C(52)	8578(3)	10714(4)	3918(2)	23(1)
C(53)	8898(3)	11176(4)	3569(2)	24(1)
C(54)	7006(3)	11122(4)	3856(2)	27(1)
C(55)	6815(4)	11169(5)	4259(2)	42(2)
N(50)	6616(2)	9028(3)	3676(1)	19(1)
N(51)	7678(2)	10301(3)	3820(1)	19(1)
O(50)	6721(2)	7267(2)	3931(1)	13(1)
S(50)	8293(1)	8343(1)	3690(1)	19(1)
N(61)	7129(2)	3868(3)	3361(1)	10(1)
C(62)	6714(3)	3125(3)	3113(1)	10(1)
C(63)	7051(3)	2742(4)	2795(1)	13(1)
C(64)	7839(3)	3138(4)	2734(1)	14(1)
C(65)	8278(3)	3900(4)	2992(1)	14(1)
C(66)	7899(3)	4247(4)	3302(1)	11(1)
C(70)	5829(3)	2751(3)	3173(1)	11(1)
C(71)	4587(3)	1826(4)	2836(1)	10(1)
C(72)	3409(3)	783(4)	2440(1)	18(1)
C(73)	3002(3)	1552(4)	2118(1)	24(1)
C(74)	4956(3)	431(4)	2392(1)	19(1)
C(75)	5274(3)	-573(4)	2630(2)	24(1)
N(70)	5444(2)	2073(3)	2902(1)	12(1)
N(71)	4334(2)	1049(3)	2575(1)	12(1)
O(70)	5561(2)	3115(2)	3469(1)	11(1)
S(70)	3781(1)	2487(1)	3023(1)	13(1)

C(80)	8325(3)	5137(3)	3570(1)	11(1)
C(81)	9636(3)	6051(4)	3795(1)	12(1)
C(82)	10957(3)	7192(4)	3896(1)	17(1)
C(83)	11731(3)	6534(4)	4099(2)	29(1)
C(84)	10431(3)	6226(4)	3267(1)	20(1)
C(85)	9823(4)	6875(5)	2961(1)	29(1)
N(80)	9136(2)	5343(3)	3553(1)	12(1)
N(81)	10302(2)	6475(3)	3665(1)	13(1)
O(80)	7839(2)	5637(3)	3766(1)	14(1)
S(80)	9506(1)	6349(1)	4269(1)	17(1)
P	1234(1)	9882(1)	3205(1)	19(1)
F(3)	1371(3)	8695(3)	3042(1)	63(1)
F(4)	1118(3)	11041(3)	3387(1)	59(1)
F(1A)	468(2)	9403(3)	3400(1)	34(1)
F(2A)	1999(4)	10323(4)	3015(2)	70(2)
F(5A)	1903(3)	9514(4)	3586(1)	62(2)
F(6A)	561(4)	10206(5)	2834(1)	84(2)
F(1B)	330(20)	9500(30)	3163(13)	34(1)
F(2B)	2210(40)	10390(40)	3279(18)	70(2)
F(5B)	1350(30)	9680(40)	3639(14)	62(2)
F(6B)	1270(40)	10390(40)	2797(13)	84(2)
Cl(1)	8251(2)	3467(2)	4301(1)	86(1)
Cl(2A)	8538(4)	2422(4)	5025(1)	141(2)
Cl(2B)	7744(11)	3689(16)	4906(5)	141(2)
C(90)	8725(6)	3568(6)	4763(2)	67(2)
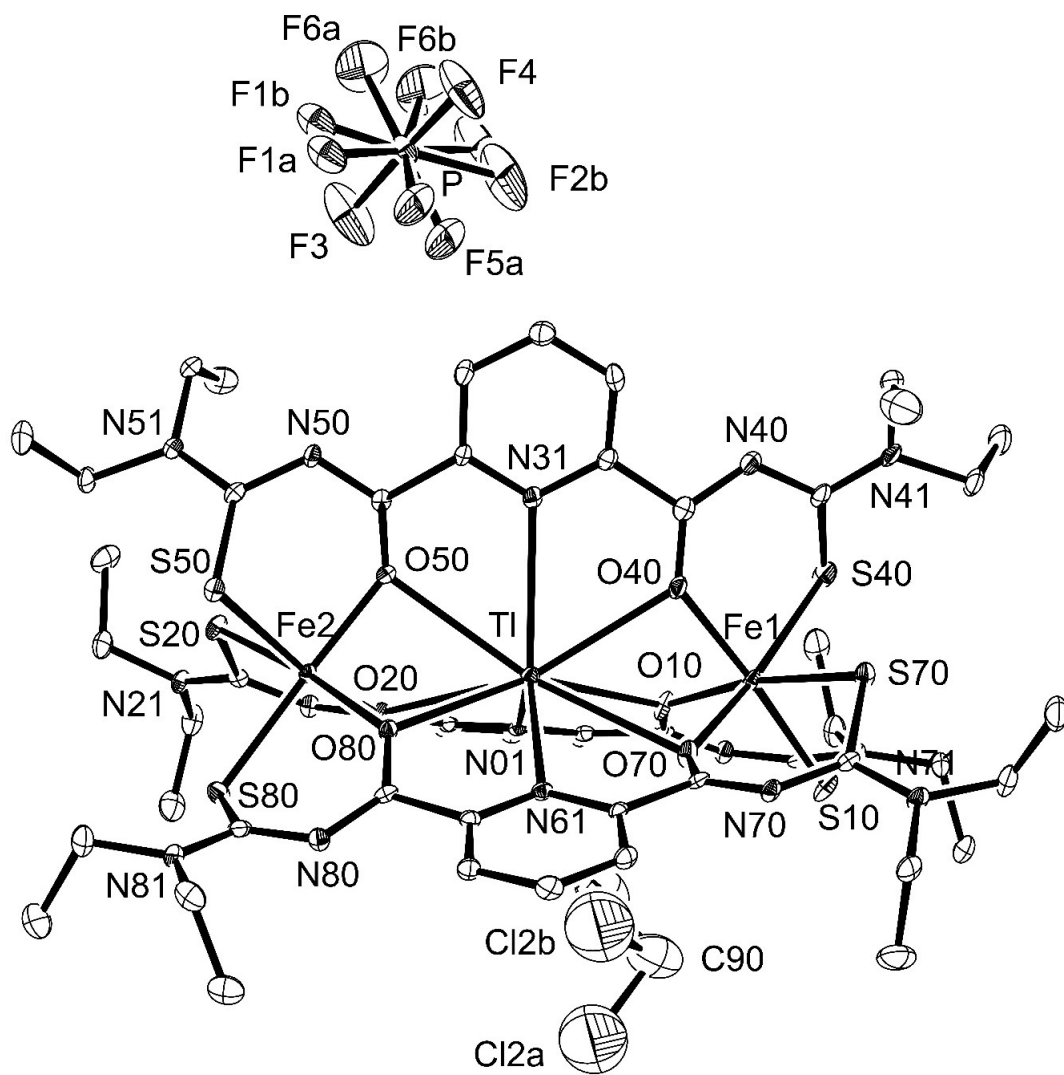
Figure 6: Ellipsoid plot (50% probability) of $\{Tl \subset [Fe_2(L^2)_3]\}(PF_6) \cdot CH_2Cl_2$.

7. $\{NH_4 \subset [Fe_2(L^2)_3]\}(PF_6) \cdot CH_2Cl_2$

Table 13. Crystal data and structure refinement for $\{NH_4 \subset [Fe_2(L^2)_3]\}(PF_6) \cdot CH_2Cl_2$.

Empirical formula	$C_{52}H_{71}O_6N_{16}S_6PF_6Cl_2Fe_2$
Formula weight	1536.17
Measurement instrument	Bruker D8 venture
Temperature	100(2) K
Wavelength	0.71073 Å
Crystal system	Monoclinic
Space group	P 2_1/c
Unit cell dimensions	a = 15.692(1) Å $\quad$ $\alpha = 90°$.
	b = 12.262(1) Å $\quad$ $\beta = 101.12(2)°$.
	c = 35.078(2) Å $\quad$ $\gamma = 90°$.
Volume	6622.8(8) Å^3
Z	4
Density (calculated)	1.541 g/cm^3
Absorption coefficient	0.809 mm^{-1}
F(000)	3176
Crystal size	0.40 x 0.20 x 0.15 mm^3
Theta range for data collection	2.272 to 24.999°.
Index ranges	-18<=h<=16, -14<=k<=12, -41<=l<=41
Reflections collected	64712
Independent reflections	11666 [R(int) = 0.0414]
Completeness to theta = 24.999°	99.9 %
Absorption correction	Semi-empirical from equivalents
Max. and min. transmission	0.7455 and 0.6085
Refinement method	Full-matrix least-squares on F^2
Data / restraints / parameters	11666 / 16 / 828
Goodness-of-fit on F^2	1.043
Final R indices [I>2sigma(I)]	R1 = 0.0515, wR2 = 0.1402
R indices (all data)	R1 = 0.0608, wR2 = 0.1473
Largest diff. peak and hole	1.889 and -2.050 e/Å^3

Table 14. Atomic coordinates (x 10^4) and equivalent isotropic displacement parameters (Å^2 x 10^3) for $\{NH_4 \subset [Fe_2(L^2)_3]\}(PF_6) \cdot CH_2Cl_2$. U(eq) is defined as one third of the trace of the orthogonalized U^{ij} tensor.

	x	y	z	U(eq)
Fe(1)	4394(1)	-1741(1)	8634(1)	9(1)
Fe(2)	8000(1)	1916(1)	9127(1)	11(1)
N	6187(2)	74(2)	8884(1)	3(1)
N(01)	6289(2)	-328(2)	9708(1)	10(1)
C(02)	5735(2)	-1035(3)	9823(1)	11(1)
C(03)	5668(2)	-1183(3)	10209(1)	14(1)
C(04)	6183(2)	-548(3)	10490(1)	15(1)
C(05)	6753(2)	192(3)	10376(1)	13(1)
C(06)	6796(2)	265(3)	9983(1)	11(1)
C(10)	5140(2)	-1667(3)	9506(1)	11(1)
C(11)	4241(2)	-3215(3)	9399(1)	14(1)
N(10)	4765(2)	-2511(3)	9634(1)	13(1)
N(11)	3690(2)	-3769(3)	9573(1)	17(1)
S(10)	4292(1)	-3505(1)	8921(1)	16(1)
O(10)	5041(2)	-1282(2)	9164(1)	13(1)
C(12)	3000(3)	-4473(3)	9358(1)	24(1)
C(13)	3177(3)	-5676(4)	9418(2)	38(1)
C(14)	3687(3)	-3596(4)	9990(1)	22(1)
C(15)	4438(3)	-4117(4)	10263(1)	25(1)
C(20)	7437(2)	1037(3)	9852(1)	11(1)
C(21)	8352(2)	2540(3)	10068(1)	12(1)
C(22)	9534(2)	3759(3)	10381(1)	19(1)
C(23)	9242(3)	4897(4)	10472(1)	25(1)
C(24)	8859(3)	2425(3)	10771(1)	18(1)
C(25)	9440(3)	1432(4)	10846(1)	33(1)
O(20)	7547(2)	935(2)	9506(1)	14(1)
N(20)	7833(2)	1700(3)	10127(1)	13(1)
N(21)	8874(2)	2908(3)	10389(1)	14(1)
S(20)	8318(1)	3248(1)	9638(1)	14(1)
N(31)	7131(2)	-1125(2)	8360(1)	10(1)
C(32)	6719(2)	-1874(3)	8110(1)	11(1)
C(33)	7059(2)	-2265(3)	7798(1)	14(1)
C(34)	7853(3)	-1870(3)	7741(1)	16(1)

C(35)	8284(2)	-1109(3)	7998(1)	14(1)
C(36)	7901(2)	-757(3)	8303(1)	11(1)
C(40)	5830(2)	-2238(3)	8171(1)	10(1)
C(41)	4589(2)	-3166(3)	7836(1)	12(1)
C(42)	3407(2)	-4219(3)	7442(1)	17(1)
C(43)	3003(3)	-3453(4)	7116(1)	25(1)
C(44)	4954(3)	-4573(3)	7397(1)	19(1)
C(45)	5275(3)	-5569(4)	7637(1)	26(1)
N(40)	5446(2)	-2927(3)	7902(1)	12(1)
N(41)	4332(2)	-3951(3)	7577(1)	13(1)
O(40)	5563(2)	-1862(2)	8464(1)	12(1)
S(40)	3782(1)	-2493(1)	8019(1)	14(1)
C(50)	8322(2)	135(3)	8572(1)	12(1)
C(51)	9634(2)	1058(3)	8800(1)	12(1)
C(52)	10954(2)	2198(3)	8903(1)	18(1)
C(53)	11727(3)	1537(4)	9110(1)	28(1)
C(54)	10431(3)	1233(4)	8274(1)	20(1)
C(55)	9822(3)	1871(4)	7964(1)	30(1)
N(50)	9134(2)	349(3)	8556(1)	13(1)
N(51)	10301(2)	1482(3)	8669(1)	14(1)
O(50)	7835(2)	622(2)	8768(1)	15(1)
S(50)	9504(1)	1352(1)	9271(1)	17(1)
N(61)	5030(2)	1906(3)	8571(1)	12(1)
C(62)	4168(2)	1770(3)	8451(1)	11(1)
C(63)	3591(2)	2641(3)	8376(1)	16(1)
C(64)	3914(3)	3696(3)	8432(1)	19(1)
C(65)	4803(3)	3840(3)	8549(1)	17(1)
C(66)	5335(2)	2933(3)	8615(1)	13(1)
C(70)	3856(2)	606(3)	8408(1)	11(1)
C(71)	2629(2)	-517(3)	8269(1)	12(1)
C(72)	1532(2)	-1797(3)	7916(1)	16(1)
C(73)	605(3)	-1704(4)	7977(1)	22(1)
C(74)	1802(2)	20(3)	7636(1)	18(1)
C(75)	2408(3)	-156(4)	7351(1)	25(1)
N(70)	3018(2)	473(3)	8269(1)	13(1)
N(71)	2001(2)	-744(3)	7968(1)	13(1)
O(70)	4426(2)	-135(2)	8497(1)	12(1)
S(70)	2865(1)	-1407(1)	8662(1)	12(1)
C(80)	6307(2)	3057(3)	8750(1)	14(1)

C(81)	7473(2)	4255(3)	8747(1)	18(1)
C(82)	8576(2)	5705(4)	8923(1)	21(1)
C(83)	8895(3)	6158(4)	8572(1)	24(1)
C(84)	7008(3)	6121(4)	8865(1)	28(1)
C(85)	6827(3)	6165(4)	9268(2)	41(1)
N(80)	6610(2)	4026(3)	8686(1)	19(1)
N(81)	7677(2)	5301(3)	8827(1)	21(1)
O(80)	6715(2)	2245(2)	8922(1)	13(1)
S(80)	8287(1)	3340(1)	8694(1)	18(1)
P	1225(1)	4876(1)	8201(1)	21(1)
F(3)	1126(3)	6021(2)	8394(1)	61(1)
F(4)	1355(3)	3702(3)	8031(1)	73(1)
F(1)	463(2)	4388(3)	8395(1)	34(1)
F(2)	1990(3)	5325(4)	8012(2)	72(2)
F(5)	1902(3)	4483(4)	8577(1)	67(1)
F(6)	537(4)	5231(5)	7838(1)	89(2)
F(1B)	345(17)	4520(20)	8175(10)	34(1)
F(2B)	2200(30)	5430(30)	8277(14)	72(2)
F(5B)	1380(20)	4670(30)	8637(11)	67(1)
F(6B)	1150(30)	5310(40)	7777(11)	89(2)
C(90)	8692(5)	8558(5)	9763(2)	54(2)
Cl(1)	8240(2)	8474(2)	9310(1)	99(1)
Cl(2)	8547(5)	7437(6)	10018(2)	269(3)
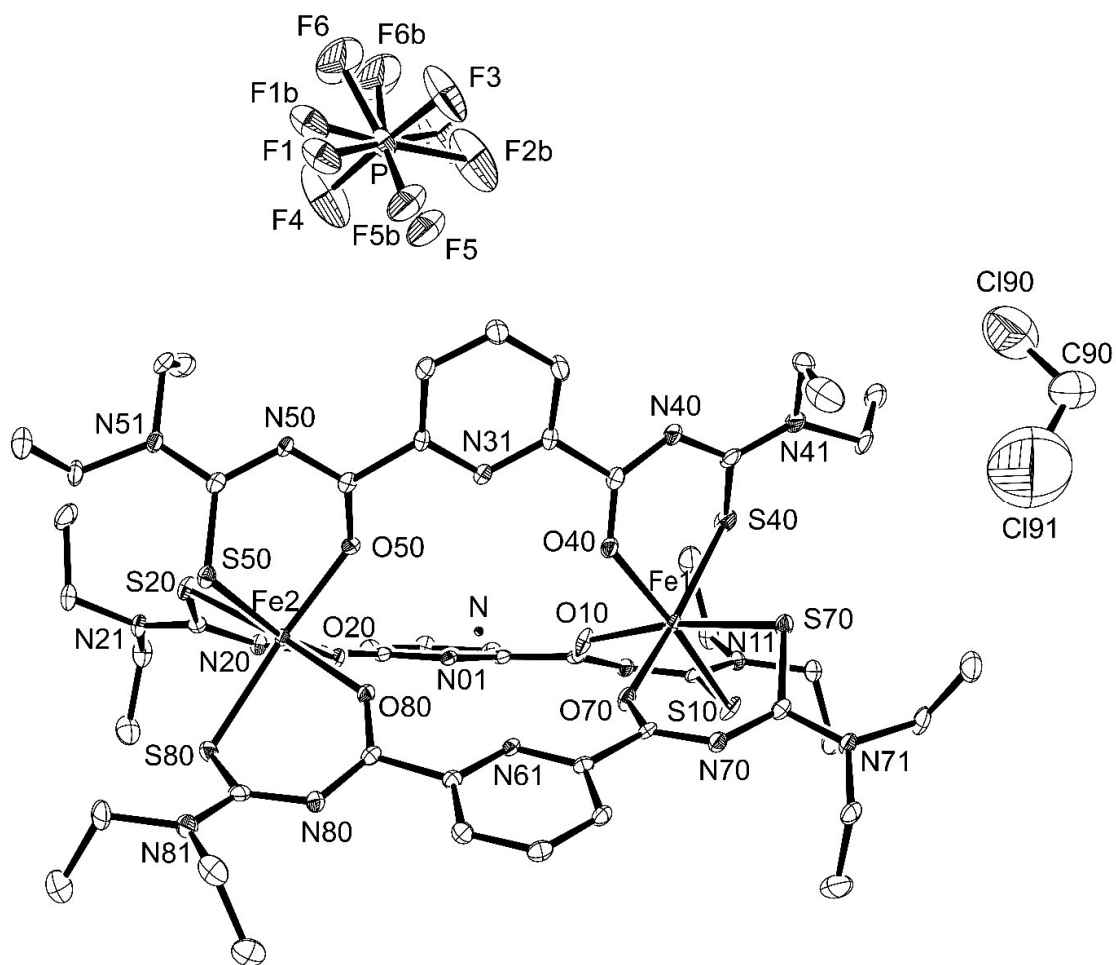
Figure 7: Ellipsoid plot (50% probability) of $\{NH_4 \subset [Fe_2(L^2)_3]\}(PF_6) \cdot CH_2Cl_2$.

8. {Rb ⊂ [In₂(L²)₃]}(PF₆) · toluene

Table 15. Crystal data and structure refinement for {Rb ⊂ [In₂(L²)₃]}(PF₆) · toluene.

Empirical formula	$C_{58}H_{77}O_6N_{15}S_6PF_6In_2Rb$
Formula weight	1732.78
Measurement instrument	STOE IPDS 2T
Temperature	200(2) K
Wavelength	0.71073 Å
Crystal system	Monoclinic
Space group	P 2₁/c
Unit cell dimensions	a = 19.601(1) Å α = 90°.
	b = 22.477(1) Å β = 113.88(1)°.
	c = 18.119(1) Å γ = 90°.
Volume	7299.4(8) Å³
Z	4
Density (calculated)	1.577 g/cm³
Absorption coefficient	1.560 mm⁻¹
F(000)	3512
Crystal size	0.25 x 0.22 x 0.19 mm³
Theta range for data collection	3.366 to 25.000°.
Index ranges	-23<=h<=23, -26<=k<=25, -21<=l<=19
Reflections collected	31896
Independent reflections	12785 [R(int) = 0.0771]
Completeness to theta = 25.000°	99.4 %
Absorption correction	None
Refinement method	Full-matrix least-squares on F²
Data / restraints / parameters	12785 / 1 / 873
Goodness-of-fit on F²	0.825
Final R indices [I>2sigma(I)]	R1 = 0.0413, wR2 = 0.0643
R indices (all data)	R1 = 0.1039, wR2 = 0.0752
Largest diff. peak and hole	0.693 and -0.781 e/Å³

Table 16. Atomic coordinates (x 10^4) and equivalent isotropic displacement parameters (Å^2 x 10^3) for {Rb $\subset$ [In$_2$(L^2)$_3$]}(PF$_6$) · toluene. U(eq) is defined as one third of the trace of the orthogonalized U^{ij} tensor.

	x	y	z	U(eq)
Rb	9898(1)	4867(1)	7291(1)	26(1)
In(2)	11989(1)	4884(1)	8433(1)	25(1)
In(1)	7821(1)	4854(1)	6143(1)	25(1)
N(01)	9894(2)	3580(2)	7567(2)	24(1)
C(02)	9227(3)	3341(2)	7453(3)	27(1)
C(03)	9158(3)	2872(3)	7897(4)	37(2)
C(04)	9780(3)	2622(3)	8491(4)	43(2)
C(05)	10470(3)	2856(3)	8602(3)	35(1)
C(06)	10504(3)	3330(2)	8147(3)	27(1)
O(10)	8617(2)	4105(2)	6478(2)	29(1)
C(10)	8541(3)	3620(2)	6806(3)	26(1)
N(10)	7931(2)	3316(2)	6630(3)	30(1)
C(11)	7235(3)	3502(2)	6148(3)	29(1)
S(10)	6865(1)	4167(1)	6325(1)	33(1)
N(11)	6817(2)	3131(2)	5586(3)	36(1)
C(12)	6036(3)	3257(3)	5024(4)	48(2)
C(13)	5495(3)	2977(4)	5320(5)	76(3)
C(14)	7118(3)	2562(3)	5469(4)	49(2)
C(15)	7540(4)	2609(4)	4931(4)	71(2)
O(20)	11244(2)	4112(2)	7937(2)	29(1)
C(20)	11246(3)	3629(2)	8305(3)	27(1)
N(20)	11830(2)	3338(2)	8812(3)	33(1)
C(21)	12519(3)	3556(3)	9200(3)	32(1)
S(20)	12707(1)	4254(1)	9665(1)	38(1)
N(21)	13079(2)	3181(2)	9313(3)	38(1)
C(22)	13874(3)	3333(3)	9819(4)	53(2)
C(23)	14271(4)	3556(4)	9304(5)	82(3)
C(24)	12923(3)	2592(3)	8922(4)	48(2)
C(25)	12797(4)	2617(4)	8053(5)	82(3)
N(31)	9733(2)	5408(2)	8714(2)	23(1)
C(32)	9059(3)	5527(2)	8707(3)	25(1)
C(33)	8952(3)	5743(3)	9365(3)	32(1)
C(34)	9572(3)	5872(3)	10065(3)	35(2)

C(35)	10275(3)	5787(3)	10065(3)	31(1)
C(36)	10334(3)	5548(2)	9390(3)	27(1)
O(40)	8510(2)	5065(2)	7413(2)	28(1)
C(40)	8406(3)	5411(2)	7906(3)	24(1)
N(40)	7792(2)	5688(2)	7844(3)	29(1)
C(41)	7183(3)	5779(2)	7157(3)	27(1)
S(40)	7174(1)	5824(1)	6193(1)	38(1)
N(41)	6566(2)	5920(2)	7260(3)	36(1)
C(42)	5844(3)	6039(3)	6575(4)	48(2)
C(43)	5380(4)	5481(3)	6319(5)	80(3)
C(44)	6578(3)	5975(3)	8078(3)	42(2)
C(45)	6876(3)	6571(3)	8439(4)	50(2)
O(50)	11079(2)	5111(2)	8794(2)	27(1)
C(50)	11078(3)	5443(2)	9354(3)	26(1)
N(50)	11650(2)	5693(2)	9946(3)	29(1)
C(51)	12338(3)	5769(2)	9972(3)	30(1)
S(50)	12545(1)	5863(1)	9128(1)	35(1)
N(51)	12878(2)	5837(2)	10709(3)	34(1)
C(52)	13658(3)	5987(3)	10855(4)	44(2)
C(53)	14154(3)	5447(3)	11054(5)	74(2)
C(54)	12698(3)	5817(3)	11425(3)	43(2)
C(55)	12444(4)	6423(3)	11587(4)	60(2)
N(61)	10057(2)	5528(2)	5931(2)	26(1)
C(62)	9459(3)	5639(2)	5237(3)	25(1)
C(63)	9520(3)	5867(3)	4557(3)	33(1)
C(64)	10227(3)	5985(3)	4582(3)	38(2)
C(65)	10844(3)	5878(3)	5297(3)	32(1)
C(66)	10738(3)	5649(2)	5947(3)	27(1)
O(70)	8714(2)	5273(2)	5900(2)	30(1)
C(70)	8707(3)	5482(2)	5240(3)	27(1)
N(70)	8139(2)	5600(2)	4565(3)	31(1)
C(71)	7424(3)	5428(3)	4380(3)	31(1)
S(70)	7167(1)	4737(1)	4620(1)	34(1)
N(71)	6901(2)	5808(2)	3921(3)	36(1)
C(72)	6098(3)	5667(3)	3578(4)	49(2)
C(73)	5708(3)	5921(3)	4069(4)	60(2)
C(74)	7121(3)	6380(3)	3695(4)	52(2)
C(75)	7355(4)	6832(3)	4376(5)	68(2)
O(80)	11235(2)	5266(2)	7285(2)	32(1)

C(80)	11384(3)	5494(3)	6727(3)	28(1)
N(80)	12040(2)	5651(2)	6757(3)	32(1)
C(81)	12705(3)	5465(3)	7307(3)	33(1)
S(80)	12879(1)	4761(1)	7750(1)	38(1)
N(81)	13263(2)	5843(3)	7444(3)	47(1)
C(84)	13121(3)	6428(3)	7055(4)	52(2)
C(85)	12801(4)	6866(3)	7470(5)	78(2)
P	4907(1)	7642(1)	7407(1)	55(1)
F(2)	4901(3)	6939(2)	7416(3)	97(2)
F(3A)	5624(5)	7687(4)	8216(6)	74(3)
F(4A)	5460(6)	7492(5)	6941(8)	108(4)
F(5A)	4121(4)	7585(3)	6692(5)	69(3)
F(6A)	4437(7)	7540(6)	7995(10)	141(5)
F(3B)	5398(8)	7592(6)	8385(9)	89(5)
F(4B)	5695(6)	7654(5)	7371(8)	77(4)
F(5B)	4454(6)	7693(4)	6430(6)	66(4)
F(6B)	4192(7)	7721(6)	7536(9)	93(5)
F(1)	4893(5)	8355(4)	7453(6)	34(3)
F(1B)	4618(11)	8244(9)	7697(12)	61(7)
F(1C)	5083(7)	8300(5)	7188(9)	48(4)
C(82A)	14064(5)	5653(5)	7884(6)	46(2)
C(83A)	14403(5)	5949(5)	8711(6)	75(4)
C(82B)	13966(14)	5906(14)	8257(17)	46(2)
C(83B)	14511(16)	5659(16)	7934(17)	75(4)
C(90A)	9089(7)	7483(6)	8898(10)	120(7)
C(91A)	9482(6)	7100(4)	8397(7)	85(4)
C(92A)	9097(5)	6786(5)	7658(8)	111(7)
C(93A)	9467(7)	6469(4)	7287(6)	89(5)
C(94A)	10263(7)	6459(4)	7675(7)	101(6)
C(95A)	10627(5)	6772(4)	8360(7)	80(4)
C(96A)	10233(6)	7090(4)	8732(7)	100(5)
C(90B)	10398(18)	7403(13)	9472(17)	80(11)
C(91B)	10233(6)	7090(4)	8732(7)	85(4)
C(92B)	9482(6)	7100(4)	8397(7)	111(7)
C(93B)	9097(5)	6786(5)	7658(8)	89(5)
C(94B)	9467(7)	6469(4)	7287(6)	101(6)
C(95B)	10263(7)	6459(4)	7675(7)	80(4)
C(96B)	10627(5)	6772(4)	8360(7)	100(5)
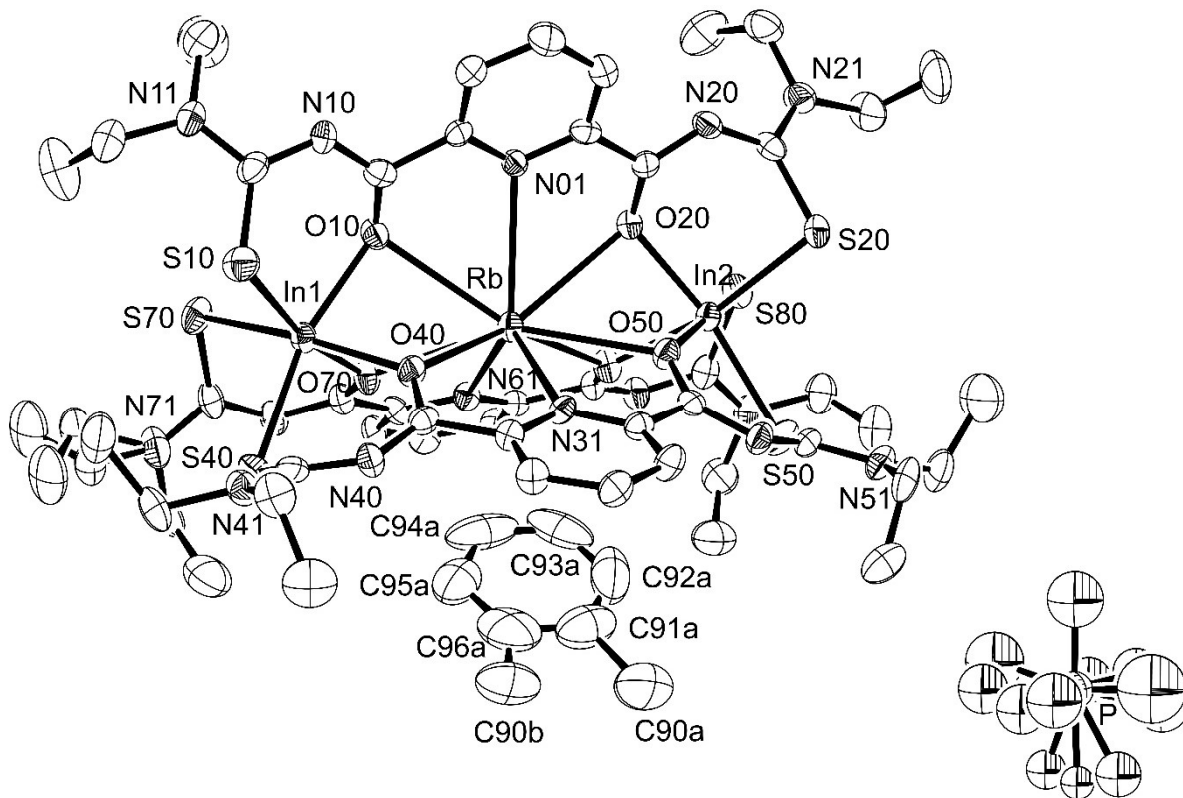
Figure 8: Ellipsoid plot (50% probability) of {Rb ⊂ [In$_2$(L^2)$_3$]}(PF$_6$) · toluene.

9. $\{K \subset [In_2(L^2)_3]\}(PF_6) \cdot$ toluene

Table 17. Crystal data and structure refinement for $\{K \subset [In_2(L^2)_3]\}(PF_6) \cdot$ toluene.

Empirical formula	$C_{58}H_{77}O_6N_{15}S_6PF_6In_2K$
Formula weight	1686.41
Measurement instrument	STOE IPDS 2T
Temperature	200(2) K
Wavelength	0.71073 Å
Crystal system	Monoclinic
Space group	P 2_1/c
Unit cell dimensions	a = 19.655(1) Å α = 90°.
	b = 22.587(1) Å β = 113.96(1)°.
	c = 18.115(1) Å γ = 90°.
Volume	7349.1(6) Å^3
Z	4
Density (calculated)	1.524 g/cm^3
Absorption coefficient	0.948 mm^{-1}
F(000)	3440
Crystal size	0.25 x 0.20 x 0.17 mm^3
Theta range for data collection	3.355 to 24.999°.
Index ranges	-23<=h<=23, -26<=k<=25, -18<=l<=21
Reflections collected	33486
Independent reflections	12873 [R(int) = 0.0863]
Completeness to theta = 24.999°	99.5 %
Absorption correction	None
Refinement method	Full-matrix least-squares on F^2
Data / restraints / parameters	12873 / 1 / 896
Goodness-of-fit on F^2	0.907
Final R indices [I>2sigma(I)]	R1 = 0.0413, wR2 = 0.0977
R indices (all data)	R1 = 0.0659, wR2 = 0.1057
Largest diff. peak and hole	0.770 and -0.842 e/Å^3

Table 18. Atomic coordinates (x 10^4) and equivalent isotropic displacement parameters (Å^2x 10^3) for $\{K \subset [In_2(L^2)_3]\}(PF_6) \cdot$ toluene. U(eq) is defined as one third of the trace of the orthogonalized U^{ij} tensor.

	x	y	z	U(eq)
In(1)	12173(1)	9860(1)	3870(1)	33(1)
In(2)	8017(1)	9898(1)	1571(1)	34(1)
K	10100(1)	9881(1)	2715(1)	36(1)
N(01)	10103(2)	8615(1)	2422(2)	34(1)
C(02)	10760(2)	8368(2)	2549(3)	35(1)
C(03)	10835(2)	7885(2)	2113(3)	49(1)
C(04)	10202(3)	7639(2)	1522(3)	57(1)
C(05)	9522(2)	7873(2)	1405(3)	48(1)
C(06)	9490(2)	8360(2)	1851(3)	36(1)
O(10)	11366(1)	9124(1)	3514(2)	37(1)
C(10)	11441(2)	8647(2)	3191(2)	33(1)
N(10)	12054(2)	8334(2)	3373(2)	40(1)
C(11)	12751(2)	8521(2)	3851(2)	36(1)
S(10)	13115(1)	9180(1)	3669(1)	44(1)
N(11)	13169(2)	8146(2)	4402(2)	46(1)
C(14)	12865(3)	7577(2)	4526(3)	60(1)
C(15)	12468(4)	7629(3)	5068(4)	94(2)
C(12)	13957(2)	8267(3)	4949(3)	67(2)
C(13)	14486(3)	7996(3)	4636(5)	103(2)
O(20)	8764(1)	9137(1)	2066(2)	39(1)
N(20)	8175(2)	8368(2)	1189(2)	48(1)
C(20)	8756(2)	8659(2)	1690(3)	36(1)
C(21)	7475(2)	8580(2)	806(3)	46(1)
S(20)	7296(1)	9273(1)	337(1)	51(1)
N(21)	6926(2)	8209(2)	701(3)	61(1)
C(22)	6126(3)	8356(3)	196(4)	84(2)
C(23)	5744(4)	8569(5)	661(5)	133(3)
C(24)	7087(3)	7616(3)	1088(4)	75(2)
C(25)	7203(4)	7644(4)	1952(5)	114(3)
N(31)	10271(2)	10412(1)	1306(2)	32(1)
C(32)	10946(2)	10527(2)	1321(2)	33(1)
C(33)	11049(2)	10738(2)	653(2)	39(1)
C(34)	10430(2)	10857(2)	-43(3)	46(1)

C(35)	9733(2)	10773(2)	-52(3)	40(1)
C(36)	9672(2)	10551(2)	632(2)	35(1)
O(40)	11471(1)	10081(1)	2613(2)	38(1)
C(40)	11587(2)	10414(2)	2109(2)	33(1)
N(40)	12209(2)	10676(2)	2176(2)	38(1)
C(41)	12816(2)	10774(2)	2864(3)	37(1)
S(40)	12825(1)	10823(1)	3828(1)	49(1)
N(41)	13428(2)	10908(2)	2755(2)	46(1)
C(42)	14154(2)	11032(2)	3443(3)	61(1)
C(43)	14615(3)	10479(3)	3717(5)	100(2)
C(44)	13408(2)	10968(2)	1939(3)	57(1)
C(45)	13117(3)	11555(2)	1574(3)	66(1)
O(50)	8934(1)	10124(1)	1236(2)	39(1)
N(50)	8364(2)	10693(2)	67(2)	40(1)
C(50)	8928(2)	10446(2)	667(2)	33(1)
C(51)	7676(2)	10775(2)	39(3)	38(1)
S(50)	7468(1)	10875(1)	880(1)	46(1)
N(51)	7138(2)	10841(2)	-702(2)	43(1)
C(52)	6363(2)	10996(2)	-852(3)	58(1)
C(53)	5867(3)	10462(3)	-1044(5)	93(2)
C(54)	7314(2)	10816(2)	-1406(3)	52(1)
C(55)	7582(3)	11411(3)	-1566(3)	70(2)
N(61)	9945(2)	10524(2)	4067(2)	36(1)
C(62)	10539(2)	10632(2)	4762(2)	35(1)
C(63)	10478(2)	10855(2)	5438(3)	46(1)
C(64)	9777(2)	10983(2)	5418(3)	48(1)
C(65)	9162(2)	10875(2)	4703(3)	43(1)
C(66)	9273(2)	10644(2)	4051(3)	37(1)
O(70)	11273(1)	10269(1)	4098(2)	38(1)
C(70)	11285(2)	10473(2)	4756(2)	35(1)
N(70)	11856(2)	10599(2)	5423(2)	41(1)
C(71)	12569(2)	10431(2)	5618(2)	41(1)
S(70)	12824(1)	9737(1)	5390(1)	44(1)
N(71)	13087(2)	10808(2)	6078(2)	49(1)
C(72)	13892(2)	10670(3)	6422(3)	62(1)
C(73)	14281(3)	10925(3)	5950(4)	81(2)
C(74)	12867(3)	11383(2)	6293(3)	64(1)
C(75)	12647(4)	11827(3)	5618(4)	90(2)
O(80)	8782(1)	10261(1)	2724(2)	41(1)

C(80)	8624(2)	10500(2)	3269(2)	37(1)
N(80)	7969(2)	10666(2)	3227(2)	44(1)
C(81)	7301(2)	10487(2)	2676(3)	44(1)
S(80)	7124(1)	9784(1)	2247(1)	50(1)
N(81)	6760(2)	10874(2)	2536(3)	64(1)
C(84)	6902(3)	11453(3)	2930(4)	71(2)
C(85)	7227(4)	11892(3)	2523(5)	101(2)
C(82A)	6044(8)	10885(7)	1781(14)	51(5)
C(83A)	5450(11)	10692(8)	2048(12)	78(6)
C(82B)	5934(7)	10653(6)	2100(6)	71(4)
C(83B)	5629(7)	10953(6)	1295(8)	107(5)
P	4905(1)	7359(1)	7353(1)	68(1)
F(3)	5381(6)	7412(4)	8328(6)	111(3)
F(4)	5683(5)	7361(4)	7350(7)	115(3)
F(5)	4490(4)	7271(4)	6365(5)	99(3)
F(6)	4126(6)	7288(5)	7345(8)	135(4)
F(3B)	5658(5)	7324(4)	8117(6)	99(3)
F(4B)	5455(6)	7538(5)	6896(8)	127(4)
F(5B)	4118(4)	7409(3)	6654(5)	82(3)
F(6B)	4445(7)	7432(5)	7926(9)	146(5)
F(2)	4909(4)	6670(3)	7438(5)	48(2)
F(2B)	4608(8)	6766(7)	7662(9)	75(4)
F(2C)	5102(5)	6695(4)	7167(6)	72(2)
F(1)	4816(5)	8037(4)	7109(11)	81(4)
F(1B)	4922(5)	8064(4)	7511(11)	84(4)
C(90A)	905(7)	2484(5)	1122(11)	174(8)
C(91A)	496(8)	2106(4)	1615(8)	136(6)
C(92A)	919(5)	1798(4)	2384(9)	156(9)
C(93A)	559(7)	1474(4)	2732(5)	115(5)
C(94A)	-247(8)	1459(4)	2342(7)	138(7)
C(95A)	-614(5)	1781(4)	1635(7)	133(8)
C(96A)	-246(6)	2101(4)	1269(6)	90(6)
C(90B)	-350(20)	2433(11)	500(20)	128(15)
C(91B)	-246(6)	2101(4)	1269(6)	240(70)
C(92B)	496(8)	2106(4)	1615(8)	156(9)
C(93B)	919(5)	1798(4)	2384(9)	115(5)
C(94B)	559(7)	1474(4)	2732(5)	138(7)
C(95B)	-247(8)	1459(4)	2342(7)	133(8)
C(96B)	-614(5)	1781(4)	1635(7)	90(6)
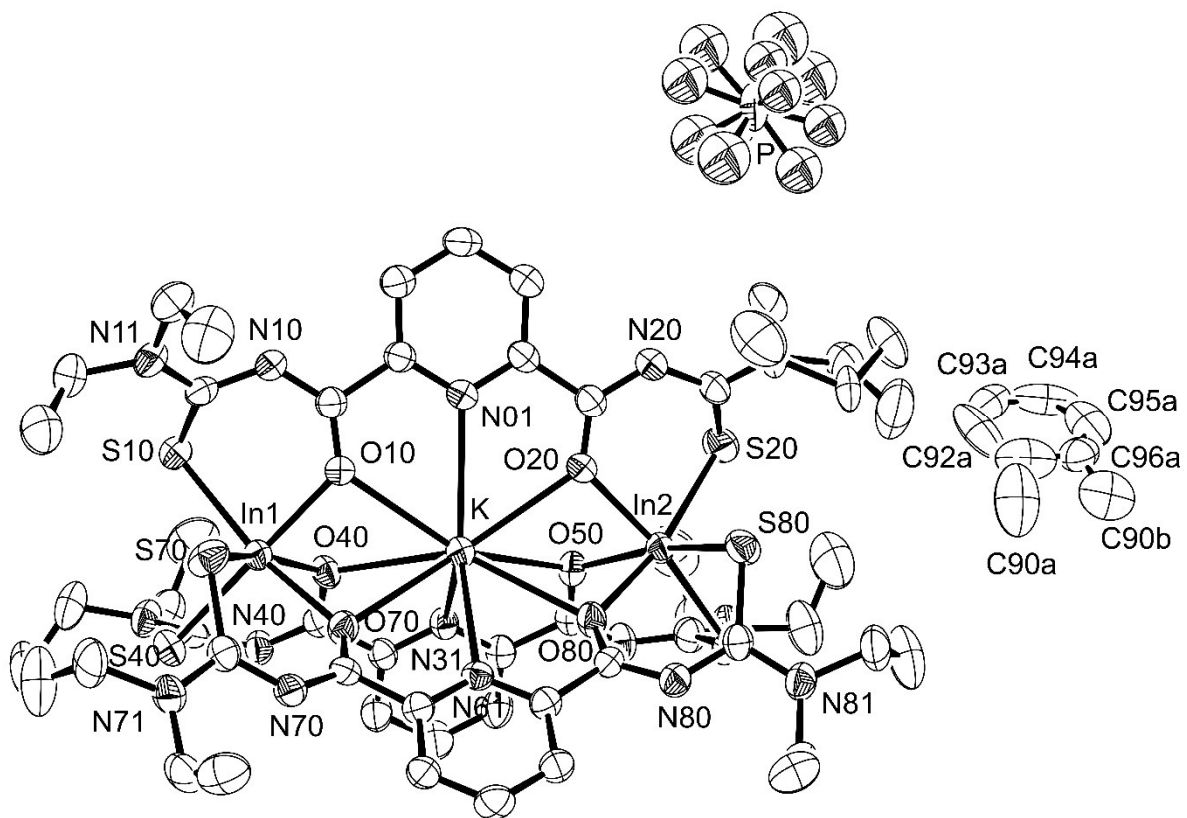
Figure 9: Ellipsoid plot (50% probability) of $\{K \subset [In_2(L^2)_3]\}(PF_6) \cdot$ toluene.

10. {NH$_4$ $\subset$ [In$_2$(L^2)$_3$]}(PF$_6$) · toluene

Table 19. Crystal data and structure refinement for {NH$_4$ $\subset$ [In$_2$(L^2)$_3$]}(PF$_6$) · toluene.

Empirical formula	C$_{58}$H$_{77}$O$_6$N$_{16}$S$_6$PF$_6$In$_2$
Formula weight	1661.32
Measurement instrument	STOE IPDS 2T
Temperature	200(2) K
Wavelength	0.71073 Å
Crystal system	Monoclinic
Space group	P 2$_1$/c
Unit cell dimensions	a = 19.632(1) Å α = 90°.
	b = 22.545(1) Å β = 113.96(1)°.
	c = 18.107(1) Å γ = 90°.
Volume	7323.6(6) Å^3
Z	4
Density (calculated)	1.507 g/cm^3
Absorption coefficient	0.895 mm^{-1}
F(000)	3392
Crystal size	0.25 x 0.20 x 0.17 mm^3
Theta range for data collection	3.360 to 24.999°.
Index ranges	-23<=h<=23, -25<=k<=26, -21<=l<=17
Reflections collected	36800
Independent reflections	12844 [R(int) = 0.0527]
Completeness to theta = 24.999°	99.6 %
Absorption correction	None
Refinement method	Full-matrix least-squares on F^2
Data / restraints / parameters	12844 / 1 / 879
Goodness-of-fit on F^2	0.898
Final R indices [I>2sigma(I)]	R1 = 0.0404, wR2 = 0.0847
R indices (all data)	R1 = 0.0752, wR2 = 0.0923
Largest diff. peak and hole	0.959 and -1.058 e/Å^3

Table 20. Atomic coordinates (x 10^4) and equivalent isotropic displacement parameters (Å^2 x 10^3) for $\{NH_4 \subset [In_2(L^2)_3]\}(PF_6) \cdot$ toluene. U(eq) is defined as one third of the trace of the orthogonalized U^{ij} tensor.

	x	y	z	U(eq)
In(1)	7824(1)	5145(1)	6142(1)	28(1)
In(2)	11984(1)	5111(1)	8431(1)	29(1)
N	9898(2)	5139(2)	7279(2)	29(1)
N(01)	9893(2)	6416(2)	7564(2)	29(1)
C(02)	9232(2)	6656(2)	7444(3)	30(1)
C(03)	9158(2)	7127(2)	7893(3)	42(1)
C(04)	9789(3)	7373(2)	8476(3)	49(1)
C(05)	10474(2)	7142(2)	8594(3)	41(1)
C(06)	10508(2)	6662(2)	8136(3)	32(1)
O(10)	8614(1)	5896(1)	6468(2)	30(1)
C(10)	8543(2)	6375(2)	6802(3)	30(1)
N(10)	7931(2)	6684(2)	6628(2)	33(1)
C(11)	7240(2)	6492(2)	6148(3)	32(1)
S(10)	6871(1)	5833(1)	6323(1)	37(1)
N(11)	6817(2)	6867(2)	5585(2)	39(1)
C(12)	6040(2)	6743(3)	5037(3)	53(1)
C(13)	5498(3)	7020(3)	5327(5)	86(2)
C(14)	7124(3)	7438(2)	5474(3)	53(1)
C(15)	7527(4)	7390(3)	4930(4)	85(2)
O(20)	11245(1)	5885(1)	7931(2)	32(1)
C(20)	11250(2)	6364(2)	8301(3)	30(1)
N(20)	11828(2)	6656(2)	8814(2)	39(1)
C(21)	12525(2)	6437(2)	9198(3)	37(1)
S(20)	12710(1)	5743(1)	9660(1)	43(1)
N(21)	13082(2)	6811(2)	9308(3)	46(1)
C(22)	13878(3)	6663(3)	9799(4)	66(2)
C(23)	14266(3)	6443(4)	9311(5)	102(3)
C(24)	12916(3)	7403(3)	8924(4)	60(2)
C(25)	12799(4)	7376(3)	8051(5)	91(2)
N(31)	10053(2)	4466(2)	5932(2)	31(1)
C(32)	9455(2)	4364(2)	5233(3)	29(1)
C(33)	9517(2)	4147(2)	4546(3)	37(1)
C(34)	10219(2)	4031(2)	4576(3)	42(1)

C(35)	10837(2)	4129(2)	5288(3)	36(1)
C(36)	10730(2)	4346(2)	5948(3)	30(1)
O(40)	8711(1)	4720(1)	5895(2)	34(1)
C(40)	8702(2)	4523(2)	5230(3)	30(1)
N(40)	8137(2)	4403(2)	4566(2)	35(1)
C(41)	7420(2)	4571(2)	4374(3)	33(1)
S(40)	7167(1)	5262(1)	4616(1)	38(1)
N(41)	6903(2)	4193(2)	3921(2)	41(1)
C(42)	6095(2)	4333(3)	3574(3)	52(1)
C(43)	5702(3)	4080(3)	4052(4)	67(2)
C(44)	7117(3)	3617(3)	3693(3)	53(1)
C(45)	7352(3)	3169(3)	4372(4)	74(2)
O(50)	11232(1)	4726(1)	7280(2)	35(1)
C(50)	11384(2)	4495(2)	6731(3)	31(1)
N(50)	12036(2)	4340(2)	6758(2)	36(1)
C(51)	12700(2)	4521(2)	7307(3)	37(1)
S(50)	12875(1)	5227(1)	7748(1)	42(1)
N(51)	13254(2)	4145(2)	7445(3)	55(1)
C(54)	13109(3)	3560(3)	7058(4)	60(2)
C(55)	12782(4)	3125(3)	7461(5)	88(2)
N(61)	9731(2)	4591(2)	8711(2)	26(1)
C(62)	9059(2)	4480(2)	8698(3)	29(1)
C(63)	8961(2)	4258(2)	9369(3)	36(1)
C(64)	9572(2)	4136(2)	10053(3)	38(1)
C(65)	10276(2)	4222(2)	10068(3)	36(1)
C(66)	10334(2)	4454(2)	9383(3)	30(1)
O(70)	8510(1)	4942(1)	7418(2)	32(1)
C(70)	8409(2)	4590(2)	7905(3)	30(1)
N(70)	7790(2)	4318(2)	7841(2)	33(1)
C(71)	7186(2)	4225(2)	7156(3)	32(1)
S(70)	7171(1)	4182(1)	6186(1)	42(1)
N(71)	6570(2)	4084(2)	7257(2)	40(1)
C(74)	6590(2)	4022(2)	8082(3)	45(1)
C(75)	6881(3)	3434(3)	8436(3)	56(2)
C(72)	5845(2)	3961(2)	6571(3)	50(1)
C(73)	5385(3)	4517(3)	6318(5)	87(2)
O(80)	11081(1)	4893(1)	8796(2)	32(1)
C(80)	11079(2)	4559(2)	9349(3)	29(1)
N(80)	11646(2)	4309(2)	9944(2)	35(1)

C(81)	12342(2)	4230(2)	9980(3)	31(1)
S(80)	12545(1)	4137(1)	9131(1)	39(1)
N(81)	12875(2)	4159(2)	10709(2)	38(1)
C(82)	13652(2)	4010(2)	10864(3)	49(1)
C(83)	14154(3)	4546(3)	11065(5)	81(2)
C(84)	12698(3)	4180(2)	11429(3)	45(1)
C(85)	12433(3)	3583(3)	11586(3)	63(2)
P	5095(1)	7361(1)	7603(1)	59(1)
F(1)	5109(2)	8059(2)	7615(3)	109(1)
C(52A)	14054(4)	4344(4)	7885(5)	55(2)
C(53A)	14389(5)	4050(5)	8701(6)	82(3)
C(52B)	13962(11)	4112(11)	8248(14)	55(2)
C(53B)	14526(12)	4325(12)	7961(14)	82(3)
F(3)	4364(5)	7330(4)	6821(5)	89(3)
F(4)	4534(5)	7502(4)	8049(7)	107(3)
F(5)	5867(4)	7418(3)	8319(5)	79(3)
F(6)	5562(6)	7454(5)	7029(8)	134(4)
F(3B)	4613(6)	7416(5)	6634(6)	92(3)
F(4B)	4302(6)	7350(5)	7598(8)	93(3)
F(5B)	5529(5)	7298(4)	8586(6)	89(4)
F(6B)	5839(6)	7289(5)	7549(8)	109(4)
F(2)	5101(4)	6662(3)	7537(5)	38(2)
F(2A)	5385(8)	6762(7)	7313(9)	70(4)
F(2B)	4911(5)	6693(4)	7793(6)	58(2)
C(90A)	9083(7)	2508(6)	8925(11)	153(8)
C(91A)	9492(7)	2889(4)	8390(8)	115(5)
C(92A)	9086(5)	3210(4)	7630(8)	139(8)
C(93A)	9472(6)	3532(3)	7308(5)	101(5)
C(94A)	10264(6)	3544(4)	7696(7)	100(5)
C(95A)	10637(5)	3227(4)	8360(6)	133(10)
C(96A)	10244(4)	2912(3)	8714(4)	58(7)
C(90B)	10412(16)	2564(10)	9590(20)	117(13)
C(91B)	10244(4)	2912(3)	8714(4)	120(30)
C(92B)	9492(7)	2889(4)	8390(8)	139(8)
C(93B)	9086(5)	3210(4)	7630(8)	101(5)
C(94B)	9472(6)	3532(3)	7308(5)	100(5)
C(95B)	10264(6)	3544(4)	7696(7)	133(10)
C(96B)	10637(5)	3227(4)	8360(6)	58(7)
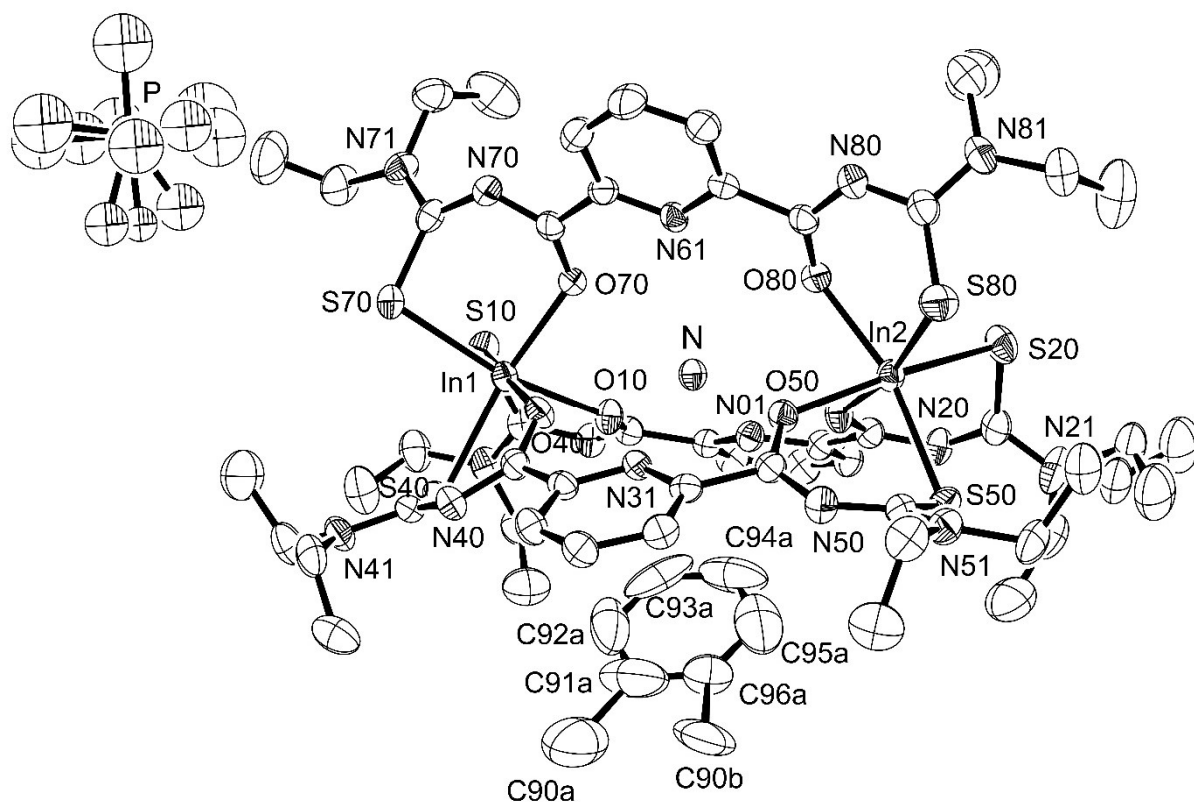
Figure 10: Ellipsoid plot (50% probability) of $\{NH_4 \subset [In_2(L^2)_3]\}(PF_6) \cdot$ toluene.

11. {Cs ⊂ [Fe₂(L³)₃]}(PF₆)

Table 21. Crystal data and structure refinement for {Cs ⊂ [Fe₂(L³)₃]}(PF₆).

Empirical formula	$C_{60}H_{84}O_{12}N_{12}S_6PF_6Fe_2Cs$
Formula weight	1747.33
Measurement instrument	STOE IPDS 2T
Temperature	200(2) K
Wavelength	0.71073 Å
Crystal system	Trigonal
Space group	R $\overline{3}$
Unit cell dimensions	a = 14.185(1) Å α = 90°.
	b = 14.185(1) Å β = 90°.
	c = 66.989(4) Å γ = 120°.
Volume	11673(2) Å³
Z	6
Density (calculated)	1.491 g/cm³
Absorption coefficient	1.092 mm⁻¹
F(000)	5376
Crystal size	0.23 x 0.20 x 0.17 mm³
Theta range for data collection	2.249 to 24.994°.
Index ranges	-16<=h<=16, -16<=k<=15, -79<=l<=79
Reflections collected	27366
Independent reflections	4566 [R(int) = 0.1085]
Completeness to theta = 24.994°	99.9 %
Absorption correction	None
Refinement method	Full-matrix least-squares on F^2
Data / restraints / parameters	4566 / 40 / 318
Goodness-of-fit on F^2	0.890
Final R indices [I>2sigma(I)]	R1 = 0.0449, wR2 = 0.1051
R indices (all data)	R1 = 0.0797, wR2 = 0.1128
Largest diff. peak and hole	1.168 and -0.778 e/Å³

Table 22. Atomic coordinates (x 10^4) and equivalent isotropic displacement parameters (Å^2 x 10^3) for {Cs $\subset$ [Fe$_2$(L^3)$_3$]}(PF$_6$). U(eq) is defined as one third of the trace of the orthogonalized U^{ij} tensor.

	x	y	z	U(eq)
Fe(1)	6667	3333	-12(1)	27(1)
Fe(2)	6667	3333	1211(1)	32(1)
Cs	6667	3333	594(1)	37(1)
C(01)	4951(4)	4777(4)	654(1)	40(1)
C(02)	5021(5)	5759(5)	699(1)	56(2)
C(03)	4584(6)	5885(6)	872(1)	73(2)
C(04)	4128(6)	5050(6)	1007(1)	78(2)
C(05)	4027(5)	4036(6)	963(1)	59(2)
C(06)	4419(4)	3899(4)	784(1)	41(1)
C(10)	5812(4)	5394(4)	340(1)	39(1)
C(11)	6203(4)	5052(4)	159(1)	31(1)
C(12)	6961(4)	5765(4)	-157(1)	33(1)
C(13)	7713(4)	6740(5)	-474(1)	48(1)
C(14)	8935(5)	7357(5)	-447(1)	64(2)
C(15)	6742(5)	7345(4)	-241(1)	47(1)
C(16)	7614(6)	8449(6)	-195(2)	98(3)
O(10)	5355(3)	4555(3)	482(1)	41(1)
O(11)	6256(3)	4194(3)	171(1)	36(1)
N(10)	6456(3)	5753(3)	14(1)	39(1)
N(11)	7144(3)	6577(3)	-283(1)	38(1)
S(10)	7429(1)	4898(1)	-228(1)	37(1)
C(20)	3760(4)	2004(4)	845(1)	48(1)
C(21)	4410(4)	2060(4)	1029(1)	37(1)
C(22)	4201(4)	1150(4)	1333(1)	40(1)
C(23)	3671(5)	-84(5)	1626(1)	64(2)
C(24)	3512(6)	453(7)	1804(1)	88(3)
C(25)	2282(5)	-274(6)	1371(1)	71(2)
C(26)	2081(7)	-1153(7)	1227(1)	107(3)
O(20)	4332(3)	2937(3)	719(1)	41(1)
O(21)	5416(3)	2714(3)	1020(1)	40(1)
N(20)	3808(3)	1353(4)	1163(1)	45(1)
N(21)	3431(4)	304(4)	1437(1)	51(1)
S(20)	5513(1)	1811(1)	1423(1)	45(1)

P(1)	3333	6667	1667	108(2)
F(1)	3328(7)	7566(5)	1804(1)	176(3)
P(2)	10000	10000	-837(1)	73(2)
F(2)	10000	10000	-610(2)	128(5)
F(3)	10000	10000	-1061(2)	184(8)
F(4)	9564(18)	8827(11)	-887(3)	154(6)
F(5)	10734(14)	9662(15)	-762(3)	132(5)
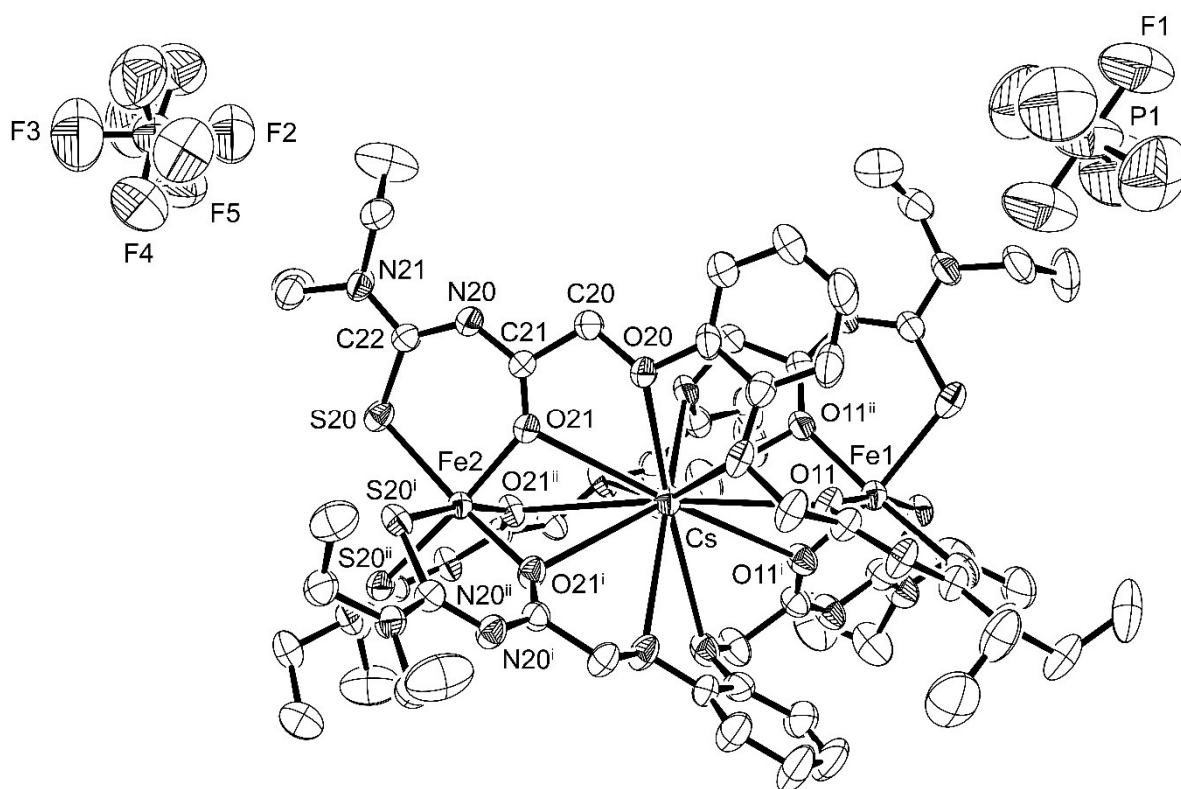
Figure 11: Ellipsoid plot (50% probability) of $\{Cs \subset [Fe_2(L^3)_3]\}(PF_6)$.

12. $\{Rb \subset [Fe_2(L^3)_3]\}(PF_6)$

Table 23. Crystal data and structure refinement for $\{Rb \subset [Fe_2(L^3)_3]\}(PF_6)$.

Empirical formula	$C_{60}H_{84}O_{12}N_{12}S_6PF_6Fe_2Rb$
Formula weight	1699.89
Measurement instrument	STOE IPDS 2T
Temperature	200(2) K
Wavelength	0.71073 Å
Crystal system	Trigonal
Space group	$R\bar{3}$
Unit cell dimensions	$a = 14.260(1)$ Å $\quad \alpha = 90°.$
	$b = 14.260(1)$ Å $\quad \beta = 90°.$
	$c = 66.790(6)$ Å $\quad \gamma = 120°.$
Volume	11762(2) Å^3
Z	6
Density (calculated)	1.440 g/cm^3
Absorption coefficient	1.243 mm^{-1}
F(000)	5268
Crystal size	0.5 x 0.26 x 0.24 mm^3
Theta range for data collection	3.313 to 24.991°.
Index ranges	-11<=h<=16, -16<=k<=16, -79<=l<=79
Reflections collected	16653
Independent reflections	4580 [R(int) = 0.0744]
Completeness to theta = 24.991°	99.7 %
Absorption correction	None
Refinement method	Full-matrix least-squares on F^2
Data / restraints / parameters	4580 / 10 / 302
Goodness-of-fit on F^2	1.054
Final R indices [I>2sigma(I)]	R1 = 0.0604, wR2 = 0.1570
R indices (all data)	R1 = 0.0842, wR2 = 0.1678
Largest diff. peak and hole	0.705 and -0.765 e/Å^3

Table 24. Atomic coordinates (x 10^4) and equivalent isotropic displacement parameters (Å^2 x 10^3) for {Rb $\subset$ [Fe$_2$(L^3)$_3$]}(PF$_6$). U(eq) is defined as one third of the trace of the orthogonalized U^{ij} tensor.

	x	y	z	U(eq)
Fe(1)	6667	3333	-13(1)	30(1)
Fe(2)	6667	3333	1203(1)	34(1)
Rb	6667	3333	589(1)	39(1)
C(01)	5273(5)	249(5)	656(1)	40(1)
C(02)	4316(6)	-668(5)	705(1)	58(2)
C(03)	4241(7)	-1227(7)	880(1)	77(2)
C(04)	5097(8)	-827(6)	1008(1)	79(3)
C(05)	6082(7)	83(6)	959(1)	60(2)
C(06)	6175(5)	607(5)	781(1)	42(1)
O(10)	5446(3)	885(3)	488(1)	44(1)
C(10)	4618(5)	456(5)	343(1)	40(1)
C(11)	4953(4)	1185(4)	161(1)	32(1)
C(12)	4233(4)	1219(4)	-158(1)	33(1)
C(13)	3278(6)	992(5)	-476(1)	49(2)
C(14)	2657(6)	1582(6)	-454(1)	66(2)
C(15)	2676(5)	-573(5)	-242(1)	48(2)
C(16)	1573(7)	-813(7)	-201(2)	94(3)
O(11)	5790(3)	2091(3)	175(1)	38(1)
N(10)	4248(4)	723(4)	15(1)	38(1)
N(11)	3439(4)	580(4)	-285(1)	41(1)
S(10)	5104(1)	2551(1)	-227(1)	39(1)
O(20)	7113(3)	1481(3)	710(1)	42(1)
C(20)	8058(5)	1865(6)	832(1)	49(2)
C(21)	8013(5)	2454(5)	1017(1)	38(1)
C(22)	8869(5)	3105(5)	1328(1)	43(1)
C(23)	10039(6)	3759(6)	1629(1)	67(2)
C(24)	9466(10)	3039(8)	1804(1)	96(3)
C(25)	10263(7)	2593(8)	1372(1)	76(2)
C(26)	11167(9)	3299(12)	1233(2)	118(4)
O(21)	7357(3)	2790(3)	1007(1)	43(1)
N(20)	8680(4)	2517(5)	1157(1)	48(1)
N(21)	9675(4)	3158(5)	1437(1)	53(1)
S(20)	8192(1)	3743(1)	1417(1)	46(1)

P(1)	3333	6667	1667	142(4)
F(1)	4208(9)	7582(9)	1537(1)	208(4)
P(2)	3333	6667	7512(1)	76(2)
F(2)	3333	6667	7736(3)	205(14)
F(3)	3333	6667	7290(3)	280(20)
F(4)	4425(14)	7356(17)	7430(3)	141(7)
F(5)	3980(20)	6160(20)	7571(4)	163(9)
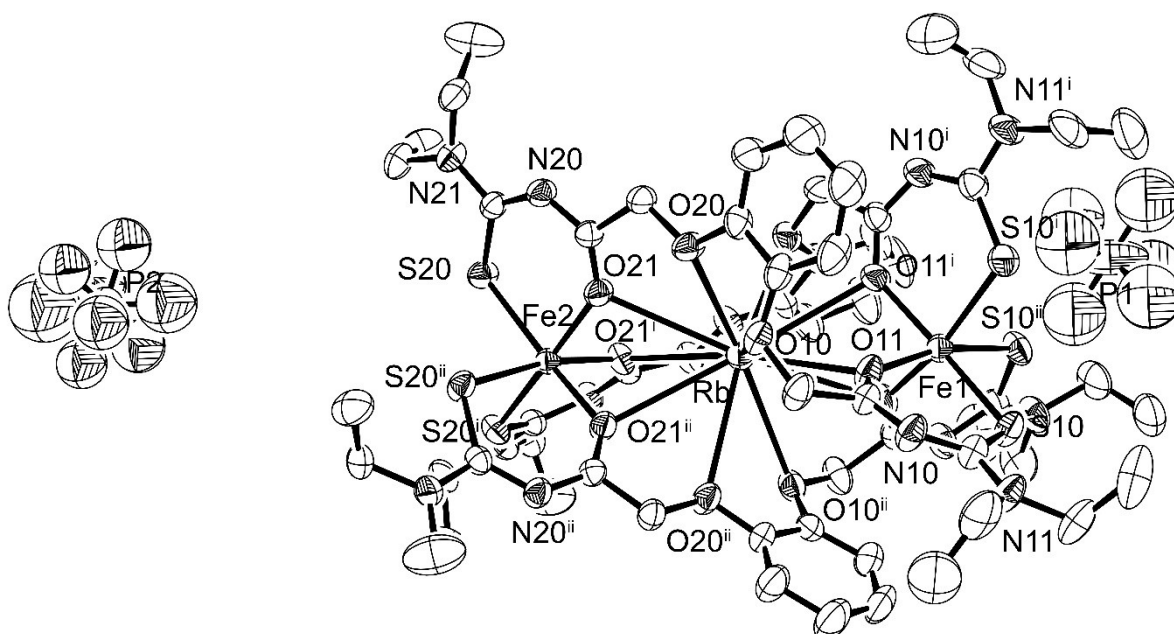
Figure 12: Ellipsoid plot (50% probability) of $\{Rb \subset [Fe_2(L^3)_3]\}(PF_6)$.

13. {K ⊂ [Fe₂(L³)₃]}(PF₆)

Table 25. Crystal data and structure refinement for {K ⊂ [Fe₂(L³)₃]}(PF₆).

Empirical formula	$C_{60}H_{84}O_{12}N_{12}S_6PF_6Fe_2K$
Formula weight	1653.52
Measurement instrument	STOE IPDS 2T
Temperature	200(2) K
Wavelength	0.71073 Å
Crystal system	Trigonal
Space group	R $\bar{3}$
Unit cell dimensions	a = 14.218(1) Å $\quad$ α = 90°.
	b = 14.218(1) Å $\quad$ β = 90°.
	c = 66.482(5) Å $\quad$ γ = 120°.
Volume	11639(2) Å³
Z	6
Density (calculated)	1.415 g/cm³
Absorption coefficient	0.686 mm⁻¹
F(000)	5160
Crystal size	0.140 x 0.100 x 0.085 mm³
Theta range for data collection	2.254 to 25.000°.
Index ranges	-16<=h<=16, -16<=k<=16, -78<=l<=78
Reflections collected	23173
Independent reflections	4557 [R(int) = 0.1190]
Completeness to theta = 25.000°	99.9 %
Absorption correction	None
Refinement method	Full-matrix least-squares on F^2
Data / restraints / parameters	4557 / 5 / 306
Goodness-of-fit on F^2	0.922
Final R indices [I>2sigma(I)]	R1 = 0.0604, wR2 = 0.1482
R indices (all data)	R1 = 0.1205, wR2 = 0.1721
Largest diff. peak and hole	0.700 and -0.567 e/Å³

Table 26. Atomic coordinates (x 10^4) and equivalent isotropic displacement parameters (Å^2 x 10^3) for $\{K \subset [Fe_2(L^3)_3]\}(PF_6)$. U(eq) is defined as one third of the trace of the orthogonalized U^{ij} tensor.

	x	y	z	U(eq)
Fe(1)	0	0	2867(1)	33(1)
Fe(2)	0	0	1651(1)	31(1)
K	0	0	2254(1)	46(1)
C(01)	-2212(4)	467(5)	2448(1)	39(1)
C(02)	-2675(5)	534(6)	2626(1)	55(2)
C(03)	-2629(6)	1512(7)	2676(1)	71(2)
C(04)	-2129(6)	2391(6)	2553(1)	67(2)
C(05)	-1635(5)	2338(5)	2378(1)	56(2)
C(06)	-1666(5)	1375(5)	2326(1)	40(1)
C(10)	-2839(5)	-1435(5)	2491(1)	45(1)
C(11)	-2211(4)	-1377(4)	2678(1)	36(1)
C(12)	-2421(4)	-2214(5)	2993(1)	39(1)
C(13)	-2953(6)	-3365(6)	3300(1)	60(2)
C(14)	-3098(7)	-2759(8)	3472(1)	82(3)
C(15)	-4339(5)	-3605(6)	3039(1)	66(2)
C(16)	-4544(8)	-4499(7)	2898(2)	104(3)
O(10)	-2256(3)	-464(3)	2372(1)	41(1)
O(11)	-1215(3)	-750(3)	2668(1)	44(1)
N(10)	-2818(4)	-2039(4)	2820(1)	44(1)
N(11)	-3181(4)	-3016(4)	3106(1)	50(1)
S(10)	-1108(1)	-1530(1)	3082(1)	43(1)
C(20)	-801(5)	2059(5)	2010(1)	42(1)
C(21)	-410(4)	1728(4)	1829(1)	32(1)
C(22)	319(4)	2438(4)	1507(1)	33(1)
C(23)	1040(5)	3382(5)	1185(1)	49(2)
C(24)	2255(5)	4009(6)	1208(1)	61(2)
C(25)	70(5)	3986(5)	1425(1)	47(2)
C(26)	962(7)	5119(6)	1468(2)	94(3)
O(20)	-1172(3)	1236(3)	2160(1)	44(1)
O(21)	-353(3)	875(3)	1841(1)	38(1)
N(20)	-171(4)	2431(4)	1681(1)	36(1)
N(21)	469(4)	3229(4)	1378(1)	38(1)
S(20)	787(1)	1569(1)	1436(1)	39(1)

P(1)	6667	3333	3333	149(4)
F(1)	6549(10)	4158(8)	3468(2)	114(4)
P(2)	0	0	4142(1)	70(2)
F(2)	0	0	3869(3)	392(17)
F(3)	0	0	4394(3)	237(16)
F(4)	-750(20)	710(20)	4132(3)	274(12)
F(5)	500(20)	1231(15)	4230(4)	266(11)
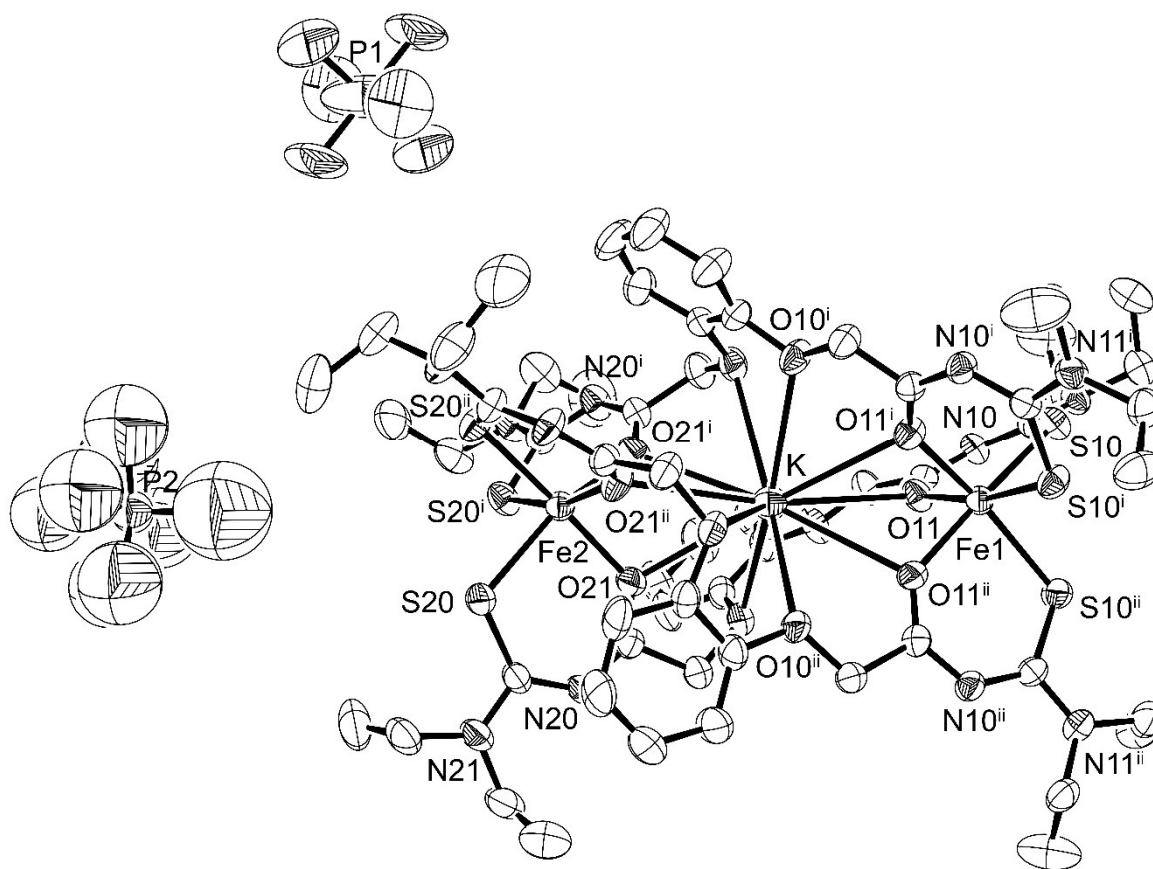
Figure 13: Ellipsoid plot (50% probability) of $\{K \subset [Fe_2(L^3)_3]\}(PF_6)$.

14. $\{Tl \subset [Fe_2(L^3)_3]\}(PF_6)$

Table 27. Crystal data and structure refinement for $\{Tl \subset [Fe_2(L^3)_3]\}(PF_6)$.

Empirical formula	$C_{60}H_{84}O_{12}N_{12}S_6PF_6Fe_2Tl$
Formula weight	1818.83
Measurement instrument	STOE IPDS 2T
Temperature	200(2) K
Wavelength	0.71073 Å
Crystal system	Trigonal
Space group	$R\bar{3}$
Unit cell dimensions	$a = 14.242(1)$ Å $\quad \alpha = 90°$.
	$b = 14.242(1)$ Å $\quad \beta = 90°$.
	$c = 66.710(5)$ Å $\quad \gamma = 120°$.
Volume	11718(2) $Å^3$
Z	6
Density (calculated)	1.546 g/cm^3
Absorption coefficient	2.681 mm^{-1}
F(000)	5531
Crystal size	0.12 x 0.10 x 0.09 mm^3
Theta range for data collection	3.318 to 24.999°.
Index ranges	$-16 \leq h \leq 16, -16 \leq k \leq 16, -78 \leq l \leq 79$
Reflections collected	26870
Independent reflections	4568 [R(int) = 0.1174]
Completeness to theta = 24.999°	99.7 %
Absorption correction	None
Refinement method	Full-matrix least-squares on F^2
Data / restraints / parameters	4568 / 40 / 318
Goodness-of-fit on F^2	0.802
Final R indices [I>2sigma(I)]	R1 = 0.0406, wR2 = 0.0659
R indices (all data)	R1 = 0.0966, wR2 = 0.0749
Largest diff. peak and hole	0.896 and -0.503 $e/Å^3$

Table 28. Atomic coordinates (x 10^4) and equivalent isotropic displacement parameters ($Å^2$ x 10^3) for {Tl $\subset$ [Fe$_2$(L^3)$_3$]}(PF$_6$). U(eq) is defined as one third of the trace of the orthogonalized U^{ij} tensor.

	x	y	z	U(eq)
C(01)	8612(5)	1701(5)	2323(1)	36(1)
C(02)	7665(5)	1666(5)	2373(1)	51(2)
C(03)	7575(6)	2120(6)	2548(1)	68(2)
C(04)	8429(7)	2591(7)	2676(1)	72(2)
C(05)	9415(7)	2666(6)	2627(1)	60(2)
C(06)	9520(5)	2238(5)	2447(1)	39(2)
C(10)	7955(4)	835(5)	2008(1)	34(1)
C(11)	8288(4)	440(4)	1827(1)	27(1)
C(12)	7571(4)	-306(4)	1509(1)	29(1)
C(13)	6602(5)	-1048(5)	1190(1)	47(2)
C(14)	5994(6)	-2262(5)	1214(1)	63(2)
C(15)	6002(5)	-83(5)	1427(1)	43(2)
C(16)	4895(6)	-967(6)	1467(1)	87(3)
C(20)	11410(5)	2867(5)	2496(1)	43(2)
C(21)	11348(5)	2230(5)	2682(1)	33(1)
C(22)	12219(5)	2441(5)	2991(1)	36(2)
C(23)	13606(6)	4326(6)	3037(1)	74(2)
C(24)	14499(8)	4524(8)	2899(2)	117(4)
C(25)	13363(6)	2945(6)	3297(1)	64(2)
C(26)	12800(8)	3106(6)	3468(1)	88(3)
O(10)	8791(3)	1258(3)	2153(1)	40(1)
O(11)	9134(3)	384(3)	1840(1)	31(1)
O(20)	10460(3)	2304(3)	2376(1)	37(1)
O(21)	10700(3)	1235(3)	2673(1)	37(1)
N(10)	7576(4)	185(4)	1681(1)	34(1)
N(11)	6762(4)	-480(4)	1383(1)	36(1)
N(20)	12028(4)	2821(4)	2821(1)	41(1)
N(21)	13013(4)	3182(4)	3104(1)	50(1)
S(10)	8435(1)	-772(1)	1438(1)	34(1)
S(20)	11530(1)	1115(1)	3082(1)	42(1)
Fe(1)	10000	0	1653(1)	26(1)
Fe(2)	10000	0	2868(1)	31(1)
Tl	10000	0	2260(1)	41(1)

176

P(1)	6667	3333	3333	146(4)
F(1)	5827(6)	3427(8)	3466(1)	135(3)
P(2)	3333	6667	818(1)	67(2)
F(4)	3978(14)	7716(8)	874(2)	238(6)
F(5)	4451(12)	7200(20)	742(3)	171(7)
F(3)	3333	6667	592(2)	167(8)
F(2)	3333	6667	1037(2)	160(7)
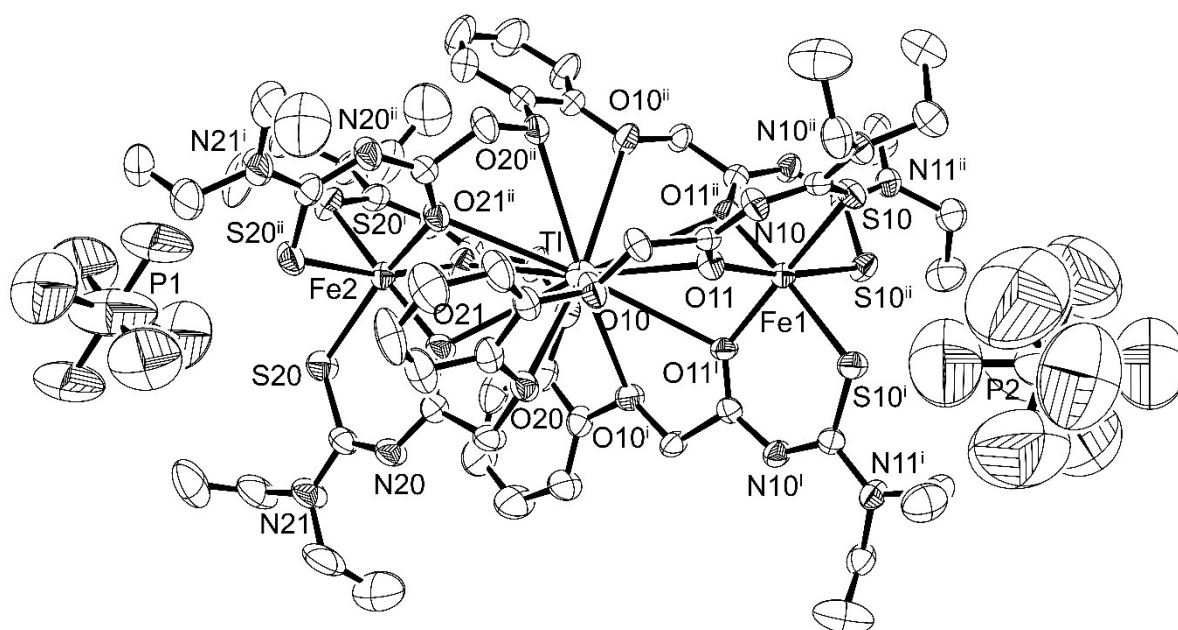
Figure 14: Ellipsoid plot (50% probability) of $\{Tl \subset [Fe_2(L^3)_3]\}(PF_6)$.

15. {NH$_4 \subset$ [Fe$_2$(L^3)$_3$]}(PF$_6$)

Table 29. Crystal data and structure refinement for {NH$_4 \subset$ [Fe$_2$(L^3)$_3$]}(PF$_6$).

Empirical formula	C$_{60}$H$_{88}$O$_{12}$N$_{13}$S$_6$PF$_6$Fe$_2$
Formula weight	1632.46
Measurement instrument	STOE IPDS 2T
Temperature	200(2) K
Wavelength	0.71073 Å
Crystal system	Trigonal
Space group	R $\overline{3}$
Unit cell dimensions	a = 14.241(6) Å $\alpha = 90°$.
	b = 14.241(6) Å $\beta = 90°$.
	c = 66.682(4) Å $\gamma = 120°$.
Volume	11712(1) Å^3
Z	6
Density (calculated)	1.389 g/cm^3
Absorption coefficient	0.629 mm^{-1}
F(000)	5112
Crystal size	0.15 x 0.099 x 0.025 mm^3
Theta range for data collection	3.318 to 24.997°.
Index ranges	-16<=h<=16, -16<=k<=16, -79<=l<=79
Reflections collected	30237
Independent reflections	4566 [R(int) = 0.1004]
Completeness to theta = 24.997°	99.7 %
Absorption correction	None
Refinement method	Full-matrix least-squares on F^2
Data / restraints / parameters	4566 / 19 / 314
Goodness-of-fit on F^2	1.057
Final R indices [I>2sigma(I)]	R1 = 0.0691, wR2 = 0.1604
R indices (all data)	R1 = 0.1033, wR2 = 0.1763
Largest diff. peak and hole	0.881 and -0.588 e/Å^3

Table 30. Atomic coordinates (x 10^4) and equivalent isotropic displacement parameters (Å^2 x 10^3) for $\{NH_4 \subset [Fe_2(L^3)_3]\}(PF_6)$. U(eq) is defined as one third of the trace of the orthogonalized U^{ij} tensor.

	x	y	z	U(eq)
Fe(1)	3333	6667	10014(1)	30(1)
Fe(2)	3333	6667	8794(1)	35(1)
C(01)	5040(4)	5284(4)	9344(1)	42(1)
C(02)	4998(5)	4326(5)	9296(1)	59(2)
C(03)	5488(7)	4267(6)	9120(1)	78(2)
C(04)	5973(7)	5129(7)	8994(1)	82(2)
C(05)	6027(6)	6101(6)	9041(1)	63(2)
C(06)	5576(4)	6189(5)	9218(1)	43(1)
C(10)	4168(4)	4620(4)	9658(1)	42(1)
C(11)	3767(4)	4953(4)	9839(1)	32(1)
C(12)	3019(4)	4226(4)	10158(1)	36(1)
C(13)	2268(5)	3268(5)	10476(1)	50(1)
C(14)	1068(5)	2668(5)	10453(1)	64(2)
C(15)	3245(5)	2664(5)	10239(1)	48(1)
C(16)	2367(7)	1562(6)	10194(2)	96(3)
O(10)	4576(3)	5453(3)	9513(1)	42(1)
O(11)	3719(3)	5806(3)	9826(1)	38(1)
N(10)	3518(3)	4239(3)	9985(1)	38(1)
N(11)	2855(3)	3430(3)	10284(1)	41(1)
S(10)	2560(1)	5103(1)	10229(1)	39(1)
C(20)	6188(4)	8075(5)	9170(1)	49(1)
C(21)	5555(4)	8013(4)	8983(1)	36(1)
C(22)	5764(4)	8879(4)	8674(1)	43(1)
C(23)	6296(6)	10039(6)	8369(1)	77(2)
C(24)	6441(7)	9463(8)	8196(1)	94(3)
C(25)	7672(6)	10292(7)	8631(1)	82(2)
C(26)	7888(8)	11157(8)	8770(2)	118(4)
O(20)	5628(3)	7123(3)	9292(1)	43(1)
O(21)	4560(3)	7343(3)	8991(1)	44(1)
N(20)	6152(3)	8697(4)	8846(1)	48(1)
N(21)	6529(4)	9689(4)	8562(1)	58(1)
S(20)	4455(1)	8201(1)	8583(1)	47(1)
P(1)	6667	3333	8333	144(3)
F(1)	5726(7)	3238(10)	8199(2)	69(3)
P(2)	3333	6667	7516(1)	64(1)

F(2)	3333	6667	7285(2)	175(11)
F(3)	3333	6667	7751(2)	160(9)
F(4)	2653(17)	7111(18)	7443(3)	267(8)
F(5)	2141(12)	5997(19)	7574(3)	307(10)
N	3333	6667	9417(1)	41(2)

Table 31. Hydrogen bonds for $\{NH_4 \subset [Fe_2(L^3)_3]\}(PF_6)$ [Å and °].

D-H...A	d(D-H)	d(H...A)	d(D...A)	<(DHA)
N-H(1)...O(10)	0.94(7)	2.21(7)	3.095(4)	155(6)
N-H(1)...O(11)	0.94(7)	2.43(8)	3.149(8)	133(6)
N-H(2)...O(21)	0.80(14)	2.54(12)	3.222(8)	143(2)
N-H(2)...O(21)#2	0.80(14)	2.54(12)	3.222(8)	143(2)
N-H(2)...O(21)#1	0.80(14)	2.54(12)	3.222(8)	143(2)

Symmetry transformations used to generate equivalent atoms: ^{i} -x+y, -x+1, z; ^{ii} -y+1, x-y+1, z
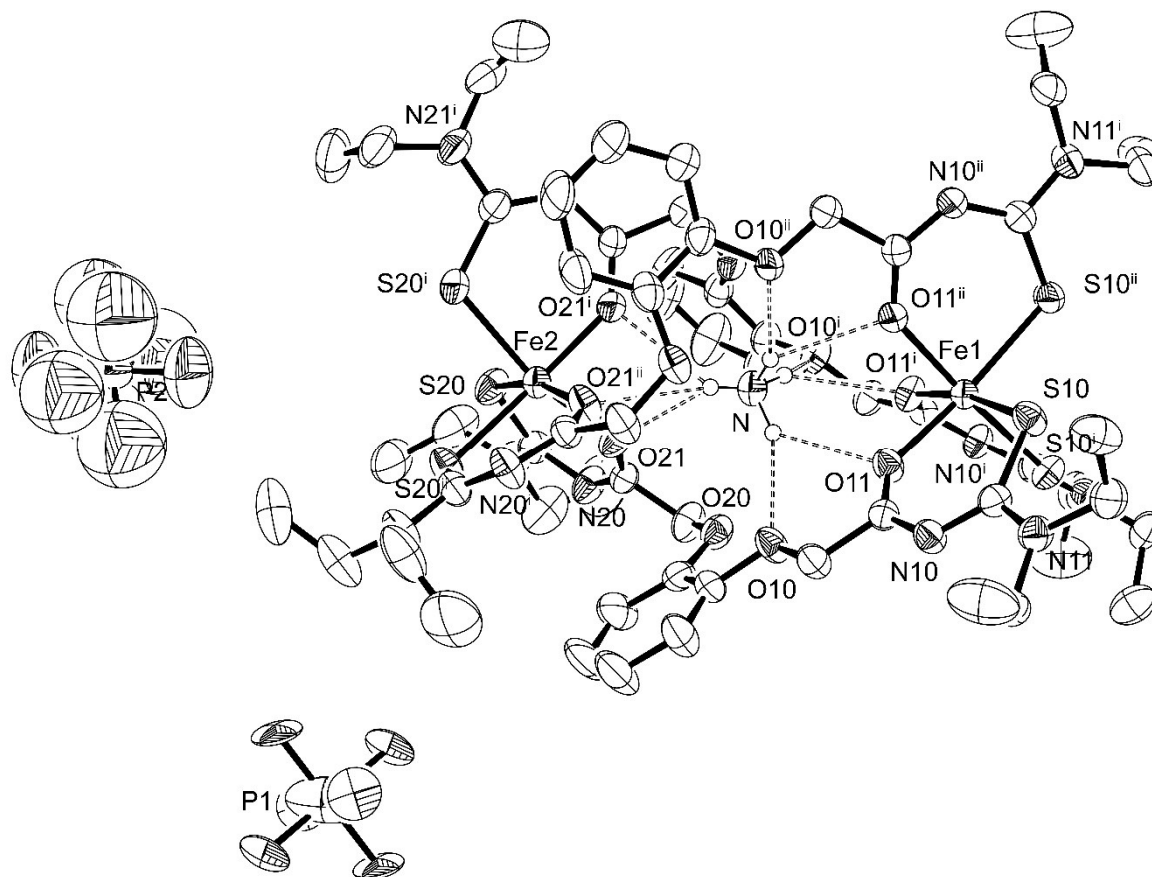
Figure 15: Ellipsoid plot (50% probability) of $\{NH_4 \subset [Fe_2(L^3)_3]\}(PF_6)$.

16. {Rb ⊂ [Co₂(L³)₃]}(PF₆) · 3 DMF

Table 32. Crystal data and structure refinement for {Rb ⊂ [Co₂(L³)₃]}(PF₆) · 3 DMF.

Empirical formula	$C_{69}H_{105}O_{15}N_{15}S_6PF_6Co_2Rb$
Formula weight	1925.33
Measurement instrument	STOE IPDS 2T
Temperature	200(2) K
Wavelength	0.71073 Å
Crystal system	Monoclinic
Space group	P 2₁/c
Unit cell dimensions	a = 24.758(2) Å $\qquad$ α = 90°.
	b = 14.029(1) Å $\qquad$ β = 126.11(1)°.
	c = 31.985(2) Å $\qquad$ γ = 90°.
Volume	8975(1) Å³
Z	4
Density (calculated)	1.425 g/cm³
Absorption coefficient	1.144 mm⁻¹
F(000)	4000
Crystal size	0.26 x 0.1 x 0.06 mm³
Theta range for data collection	3.305 to 24.999°.
Index ranges	-29<=h<=29, -15<=k<=16, -33<=l<=38
Reflections collected	56914
Independent reflections	15774 [R(int) = 0.1380]
Completeness to theta = 24.999°	99.7 %
Absorption correction	None
Refinement method	Full-matrix least-squares on F^2
Data / restraints / parameters	15774 / 0 / 1081
Goodness-of-fit on F^2	0.897
Final R indices [I>2sigma(I)]	R1 = 0.0595, wR2 = 0.1163
R indices (all data)	R1 = 0.1251, wR2 = 0.1390
Largest diff. peak and hole	0.681 and -0.725 e/Å³

Table 33. Atomic coordinates (x 10^4) and equivalent isotropic displacement parameters (Å^2 x 10^3) for {Rb $\subset$ [Co$_2$(L^3)$_3$]}(PF$_6$) $\cdot$ 3 DMF. U(eq) is defined as one third of the trace of the orthogonalized U^{ij} tensor.

	x	y	z	U(eq)
Co(1)	9325(1)	2427(1)	4199(1)	37(1)
Co(2)	6311(1)	2849(1)	4501(1)	37(1)
Rb	7873(1)	2591(1)	4394(1)	43(1)
C(01)	8259(2)	220(4)	5095(2)	46(1)
C(02)	8557(3)	-175(5)	5578(2)	63(2)
C(03)	8166(3)	-612(5)	5702(3)	69(2)
C(04)	7481(3)	-616(5)	5347(3)	64(2)
C(05)	7175(3)	-230(4)	4863(2)	55(2)
C(06)	7562(2)	190(4)	4727(2)	41(1)
C(10)	9303(2)	668(4)	5273(2)	50(2)
C(11)	9585(2)	1196(4)	5024(2)	38(1)
C(12)	10649(2)	1666(4)	5262(2)	46(1)
C(13)	11550(3)	747(6)	6006(3)	91(3)
C(14)	11945(7)	1036(9)	6514(4)	222(9)
O(10)	8589(2)	681(3)	4926(1)	54(1)
O(11)	9179(2)	1572(2)	4596(1)	39(1)
N(10)	10246(2)	1154(3)	5330(2)	45(1)
N(11)	11301(2)	1485(5)	5607(2)	83(2)
S(10)	10423(1)	2497(1)	4787(1)	47(1)
C(20)	6624(2)	478(4)	3852(2)	49(2)
C(21)	6229(2)	1202(4)	3922(2)	40(1)
C(22)	5122(2)	1643(4)	3575(2)	40(1)
C(23)	4325(3)	408(4)	2993(2)	53(2)
C(24)	4327(4)	-376(5)	3318(3)	86(2)
C(25)	3915(2)	1895(5)	3143(2)	58(2)
C(26)	3659(3)	2576(5)	2705(2)	69(2)
O(20)	7327(2)	545(3)	4250(1)	43(1)
O(21)	6566(2)	1877(3)	4226(1)	41(1)
N(20)	5584(2)	1016(3)	3642(2)	44(1)
N(21)	4485(2)	1328(3)	3255(2)	44(1)
S(20)	5247(1)	2779(1)	3828(1)	48(1)
C(30)	7289(2)	3840(4)	3131(2)	40(1)
C(31)	7501(3)	4053(5)	2824(2)	53(2)

C(32)	7613(3)	4980(5)	2760(2)	58(2)
C(33)	7534(3)	5703(5)	3002(2)	55(2)
C(34)	7340(2)	5515(4)	3322(2)	46(1)
C(35)	7222(2)	4583(4)	3388(2)	42(1)
C(40)	7259(2)	2160(4)	2997(2)	50(2)
C(41)	8004(2)	1981(4)	3277(2)	41(1)
C(42)	8745(3)	1028(4)	3227(2)	48(1)
C(43)	8128(4)	69(6)	2416(3)	84(2)
C(44)	7953(4)	646(8)	1966(3)	117(3)
C(45)	9382(5)	-37(8)	3039(4)	133(5)
C(46)	9477(7)	-920(11)	3263(5)	215(9)
O(40)	7133(2)	2946(3)	3209(1)	45(1)
O(41)	8371(2)	2386(3)	3707(1)	41(1)
N(40)	8134(2)	1398(3)	3028(2)	47(1)
N(41)	8748(2)	389(4)	2915(2)	68(2)
S(40)	9490(1)	1249(1)	3822(1)	47(1)
C(50)	6907(3)	5037(4)	3941(2)	45(1)
C(51)	6659(2)	4586(4)	4224(2)	37(1)
C(52)	6378(2)	5057(4)	4786(2)	45(1)
C(53)	6606(3)	6765(5)	4976(3)	66(2)
C(54)	6120(4)	7286(5)	4485(3)	88(2)
C(55)	6144(4)	5801(6)	5365(3)	76(2)
C(56)	5483(5)	6286(9)	5115(4)	141(4)
O(50)	7042(2)	4299(3)	3701(1)	47(1)
O(51)	6528(2)	3711(3)	4153(1)	39(1)
N(50)	6619(2)	5228(3)	4502(2)	46(1)
N(51)	6363(2)	5837(4)	5022(2)	56(1)
S(50)	6085(1)	3996(1)	4853(1)	50(1)
C(60)	8582(2)	4728(4)	5310(2)	41(1)
C(61)	8563(3)	5702(4)	5355(2)	48(1)
C(62)	8387(3)	6068(5)	5670(2)	62(2)
C(63)	8240(3)	5458(5)	5926(2)	63(2)
C(64)	8267(3)	4480(5)	5880(2)	53(2)
C(65)	8449(2)	4106(4)	5582(2)	40(1)
C(70)	8936(3)	4886(4)	4761(2)	44(1)
C(71)	9127(2)	4296(4)	4469(2)	38(1)
C(72)	9411(3)	4562(4)	3891(2)	53(2)
C(75)	9799(4)	5101(6)	3373(3)	81(2)
C(76)	9228(4)	5075(9)	2836(4)	135(4)

O(70)	8719(2)	4288(3)	4993(1)	43(1)
O(71)	9150(2)	3413(3)	4525(1)	37(1)
N(70)	9250(3)	4860(4)	4208(2)	62(1)
N(71)	9539(4)	5261(4)	3681(3)	91(2)
S(70)	9445(1)	3419(1)	3720(1)	48(1)
C(80)	8337(2)	2492(4)	5756(2)	47(1)
C(81)	7581(2)	2420(4)	5460(2)	40(1)
C(82)	6775(3)	1570(4)	5480(2)	48(1)
C(83)	7309(4)	754(7)	6313(3)	94(3)
C(84)	7455(5)	1552(9)	6690(3)	130(4)
C(85)	6076(3)	631(7)	5649(3)	90(3)
C(86)	5929(4)	-361(7)	5420(4)	131(4)
O(80)	8520(2)	3154(3)	5524(1)	43(1)
O(81)	7244(2)	2885(3)	5047(1)	43(1)
N(80)	7409(2)	1850(4)	5691(2)	50(1)
N(81)	6717(2)	995(4)	5788(2)	67(2)
S(80)	6061(1)	1791(1)	4875(1)	49(1)
C(90)	5229(6)	8104(8)	7696(4)	108(3)
C(91)	5601(4)	6530(7)	8009(4)	135(4)
C(92)	4469(4)	6847(10)	7233(3)	167(6)
O(90)	5788(5)	8438(7)	8053(3)	173(4)
N(90)	5096(3)	7168(5)	7639(2)	75(2)
C(100)	3722(6)	9864(8)	7703(5)	132(4)
C(101)	3954(5)	10169(9)	8541(4)	141(4)
C(102)	4804(5)	9507(10)	8479(5)	183(6)
O(100)	3822(4)	9604(6)	7384(3)	134(3)
N(100)	4145(3)	9832(6)	8202(3)	96(2)
C(110)	9922(5)	7719(14)	7652(4)	209(9)
C(111)	10731(4)	7443(13)	7572(4)	202(8)
C(112)	9526(4)	7410(11)	6829(3)	167(6)
O(110)	10335(5)	7972(12)	8115(4)	303(9)
N(110)	10048(3)	7495(5)	7358(2)	84(2)
C(15A)	11798(5)	1760(11)	5489(5)	58(4)
C(16A)	12116(8)	2619(12)	5778(8)	92(4)
C(15B)	11783(7)	2412(14)	5734(6)	59(5)
C(16B)	12194(10)	2127(13)	5564(9)	92(4)
C(73A)	9254(5)	6258(10)	3619(4)	54(3)
C(74A)	9833(6)	6802(14)	4040(5)	72(4)
C(74B)	9160(12)	6830(20)	3708(9)	96(9)

C(73B)	9799(10)	6268(18)	3993(9)	54(3)
P	7666(1)	7680(1)	6743(1)	54(1)
F(1)	8156(3)	8452(4)	6783(3)	155(3)
F(2)	7196(3)	6948(4)	6715(4)	184(3)
F(3)	7495(7)	8527(8)	6947(5)	96(2)
F(4)	7802(9)	6765(11)	6543(5)	148(4)
F(5)	6984(6)	7888(9)	6212(6)	136(4)
F(6)	8312(7)	7450(10)	7261(4)	119(3)
F(3B)	8207(5)	6922(6)	6888(5)	96(2)
F(5B)	7185(6)	8560(11)	6661(6)	136(4)
F(4B)	7912(8)	7627(9)	7318(4)	148(4)
F(6B)	7474(6)	7793(8)	6197(3)	119(3)
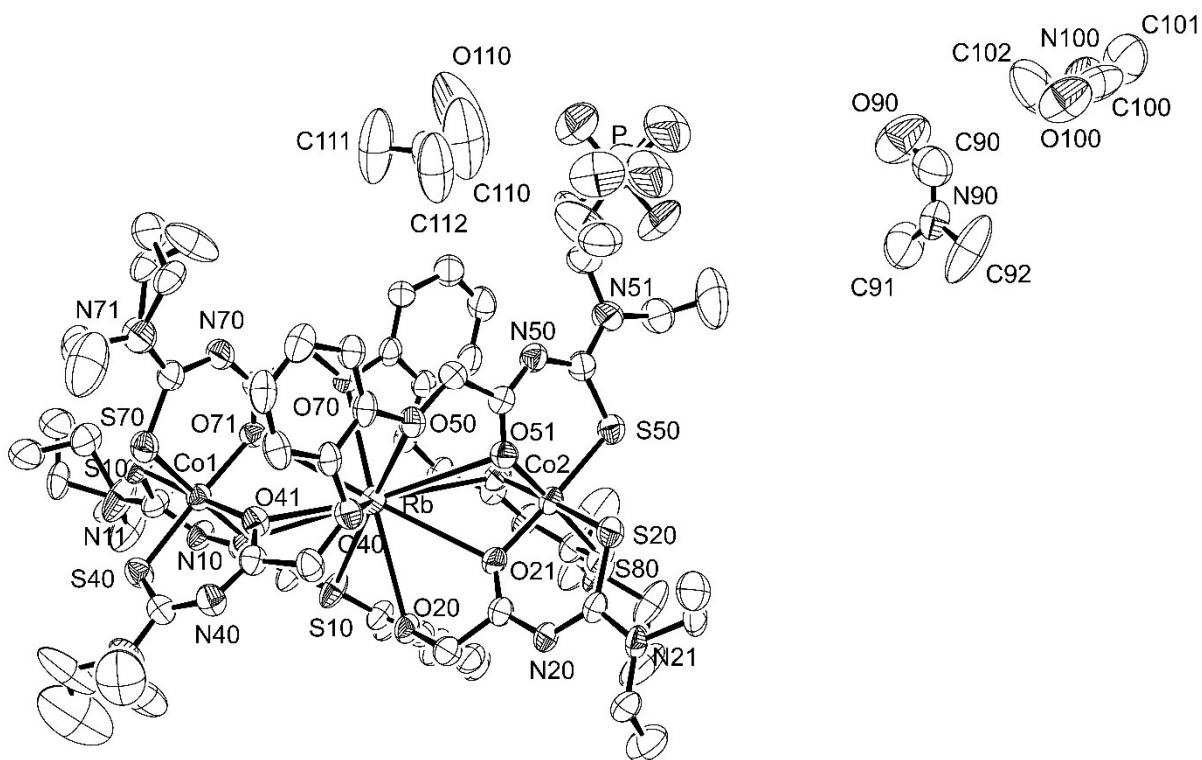
Figure 16: Ellipsoid plot (50% probability) of $\{Rb \subset [Co_2(L^3)_3]\}(PF_6) \cdot 3$ DMF.

187

17. {K ⊂ [Co₂(L³)₃]}(PF₆) · CH₃OH

Table 34. Crystal data and structure refinement for {K ⊂ [Co₂(L³)₃]}(PF₆) · CH₃OH.

Empirical formula	$C_{61}H_{88}O_{13}N_{12}S_6PF_6Co_2K$
Formula weight	1691.72
Measurement instrument	STOE IPDS 2T
Temperature	200(2) K
Wavelength	0.71073 Å
Crystal system	Triclinic
Space group	P $\bar{1}$
Unit cell dimensions	a = 14.909(1) Å α = 83.79(1)°.
	b = 16.089(1) Å β = 67.57(1)°.
	c = 18.049(1) Å γ = 81.34(1)°.
Volume	3950.2(5) Å³
Z	2
Density (calculated)	1.422 g/cm³
Absorption coefficient	0.729 mm⁻¹
F(000)	1760
Crystal size	0.4 x 0.35 x 0.27 mm³
Theta range for data collection	2.343 to 24.999°.
Index ranges	-17<=h<=17, -15<=k<=19, -21<=l<=21
Reflections collected	27898
Independent reflections	13813 [R(int) = 0.1049]
Completeness to theta = 24.999°	99.4 %
Absorption correction	None
Refinement method	Full-matrix least-squares on F²
Data / restraints / parameters	13813 / 8 / 939
Goodness-of-fit on F²	0.888
Final R indices [I>2sigma(I)]	R1 = 0.0623, wR2 = 0.1276
R indices (all data)	R1 = 0.1458, wR2 = 0.1571
Largest diff. peak and hole	1.032 and -0.475 e/Å³

Table 35. Atomic coordinates (x 10^4) and equivalent isotropic displacement parameters (Å^2 x 10^3) for $\{K \subset [Co_2(L^3)_3]\}(PF_6) \cdot CH_3OH$. U(eq) is defined as one third of the trace of the orthogonalized U^{ij} tensor.

	x	y	z	U(eq)
Co(1)	7120(1)	4950(1)	7455(1)	28(1)
Co(2)	5448(1)	9795(1)	7197(1)	29(1)
K	6367(1)	7341(1)	7315(1)	39(1)
C(01)	5003(5)	7567(4)	9584(4)	37(2)
C(02)	4148(5)	7622(5)	10238(5)	57(2)
C(03)	3915(5)	8290(5)	10737(5)	58(2)
C(04)	4547(5)	8876(5)	10579(4)	51(2)
C(05)	5419(5)	8826(4)	9920(4)	40(2)
C(06)	5663(4)	8162(4)	9420(4)	33(1)
C(10)	4766(5)	6245(4)	9265(4)	44(2)
C(11)	5301(5)	5569(4)	8677(4)	37(2)
C(12)	5056(5)	4248(4)	8363(4)	42(2)
C(13)	3283(6)	4031(5)	9065(6)	68(2)
C(14)	3147(10)	3711(8)	9860(8)	122(4)
C(15)	4574(6)	2912(4)	8195(5)	55(2)
C(16)	4334(6)	2959(5)	7463(6)	68(2)
O(10)	5302(3)	6946(3)	9039(3)	46(1)
O(11)	6132(3)	5683(3)	8193(3)	33(1)
N(10)	4782(4)	4933(4)	8806(4)	53(2)
N(11)	4376(5)	3727(4)	8551(4)	66(2)
S(10)	6150(1)	3983(1)	7590(1)	37(1)
C(20)	7144(4)	8665(4)	8532(4)	34(2)
C(21)	6783(4)	9359(4)	8038(4)	30(1)
C(22)	7189(4)	10646(4)	7317(4)	33(1)
C(25)	7754(6)	11981(4)	6611(5)	55(2)
C(26)	8220(7)	11817(6)	5750(5)	71(3)
O(20)	6541(3)	8008(3)	8789(2)	35(1)
O(21)	6022(3)	9244(3)	7933(2)	35(1)
N(20)	7334(3)	9974(3)	7793(3)	32(1)
N(21)	7822(4)	11215(3)	7139(4)	39(1)
S(20)	6288(1)	10874(1)	6922(1)	37(1)
C(31)	8899(4)	7997(4)	6610(3)	28(1)
C(32)	9545(4)	8333(4)	6841(4)	36(2)

190

C(33)	9853(5)	9103(4)	6517(4)	43(2)
C(34)	9520(5)	9532(5)	5955(4)	46(2)
C(35)	8886(4)	9198(4)	5702(4)	39(2)
C(36)	8591(4)	8429(4)	6013(4)	29(1)
C(40)	8848(4)	6782(4)	7497(4)	31(1)
C(41)	8447(4)	5938(4)	7678(4)	32(1)
C(42)	8449(4)	4716(4)	8505(4)	37(2)
C(43)	9612(6)	4708(6)	9177(6)	81(3)
C(44)	10617(7)	4494(9)	8558(8)	130(5)
O(40)	8520(3)	7259(3)	6917(3)	38(1)
O(41)	7903(3)	5834(3)	7317(2)	32(1)
N(40)	8762(4)	5449(3)	8175(3)	40(1)
N(41)	8892(5)	4307(4)	8990(4)	60(2)
S(40)	7534(1)	4236(1)	8416(1)	41(1)
C(50)	7566(5)	8482(4)	5261(4)	37(2)
C(51)	6799(4)	9193(4)	5670(4)	32(1)
C(52)	5827(5)	10387(4)	5394(4)	37(2)
C(53)	6588(5)	11022(5)	4037(4)	49(2)
C(54)	7386(7)	11509(8)	3967(7)	107(4)
C(55)	5012(6)	11695(5)	4980(5)	59(2)
C(56)	5198(8)	12433(6)	5338(6)	84(3)
O(50)	7971(3)	8018(3)	5805(3)	34(1)
O(51)	6467(3)	9116(3)	6420(3)	32(1)
N(50)	6614(4)	9786(3)	5160(3)	38(1)
N(51)	5806(4)	10999(3)	4840(3)	41(1)
S(50)	4837(1)	10394(1)	6296(1)	41(1)
C(61)	4831(4)	6240(4)	6456(4)	36(2)
C(62)	4669(5)	5493(5)	6239(5)	53(2)
C(63)	3807(6)	5154(5)	6657(6)	65(2)
C(64)	3095(6)	5557(5)	7303(6)	61(2)
C(65)	3258(5)	6302(5)	7530(5)	47(2)
C(66)	4118(5)	6634(4)	7110(4)	37(2)
C(70)	6470(5)	6171(4)	5500(4)	39(2)
C(71)	6959(4)	5505(4)	5926(4)	29(1)
C(72)	8256(4)	4407(4)	5641(4)	31(1)
C(73)	8960(6)	4187(5)	4197(4)	56(2)
C(74)	8416(6)	3602(6)	3970(5)	69(2)
C(75)	9730(4)	3394(4)	5108(5)	45(2)
C(76)	10632(5)	3810(5)	4975(6)	62(2)

O(70)	5639(3)	6648(3)	6047(3)	37(1)
O(71)	6725(3)	5604(3)	6659(2)	31(1)
N(70)	7594(3)	4957(3)	5441(3)	34(1)
N(71)	8931(4)	3991(3)	5030(3)	37(1)
S(70)	8344(1)	4188(1)	6574(1)	35(1)
C(80)	3603(4)	7847(4)	7876(4)	36(2)
C(81)	3920(4)	8706(4)	7873(4)	31(1)
C(82)	3270(4)	9979(4)	8545(4)	36(2)
C(83)	1578(5)	9931(5)	9462(5)	56(2)
C(84)	1545(7)	9456(7)	10224(6)	100(4)
C(85)	2410(5)	11201(5)	9340(5)	49(2)
C(86)	2047(6)	11890(5)	8846(5)	65(2)
O(80)	4360(3)	7362(3)	7290(3)	43(1)
O(81)	4765(3)	8827(3)	7409(3)	34(1)
N(80)	3217(4)	9190(3)	8381(4)	44(1)
N(81)	2470(3)	10351(3)	9079(3)	40(1)
S(80)	4270(1)	10536(1)	8131(1)	44(1)
P	285(1)	7773(2)	8839(1)	54(1)
F(1)	-786(3)	7931(5)	8848(3)	103(2)
F(2)	560(4)	7195(5)	8120(4)	118(2)
F(3)	1350(3)	7643(5)	8831(4)	109(2)
F(6)	4(4)	8360(5)	9546(4)	128(3)
F(5)	576(7)	8515(5)	8200(5)	152(3)
F(4)	5(6)	7034(5)	9467(5)	144(3)
C(45A)	8456(19)	3646(16)	9558(17)	40(3)
C(46A)	9013(17)	2870(20)	9130(16)	88(5)
C(45B)	8753(11)	3423(10)	9308(10)	40(3)
C(46B)	7933(12)	3528(12)	10104(12)	88(5)
C(23A)	8635(6)	11084(6)	7419(6)	69(3)
C(24A)	9446(17)	11457(19)	7003(16)	78(4)
C(23B)	8635(6)	11084(6)	7419(6)	69(3)
C(24B)	8713(10)	11740(10)	7859(9)	78(4)
C(90)	2260(16)	1077(16)	6788(15)	97(5)
O(90)	1547(9)	607(9)	7295(8)	93(5)
C(91)	1936(15)	3307(11)	6686(14)	97(5)
O(91)	2259(11)	2503(9)	6489(9)	109(6)
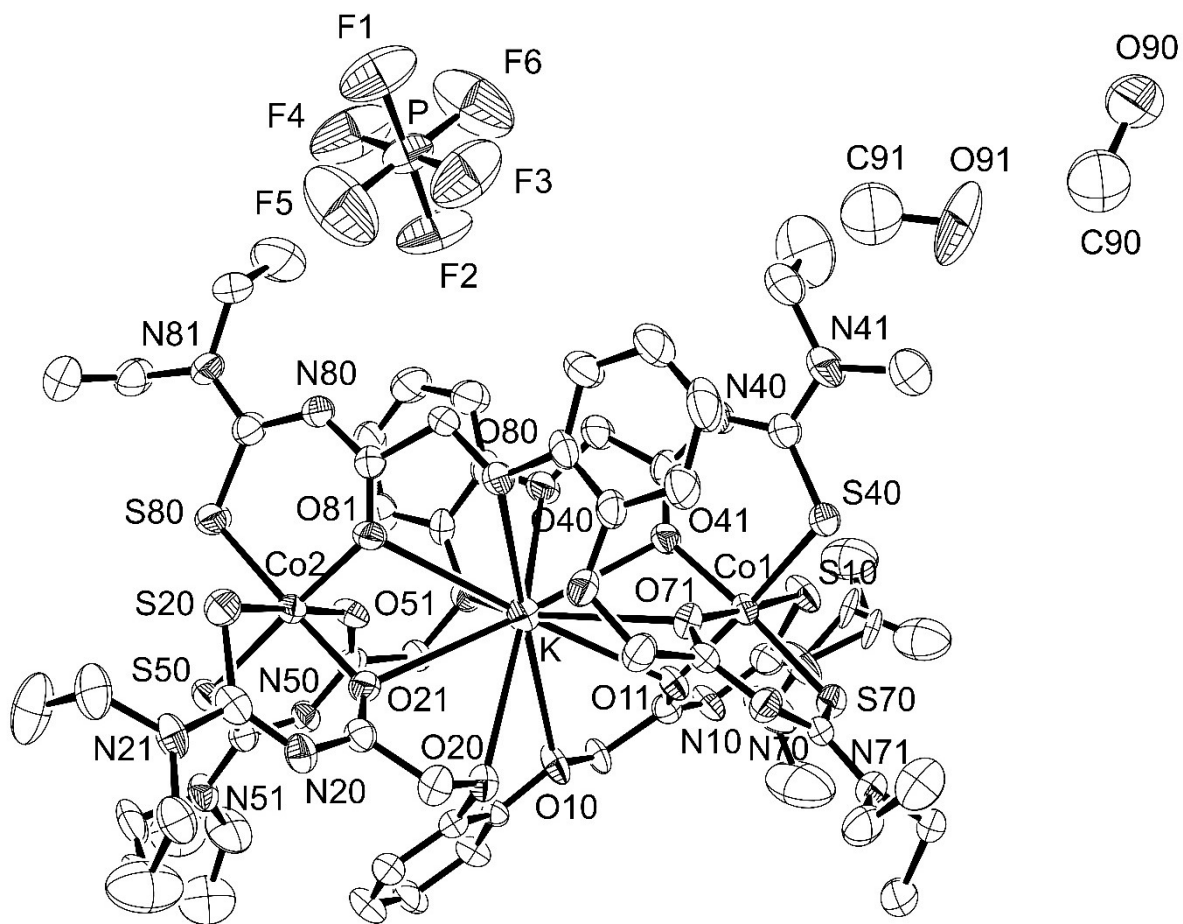
Figure 17: Ellipsoid plot (50% probability) of $\{K \subset [Co_2(L^3)_3]\}(PF_6) \cdot CH_3OH$.

18. {Tl ⊂ [Co₂(L³)₃]}(PF₆) · toluene

Table 36. Crystal data and structure refinement for {Tl ⊂ [Co₂(L³)₃]}(PF₆) · toluene.

Empirical formula	$C_{67}H_{92}O_{12}N_{12}S_6PF_6Co_2Tl$
Formula weight	1917.15
Measurement instrument	STOE IPDS 2T
Temperature	200(2) K
Wavelength	0.71073 Å
Crystal system	Triclinic
Space group	P $\bar{1}$
Unit cell dimensions	a = 15.119(1) Å α = 84.29(1)°.
	b = 16.092(1) Å β = 68.16(1)°.
	c = 18.178(1) Å γ = 80.78(1)°.
Volume	4048.3(5) $Å^3$
Z	2
Density (calculated)	1.573 g/cm^3
Absorption coefficient	2.642 mm^{-1}
F(000)	1948
Crystal size	0.25 x 0.13 x 0.06 mm^3
Theta range for data collection	3.236 to 24.998°.
Index ranges	-17<=h<=17, -18<=k<=19, -21<=l<=21
Reflections collected	30092
Independent reflections	14176 [R(int) = 0.0996]
Completeness to theta = 24.998°	99.5 %
Absorption correction	Integration
Max. and min. transmission	0.7203 and 0.5406
Refinement method	Full-matrix least-squares on F^2
Data / restraints / parameters	14176 / 0 / 964
Goodness-of-fit on F^2	0.889
Final R indices [I>2sigma(I)]	R1 = 0.0634, wR2 = 0.1403
R indices (all data)	R1 = 0.1157, wR2 = 0.1569
Largest diff. peak and hole	2.660 and -2.290 $e/Å^3$

Table 37. Atomic coordinates (x 10^4) and equivalent isotropic displacement parameters (Å^2 x 10^3) for $\{Tl \subset [Co_2(L^3)_3]\}(PF_6) \cdot$ toluene. U(eq) is defined as one third of the trace of the orthogonalized U^{ij} tensor.

	x	y	z	U(eq)
Co(2)	455(1)	4815(1)	2188(1)	29(1)
Co(1)	2152(1)	-102(1)	2468(1)	28(1)
Tl	1347(1)	2333(1)	2320(1)	38(1)
C(01)	-187(6)	1202(6)	1458(6)	37(2)
C(02)	-323(7)	443(7)	1278(7)	50(3)
C(03)	-1191(9)	138(7)	1684(8)	62(3)
C(04)	-1932(8)	608(7)	2278(8)	59(3)
C(05)	-1765(7)	1377(6)	2454(7)	43(3)
C(06)	-921(6)	1682(6)	2068(5)	34(2)
C(10)	1446(6)	1090(6)	546(6)	39(2)
C(11)	1942(6)	444(5)	979(5)	28(2)
C(12)	3262(6)	-635(5)	668(6)	36(2)
C(13)	4771(6)	-1622(6)	128(7)	46(3)
C(14)	5626(6)	-1164(7)	-40(7)	51(3)
C(15)	3937(8)	-873(7)	-747(6)	56(3)
C(16)	3408(10)	-1450(9)	-978(9)	79(4)
O(10)	634(4)	1591(4)	1079(3)	32(1)
O(11)	1706(4)	542(4)	1694(4)	31(1)
N(10)	2589(5)	-100(5)	472(4)	36(2)
N(11)	3942(5)	-1048(5)	41(5)	41(2)
S(10)	3364(2)	-861(2)	1586(2)	35(1)
C(20)	-1411(6)	2931(6)	2789(6)	40(2)
C(21)	-1099(6)	3775(6)	2797(5)	32(2)
C(22)	-1716(6)	5056(6)	3438(6)	37(2)
C(23)	-2584(7)	6264(7)	4289(6)	47(3)
C(24)	-2921(8)	7000(7)	3837(8)	59(3)
C(25)	-3422(7)	5040(7)	4270(8)	59(3)
C(26)	-3471(11)	4513(11)	5024(10)	105(6)
O(20)	-688(4)	2426(4)	2187(4)	38(2)
O(21)	-232(4)	3860(4)	2363(4)	32(2)
N(20)	-1803(5)	4301(5)	3257(5)	42(2)
N(21)	-2524(5)	5449(5)	3963(5)	44(2)
S(20)	-722(2)	5584(2)	3098(2)	42(1)

C(31)	3899(6)	2943(5)	1595(5)	32(2)
C(32)	4527(7)	3285(6)	1828(6)	39(2)
C(33)	4833(7)	4044(7)	1500(7)	49(3)
C(34)	4501(7)	4473(7)	935(7)	48(3)
C(35)	3860(6)	4138(6)	705(6)	41(2)
C(36)	3571(6)	3379(5)	1020(5)	30(2)
C(40)	3846(6)	1744(5)	2489(5)	29(2)
C(41)	3459(6)	908(5)	2672(5)	30(2)
C(42)	3488(6)	-311(6)	3511(5)	32(2)
C(43)	3722(8)	-1536(8)	4379(7)	61(3)
C(44)	2915(10)	-1448(11)	5154(9)	100(6)
C(45)	4614(8)	-297(8)	4186(7)	55(3)
C(46)	5630(8)	-498(11)	3616(10)	95(5)
O(40)	3543(5)	2209(4)	1900(4)	38(2)
O(41)	2916(4)	791(4)	2325(4)	31(1)
N(40)	3771(5)	425(5)	3180(4)	33(2)
N(41)	3931(5)	-709(5)	3982(5)	41(2)
S(40)	2607(2)	-811(2)	3402(2)	39(1)
C(50)	2540(7)	3423(6)	290(6)	38(2)
C(51)	1796(6)	4167(5)	689(5)	28(2)
C(52)	859(6)	5362(6)	384(6)	34(2)
C(53)	118(7)	6699(7)	-75(7)	54(3)
C(54)	384(8)	7435(7)	210(8)	63(3)
C(55)	1628(7)	5894(7)	-978(6)	49(3)
C(56)	2475(9)	6296(11)	-1061(9)	90(5)
O(50)	2963(4)	2964(4)	818(4)	33(1)
O(51)	1473(4)	4116(4)	1432(4)	32(2)
N(50)	1614(5)	4739(5)	176(5)	37(2)
N(51)	858(5)	5952(5)	-184(5)	40(2)
S(50)	-121(2)	5433(2)	1280(2)	40(1)
C(61)	75(6)	2528(6)	4606(6)	37(2)
C(62)	-746(7)	2578(7)	5281(7)	54(3)
C(63)	-968(8)	3240(8)	5773(7)	57(3)
C(64)	-384(8)	3856(6)	5592(7)	50(3)
C(65)	447(8)	3804(7)	4915(6)	44(3)
C(66)	683(7)	3142(6)	4435(5)	35(2)
C(70)	-149(7)	1191(7)	4268(6)	49(3)
C(71)	354(7)	523(6)	3682(6)	38(2)
C(72)	107(7)	-779(6)	3339(6)	36(2)

C(73)	-383(7)	-2099(7)	3138(7)	50(3)
C(74)	-589(9)	-2050(7)	2390(8)	64(3)
C(75)	-1627(8)	-957(7)	3960(8)	59(3)
C(76)	-1852(10)	-1238(10)	4771(9)	91(5)
O(70)	366(5)	1890(4)	4072(4)	47(2)
O(71)	1185(4)	626(4)	3216(4)	34(2)
N(70)	-169(6)	-85(5)	3770(5)	49(2)
N(71)	-561(6)	-1287(5)	3486(6)	50(2)
S(70)	1217(2)	-1079(1)	2603(2)	35(1)
C(80)	2109(6)	3647(6)	3530(6)	36(2)
C(81)	1751(6)	4344(5)	3048(5)	31(2)
C(82)	2202(6)	5606(6)	2328(5)	35(2)
C(83)	2792(7)	6930(6)	1658(7)	48(3)
C(84)	3243(9)	6783(8)	795(7)	64(4)
C(85)	3666(7)	5993(7)	2422(7)	53(3)
C(86)	3507(10)	6493(12)	3135(9)	97(5)
O(80)	1536(4)	2994(4)	3787(3)	31(1)
O(81)	986(4)	4251(4)	2944(4)	31(1)
N(80)	2314(5)	4936(5)	2796(5)	35(2)
N(81)	2826(5)	6165(5)	2164(5)	40(2)
S(80)	1295(2)	5880(2)	1936(2)	38(1)
P	5270(2)	2808(3)	3815(2)	61(1)
F(1)	6336(4)	2765(6)	3779(5)	102(3)
F(2)	5131(9)	1997(9)	4344(7)	153(5)
F(3)	4213(5)	2879(8)	3828(6)	122(4)
F(4)	5420(8)	3581(7)	3238(8)	144(4)
F(5)	5571(7)	2258(7)	3063(5)	117(3)
F(6)	4946(6)	3306(10)	4567(6)	164(6)
C(90)	3587(13)	4103(12)	7854(15)	141(8)
C(91)	3416(10)	3182(12)	8053(9)	90(5)
C(92)	4181(11)	2587(12)	7991(10)	93(5)
C(93)	4071(12)	1735(13)	8155(10)	102(6)
C(94)	3164(11)	1514(13)	8449(11)	109(6)
C(95)	2427(13)	2106(16)	8513(11)	109(7)
C(96)	2536(11)	2942(17)	8312(9)	108(7)
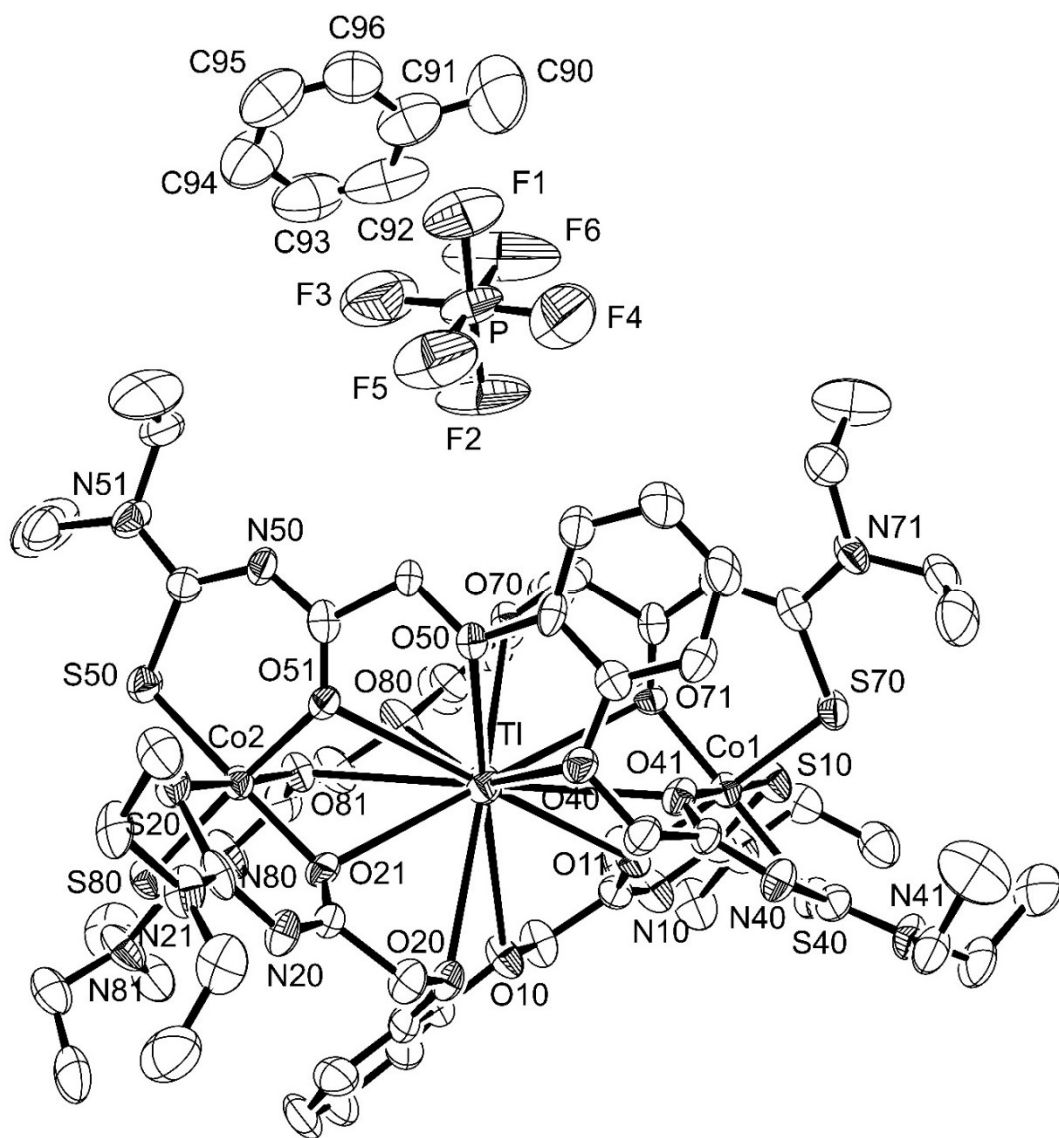
Figure 18: Ellipsoid plot (50% probability) of $\{Tl \subset [Co_2(L^3)_3]\}(PF_6) \cdot$ toluene.

19. {NH$_4$ ⊂ [Co$_2$(L^3)$_3$)]}(PF$_6$) · toluene

Table 38. Crystal data and structure refinement for {NH$_4$ ⊂ [Co$_2$(L^3)$_3$)]}(PF$_6$) · toluene.

Empirical formula	C$_{67}$H$_{96}$O$_{12}$N$_{13}$S$_6$PF$_6$Co$_2$
Formula weight	1730.75
Measurement instrument	Bruker D8 Venture
Temperature	136(2) K
Wavelength	0.71073 Å
Crystal system	Triclinic
Space group	P $\bar{1}$
Unit cell dimensions	a = 14.998(2) Å α = 84.61(1)°
	b = 15.984(2) Å β = 68.37(1)°.
	c = 17.973(2) Å γ = 81.11(1)°.
Volume	3953.9(8) Å^3
Z	2
Density (calculated)	1.454 g/cm^3
Absorption coefficient	0.678 mm^{-1}
F(000)	1808
Crystal size	0.19 x 0.12 x 0.08 mm^3
Theta range for data collection	2.353 to 24.999°.
Index ranges	-17<=h<=17, -19<=k<=19, -21<=l<=21
Reflections collected	66785
Independent reflections	13894 [R(int) = 0.1137]
Completeness to theta = 24.999°	99.9 %
Absorption correction	Semi-empirical from equivalents
Max. and min. transmission	0.7456 and 0.6187
Refinement method	Full-matrix least-squares on F^2
Data / restraints / parameters	13894 / 0 / 980
Goodness-of-fit on F^2	1.045
Final R indices [I>2sigma(I)]	R1 = 0.0470, wR2 = 0.0926
R indices (all data)	R1 = 0.0830, wR2 = 0.1077
Largest diff. peak and hole	0.593 and -0.425 e/Å^3

Table 39. Atomic coordinates (x 10^4) and equivalent isotropic displacement parameters (Å^2 x 10^3) for {NH$_4$ $\subset$ [Co$_2$(L^3)$_3$)]}(PF$_6$) · toluene. U(eq) is defined as one third of the trace of the orthogonalized U^{ij} tensor.

	x	y	z	U(eq)
Co(1)	2836(1)	5106(1)	2534(1)	11(1)
Co(2)	4539(1)	177(1)	2823(1)	12(1)
N	3632(3)	2673(3)	2695(2)	13(1)
C(01)	4913(2)	2464(2)	371(2)	17(1)
C(02)	5736(3)	2433(2)	-313(2)	23(1)
C(03)	5954(3)	1752(2)	-816(2)	25(1)
C(04)	5373(3)	1130(2)	-621(2)	22(1)
C(05)	4545(3)	1163(2)	62(2)	19(1)
C(06)	4300(2)	1851(2)	551(2)	15(1)
C(10)	5156(3)	3801(2)	710(2)	22(1)
C(11)	4648(2)	4484(2)	1314(2)	15(1)
C(12)	4899(2)	5783(2)	1678(2)	18(1)
C(13)	5397(3)	7116(2)	1888(2)	21(1)
C(14)	5593(3)	7070(2)	2658(2)	27(1)
C(15)	6622(3)	5980(3)	1055(2)	26(1)
C(16)	6894(3)	6248(3)	194(2)	37(1)
N(10)	5185(2)	5079(2)	1237(2)	22(1)
N(11)	5583(2)	6276(2)	1540(2)	21(1)
O(10)	4625(2)	3101(2)	917(1)	20(1)
O(11)	3811(2)	4373(1)	1777(1)	13(1)
S(10)	3777(1)	6092(1)	2404(1)	14(1)
C(20)	2872(2)	1339(2)	1477(2)	17(1)
C(21)	3240(2)	632(2)	1958(2)	13(1)
C(22)	2789(2)	-637(2)	2679(2)	14(1)
C(23)	2182(3)	-1951(2)	3360(2)	22(1)
C(24)	1708(3)	-1792(3)	4246(2)	28(1)
C(25)	1318(3)	-1030(2)	2582(2)	22(1)
C(26)	1488(3)	-1515(3)	1846(2)	37(1)
N(20)	2658(2)	45(2)	2215(2)	15(1)
N(21)	2142(2)	-1180(2)	2856(2)	17(1)
O(20)	3465(2)	1992(1)	1210(1)	15(1)
O(21)	4011(2)	729(1)	2052(1)	13(1)
S(20)	3691(1)	-893(1)	3080(1)	16(1)

C(31)	1091(2)	2031(2)	3388(2)	12(1)
C(32)	461(2)	1681(2)	3144(2)	17(1)
C(33)	165(2)	904(2)	3480(2)	20(1)
C(34)	497(2)	482(2)	4044(2)	19(1)
C(35)	1126(2)	834(2)	4298(2)	18(1)
C(36)	1415(2)	1608(2)	3979(2)	13(1)
C(40)	1135(2)	3238(2)	2492(2)	14(1)
C(41)	1520(2)	4086(2)	2319(2)	13(1)
C(42)	1488(2)	5319(2)	1490(2)	14(1)
C(43)	1275(3)	6524(3)	595(2)	28(1)
C(44)	2107(3)	6395(3)	-195(2)	45(1)
C(45)	349(2)	5303(2)	810(2)	21(1)
C(46)	-676(3)	5503(3)	1395(2)	38(1)
N(40)	1197(2)	4566(2)	1812(2)	16(1)
N(41)	1042(2)	5710(2)	1011(2)	17(1)
O(40)	1452(2)	2780(1)	3088(1)	16(1)
O(41)	2069(2)	4204(1)	2677(1)	12(1)
S(40)	2389(1)	5811(1)	1593(1)	16(1)
C(50)	2447(2)	1585(2)	4720(2)	15(1)
C(51)	3193(2)	844(2)	4331(2)	14(1)
C(52)	4128(2)	-362(2)	4642(2)	15(1)
C(53)	4856(3)	-1697(2)	5107(2)	24(1)
C(54)	4546(3)	-2443(2)	4840(2)	31(1)
C(55)	3339(3)	-886(2)	6017(2)	21(1)
C(56)	2448(3)	-1245(3)	6087(3)	44(1)
N(50)	3373(2)	272(2)	4846(2)	16(1)
N(51)	4116(2)	-944(2)	5221(2)	18(1)
O(50)	2016(2)	2032(1)	4192(1)	14(1)
O(51)	3513(2)	889(1)	3576(1)	12(1)
S(50)	5113(1)	-433(1)	3745(1)	17(1)
C(61)	5191(2)	3817(2)	3558(2)	15(1)
C(62)	5336(3)	4599(2)	3733(2)	21(1)
C(63)	6220(3)	4896(2)	3324(2)	25(1)
C(64)	6940(3)	4436(2)	2740(2)	23(1)
C(65)	6793(3)	3654(2)	2551(2)	20(1)
C(66)	5924(2)	3349(2)	2952(2)	15(1)
C(70)	3559(2)	3930(2)	4480(2)	16(1)
C(71)	3041(2)	4576(2)	4054(2)	12(1)
C(72)	1717(2)	5662(2)	4350(2)	14(1)

C(73)	192(2)	6628(2)	4894(2)	18(1)
C(74)	-666(2)	6154(2)	5055(2)	23(1)
C(75)	1016(3)	5890(2)	5793(2)	23(1)
C(76)	1556(3)	6486(3)	6018(2)	29(1)
N(70)	2399(2)	5127(2)	4543(2)	15(1)
N(71)	1025(2)	6060(2)	4972(2)	16(1)
O(70)	4370(2)	3434(1)	3943(1)	14(1)
O(71)	3277(2)	4468(1)	3318(1)	11(1)
S(70)	1613(1)	5864(1)	3420(1)	14(1)
C(80)	6417(2)	2085(2)	2221(2)	16(1)
C(81)	6088(2)	1237(2)	2222(2)	14(1)
C(82)	6735(2)	-70(2)	1570(2)	17(1)
C(83)	7597(2)	-1275(2)	711(2)	19(1)
C(84)	7956(3)	-2015(2)	1160(2)	26(1)
C(85)	8437(3)	-48(2)	729(2)	25(1)
C(86)	8496(3)	488(3)	-21(2)	37(1)
N(80)	6811(2)	711(2)	1761(2)	18(1)
N(81)	7545(2)	-451(2)	1047(2)	19(1)
O(80)	5686(2)	2593(2)	2821(1)	17(1)
O(81)	5226(2)	1154(1)	2638(1)	14(1)
S(80)	5728(1)	-599(1)	1920(1)	18(1)
P	9729(1)	2176(1)	1180(1)	25(1)
F(1)	10821(2)	2104(2)	1139(1)	44(1)
F(2)	8640(2)	2245(2)	1225(1)	39(1)
F(3)	9389(2)	2727(2)	1956(1)	44(1)
F(4)	10067(2)	1642(2)	402(1)	62(1)
F(5)	9874(2)	3021(2)	633(2)	61(1)
F(6)	9589(2)	1340(2)	1739(2)	59(1)
C(92)	2476(3)	2013(3)	6670(2)	34(1)
C(96)	787(3)	2437(3)	7044(2)	35(1)
C(93)	2638(3)	2844(3)	6449(2)	34(1)
C(91)	1552(3)	1801(3)	6972(2)	32(1)
C(95)	949(3)	3271(3)	6827(2)	38(1)
C(94)	1881(3)	3483(3)	6528(2)	38(1)
C(90)	1382(3)	892(3)	7215(3)	52(1)

Table 40. Hydrogen bonds for $\{NH_4 \subset [Co_2(L^3)_3)]\}(PF_6) \cdot$ toluene [Å and °].

D-H...A	d(D-H)	d(H...A)	d(D...A)	<(DHA)
N-H(1)...O(10)	0.85(4)	2.22(4)	3.048(4)	165(3)
N-H(1)...O(11)	0.85(4)	2.59(4)	3.039(5)	114(3)
N-H(1)...O(20)	0.85(4)	2.50(4)	3.081(4)	126(3)
N-H(2)...O(70)	0.76(5)	2.56(5)	3.241(4)	150(5)
N-H(2)...O(71)	0.76(5)	2.46(5)	3.076(4)	139(5)
N-H(3)...O(40)	0.88(6)	2.27(6)	3.060(4)	149(5)
N-H(3)...O(50)	0.88(6)	2.35(6)	3.100(4)	143(5)
N-H(4)...O(51)	0.69(6)	2.60(7)	3.126(5)	135(6)
N-H(4)...O(81)	0.69(6)	2.46(6)	3.114(4)	159(6)
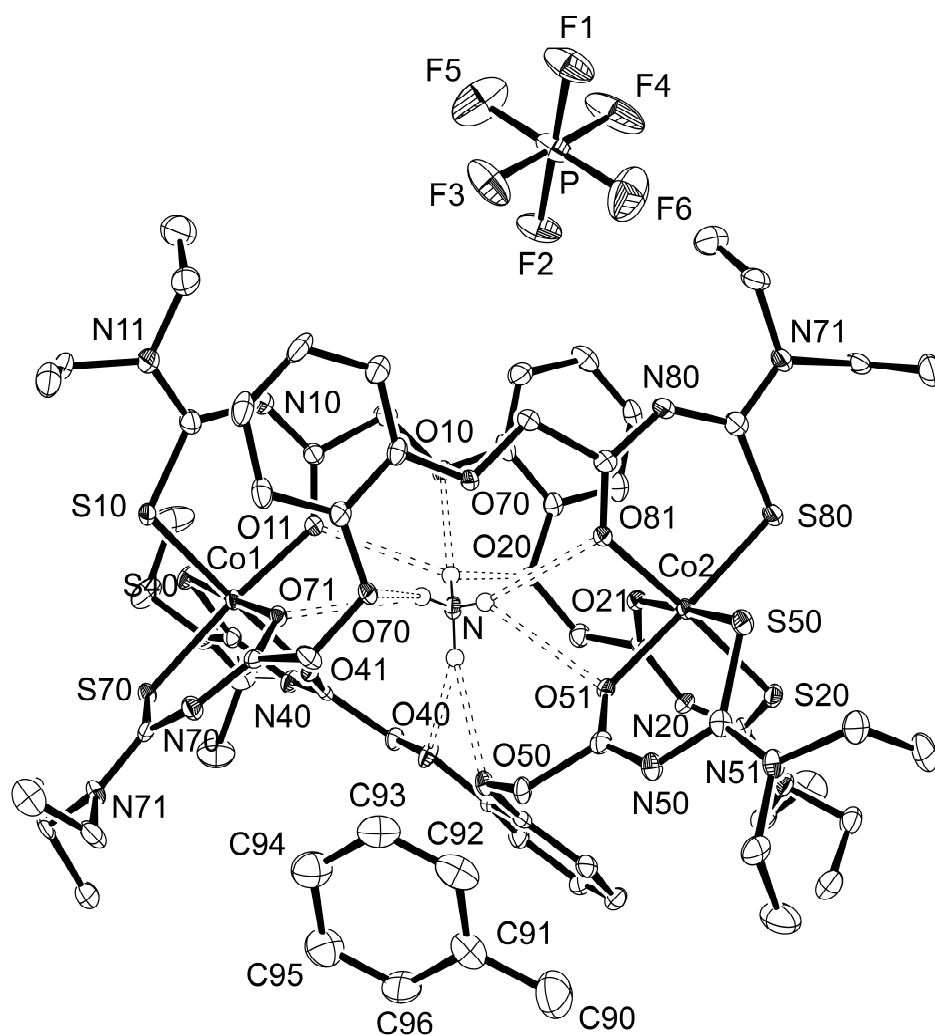
Figure 19: Ellipsoid plot (50% probability) of $\{NH_4 \subset [Co_2(L^3)_3)]\}(PF_6) \cdot$ toluene.

20. $\{Cs \subset [Cu_3(L^3)_3]\}(PF_6)$

Table 41. Crystal data and structure refinement for $\{Cs \subset [Cu_3(L^3)_3]\}(PF_6)$.

Empirical formula	$C_{60}H_{84}O_{12}N_{12}S_6PF_6Cu_3Cs$
Formula weight	1826.31
Measurement instrument	STOE IPDS 2T
Temperature	200(2) K
Wavelength	0.71073 Å
Crystal system	Triclinic
Space group	$P\bar{1}$
Unit cell dimensions	$a = 16.070(1)$ Å $\quad \alpha = 84.61(1)°$.
	$b = 16.190(1)$ Å $\quad \beta = 64.75(1)°$.
	$c = 16.856(1)$ Å $\quad \gamma = 74.98(1)°$.
Volume	$3830.3(5)$ Å^3
Z	2
Density (calculated)	1.584 g/cm^3
Absorption coefficient	1.556 mm^{-1}
F(000)	1862
Crystal size	$0.184 \times 0.054 \times 0.03$ mm^3
Theta range for data collection	3.212 to 24.998°.
Index ranges	-19<=h<=19, -18<=k<=19, -20<=l<=20
Reflections collected	29985
Independent reflections	13397 [R(int) = 0.0985]
Completeness to theta = 24.998°	99.4 %
Absorption correction	None
Refinement method	Full-matrix least-squares on F^2
Data / restraints / parameters	13397 / 7 / 910
Goodness-of-fit on F^2	0.971
Final R indices [I>2sigma(I)]	R1 = 0.0642, wR2 = 0.1597
R indices (all data)	R1 = 0.1022, wR2 = 0.1748
Largest diff. peak and hole	0.985 and -1.207 e/Å^3

Table 42. Atomic coordinates (x 10^4) and equivalent isotropic displacement parameters (Å^2 x 10^3) for $\{Cs \subset [Cu_3(L^3)_3]\}(PF_6)$. U(eq) is defined as one third of the trace of the orthogonalized U^{ij} tensor.

	x	y	z	U(eq)
Cs	2756(1)	3723(1)	1182(1)	48(1)
Cu(1)	4902(1)	3408(1)	-1341(1)	48(1)
Cu(2)	336(1)	4417(1)	3681(1)	48(1)
Cu(3)	1955(1)	1629(1)	233(1)	47(1)
C(01)	4207(5)	4641(5)	2078(5)	51(2)
C(02)	4666(6)	4373(6)	2618(6)	65(2)
C(03)	4240(7)	4649(6)	3486(6)	73(3)
C(04)	3344(6)	5177(6)	3827(6)	71(2)
C(05)	2865(6)	5453(6)	3297(5)	60(2)
C(06)	3292(5)	5201(5)	2431(5)	47(2)
C(10)	5448(5)	3852(6)	833(6)	70(3)
C(11)	5572(5)	3417(5)	19(5)	50(2)
C(12)	6706(4)	2312(4)	-986(5)	41(2)
C(13)	7829(6)	988(6)	-1747(6)	70(3)
C(14)	7320(7)	266(6)	-1452(8)	90(3)
C(15)	7838(5)	1501(5)	-403(5)	55(2)
C(16)	8638(6)	1938(7)	-677(7)	79(3)
N(10)	6387(4)	2847(4)	-284(4)	49(2)
N(11)	7424(4)	1642(4)	-1052(4)	51(2)
O(10)	4516(3)	4404(4)	1224(3)	61(2)
O(11)	4909(3)	3623(3)	-235(3)	57(1)
S(10)	6301(1)	2443(1)	-1798(1)	52(1)
C(20)	2037(5)	6097(5)	2127(5)	54(2)
C(21)	1171(5)	5834(5)	2800(5)	53(2)
C(22)	-384(5)	6462(5)	3853(6)	56(2)
C(23)	-1929(5)	7331(6)	4841(6)	67(2)
C(24)	-2622(7)	7226(9)	4520(8)	111(4)
C(25)	-767(7)	8045(6)	3502(8)	88(2)
C(26)	-371(11)	8373(12)	3933(11)	158(7)
N(20)	485(4)	6494(4)	3206(5)	64(2)
N(21)	-976(5)	7216(5)	4109(6)	87(2)
O(20)	2890(3)	5433(3)	1848(3)	51(1)
O(21)	1208(3)	5033(3)	2840(3)	57(1)

S(20)	-758(2)	5587(1)	4370(2)	72(1)
C(31)	4026(5)	2189(5)	2476(5)	49(2)
C(32)	4421(6)	2201(6)	3040(6)	63(2)
C(33)	5370(5)	1779(6)	2821(6)	64(2)
C(34)	5887(5)	1358(5)	2031(5)	57(2)
C(35)	5497(5)	1361(5)	1429(5)	45(2)
C(36)	4555(4)	1784(4)	1657(4)	41(2)
C(40)	2435(4)	2086(5)	2944(5)	52(2)
C(41)	1436(4)	2658(5)	3307(5)	46(2)
C(42)	-158(5)	2577(5)	4147(5)	48(2)
C(43)	-1736(5)	2253(5)	4778(5)	57(2)
C(44)	-2124(6)	2179(7)	5771(6)	83(3)
C(45)	-262(6)	1091(5)	4159(6)	62(2)
C(46)	-9(7)	881(6)	3218(6)	81(3)
N(40)	798(4)	2217(4)	3754(4)	53(2)
N(41)	-679(4)	2005(4)	4351(4)	51(2)
O(40)	3075(3)	2643(3)	2703(3)	48(1)
O(41)	1339(3)	3431(3)	3106(4)	60(1)
S(40)	-703(1)	3633(1)	4461(1)	58(1)
C(50)	4576(4)	1332(5)	346(4)	45(2)
C(51)	3905(5)	1389(5)	-104(5)	44(2)
C(52)	3905(5)	910(5)	-1376(5)	49(2)
C(53)	4085(6)	694(6)	-2870(5)	60(2)
C(54)	3641(9)	1539(7)	-3164(8)	100(4)
C(55)	5426(5)	902(5)	-2622(5)	53(2)
C(56)	6106(5)	24(5)	-2771(5)	60(2)
N(50)	4341(4)	996(4)	-859(4)	45(1)
N(51)	4433(4)	827(4)	-2229(4)	51(2)
O(50)	4088(3)	1824(3)	1131(3)	48(1)
O(51)	3064(3)	1836(3)	295(3)	55(1)
S(50)	2744(1)	813(2)	-978(1)	61(1)
C(61)	899(5)	5461(5)	593(5)	49(2)
C(62)	610(6)	6309(5)	406(6)	63(2)
C(63)	-285(6)	6786(6)	948(7)	70(2)
C(64)	-843(6)	6434(5)	1662(6)	67(2)
C(65)	-566(5)	5579(5)	1853(5)	58(2)
C(66)	301(5)	5085(5)	1311(5)	47(2)
C(70)	1975(6)	4573(9)	-633(6)	100(4)
C(71)	3010(6)	4254(6)	-1235(5)	60(2)

C(72)	4000(5)	3922(5)	-2736(5)	54(2)
C(73)	4901(6)	3884(5)	-4347(5)	59(2)
C(74)	5087(7)	3055(7)	-4765(7)	86(3)
C(75)	3180(6)	4573(6)	-3652(5)	61(2)
C(76)	2970(7)	5525(6)	-3564(7)	87(3)
N(70)	3166(4)	4246(4)	-2069(4)	58(2)
N(71)	4026(4)	4106(4)	-3524(4)	57(2)
O(70)	1831(3)	4999(4)	92(3)	61(2)
O(71)	3577(3)	4042(4)	-867(3)	60(2)
S(70)	4998(2)	3261(2)	-2676(1)	76(1)
C(80)	-55(5)	3751(5)	1817(6)	54(2)
C(81)	321(4)	2860(5)	1415(5)	44(2)
C(82)	-280(4)	1717(5)	1255(5)	45(2)
C(83)	-1135(5)	657(5)	1247(6)	59(2)
C(84)	-963(7)	-107(6)	1802(6)	76(3)
C(85)	-1977(5)	1962(5)	2252(5)	58(2)
C(86)	-2508(6)	2663(6)	1854(6)	72(2)
N(80)	-376(4)	2495(4)	1564(4)	49(2)
N(81)	-1076(4)	1450(4)	1558(4)	50(2)
O(80)	632(3)	4238(3)	1423(4)	59(1)
O(81)	1218(3)	2602(3)	1017(4)	58(1)
S(80)	734(1)	1065(1)	505(2)	59(1)
P	6927(2)	407(2)	4551(2)	70(1)
F(1)	8014(4)	374(6)	4043(5)	136(3)
F(2)	7060(9)	-471(5)	4942(8)	202(5)
F(3)	6892(7)	847(6)	5338(4)	157(4)
F(4)	5851(5)	522(9)	5055(7)	202(5)
F(5)	6807(7)	1341(6)	4139(6)	169(4)
F(6)	6956(8)	39(9)	3743(6)	227(7)
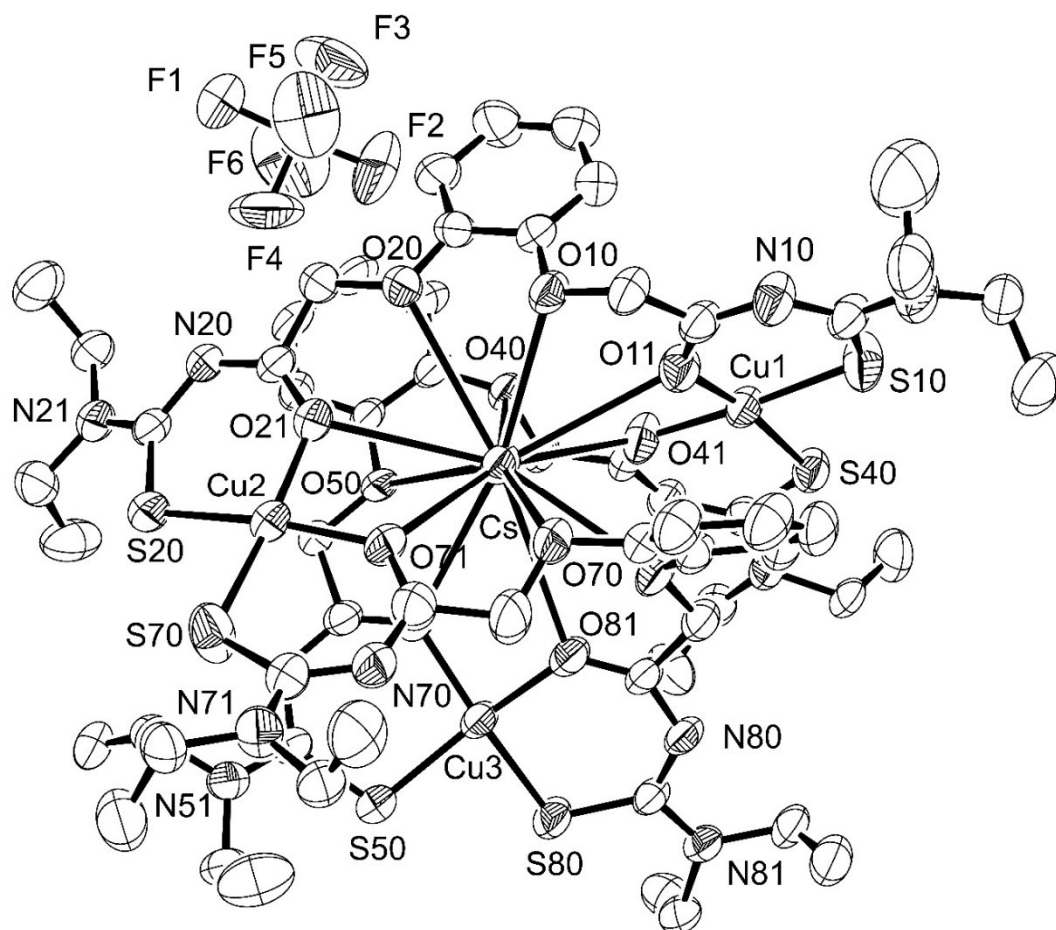
Figure 20: Ellipsoid plot (50% probability) of $\{Cs \subset [Cu_3(L^3)_3]\}(PF_6)$.

21. $\{(CH_3OH)Rb \subset [Cu_2(L^3)_2]\}(PF_6)$

Table 43. Crystal data and structure refinement for $\{(CH_3OH)Rb \subset [Cu_2(L^3)_2]\}(PF_6)$.

Empirical formula	$C_{41}H_{60}O_9N_8S_4PF_6Cu_2Rb$
Formula weight	1294.73
Measurement instrument	STOE IPDS 2T
Temperature	200(2) K
Wavelength	0.71073 Å
Crystal system	Monoclinic
Space group	C 2/c
Unit cell dimensions	a = 29.134(3) Å $\alpha = 90°$.
	b = 13.123(2) Å $\beta = 133.08(2)°$.
	c = 20.985(1) Å $\gamma = 90°$.
Volume	5860(2) Å^3
Z	4
Density (calculated)	1.468 g/cm^3
Absorption coefficient	1.793 mm^{-1}
F(000)	2648
Crystal size	0.25 x 0.22 x 0.20 mm^3
Theta range for data collection	3.377 to 24.999°.
Index ranges	-34<=h<=34, -15<=k<=15, -24<=l<=21
Reflections collected	21310
Independent reflections	5146 [R(int) = 0.1062]
Completeness to theta = 24.999°	99.7 %
Absorption correction	None
Refinement method	Full-matrix least-squares on F^2
Data / restraints / parameters	5146 / 20 / 343
Goodness-of-fit on F^2	0.969
Final R indices [I>2sigma(I)]	R1 = 0.0640, wR2 = 0.1553
R indices (all data)	R1 = 0.1097, wR2 = 0.1763
Largest diff. peak and hole	0.909 and -0.642 e/Å^3

Table 44. Atomic coordinates (x 10^4) and equivalent isotropic displacement parameters ($Å^2$ x 10^3) for $\{(CH_3OH)Rb \subset [Cu_2(L^3)_2]\}(PF_6)$. U(eq) is defined as one third of the trace of the orthogonalized U^{ij} tensor.

	x	y	z	U(eq)
Cu	960(1)	514(1)	1673(1)	45(1)
Rb	0	671(1)	2500	59(1)
C(01)	1729(3)	597(5)	4415(4)	55(2)
C(02)	2310(3)	619(6)	4670(5)	69(2)
C(03)	2709(4)	-204(8)	5117(6)	89(3)
C(04)	2539(4)	-1021(8)	5292(6)	91(3)
C(05)	1942(3)	-1066(7)	5020(5)	76(2)
C(06)	1544(3)	-244(6)	4582(5)	58(2)
C(10)	1445(3)	2249(5)	3743(5)	61(2)
C(11)	1400(3)	2025(5)	3003(5)	52(2)
C(12)	1846(3)	2469(5)	2445(5)	53(2)
C(13)	2381(13)	3184(15)	1878(11)	274(19)
C(14)	1887(10)	3517(14)	1270(18)	233(13)
C(15)	2206(4)	4239(5)	2850(7)	80(3)
C(16)	1626(5)	4902(7)	2396(8)	106(3)
O(10)	1297(2)	1389(3)	3998(3)	54(1)
O(11)	984(2)	1358(3)	2452(3)	57(1)
N(10)	1771(2)	2571(4)	3000(4)	54(1)
N(11)	2059(3)	3288(5)	2355(5)	70(2)
S(10)	1752(1)	1347(1)	1935(1)	60(1)
C(20)	766(3)	-1005(5)	4507(5)	57(2)
C(21)	151(3)	-779(4)	4248(4)	49(2)
C(22)	-454(3)	-1498(5)	4516(5)	52(2)
C(23)	-913(4)	-2378(6)	5007(6)	78(2)
C(24)	-1424(5)	-3107(8)	4352(8)	110(4)
C(25)	86(4)	-3029(7)	5429(8)	106(4)
C(26)	11(6)	-3747(8)	4825(12)	192(9)
O(20)	946(2)	-190(3)	4279(3)	58(1)
O(21)	-179(2)	-36(3)	3733(3)	51(1)
S(20)	-1094(1)	-711(1)	3917(2)	70(1)
N(20)	47(2)	-1441(4)	4603(4)	59(2)
N(21)	-440(3)	-2261(4)	4950(4)	67(2)
P	0	4432(3)	2500	125(2)

F(1)	-640(4)	4381(6)	1482(7)	199(4)
F(3)	0	3237(9)	2500	228(8)
F(4)	425(7)	4396(14)	2352(12)	322(10)
F(6)	0	5537(8)	2500	364(17)
O(90)	333(6)	-1574(11)	2621(8)	100(4)
C(90A)	866(8)	-2230(15)	2720(11)	53(4)
C(90B)	787(18)	-2690(30)	3040(20)	53(4)
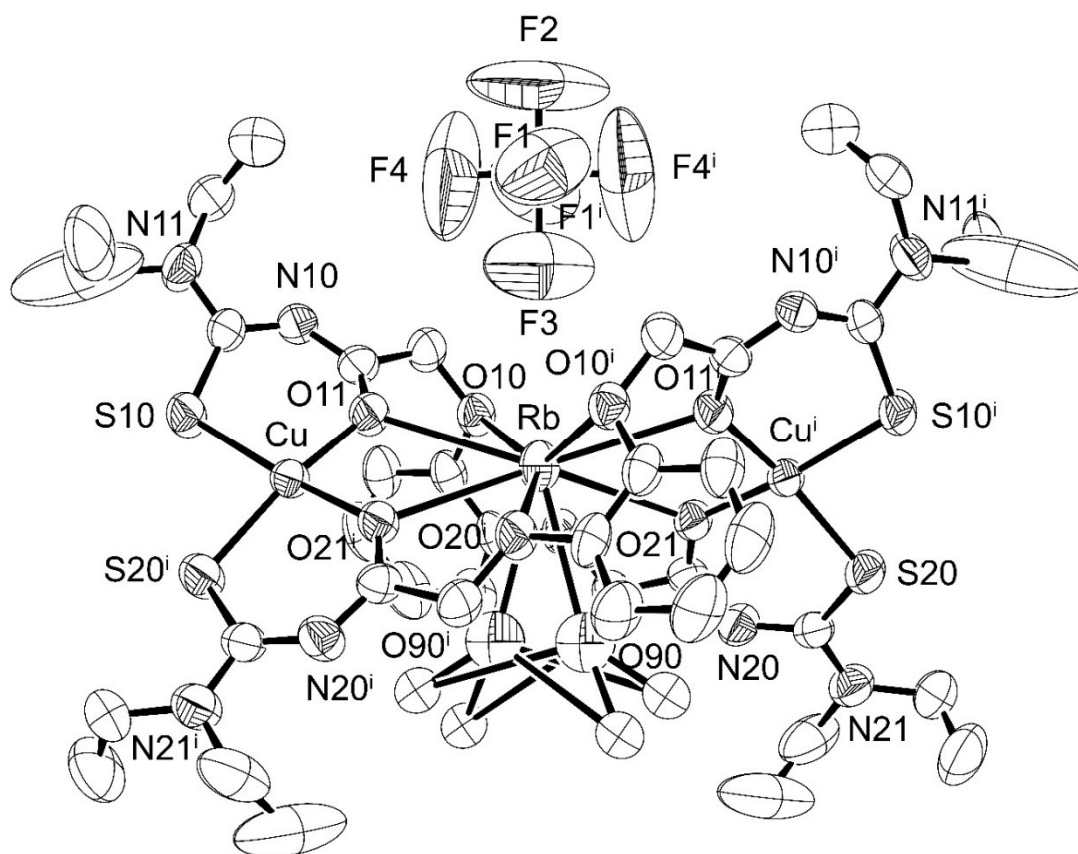
Figure 20: Ellipsoid plot (50% probability) of $\{(CH_3OH)Rb \subset [Cu_2(L^3)_2]\}(PF_6)$.

215

22. $\{(CH_3OH)K \subset [Cu_2(L^3)_2]\}(PF_6)$

Table 45. Crystal data and structure refinement for $\{(CH_3OH)K \subset [Cu_2(L^3)_2]\}(PF_6)$.

Empirical formula	$C_{41}H_{60}O_9N_8S_4PF_6Cu_2K$
Formula weight	1248.36
Measurement instrument	STOE IPDS 2T
Temperature	200(2) K
Wavelength	0.71073 Å
Crystal system	Monoclinic
Space group	C 2/c
Unit cell dimensions	a = 28.922(3) Å $\quad$ $\alpha = 90°$.
	b = 13.289(1) Å $\quad$ $\beta = 133.27(1)°$.
	c = 20.762(3) Å $\quad$ $\gamma = 90°$.
Volume	5810.3(14) Å^3
Z	4
Density (calculated)	1.427 g/cm^3
Absorption coefficient	1.047 mm^{-1}
F(000)	2576
Crystal size	0.23 x 0.20 x 0.17 mm^3
Theta range for data collection	3.322 to 24.998°.
Index ranges	-34<=h<=34, -15<=k<=15, -24<=l<=22
Reflections collected	22097
Independent reflections	5110 [R(int) = 0.1095]
Completeness to theta = 24.998°	99.8 %
Absorption correction	None
Refinement method	Full-matrix least-squares on F^2
Data / restraints / parameters	5110 / 27 / 359
Goodness-of-fit on F^2	0.899
Final R indices [I>2sigma(I)]	R1 = 0.0629, wR2 = 0.1476
R indices (all data)	R1 = 0.1253, wR2 = 0.1700
Largest diff. peak and hole	0.767 and -0.596 e/Å^3

Table 46. Atomic coordinates (x 10^4) and equivalent isotropic displacement parameters (Å^2 x 10^3) for $\{(CH_3OH)K \subset [Cu_2(L^3)_2]\}(PF_6)$. U(eq) is defined as one third of the trace of the orthogonalized U^{ij} tensor.

	x	y	z	U(eq)
K	0	4473(2)	2500	62(1)
Cu	-940(1)	4511(1)	3352(1)	43(1)
C(1)	1541(3)	5178(5)	4556(5)	55(2)
C(2)	1986(4)	5954(6)	5033(6)	78(2)
C(3)	2576(4)	5829(8)	5311(6)	88(3)
C(4)	2726(4)	4960(8)	5119(6)	82(3)
C(5)	2283(3)	4209(6)	4646(5)	65(2)
C(6)	1697(3)	4300(5)	4375(5)	51(2)
C(10)	797(3)	6010(4)	4523(5)	51(2)
C(11)	161(3)	5806(4)	4242(5)	47(2)
C(12)	-432(3)	6524(4)	4534(4)	47(2)
C(13)	90(4)	8076(5)	5394(6)	75(2)
C(14)	9(5)	8729(6)	4719(8)	102(3)
C(15)	-866(4)	7424(5)	5060(6)	67(2)
C(16)	-1392(4)	8155(7)	4398(8)	105(3)
N(10)	71(2)	6472(4)	4618(4)	53(1)
O(10)	940(2)	5203(3)	4237(3)	57(1)
O(11)	-174(2)	5087(3)	3722(3)	53(1)
N(11)	-415(3)	7302(4)	4956(4)	56(2)
S(10)	-1072(1)	5728(1)	3954(2)	60(1)
C(20)	1335(4)	2716(5)	3635(5)	61(2)
C(21)	1326(3)	2973(4)	2914(5)	51(2)
C(22)	1836(3)	2577(4)	2426(5)	48(2)
C(23)	2204(4)	841(5)	2824(6)	67(2)
C(24)	1624(5)	205(6)	2353(8)	100(3)
O(20)	1230(2)	3597(3)	3929(3)	52(1)
O(21)	917(2)	3624(3)	2360(3)	55(1)
N(20)	1725(3)	2437(4)	2958(4)	52(1)
N(21)	2082(3)	1789(4)	2361(4)	59(2)
S(20)	1769(1)	3715(1)	1973(1)	58(1)
C(25A)	2305(7)	1848(10)	1903(9)	78(5)
C(26A)	1826(10)	1414(12)	1002(13)	146(8)
C(25B)	2000(30)	1690(40)	1530(50)	59(2)

C(26B)	2650(20)	2010(40)	1820(40)	100(20)
P	0	286(3)	2500	114(2)
F(1)	707(11)	247(16)	3101(17)	206(9)
F(2)	16(8)	1345(12)	2186(10)	159(7)
F(5)	119(9)	-688(12)	3038(11)	168(7)
F(3)	431(14)	-306(19)	2417(19)	211(11)
F(4)	352(10)	803(17)	2223(15)	179(9)
F(6)	609(8)	566(11)	3561(12)	137(7)
O(90)	312(6)	6564(10)	2628(9)	106(4)
C(90A)	842(14)	7650(20)	3120(20)	56(5)
C(90B)	873(11)	7209(16)	2785(16)	56(5)
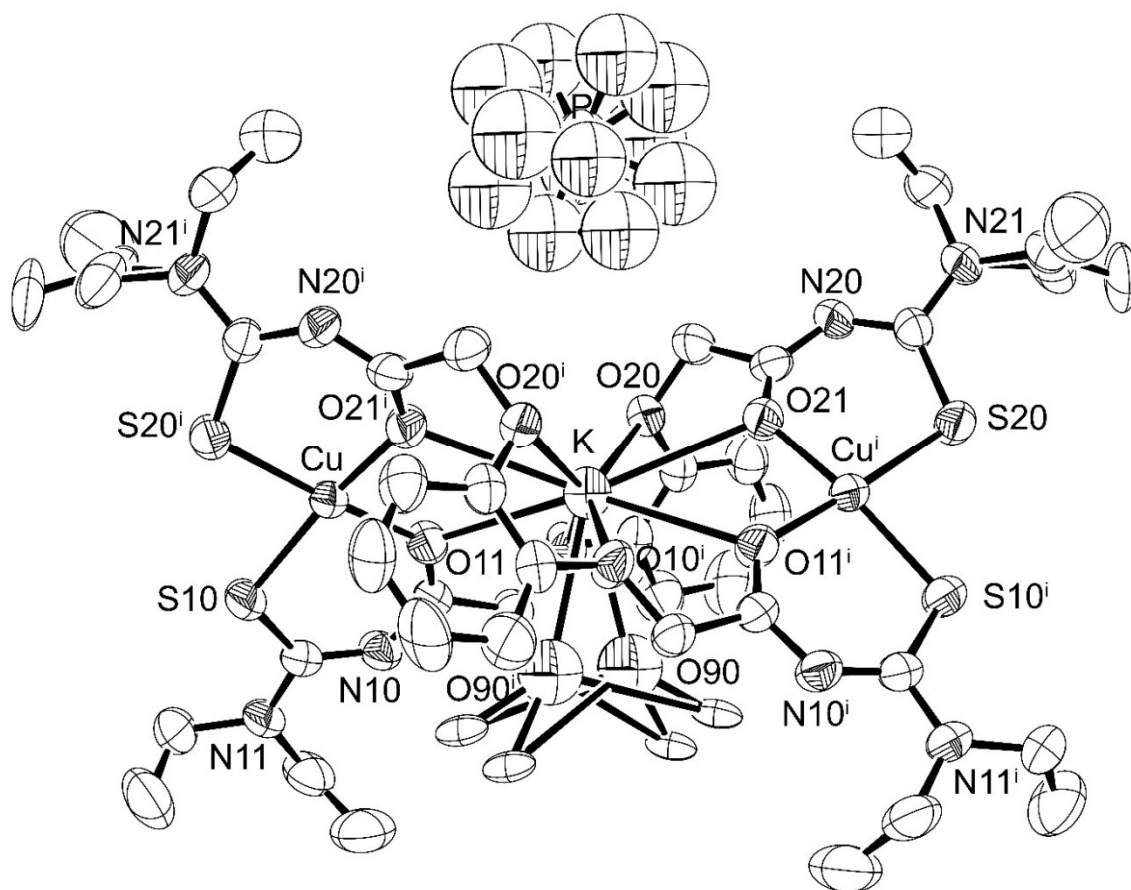
Figure 22: Ellipsoid plot (50% probability) of $\{(CH_3OH)K \subset [Cu_2(L^3)_2]\}(PF_6)$.

23. {(CH₃OH)Tl ⊂ [Cu₂(L³)₂]}(PF₆)

Table 47. Crystal data and structure refinement for {(CH₃OH)Tl ⊂ [Cu₂(L³)₂]}(PF₆).

Empirical formula	$C_{41}H_{60}O_9N_8S_4PF_6Cu_2Tl$
Formula weight	1413.63
Measurement instrument	STOE IPDS 2T
Temperature	200(2) K
Wavelength	0.71073 Å
Crystal system	Monoclinic
Space group	C 2/c
Unit cell dimensions	a = 29.146(4) Å $\quad$ α = 90°.
	b = 13.167(2) Å $\quad$ β = 133.31(1)°.
	c = 20.917(3) Å $\quad$ γ = 90°.
Volume	5841.0(16) Å³
Z	4
Density (calculated)	1.608 g/cm³
Absorption coefficient	3.716 mm⁻¹
F(000)	2824
Crystal size	0.13 x 0.10 x 0.07 mm³
Theta range for data collection	1.949 to 25.000°.
Index ranges	-34<=h<=34, -15<=k<=15, -24<=l<=24
Reflections collected	20761
Independent reflections	5145 [R(int) = 0.1169]
Completeness to theta = 25.000°	99.9 %
Absorption correction	Integration
Max. and min. transmission	0.8066 and 0.4278
Refinement method	Full-matrix least-squares on F²
Data / restraints / parameters	5145 / 40 / 348
Goodness-of-fit on F²	0.880
Final R indices [I>2sigma(I)]	R1 = 0.0521, wR2 = 0.0951
R indices (all data)	R1 = 0.1149, wR2 = 0.1125
Largest diff. peak and hole	0.839 and -0.622 e/Å³

Table 48. Atomic coordinates (x 10^4) and equivalent isotropic displacement parameters (Å^2 x 10^3) for {(CH$_3$OH)Tl ⊂ [Cu$_2$(L^3)$_2$]}(PF$_6$). U(eq) is defined as one third of the trace of the orthogonalized U^{ij} tensor.

	x	y	z	U(eq)
Cu	-960(1)	4509(1)	3329(1)	45(1)
Tl	0	4378(1)	2500	61(1)
C(01)	1549(4)	5227(7)	4592(6)	59(2)
C(02)	1960(5)	6043(8)	5039(7)	77(3)
C(03)	2552(5)	5963(11)	5307(7)	94(4)
C(04)	2721(5)	5132(12)	5122(7)	91(4)
C(05)	2307(4)	4343(9)	4682(6)	71(3)
C(06)	1727(4)	4369(8)	4418(5)	54(2)
O(10)	958(2)	5178(4)	4298(4)	56(2)
O(11)	-175(2)	5060(4)	3743(4)	53(1)
C(10)	782(4)	6003(6)	4525(6)	53(2)
C(11)	161(4)	5789(6)	4261(5)	47(2)
C(12)	-438(4)	6505(6)	4531(5)	50(2)
C(13)	92(5)	8049(9)	5427(9)	100(3)
C(14)	25(6)	8727(9)	4775(9)	123(4)
C(15)	-886(5)	7393(8)	5038(7)	80(3)
C(16)	-1401(6)	8135(9)	4390(8)	106(4)
N(10)	60(3)	6457(5)	4625(5)	54(2)
N(11)	-419(4)	7277(5)	4969(5)	62(2)
S(10)	-1089(1)	5734(2)	3926(2)	67(1)
O(20)	1288(3)	3600(4)	3996(4)	54(1)
O(21)	977(3)	3663(4)	2439(4)	55(2)
C(20)	1420(4)	2741(6)	3732(6)	59(2)
C(21)	1385(4)	2999(6)	2982(6)	53(2)
C(22)	1854(4)	2566(6)	2457(5)	50(2)
C(23)	2212(5)	811(7)	2852(7)	72(3)
C(24)	1626(6)	142(9)	2391(8)	102(4)
N(20)	1766(3)	2439(5)	3004(4)	52(2)
N(21)	2068(4)	1741(6)	2360(5)	65(2)
S(20)	1767(1)	3691(2)	1962(2)	59(1)
C(25A)	2279(8)	1780(20)	1887(12)	79(6)
C(26A)	1765(12)	1420(17)	982(17)	123(7)
C(25B)	1980(18)	1690(50)	1570(19)	79(6)

C(26B)	2610(30)	1920(30)	1890(30)	123(7)
P	0	417(4)	2500	119(2)
F(2)	-33(11)	1541(17)	2756(13)	166(11)
F(3)	-94(16)	-580(20)	2009(17)	209(13)
F(5)	-318(11)	942(19)	2788(13)	166(11)
F(4)	414(18)	-200(20)	2420(20)	224(14)
F(1)	633(7)	576(12)	3555(12)	160(9)
F(6)	730(15)	370(20)	3130(20)	157(17)
O(90)	344(8)	6512(12)	2608(10)	98(4)
C(90A)	880(11)	7189(18)	2747(15)	49(5)
C(90B)	790(20)	7600(40)	3060(30)	49(5)
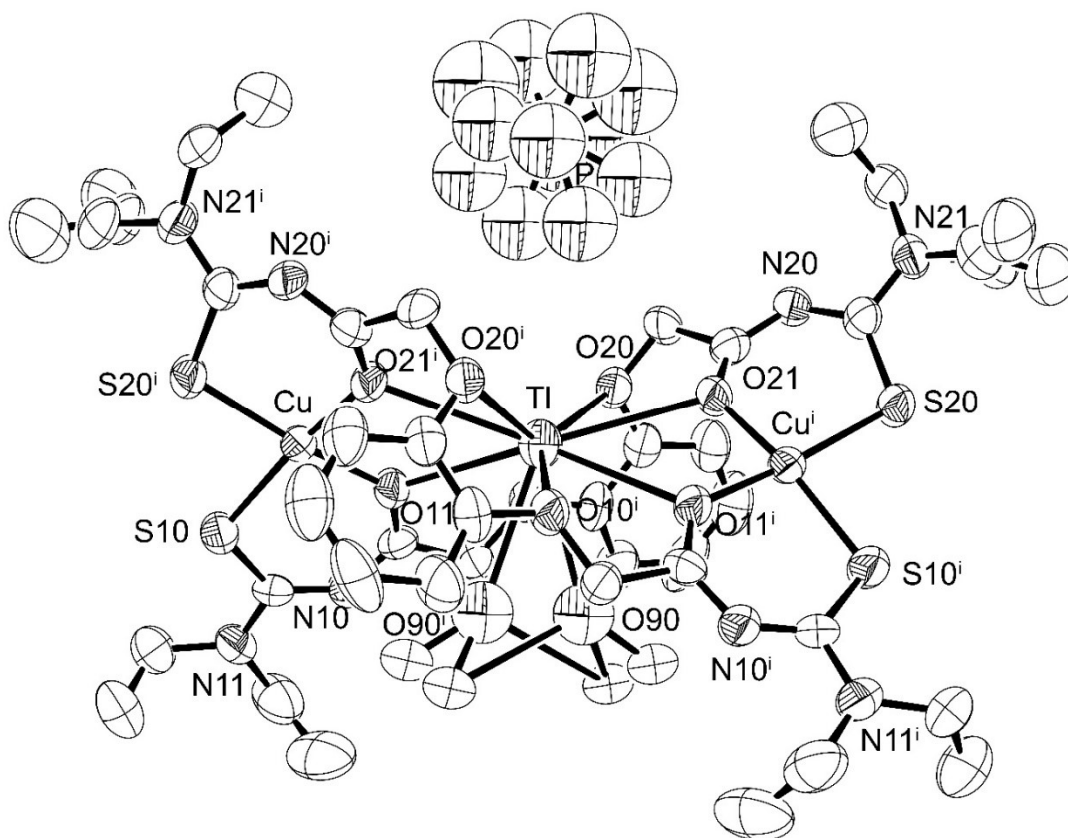
Figure 23: Ellipsoid plot (50% probability) of $\{(CH_3OH)Tl \subset [Cu_2(L^3)_2]\}(PF_6)$.

24. $\{Cs \subset [Ni_3(L^3)_3]\}(PF_6) \cdot 2\ CH_3OH$

Table 49. Crystal data and structure refinement for $\{Cs \subset [Ni_3(L^3)_3]\}(PF_6) \cdot 2\ CH_3OH$.

Empirical formula	$C_{62}H_{92}O_{14}N_{12}S_6PF_6Ni_3Cs$
Formula weight	1875.83
Measurement instrument	Bruker D8 Venture
Temperature	100(2) K
Wavelength	0.71073 Å
Crystal system	Triclinic
Space group	$P\bar{1}$
Unit cell dimensions	$a = 14.175(1)$ Å $\qquad \alpha = 89.54(1)°$.
	$b = 15.788(1)$ Å $\qquad \beta = 88.48(1)°$.
	$c = 18.292(1)$ Å $\qquad \gamma = 81.24(1)°$.
Volume	4044.4(4) Å^3
Z	2
Density (calculated)	1.540 g/cm^3
Absorption coefficient	1.388 mm^{-1}
F(000)	1928
Crystal size	0.18 x 0.16 x 0.03 mm^3
Theta range for data collection	2.228 to 24.999°.
Index ranges	-15<=h<=16, -18<=k<=18, -21<=l<=21
Reflections collected	36661
Independent reflections	13997 [R(int) = 0.0380]
Completeness to theta = 24.999°	98.3 %
Absorption correction	Semi-empirical from equivalents
Max. and min. transmission	0.7456 and 0.6230
Refinement method	Full-matrix least-squares on F^2
Data / restraints / parameters	13997 / 24 / 1006
Goodness-of-fit on F^2	1.036
Final R indices [I>2sigma(I)]	R1 = 0.0402, wR2 = 0.0749
R indices (all data)	R1 = 0.0713, wR2 = 0.0887
Largest diff. peak and hole	1.295 and -0.715 e/Å^3

Table 50. Atomic coordinates (x 10^4) and equivalent isotropic displacement parameters (Å^2 x 10^3) for $\{Cs \subset [Ni_3(L^3)_3]\}(PF_6) \cdot 2\ CH_3OH$. U(eq) is defined as one third of the trace of the orthogonalized U^{ij} tensor.

	x	y	z	U(eq)
Cs	1306(1)	3945(1)	1870(1)	19(1)
Ni(1)	-1252(1)	5393(1)	2034(1)	24(1)
Ni(2)	3917(1)	2419(1)	1315(1)	31(1)
Ni(3)	221(1)	2296(1)	3536(1)	22(1)
C(01)	2426(3)	6002(3)	1086(2)	26(1)
C(02)	2976(3)	6631(3)	1230(3)	35(1)
C(03)	3834(4)	6642(3)	840(3)	44(1)
C(04)	4143(3)	6029(3)	334(3)	41(1)
C(05)	3595(3)	5395(3)	187(2)	32(1)
C(06)	2735(3)	5381(3)	558(2)	26(1)
C(10)	1180(3)	6596(3)	1918(2)	27(1)
C(11)	220(3)	6425(3)	2213(2)	25(1)
C(12)	-974(3)	6927(3)	3076(2)	30(1)
C(13)	-1959(4)	7442(4)	4158(3)	54(2)
C(14)	-1668(4)	6878(5)	4807(3)	68(2)
C(15)	-541(4)	8122(3)	3779(3)	41(1)
C(16)	-846(5)	8937(3)	3341(3)	64(2)
N(10)	-176(3)	7011(2)	2671(2)	27(1)
N(11)	-1158(3)	7470(3)	3635(2)	36(1)
O(10)	1564(2)	5935(2)	1426(2)	28(1)
O(11)	-57(2)	5749(2)	1981(2)	25(1)
S(10)	-1761(1)	6210(1)	2939(1)	31(1)
C(20)	2380(3)	4172(3)	-113(2)	32(1)
C(21)	3083(3)	3418(3)	113(2)	28(1)
C(22)	4061(3)	2220(3)	-410(3)	35(1)
O(20)	2117(2)	4802(2)	441(2)	27(1)
O(21)	3160(2)	3275(2)	792(2)	32(1)
N(20)	3489(3)	2985(2)	-454(2)	32(1)
N(21)	4308(3)	1831(3)	-1044(2)	46(1)
S(20)	4517(1)	1707(1)	375(1)	45(1)
C(31)	2640(3)	5219(3)	3196(2)	23(1)
C(32)	3236(4)	5841(3)	3201(3)	35(1)
C(33)	2930(5)	6613(3)	3548(3)	50(2)

C(34)	2048(5)	6754(3)	3892(3)	48(2)
C(35)	1451(4)	6138(3)	3898(2)	34(1)
C(36)	1743(3)	5369(3)	3538(2)	23(1)
C(40)	3221(3)	3741(3)	3274(2)	28(1)
C(41)	3618(3)	2980(3)	2802(2)	25(1)
C(42)	4519(3)	1615(3)	2854(3)	31(1)
C(43)	5309(4)	132(3)	3079(3)	43(1)
C(44)	6387(4)	93(3)	3051(4)	56(2)
C(45)	4651(3)	1083(3)	4112(3)	32(1)
C(46)	3691(4)	836(4)	4345(3)	58(2)
O(40)	2934(2)	4468(2)	2818(1)	22(1)
O(41)	3405(2)	3056(2)	2130(2)	30(1)
N(40)	4088(3)	2345(2)	3169(2)	28(1)
N(41)	4817(3)	983(2)	3315(2)	32(1)
S(40)	4774(1)	1437(1)	1928(1)	42(1)
C(50)	296(3)	4853(3)	3846(2)	27(1)
C(51)	-204(3)	4085(3)	3748(2)	25(1)
C(52)	-1540(3)	3518(3)	4170(2)	29(1)
C(53)	-3084(3)	3040(3)	4435(2)	33(1)
C(54)	-3398(4)	2600(4)	3768(3)	57(2)
C(55)	-2984(3)	4580(3)	4138(3)	36(1)
C(56)	-3205(4)	5056(3)	4853(3)	49(2)
O(50)	1200(2)	4720(2)	3482(2)	22(1)
O(51)	229(2)	3472(2)	3358(2)	28(1)
N(50)	-1048(3)	4177(2)	4076(2)	27(1)
N(51)	-2478(3)	3702(2)	4241(2)	27(1)
S(50)	-995(1)	2456(1)	4282(1)	44(1)
C(61)	833(3)	2598(3)	158(2)	24(1)
C(62)	798(3)	2570(3)	-595(2)	33(1)
C(63)	1337(4)	1911(3)	-978(3)	43(1)
C(64)	1924(4)	1277(3)	-614(3)	41(1)
C(65)	1980(4)	1313(3)	147(2)	33(1)
C(66)	1439(3)	1960(3)	535(2)	24(1)
C(70)	-498(3)	3725(3)	272(2)	25(1)
C(71)	-1108(3)	4107(3)	911(2)	26(1)
C(72)	-2563(3)	4058(3)	1546(2)	30(1)
C(73)	-4119(4)	3847(4)	2085(3)	45(1)
C(74)	-4911(4)	4428(4)	1697(3)	55(2)
C(75)	-3271(4)	2815(3)	1171(3)	42(1)

C(76)	-2727(5)	2035(4)	1549(3)	66(2)
O(70)	320(2)	3224(2)	585(2)	27(1)
O(71)	-765(2)	4691(2)	1248(2)	28(1)
N(70)	-1881(3)	3762(2)	1039(2)	29(1)
N(71)	-3278(3)	3603(3)	1607(2)	36(1)
S(70)	-2626(1)	4974(1)	2077(1)	36(1)
C(80)	1859(3)	1340(3)	1695(2)	25(1)
C(81)	1492(3)	1391(3)	2481(2)	20(1)
C(82)	1380(3)	435(3)	3468(2)	22(1)
C(83)	1440(3)	-675(3)	4435(2)	26(1)
C(84)	2046(4)	-483(3)	5070(3)	42(1)
C(85)	2526(3)	-870(3)	3329(3)	34(1)
C(86)	2140(4)	-1371(3)	2728(3)	44(1)
O(80)	1422(2)	2056(2)	1285(2)	25(1)
O(81)	1069(2)	2099(2)	2722(2)	23(1)
N(80)	1712(2)	638(2)	2805(2)	23(1)
N(81)	1758(2)	-324(2)	3738(2)	23(1)
S(80)	457(1)	1024(1)	3971(1)	37(1)
O(90)	67(4)	396(4)	1025(3)	105(2)
C(90)	-344(6)	269(6)	1705(5)	118(3)
O(91)	1211(5)	9288(4)	106(3)	133(2)
C(91)	1447(6)	8529(4)	441(5)	99(3)
P(1A)	5258(2)	7383(5)	4009(2)	26(1)
F(2A)	4651(5)	7540(6)	3277(4)	42(2)
F(4A)	5750(7)	8221(6)	3813(7)	51(3)
F(5A)	4777(4)	6569(4)	4214(3)	32(2)
F(6A)	6095(5)	6802(4)	3577(4)	37(2)
P(1B)	5204(2)	7876(3)	4044(1)	23(1)
F(2B)	4533(3)	8174(4)	3370(2)	31(1)
F(4B)	6100(5)	8039(6)	3548(4)	39(2)
F(5B)	5081(4)	8847(3)	4317(2)	40(2)
F(6B)	5312(5)	6898(4)	3772(3)	48(2)
F(1)	5871(2)	7454(2)	4722(2)	60(1)
F(3)	4325(2)	7844(2)	4501(2)	60(1)
C(23)	4838(4)	953(3)	-1101(3)	54(2)
C(24A)	5767(14)	1050(18)	-1498(13)	29(6)
C(24B)	5934(10)	866(11)	-1141(18)	100(8)
C(25A)	3861(7)	2274(7)	-1739(5)	45(1)
C(26A)	4347(6)	3032(5)	-2024(4)	39(2)

C(25B)	4240(10)	2245(11)	-1752(7)	45(1)
C(26B)	3318(9)	2035(8)	-2003(6)	39(2)
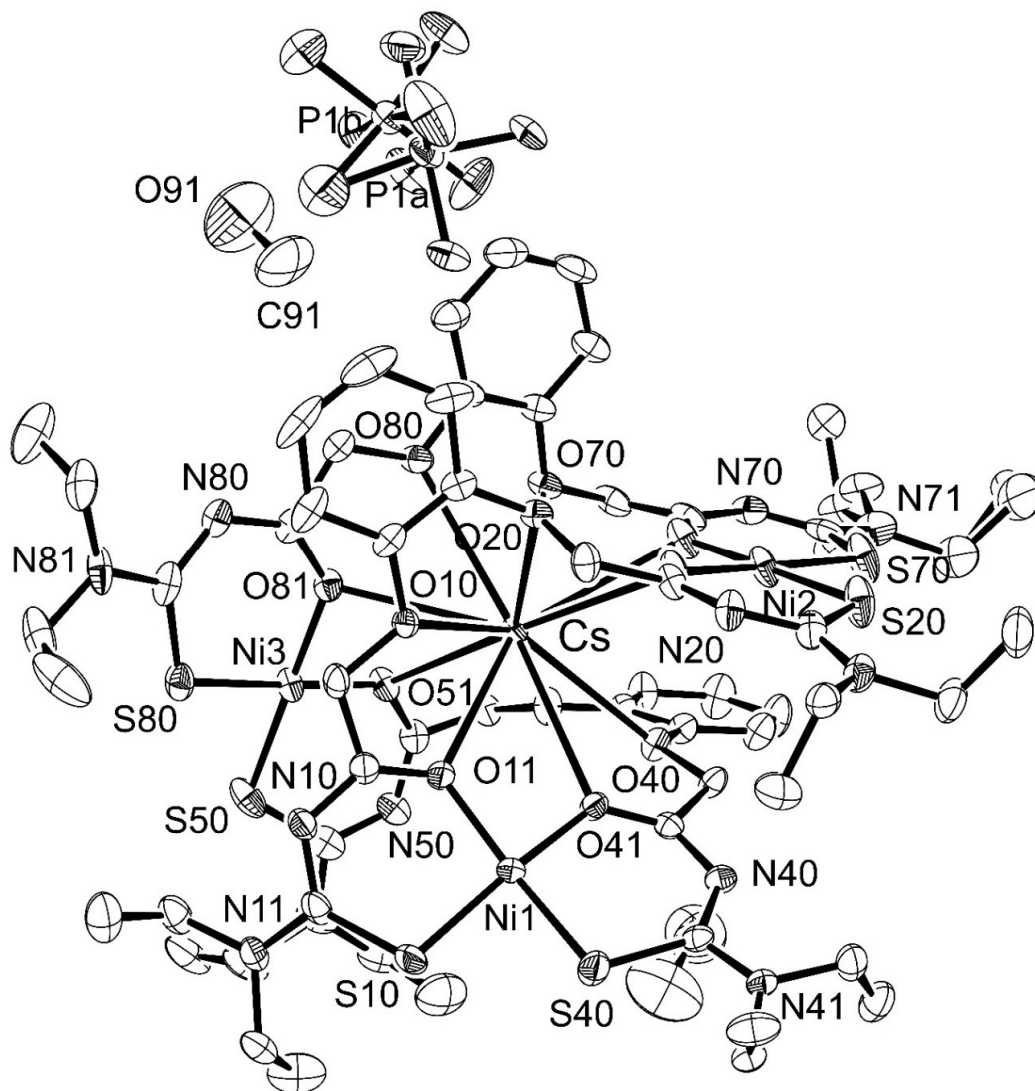
Figure 24: Ellipsoid plot (50% probability) of $\{Cs \subset [Ni_3(L^3)_3]\}(PF_6) \cdot 2\ CH_3OH$.

25. $\{(CH_3OH)(Cl)Rb \subset [Ni_2(L^3)_2)]\} \cdot H_2O$

Table 51. Crystal data and structure refinement for $\{(CH_3OH)(Cl)Rb \subset [Ni_2(L^3)_2)]\} \cdot H_2O$.

Empirical formula	$C_{41}H_{60}O_{10}N_8S_4ClNi_2Rb$
Formula weight	1191.55
Measurement instrument	STOE IPDS 2T
Temperature	200(2) K
Wavelength	0.71073 Å
Crystal system	Monoclinic
Space group	C 2/c
Unit cell dimensions	a = 29.181(3) Å $\quad$ α = 90°.
	b = 12.414(1) Å $\quad$ β = 131.16(1)°.
	c = 21.383(2) Å $\quad$ γ = 90°.
Volume	5831.8(12) Å^3
Z	4
Density (calculated)	1.357 g/cm^3
Absorption coefficient	1.717 mm^{-1}
F(000)	2464
Crystal size	0.25 x 0.22 x 0.19 mm^3
Theta range for data collection	3.282 to 24.999°.
Index ranges	-34<=h<=34, -14<=k<=14, -25<=l<=24
Reflections collected	21236
Independent reflections	5127 [R(int) = 0.0911]
Completeness to theta = 24.999°	99.7 %
Absorption correction	None
Refinement method	Full-matrix least-squares on F^2
Data / restraints / parameters	5127 / 20 / 323
Goodness-of-fit on F^2	0.970
Final R indices [I>2sigma(I)]	R1 = 0.0622, wR2 = 0.1552
R indices (all data)	R1 = 0.1037, wR2 = 0.1708
Largest diff. peak and hole	1.249 and -0.475 e/Å^3

Table 52. Atomic coordinates (x 10^4) and equivalent isotropic displacement parameters (Å^2 x 10^3) for {(CH$_3$OH)(Cl)Rb $\subset$ [Ni$_2$(L^3)$_2$)]} · H$_2$O. U(eq) is defined as one third of the trace of the orthogonalized U^{ij} tensor.

	x	y	z	U(eq)
Ni	9047(1)	4434(1)	3335(1)	28(1)
Rb	10000	4263(1)	2500	40(1)
C(01)	11666(3)	4415(6)	4361(4)	38(2)
C(02)	12247(3)	4394(7)	4641(5)	54(2)
C(03)	12640(4)	5251(8)	5102(6)	69(3)
C(04)	12450(4)	6131(8)	5276(6)	63(2)
C(05)	11851(3)	6179(6)	4967(5)	49(2)
C(06)	11456(3)	5319(5)	4504(4)	38(2)
O(10)	11245(2)	3606(4)	3926(3)	38(1)
O(11)	8991(2)	3691(3)	2524(3)	39(1)
C(10)	11400(4)	2709(6)	3693(5)	47(2)
C(11)	8620(3)	2956(5)	2025(4)	35(2)
C(12)	8221(3)	2378(5)	2619(4)	33(1)
C(13)	7979(5)	1379(7)	3388(6)	67(3)
C(14)	7393(5)	1695(9)	3117(8)	94(4)
C(15)	7835(4)	528(6)	2182(5)	53(2)
C(16)	8357(5)	-202(7)	2525(7)	74(3)
N(10)	8286(3)	2297(4)	2060(4)	36(1)
N(11)	8004(3)	1498(4)	2708(4)	46(2)
S(10)	8336(1)	3528(1)	3163(1)	40(1)
O(20)	10866(2)	5267(3)	4181(3)	38(1)
O(21)	9745(2)	5087(3)	3630(3)	34(1)
C(20)	10657(3)	6154(5)	4338(5)	36(2)
C(21)	10034(3)	5912(5)	4067(4)	33(1)
C(22)	9446(3)	6567(5)	4376(4)	31(1)
C(23)	8980(3)	7359(6)	4902(5)	43(2)
C(24)	8362(4)	7821(7)	4240(7)	74(3)
C(25)	9682(3)	8432(5)	4863(5)	45(2)
C(26)	10292(4)	8453(7)	5738(6)	73(3)
N(20)	9890(2)	6671(4)	4346(4)	34(1)
N(21)	9362(3)	7406(4)	4682(4)	39(1)
S(20)	9005(1)	5433(1)	4115(1)	40(1)
Cl	10000	1452(3)	2500	122(2)

O(90)	10432(6)	6645(11)	2667(10)	82(4)
C(90A)	10949(7)	7218(13)	2810(10)	26(3)
C(90B)	10560(20)	7570(30)	2690(30)	26(3)
O(91)	10716(9)	9650(20)	4110(11)	184(12)
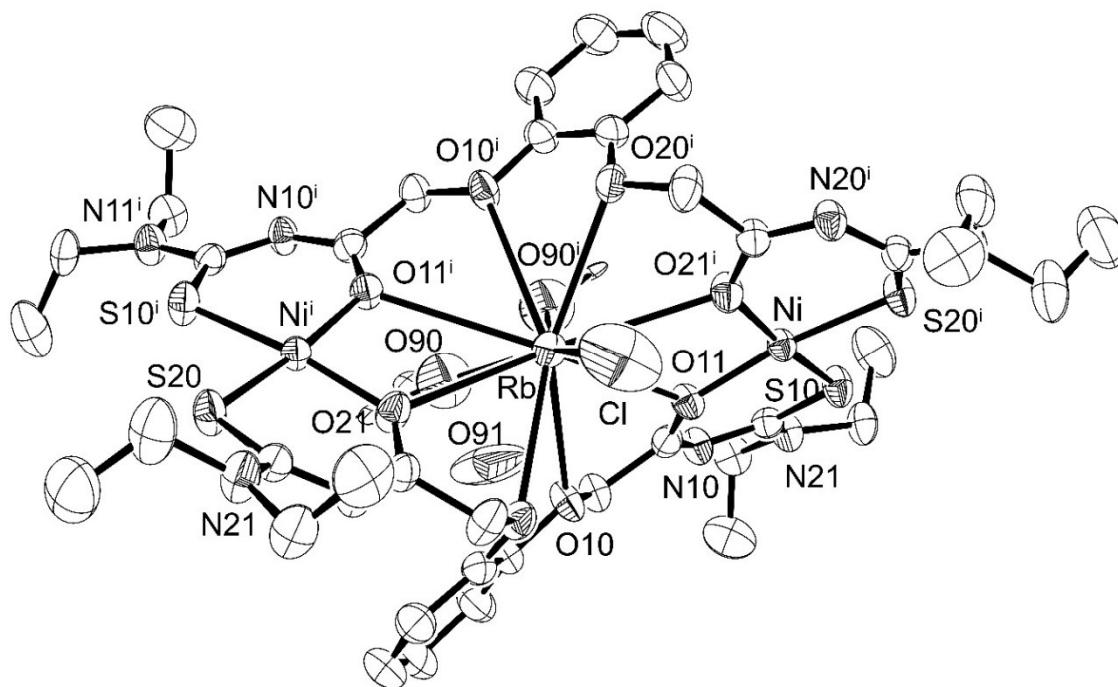
Figure 25: Ellipsoid plot (50% probability) of $\{(CH_3OH)(Cl)Rb \subset [Ni_2(L^3)_2)]\} \cdot H_2O$.

26. {Ba ⊂ [Ni$_2$(L^3)$_3$]} · 0.75 CH$_2$Cl$_2$

Table 53. Crystal data and structure refinement for {Ba ⊂ [Ni$_2$(L^3)$_3$]} · 0.75 CH$_2$Cl$_2$.

Empirical formula	C$_{61.5}$H$_{87}$O$_{12}$N$_{12}$S$_6$Cl$_3$Ni$_2$Ba
Formula weight	1739.90
Measurement instrument	STOE IPDS 2T
Temperature	200(2) K
Wavelength	0.71073 Å
Crystal system	Monoclinic
Space group	C 2/c
Unit cell dimensions	a = 24.578(2) Å　　α = 90°.
	b = 17.672(2) Å　　β = 106.31(1)°.
	c = 18.774(3) Å　　γ = 90°.
Volume	7826.2(17) Å^3
Z	4
Density (calculated)	1.477 g/cm^3
Absorption coefficient	1.298 mm^{-1}
F(000)	3580
Crystal size	0.184 x 0.05 x 0.03 mm^3
Theta range for data collection	2.770 to 24.997°.
Index ranges	-28<=h<=29, -21<=k<=20, -22<=l<=22
Reflections collected	26880
Independent reflections	6871 [R(int) = 0.0797]
Completeness to theta = 24.997°	99.7 %
Absorption correction	None
Refinement method	Full-matrix least-squares on F^2
Data / restraints / parameters	6871 / 2 / 461
Goodness-of-fit on F^2	0.803
Final R indices [I>2sigma(I)]	R1 = 0.0390, wR2 = 0.0676
R indices (all data)	R1 = 0.0853, wR2 = 0.0739
Largest diff. peak and hole	0.913 and -0.436 e/Å^3

Table 54. Atomic coordinates (x 10^4) and equivalent isotropic displacement parameters ($Å^2$ x 10^3) for {Ba $\subset$ [Ni$_2$(L^3)$_3$]} · 0.75 CH$_2$Cl$_2$. U(eq) is defined as one third of the trace of the orthogonalized U^{ij} tensor.

	x	y	z	U(eq)
Ba	0	3234(1)	2500	30(1)
Ni(1)	342(1)	2632(1)	4429(1)	33(1)
C(01)	-104(2)	5481(2)	2810(2)	29(1)
C(02)	-214(2)	6164(3)	3106(3)	40(1)
C(03)	-110(2)	6841(3)	2799(2)	45(1)
C(10)	-366(2)	4817(3)	3762(2)	42(1)
C(11)	-352(2)	4041(3)	4106(2)	32(1)
C(12)	-685(2)	3404(3)	5014(2)	35(1)
C(13)	-1147(2)	2929(3)	5923(3)	54(2)
C(14)	-1663(3)	2482(4)	5548(4)	88(2)
C(15)	-1232(2)	4298(3)	5559(3)	61(2)
C(16)	-1792(3)	4426(4)	5101(6)	155(5)
O(10)	-174(1)	4783(2)	3111(2)	33(1)
O(11)	-115(1)	3525(2)	3851(2)	36(1)
N(10)	-606(2)	4041(2)	4639(2)	38(1)
N(11)	-1010(2)	3528(2)	5465(2)	46(1)
S(10)	-416(1)	2518(1)	4978(1)	41(1)
C(21)	1479(2)	3074(3)	2290(2)	41(1)
C(22)	1859(2)	3416(3)	1969(3)	58(2)
C(23)	2135(2)	2992(4)	1568(3)	69(2)
C(24)	2031(2)	2236(4)	1472(3)	63(2)
C(25)	1645(2)	1894(3)	1776(3)	55(2)
C(26)	1368(2)	2306(3)	2202(2)	39(1)
C(30)	1509(3)	3763(3)	3398(3)	66(2)
C(31)	1321(2)	3386(3)	4017(2)	41(1)
C(32)	1551(2)	3420(3)	5324(3)	46(1)
C(33)	1966(3)	3332(4)	6669(3)	80(2)
C(34)	1894(3)	4056(5)	7054(4)	104(3)
O(30)	1184(1)	3505(2)	2676(2)	45(1)
O(31)	887(1)	2987(2)	3835(2)	39(1)
N(30)	1673(2)	3546(3)	4671(2)	53(1)
N(31)	2002(2)	3451(3)	5920(2)	74(2)
S(30)	903(1)	3317(1)	5454(1)	58(1)

C(40)	-740(2)	1314(3)	2689(3)	53(2)
C(41)	-244(2)	1428(3)	3370(3)	39(1)
C(42)	382(3)	739(3)	4332(3)	54(2)
C(43)	997(3)	-183(4)	5175(4)	94(2)
C(44)	1555(3)	-255(5)	5051(5)	134(3)
C(45)	230(3)	-619(4)	4085(4)	90(2)
C(46)	467(4)	-818(4)	3471(4)	114(3)
O(40)	-1009(1)	2013(2)	2436(2)	47(1)
O(41)	-39(1)	2077(2)	3453(2)	38(1)
N(40)	-83(2)	802(2)	3746(3)	52(1)
N(41)	533(2)	20(3)	4522(3)	67(1)
S(40)	765(1)	1456(1)	4866(1)	57(1)
C(35A)	2624(8)	3365(11)	5832(11)	89(6)
C(36A)	2950(6)	4045(8)	6177(8)	100(4)
C(35B)	2529(9)	3815(13)	5856(13)	89(6)
C(36B)	2895(7)	3145(9)	5837(9)	100(4)
C(50)	1631(4)	1304(5)	6839(5)	92(3)
Cl(1A)	1282(3)	1856(3)	7441(3)	80(2)
Cl(2A)	1772(3)	433(3)	7248(3)	80(2)
Cl(1B)	1233(3)	1446(6)	7327(4)	105(2)
Cl(2B)	1982(3)	413(4)	6896(5)	105(2)
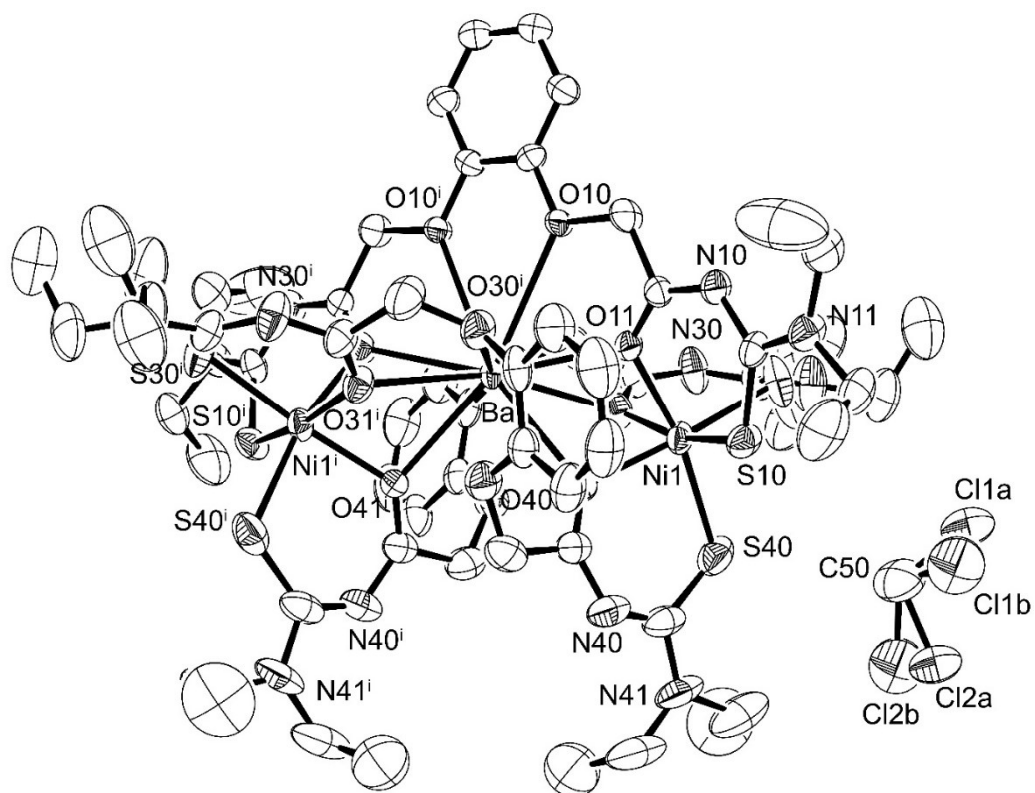
Figure 26: Ellipsoid plot (50% probability) of $\{Ba \subset [Ni_2(L^3)_3]\} \cdot 0.75\ CH_2Cl_2$.

27. $\{(CH_3OH)_2Sr_2 \subset [Ni_2(L^3)_2(L^{3'})_2]\} \cdot 1.5\ CH_3OH$

Table 55. Crystal data and structure refinement for $\{(CH_3OH)_2Sr_2 \subset [Ni_2(L^3)_2(L^{3'})_2]\} \cdot 1.5\ CH_3OH$.

Empirical formula	$C_{69.5}H_{102}O_{17.5}N_{12}S_6Ni_2Sr_2$
Formula weight	935.33
Measurement instrument	STOE IPDS 2T
Temperature	200(2) K
Wavelength	0.71073 Å
Crystal system	Triclinic
Space group	$P\bar{1}$
Unit cell dimensions	$a = 11.672(1)$ Å $\qquad \alpha = 84.08(1)°.$
	$b = 12.471(1)$ Å $\qquad \beta = 87.08(1)°.$
	$c = 16.534(2)$ Å $\qquad \gamma = 63.45(1)°.$
Volume	$2141.4(4)$ Å^3
Z	1
Density (calculated)	1.451 g/cm^3
Absorption coefficient	1.887 mm^{-1}
F(000)	971
Crystal size	0.184 x 0.05 x 0.03 mm^3
Theta range for data collection	2.305 to 25.000°.
Index ranges	-13<=h<=13, -14<=k<=14, -17<=l<=19
Reflections collected	15075
Independent reflections	7466 [R(int) = 0.1037]
Completeness to theta = 25.000°	99.0 %
Absorption correction	Integration
Max. and min. transmission	0.7002 and 0.5542
Refinement method	Full-matrix least-squares on F^2
Data / restraints / parameters	7466 / 15 / 502
Goodness-of-fit on F^2	0.904
Final R indices [I>2sigma(I)]	R1 = 0.0524, wR2 = 0.1160
R indices (all data)	R1 = 0.0892, wR2 = 0.1294
Largest diff. peak and hole	0.950 and -0.825 e/Å^3

Table 56. Atomic coordinates (x 10^4) and equivalent isotropic displacement parameters (Å^2 x 10^3) for $\{(CH_3OH)_2Sr_2 \subset [Ni_2(L^3)_2(L^{3'})_2]\} \cdot 1.5\ CH_3OH$. U(eq) is defined as one third of the trace of the orthogonalized U^{ij} tensor.

	x	y	z	U(eq)
Ni(1)	252(1)	1891(1)	2365(1)	34(1)
Sr(1)	309(1)	1159(1)	413(1)	30(1)
C(01)	2954(5)	-921(4)	-866(3)	32(1)
C(02)	3483(5)	-1754(5)	-1431(3)	41(1)
C(03)	4732(5)	-2646(5)	-1332(4)	45(1)
C(04)	5426(5)	-2677(5)	-678(4)	45(1)
C(05)	4907(5)	-1856(5)	-107(3)	43(1)
C(06)	3652(5)	-955(5)	-202(3)	34(1)
C(10)	3759(5)	-136(5)	1025(3)	37(1)
C(11)	2902(5)	725(5)	1613(3)	35(1)
C(12)	3035(6)	1739(5)	2691(3)	45(1)
C(13)	3497(8)	2526(7)	3890(4)	74(2)
C(14)	3922(11)	3498(9)	3635(6)	113(3)
C(15)	5132(7)	669(7)	3323(4)	71(2)
C(16)	5106(8)	-433(8)	3801(5)	91(3)
O(10)	3043(3)	-80(3)	331(2)	36(1)
O(11)	1713(3)	1121(3)	1528(2)	35(1)
N(10)	3548(4)	914(4)	2162(3)	43(1)
N(11)	3848(5)	1665(5)	3271(3)	57(1)
S(10)	1485(2)	2905(1)	2692(1)	50(1)
C(20)	1302(5)	569(5)	-1735(3)	34(1)
C(21)	-636(5)	-43(5)	2221(3)	34(1)
C(22)	459(5)	-561(5)	3479(3)	38(1)
C(23)	2873(7)	-2207(8)	4705(5)	91(3)
C(24)	1484(6)	-1379(6)	4820(4)	60(2)
C(25)	206(8)	-2264(6)	4209(4)	67(2)
C(26)	-1103(10)	-1821(9)	4561(5)	103(3)
O(20)	1703(3)	-14(3)	-932(2)	35(1)
O(21)	-480(3)	847(3)	1898(2)	33(1)
N(20)	-303(4)	-657(4)	2940(2)	37(1)
N(21)	689(5)	-1341(4)	4143(3)	46(1)
S(20)	1202(1)	369(1)	3411(1)	42(1)
C(31)	-1977(5)	1975(4)	-1002(3)	31(1)
C(32)	-2481(5)	1968(5)	-1749(3)	37(1)
C(33)	-3516(5)	2960(5)	-2091(3)	47(1)

C(34)	-4115(6)	3992(5)	-1682(4)	51(2)
C(35)	-3629(5)	4037(5)	-944(3)	42(1)
C(36)	-2580(5)	3060(5)	-619(3)	35(1)
C(40)	-2484(5)	4076(5)	509(3)	41(1)
C(41)	-1746(5)	3830(5)	1286(3)	38(1)
C(42)	-2157(6)	4434(6)	2611(4)	58(2)
C(45)	-3397(10)	6680(8)	2545(5)	94(2)
C(46)	-2497(9)	7140(8)	2370(5)	98(2)
O(40)	-1992(3)	3012(3)	103(2)	34(1)
O(41)	-636(3)	2971(3)	1332(2)	36(1)
N(40)	-2380(5)	4614(4)	1812(3)	53(1)
N(41)	-2574(8)	5416(7)	3007(4)	94(2)
S(40)	-1549(2)	3055(1)	3161(1)	56(1)
O(50)	-988(3)	1035(3)	-652(2)	34(1)
C(60)	1509(7)	3252(7)	-142(5)	72(2)
O(60)	681(4)	2839(3)	-458(2)	47(1)
C(70)	8877(9)	4185(8)	7812(6)	69(3)
O(70)	9066(6)	4646(5)	8485(4)	64(2)
C(43A)	-2515(13)	5389(8)	3913(5)	116(4)
C(44A)	-1060(20)	5125(16)	4164(11)	127(6)
C(43B)	-2515(13)	5389(8)	3913(5)	116(4)
C(44B)	-3900(30)	5360(30)	4248(16)	127(6)
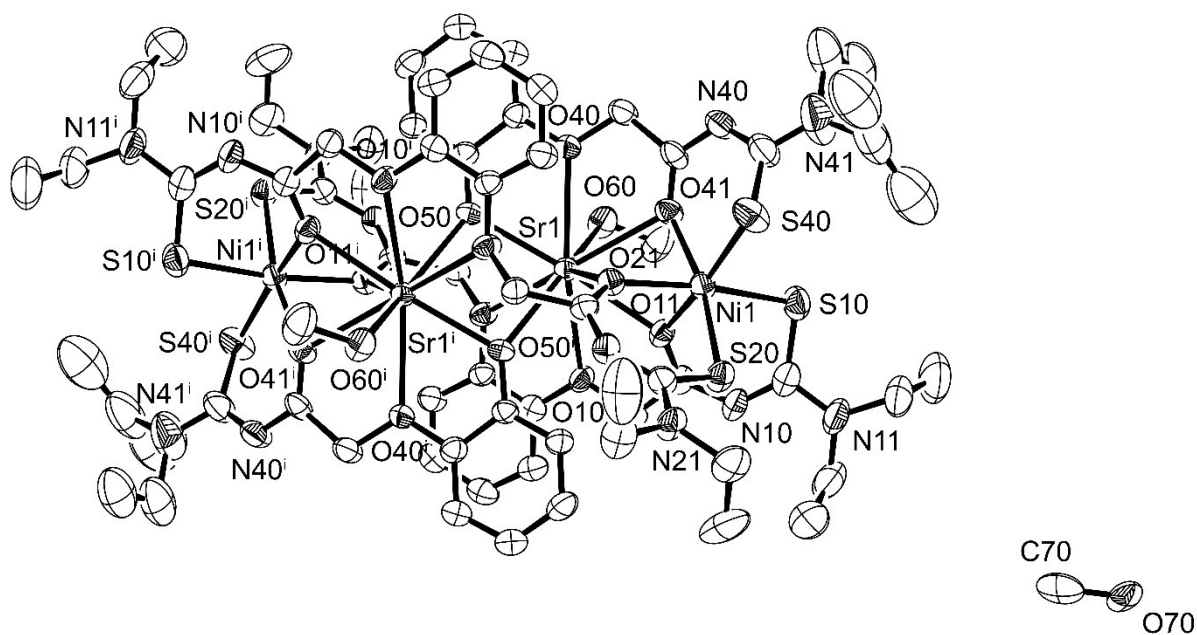
Figure 27: Ellipsoid plot (50% probability) of $\{(CH_3OH)_2Sr_2 \subset [Ni_2(L^3)_2(L^{3'})_2]\} \cdot 1.5\ CH_3OH$.

241

28. {(CH$_3$OH)$_2$Ca$_2 \subset$ [Ni$_2$(L^3)$_2$(L$^{3'}$)$_2$]} · 2 CH$_3$OH

Table 57. Crystal data and structure refinement for {(CH$_3$OH)$_2$Ca$_2 \subset$ [Ni$_2$(L^3)$_2$(L$^{3'}$)$_2$]} · 2 CH$_3$OH.

Empirical formula	C$_{70}$H$_{104}$O$_{18}$N$_{12}$S$_6$Ni$_2$Ca$_2$
Formula weight	1791.59
Measurement instrument	Bruker D8 Venture
Temperature	100(2) K
Wavelength	0.71073 Å
Crystal system	Triclinic
Space group	P $\bar{1}$
Unit cell dimensions	a = 10.952(1) Å α = 93.97(3)°.
	b = 12.870(1) Å β = 105.17(3)°.
	c = 15.549(1) Å γ = 99.16(3)°.
Volume	2074.2(3) Å^3
Z	1
Density (calculated)	1.434 g/cm^3
Absorption coefficient	0.800 mm^{-1}
F(000)	944
Crystal size	0.25 x 0.21 x 0.15 mm^3
Theta range for data collection	2.233 to 24.999°.
Index ranges	-13<=h<=13, -15<=k<=15, -18<=l<=18
Reflections collected	58508
Independent reflections	7308 [R(int) = 0.0401]
Completeness to theta = 24.999°	99.9 %
Absorption correction	Semi-empirical from equivalents
Max. and min. transmission	0.7455 and 0.6177
Refinement method	Full-matrix least-squares on F^2
Data / restraints / parameters	7308 / 0 / 500
Goodness-of-fit on F^2	1.039
Final R indices [I>2sigma(I)]	R1 = 0.0291, wR2 = 0.0754
R indices (all data)	R1 = 0.0345, wR2 = 0.0791
Largest diff. peak and hole	1.297 and -0.444 e/Å^3

Table 58. Atomic coordinates (x 10^4) and equivalent isotropic displacement parameters (Å^2 x 10^3) for {(CH$_3$OH)$_2$Ca$_2 \subset$ [Ni$_2$(L^3)$_2$(L$^{3'}$)$_2$]} · 2 CH$_3$OH. U(eq) is defined as one third of the trace of the orthogonalized U^{ij} tensor.

	x	y	z	U(eq)
Ca	865(1)	4063(1)	4614(1)	12(1)
Ni	737(1)	2555(1)	2736(1)	11(1)
C(01)	-1089(2)	2480(2)	6046(1)	13(1)
C(02)	-2079(2)	1743(2)	6171(1)	18(1)
C(03)	-2676(2)	1966(2)	6834(1)	20(1)
C(04)	-2278(2)	2917(2)	7381(1)	19(1)
C(05)	-1269(2)	3659(2)	7271(1)	17(1)
C(06)	-681(2)	3443(2)	6610(1)	13(1)
C(10)	-836(2)	1346(2)	4860(1)	15(1)
C(11)	-214(2)	1369(2)	4100(1)	13(1)
C(12)	154(2)	174(2)	3006(1)	14(1)
C(13)	55(2)	-1150(2)	1754(2)	22(1)
C(14)	-493(3)	-728(2)	878(2)	36(1)
C(15)	-1556(2)	-1384(2)	2654(2)	22(1)
C(16)	-2796(3)	-1004(3)	2232(2)	45(1)
N(10)	-390(2)	418(1)	3664(1)	15(1)
N(11)	-413(2)	-742(1)	2495(1)	17(1)
O(10)	-447(1)	2343(1)	5411(1)	15(1)
O(11)	300(1)	2255(1)	3934(1)	12(1)
S(10)	1538(1)	903(1)	2844(1)	16(1)
O(20)	305(1)	4142(1)	6445(1)	15(1)
C(20)	1240(2)	4730(2)	7216(1)	13(1)
C(21)	913(2)	5762(2)	7547(1)	11(1)
C(22)	1754(2)	7149(2)	8748(1)	12(1)
C(23)	2424(2)	8252(2)	10216(2)	24(1)
C(24)	3767(3)	8905(2)	10443(2)	55(1)
C(25)	2719(2)	6378(2)	10104(1)	21(1)
C(26)	1625(3)	5665(2)	10308(2)	34(1)
O(21)	-16(1)	6090(1)	7043(1)	12(1)
N(20)	1667(2)	6154(1)	8347(1)	13(1)
N(21)	2298(2)	7271(1)	9637(1)	14(1)
S(20)	1368(1)	8231(1)	8214(1)	14(1)
C(31)	3313(2)	6176(2)	5297(1)	13(1)
C(32)	4514(2)	6819(2)	5524(1)	16(1)
C(33)	4820(2)	7653(2)	6212(1)	19(1)

C(34)	3912(2)	7828(2)	6651(1)	18(1)
C(35)	2699(2)	7180(2)	6417(1)	14(1)
C(36)	2363(2)	6336(2)	5730(1)	11(1)
C(40)	3647(2)	5231(2)	4018(1)	13(1)
C(41)	3032(2)	4258(2)	3350(1)	13(1)
C(42)	2976(2)	3574(2)	1883(1)	16(1)
C(43)	3531(2)	2744(2)	595(2)	33(1)
C(44)	3805(4)	1697(3)	772(2)	60(1)
C(45)	5173(2)	4036(2)	1755(2)	24(1)
C(46)	5294(2)	5113(2)	1420(2)	30(1)
N(40)	3424(2)	4302(1)	2622(1)	16(1)
N(41)	3842(2)	3457(2)	1432(1)	23(1)
O(40)	2912(1)	5304(1)	4644(1)	16(1)
O(41)	2314(1)	3528(1)	3591(1)	13(1)
S(40)	1409(1)	2928(1)	1456(1)	17(1)
O(50)	1223(1)	5691(1)	5476(1)	12(1)
C(60)	3443(2)	3527(2)	6399(2)	26(1)
C(61)	3819(2)	898(2)	5377(2)	33(1)
O(60)	2466(2)	3267(1)	5594(1)	29(1)
O(61)	2670(2)	1286(1)	5019(1)	30(1)
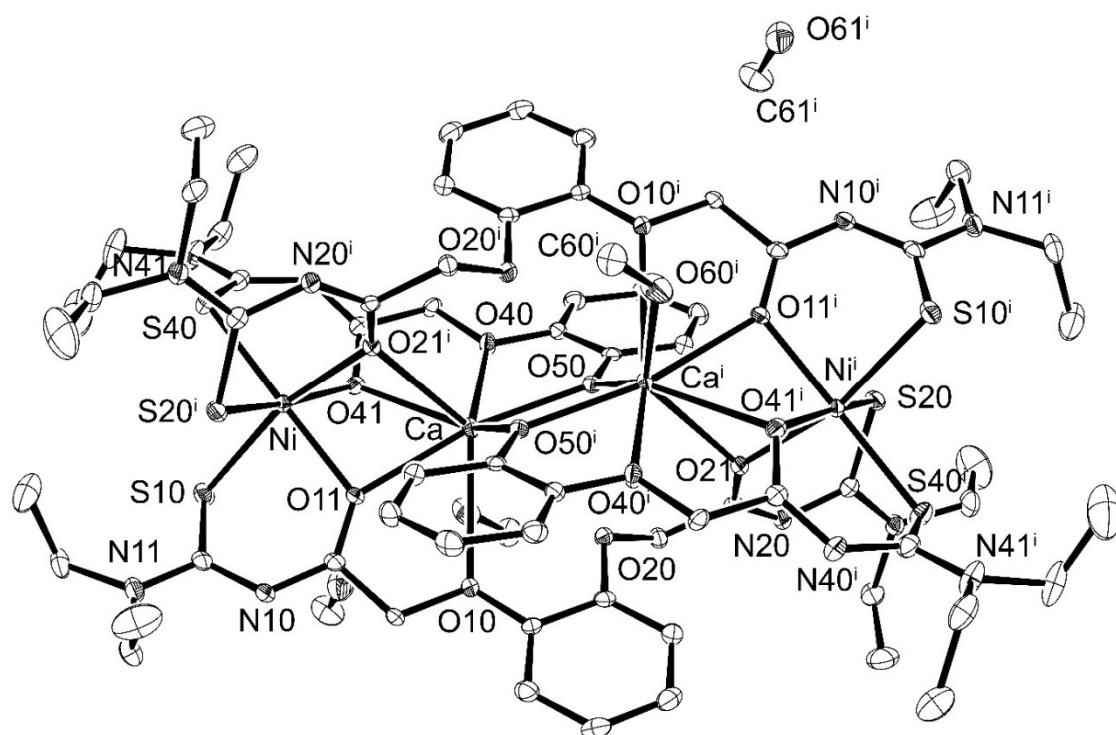
Figure 28: Ellipsoid plot (50% probability) of $\{(CH_3OH)_2Ca_2 \subset [Ni_2(L^3)_2(L^{3'})_2]\} \cdot 2\ CH_3OH$.

29. {(AcO)$_2$La$_2$ ⊂ [Ni$_2$(L^3)$_2$(L$^{3'}$)$_2$]} · CH$_3$OH

Table 59. Crystal data and structure refinement for {(AcO)$_2$La$_2$ ⊂ [Ni$_2$(L^3)$_2$(L$^{3'}$)$_2$]} · CH$_3$OH.

Empirical formula	C$_{71}$H$_{98}$O$_{19}$N$_{12}$S$_6$Ni$_2$La$_2$
Formula weight	1005.61
Measurement instrument	STOE IPDS 2T
Temperature	200(2) K
Wavelength	0.71073 Å
Crystal system	Monoclinic
Space group	P 2$_1$/c
Unit cell dimensions	a = 10.779(1) Å α = 90°.
	b = 25.164(2) Å β = 91.05(1)°.
	c = 16.518(1) Å γ = 90°.
Volume	4479.6(6) Å^3
Z	2
Density (calculated)	1.491 g/m^3
Absorption coefficient	1.556 mm^{-1}
F(000)	2052
Crystal size	0.18 x 0.054 x 0.03 mm^3
Theta range for data collection	2.379 to 24.999°.
Index ranges	-12<=h<=12, -29<=k<=29, -19<=l<=19
Reflections collected	22522
Independent reflections	7841 [R(int) = 0.1307]
Completeness to theta = 24.999°	99.5 %
Absorption correction	None
Refinement method	Full-matrix least-squares on F^2
Data / restraints / parameters	7839 / 33 / 521
Goodness-of-fit on F^2	0.801
Final R indices [I>2sigma(I)]	R1 = 0.0467, wR2 = 0.0772
R indices (all data)	R1 = 0.1090, wR2 = 0.0894
Largest diff. peak and hole	0.574 and -0.916 e/Å^3

Table 60. Atomic coordinates (x 10^4) and equivalent isotropic displacement parameters ($Å^2$x 10^3) for $\{(AcO)_2La_2 \subset [Ni_2(L^3)_2(L^{3'})_2]\} \cdot CH_3OH$. U(eq) is defined as one third of the trace of the orthogonalized U^{ij} tensor.

	x	y	z	U(eq)
Ni	1885(1)	4149(1)	2659(1)	38(1)
La	1298(1)	5067(1)	4156(1)	29(1)
C(01)	3048(6)	4873(3)	5896(4)	34(2)
C(02)	4080(6)	4868(3)	6393(4)	39(2)
C(03)	4040(6)	5113(3)	7143(4)	47(2)
C(04)	2957(7)	5353(3)	7387(5)	43(2)
C(05)	1910(6)	5354(3)	6893(4)	35(2)
C(06)	1921(5)	5108(3)	6152(4)	30(2)
C(10)	4000(6)	4343(3)	4877(4)	33(2)
C(11)	3741(6)	4159(3)	4023(5)	37(2)
C(12)	4245(6)	3448(3)	3157(5)	44(2)
C(13)	5357(8)	2863(3)	2199(6)	69(3)
C(14)	5696(11)	3182(5)	1460(6)	107(4)
C(15)	6445(7)	3245(3)	3431(6)	64(3)
C(16)	6545(8)	2807(3)	4034(6)	76(3)
O(10)	2972(4)	4656(2)	5120(3)	33(1)
O(11)	3058(4)	4459(2)	3575(3)	35(1)
N(10)	4345(5)	3727(2)	3855(4)	41(2)
N(11)	5301(5)	3203(2)	2929(4)	50(2)
S(10)	2886(2)	3325(1)	2637(1)	52(1)
O(20)	938(3)	5091(2)	5616(2)	30(1)
C(31)	-1014(6)	6055(3)	3451(4)	36(2)
C(32)	-1988(6)	6268(3)	3002(5)	45(2)
C(33)	-2794(6)	6627(3)	3336(5)	50(2)
C(34)	-2633(7)	6787(3)	4126(6)	51(2)
C(35)	-1687(6)	6571(3)	4602(5)	42(2)
C(36)	-876(6)	6210(2)	4269(5)	34(2)
C(40)	-87(7)	5636(3)	2315(4)	47(2)
C(41)	828(6)	5209(3)	2124(5)	42(2)
O(40)	-153(4)	5695(2)	3182(3)	36(1)
O(41)	1106(4)	4891(2)	2686(3)	37(1)
N(40)	1142(6)	5223(2)	1371(4)	51(2)
S(40)	2950(2)	4437(1)	1504(1)	59(1)

C(50)	647(6)	6284(3)	5345(4)	36(2)
O(50)	95(4)	5973(2)	4696(3)	37(1)
C(51)	-27(6)	6279(3)	6140(4)	33(2)
C(52)	100(6)	6731(3)	7387(5)	40(2)
C(53)	-150(8)	7401(4)	8471(5)	67(3)
C(54)	993(10)	7407(4)	9038(7)	102(4)
C(55)	478(10)	7668(4)	7089(7)	86(3)
C(56)	-598(14)	7824(4)	6548(8)	123(5)
O(51)	-855(4)	5927(2)	6266(3)	31(1)
N(50)	355(5)	6670(2)	6601(4)	40(2)
N(51)	165(6)	7239(3)	7641(4)	51(2)
S(50)	-166(2)	6233(1)	8071(1)	49(1)
C(60)	3034(7)	5983(3)	3957(5)	42(2)
C(61)	3783(7)	6461(3)	3902(5)	57(2)
O(60)	2954(4)	5745(2)	4615(3)	45(1)
O(61)	2461(5)	5814(2)	3346(3)	57(2)
O(90)	3094(10)	6389(4)	1943(6)	46(3)
C(90)	4101(16)	6160(7)	1707(8)	57(5)
N(41)	2133(6)	4970(4)	230(4)	74(2)
C(42)	2029(7)	4899(3)	1031(5)	54(2)
C(43)	1443(9)	5389(4)	-207(6)	83(3)
C(44)	2103(14)	5907(6)	-161(7)	146(6)
C(45A)	2973(12)	4636(6)	-278(7)	121(2)
C(46A)	2346(15)	4095(7)	-483(10)	122(3)
C(45B)	2973(12)	4636(6)	-278(7)	121(2)
C(46B)	4050(30)	5035(16)	-380(20)	122(3)
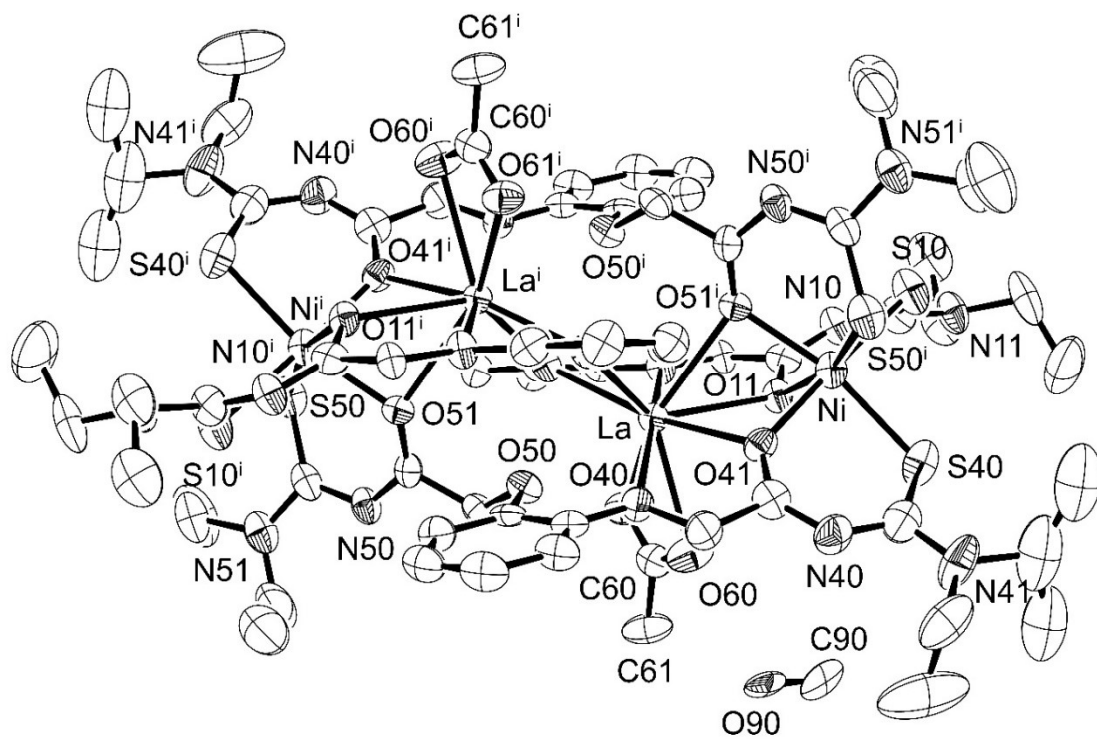
Figure 29: Ellipsoid plot (50% probability) of $\{(AcO)_2La_2 \subset [Ni_2(L^3)_2(L^{3'})_2]\} \cdot CH_3OH$.

30. {(AcO)$_2$Ce$_2$ ⊂ [Ni$_2$(L^3)$_2$(L$^{3'}$)$_2$]} · CH$_3$OH

Table 61. Crystal data and structure refinement for {(AcO)$_2$Ce$_2$ ⊂ [Ni$_2$(L^3)$_2$(L$^{3'}$)$_2$]} · CH$_3$OH.

Empirical formula	C$_{71}$H$_{98}$O$_{19}$N$_{12}$S$_6$Ni$_2$Ce$_2$
Formula weight	2013.63
Measurement instrument	STOE IPDS 2T
Temperature	200(2) K
Wavelength	0.71073 Å
Crystal system	Monoclinic
Space group	P 2$_1$/c
Unit cell dimensions	a = 10.759(1) Å α = 90°.
	b = 25.237(2) Å β = 90.97(1)°.
	c = 16.509(1) Å γ = 90°.
Volume	4482.0(6) Å^3
Z	2
Density (calculated)	1.492 g/cm^3
Absorption coefficient	1.618 mm^{-1}
F(000)	2056
Crystal size	0.18 x 0.054 x 0.03 mm^3
Theta range for data collection	2.596 to 25.000°.
Index ranges	-12<=h<=9, -30<=k<=30, -19<=l<=19
Reflections collected	21701
Independent reflections	7833 [R(int) = 0.0752]
Completeness to theta = 25.000°	99.3 %
Absorption correction	Integration
Max. and min. transmission	0.9271 and 0.7567
Refinement method	Full-matrix least-squares on F^2
Data / restraints / parameters	7833 / 32 / 520
Goodness-of-fit on F^2	0.880
Final R indices [I>2sigma(I)]	R1 = 0.0478, wR2 = 0.0978
R indices (all data)	R1 = 0.0950, wR2 = 0.1119
Largest diff. peak and hole	0.796 and -1.018 e/Å^3

Table 62. Atomic coordinates (x 10^4) and equivalent isotropic displacement parameters (Å^2x 10^3) for {(AcO)$_2$Ce$_2$ $\subset$ [Ni$_2$(L^3)$_2$(L$^{3'}$)$_2$]} · CH$_3$OH. U(eq) is defined as one third of the trace of the orthogonalized U^{ij} tensor.

	x	y	z	U(eq)
Ni(1)	3122(1)	9151(1)	2340(1)	39(1)
Ce(1)	3707(1)	10063(1)	844(1)	30(1)
C(01)	6019(7)	11056(3)	1536(4)	38(2)
C(02)	6989(7)	11263(3)	1992(5)	48(2)
C(03)	7781(7)	11624(3)	1662(5)	52(2)
C(04)	7622(7)	11779(3)	873(5)	53(2)
C(05)	6677(7)	11572(3)	396(4)	42(2)
C(06)	5869(6)	11210(3)	729(4)	37(2)
C(10)	5088(8)	10635(3)	2674(4)	51(2)
C(11)	4190(7)	10205(3)	2869(4)	44(2)
C(12)	2982(8)	9887(4)	3966(4)	60(2)
C(15)	3531(10)	10391(5)	5196(5)	86(3)
C(16)	2865(16)	10904(7)	5163(8)	151(7)
O(10)	5165(4)	10694(2)	1816(3)	40(1)
O(11)	3898(4)	9890(2)	2305(2)	41(1)
N(10)	3843(6)	10220(3)	3634(3)	53(2)
N(11)	2873(8)	9975(4)	4759(4)	79(2)
S(10)	2054(2)	9435(1)	3496(1)	61(1)
C(20)	4332(6)	11281(3)	-337(4)	39(2)
O(20)	4909(4)	10975(2)	304(3)	36(1)
C(21)	5019(6)	11278(3)	-1136(4)	35(2)
C(22)	4889(7)	11731(3)	-2395(4)	46(2)
C(23)	5153(9)	12394(4)	-3471(5)	70(3)
C(24)	4001(11)	12399(5)	-4024(7)	104(4)
C(25)	4559(11)	12666(4)	-2077(7)	85(3)
C(26)	5596(16)	12832(5)	-1547(8)	127(5)
O(21)	5835(4)	10924(2)	-1265(2)	36(1)
N(20)	4644(6)	11668(2)	-1596(4)	44(1)
N(21)	4848(6)	12233(3)	-2644(4)	55(2)
S(20)	5164(2)	11231(1)	-3073(1)	50(1)
C(31)	1975(6)	9873(3)	-893(3)	34(1)
C(32)	929(6)	9865(3)	-1387(4)	41(2)
C(33)	967(7)	10118(3)	-2135(4)	46(2)

|				
C(34)	2054(7)	10356(3)	-2377(4)	46(2)
C(35)	3111(6)	10351(3)	-1881(4)	38(2)
C(36)	3096(6)	10107(2)	-1126(3)	30(1)
C(40)	1014(6)	9340(3)	132(4)	35(2)
C(41)	1272(6)	9158(3)	977(4)	35(2)
C(42)	761(6)	8446(3)	1843(4)	43(2)
C(43)	-349(9)	7861(4)	2787(5)	69(3)
C(44)	-706(13)	8172(5)	3530(7)	110(4)
C(45)	-1434(8)	8246(4)	1579(6)	65(2)
C(46)	-1545(9)	7809(4)	983(6)	82(3)
O(40)	2044(4)	9654(2)	-118(2)	34(1)
O(41)	1954(4)	9458(2)	1432(2)	35(1)
N(40)	660(5)	8730(2)	1155(3)	43(1)
N(41)	-289(6)	8204(3)	2070(4)	53(2)
S(40)	2116(2)	8327(1)	2362(1)	56(1)
O(50)	4075(4)	10091(2)	-610(2)	29(1)
C(60)	1994(7)	10968(3)	1046(4)	44(2)
C(61)	1216(9)	11467(3)	1084(6)	67(2)
O(60)	2072(5)	10729(2)	385(3)	48(1)
O(61)	2558(5)	10803(2)	1667(3)	62(2)
C(70)	940(20)	1161(8)	3282(9)	72(6)
O(70)	1915(12)	1394(4)	3039(6)	53(3)
C(13A)	2029(15)	9632(7)	5254(7)	126(2)
C(14A)	2710(18)	9102(8)	5494(9)	130(3)
C(13B)	2029(15)	9632(7)	5254(7)	126(2)
C(14B)	920(50)	10030(20)	5360(30)	130(3)
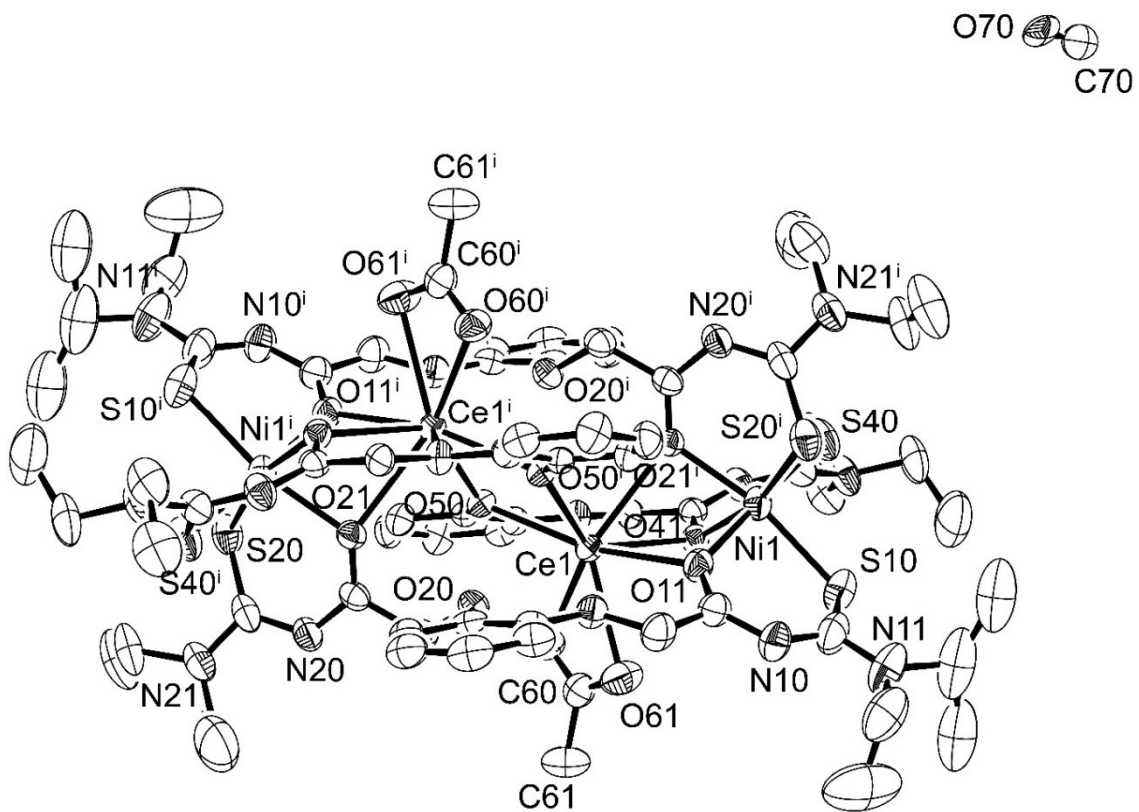
Figure 30: Ellipsoid plot (50% probability) of $\{(AcO)_2Ce_2 \subset [Ni_2(L^3)_2(L^{3'})_2]\} \cdot CH_3OH$.

31. $\{(AcO)_2Pr_2 \subset [Ni_2(L^3)_2(L^{3'})_2]\}$

Table 63. Crystal data and structure refinement for $\{(AcO)_2Pr_2 \subset [Ni_2(L^3)_2(L^{3'})_2]\}$.

Empirical formula	$C_{70}H_{94}O_{18}N_{12}S_6Ni_2Pr_2$
Formula weight	1983.17
Measurement instrument	STOE IPDS 2T
Temperature	200(2) K
Wavelength	0.71073 Å
Crystal system	Monoclinic
Space group	P 2_1/c
Unit cell dimensions	a = 12.913(1) Å $\qquad$ $\alpha = 90°$.
	b = 18.105(1) Å $\qquad$ $\beta = 120.25(1)°$.
	c = 20.522(1) Å $\qquad$ $\gamma = 90°$.
Volume	4144.5(4) Å^3
Z	2
Density (calculated)	1.589 g/cm^3
Absorption coefficient	1.825 mm^{-1}
F(000)	2024
Crystal size	0.18 x 0.054 x 0.03 mm^3
Theta range for data collection	2.094 to 24.998°.
Index ranges	-15<=h<=14, -21<=k<=21, -24<=l<=24
Reflections collected	19695
Independent reflections	7251 [R(int) = 0.0923]
Completeness to theta = 24.998°	99.3 %
Absorption correction	None
Refinement method	Full-matrix least-squares on F^2
Data / restraints / parameters	7251 / 0 / 497
Goodness-of-fit on F^2	0.836
Final R indices [I>2sigma(I)]	R1 = 0.0402, wR2 = 0.0532
R indices (all data)	R1 = 0.0851, wR2 = 0.0607
Largest diff. peak and hole	0.451 and -0.841 e/Å^3

Table 64. Atomic coordinates (x 10^4) and equivalent isotropic displacement parameters (Å^2 x 10^3) for $\{(AcO)_2Pr_2 \subset [Ni_2(L^3)_2(L^{3'})_2]\}$. U(eq) is defined as one third of the trace of the orthogonalized U^{ij} tensor.

	x	y	z	U(eq)
Ni	194(1)	8829(1)	2205(1)	24(1)
Pr	75(1)	9039(1)	497(1)	21(1)
C(01)	3035(4)	8972(3)	653(2)	26(1)
C(02)	4262(5)	8983(3)	972(3)	33(1)
C(03)	4778(5)	9129(3)	537(3)	47(2)
C(04)	4046(5)	9261(3)	-229(3)	45(2)
C(05)	2818(5)	9248(3)	-550(3)	41(2)
C(06)	2292(5)	9119(3)	-114(2)	26(1)
C(10)	3139(5)	8442(3)	1756(3)	33(1)
C(11)	2408(5)	8399(3)	2144(2)	25(1)
C(12)	2535(5)	7929(3)	3246(3)	30(1)
C(13)	4628(6)	8046(4)	4222(3)	63(2)
C(14)	4892(7)	8865(5)	4220(3)	87(3)
C(15)	3106(6)	7720(3)	4587(3)	49(2)
C(16)	3217(7)	8374(4)	5072(3)	60(2)
N(10)	2987(4)	8072(2)	2797(2)	35(1)
N(11)	3379(5)	7892(3)	3988(2)	41(1)
O(10)	2442(3)	8833(2)	1048(2)	26(1)
O(11)	1395(3)	8722(2)	1835(2)	26(1)
S(10)	1058(2)	7739(1)	2952(1)	36(1)
C(20)	364(5)	8922(3)	-1192(2)	27(1)
C(21)	183(5)	9564(3)	-1720(2)	23(1)
C(22)	-476(5)	9700(3)	-3024(3)	27(1)
C(23)	593(7)	8778(3)	-3350(3)	49(2)
C(24)	1894(7)	8977(5)	-2982(4)	86(2)
C(25)	-570(6)	9797(3)	-4245(3)	43(2)
C(26)	-1782(7)	9513(4)	-4860(3)	64(2)
N(20)	-15(4)	9307(2)	-2368(2)	30(1)
N(21)	-190(4)	9447(2)	-3520(2)	33(1)
O(20)	1076(3)	9095(2)	-396(1)	25(1)
O(21)	245(3)	10224(2)	-1493(2)	24(1)
S(20)	-1458(1)	10422(1)	-3262(1)	31(1)
C(31)	-2892(5)	9164(3)	-992(2)	28(1)
C(32)	-4044(5)	8949(3)	-1493(3)	36(1)
C(33)	-4539(5)	9158(3)	-2249(3)	38(1)

C(34)	-3842(5)	9538(3)	-2470(3)	34(1)
C(35)	-2683(5)	9734(3)	-1957(2)	27(1)
C(36)	-2173(5)	9566(3)	-1193(2)	22(1)
C(40)	-2829(5)	8431(3)	2(3)	32(1)
C(41)	-2057(5)	8331(3)	845(3)	27(1)
C(42)	-2272(5)	8159(3)	1915(3)	30(1)
C(43)	-3614(5)	7107(3)	1585(3)	39(1)
C(44)	-2995(7)	6489(3)	1415(3)	56(2)
C(45)	-2460(5)	7545(3)	2917(3)	38(2)
C(46)	-3297(6)	7971(4)	3093(3)	54(2)
N(40)	-2700(4)	8163(2)	1153(2)	33(1)
N(41)	-2763(4)	7636(2)	2129(2)	32(1)
O(40)	-2301(3)	8999(2)	-213(2)	26(1)
O(41)	-930(3)	8395(2)	1130(2)	26(1)
S(40)	-1356(1)	8826(1)	2510(1)	40(1)
O(50)	-1063(3)	9772(2)	-652(2)	22(1)
C(60)	-1(5)	7537(3)	-40(3)	30(1)
C(61)	37(6)	6816(3)	-334(3)	45(2)
O(60)	827(4)	7717(2)	611(2)	40(1)
O(61)	-823(3)	7991(2)	-424(2)	32(1)
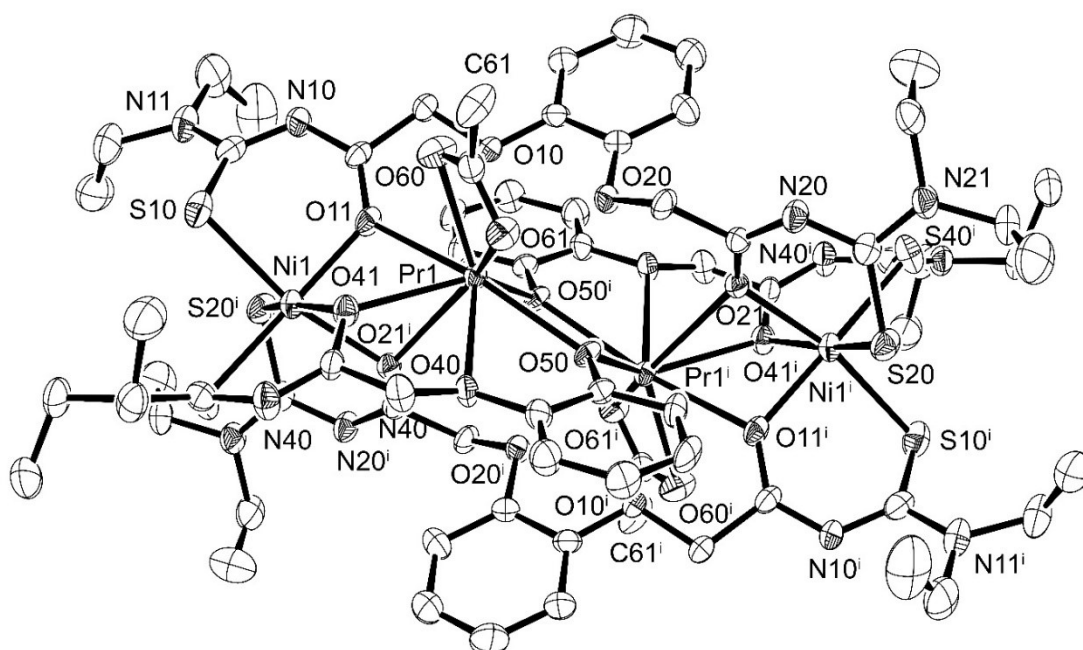
Figure 31: Ellipsoid plot (50% probability) of $\{(AcO)_2Pr_2 \subset [Ni_2(L^3)_2(L^{3'})_2]\}$.

32. {(CH₃OH)Ba ⊂ [Ag₂(L³)₂]}

Table 65. Crystal data and structure refinement for {(CH₃OH)Ba ⊂ [Ag₂(L³)₂]}.

Empirical formula	$C_{41}H_{60}O_9N_8S_4Ag_2Ba$
Formula weight	1290.29
Measurement instrument	Bruker D8 Venture
Temperature	100(2) K
Wavelength	0.71073 Å
Crystal system	Triclinic
Space group	P $\bar{1}$
Unit cell dimensions	a = 11.119(1) Å α = 95.95(4)°.
	b = 11.226(1) Å β = 110.76(4)°.
	c = 13.775(2) Å γ = 114.24(3)°.
Volume	1402.1(3) Å³
Z	1
Density (calculated)	1.528 g/cm³
Absorption coefficient	1.587 mm⁻¹
F(000)	648
Crystal size	0.23 x 0.14 x 0.02 mm³
Theta range for data collection	2.202 to 24.998°.
Index ranges	-13<=h<=13, -13<=k<=13, -16<=l<=16
Reflections collected	19354
Independent reflections	4897 [R(int) = 0.0480]
Completeness to theta = 24.998°	99.0 %
Absorption correction	Semi-empirical from equivalents
Max. and min. transmission	0.7454 and 0.6314
Refinement method	Full-matrix least-squares on F^2
Data / restraints / parameters	4897 / 2 / 329
Goodness-of-fit on F^2	1.100
Final R indices [I>2sigma(I)]	R1 = 0.0530, wR2 = 0.1393
R indices (all data)	R1 = 0.0749, wR2 = 0.1550
Largest diff. peak and hole	2.023 and -0.720 e/Å³

Table 66. Atomic coordinates (x 10^4) and equivalent isotropic displacement parameters (Å^2x 10^3) for $\{(CH_3OH)Ba \subset [Ag_2(L^3)_2]\}$. U(eq) is defined as one third of the trace of the orthogonalized U^{ij} tensor.

	x	y	z	U(eq)
Ag	5659(1)	8983(1)	5695(1)	31(1)
Ba	0	5000	5000	39(1)
C(01)	1084(8)	2408(7)	4234(6)	29(2)
C(02)	1601(8)	1894(8)	3639(6)	36(2)
C(03)	823(9)	524(9)	3053(6)	41(2)
C(04)	-460(9)	-317(9)	3083(6)	43(2)
C(05)	-1014(8)	180(7)	3688(6)	34(2)
C(06)	-260(8)	1538(7)	4263(6)	29(2)
O(10)	1713(6)	3746(5)	4817(5)	42(1)
O(11)	2871(7)	5898(7)	6387(5)	55(2)
C(10)	3242(8)	4611(8)	5148(6)	34(2)
C(11)	3797(8)	5720(8)	6152(6)	32(2)
C(12)	5833(11)	7473(9)	7594(7)	50(2)
N(10)	5208(7)	6346(6)	6733(5)	34(1)
S(10)	5820(2)	8948(2)	7504(2)	38(1)
C(20)	-1960(8)	1345(7)	4970(6)	29(2)
C(21)	-2157(8)	2203(7)	5760(6)	30(2)
C(22)	-3484(8)	2087(7)	6763(6)	29(2)
C(23)	-3274(12)	3013(10)	8564(7)	56(3)
C(24)	-4329(14)	1865(12)	8818(9)	73(3)
C(25)	-1394(11)	2414(10)	8403(8)	58(3)
C(26)	-40(11)	3714(13)	8637(9)	79(4)
N(20)	-3019(6)	1478(6)	6170(5)	28(1)
N(21)	-2754(7)	2493(6)	7851(5)	40(2)
O(20)	-660(6)	2179(5)	4887(5)	36(1)
O(21)	-1556(6)	3471(5)	5941(5)	44(1)
S(20)	-5014(2)	2230(2)	6148(1)	29(1)
N(11A)	7010(14)	7585(13)	8499(10)	40(2)
C(13A)	7940(30)	8780(20)	9454(16)	54(6)
C(14A)	7200(40)	8850(30)	10170(18)	90(10)
C(15A)	7170(20)	6379(18)	8612(14)	55(3)
C(16A)	8465(19)	6392(19)	8412(14)	60(4)
N(11B)	5996(16)	7148(14)	8598(12)	40(2)

C(13B)	6700(30)	8260(30)	9650(20)	63(7)
C(14B)	8350(40)	9050(30)	10000(30)	72(9)
C(15B)	5557(19)	5721(17)	8695(17)	55(3)
C(16B)	3940(20)	5120(20)	8601(16)	60(4)
O(30)	1594(14)	6906(13)	7157(10)	53(3)
C(30)	2068(19)	7819(18)	8073(10)	41(4)
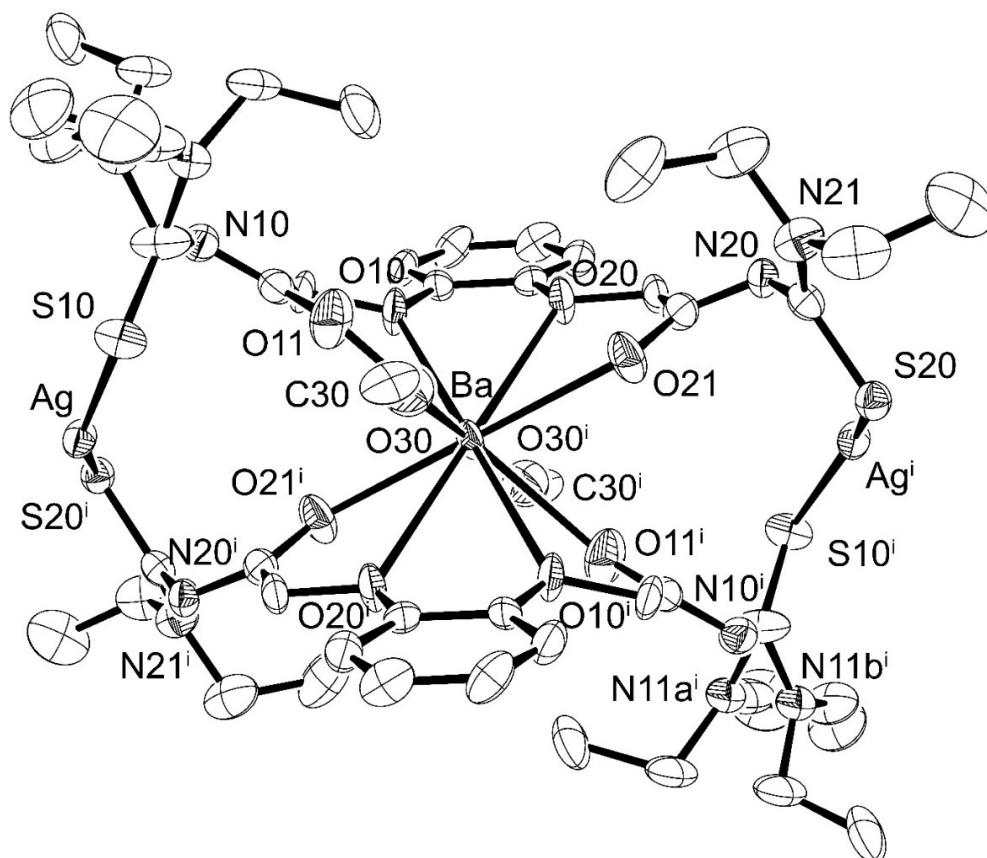
Figure 32: Ellipsoid plot (50% probability) of $\{(CH_3OH)Ba \subset [Ag_2(L^3)_2]\}$.

33. {(CH₃OH)Sr ⊂ [Ag₂(L³)₂]} · 0.75 CH₃OH

Table 67. Crystal data and structure refinement for {(CH$_3$OH)Sr ⊂ [Ag$_2$(L^3)$_2$]} · 0.75 CH$_3$OH.

Empirical formula	C$_{41.75}$H$_{63}$O$_{9.75}$N$_8$S$_4$Ag$_2$Sr
Formula weight	1264.60
Measurement instrument	STOE IPDS 2T
Temperature	200(2) K
Wavelength	0.71073 Å
Crystal system	Triclinic
Space group	P $\bar{1}$
Unit cell dimensions	a = 11.582(1) Å α = 86.84(1)°.
	b = 13.124(2) Å β = 76.11(1)°.
	c = 17.957(2) Å γ = 76.96(1)°.
Volume	2581.4(6) Å^3
Z	2
Density (calculated)	1.627 g/cm^3
Absorption coefficient	2.002 mm^{-1}
F(000)	1287
Crystal size	0.184 x 0.054 x 0.03 mm^3
Theta range for data collection	2.165 to 24.999°.
Index ranges	-13<=h<=13, -15<=k<=15, -21<=l<=21
Reflections collected	18425
Independent reflections	9017 [R(int) = 0.1170]
Completeness to theta = 24.999°	99.2 %
Absorption correction	None
Refinement method	Full-matrix least-squares on F^2
Data / restraints / parameters	9017 / 0 / 621
Goodness-of-fit on F^2	0.884
Final R indices [I>2sigma(I)]	R1 = 0.0429, wR2 = 0.0957
R indices (all data)	R1 = 0.0686, wR2 = 0.1031
Largest diff. peak and hole	0.615 and -1.310 e/Å^3

Table 68. Atomic coordinates (x 10^4) and equivalent isotropic displacement parameters (Å^2 x 10^3) for $\{(CH_3OH)Sr \subset [Ag_2(L^3)_2]\} \cdot 0.75\ CH_3OH$. U(eq) is defined as one third of the trace of the orthogonalized U^{ij} tensor.

	x	y	z	U(eq)
Sr	3751(1)	8399(1)	7410(1)	24(1)
Ag(1)	4182(1)	10719(1)	9367(1)	52(1)
Ag(2)	3586(1)	5242(1)	5391(1)	33(1)
C(01)	3512(5)	6386(4)	8965(3)	30(1)
C(02)	3713(5)	5806(4)	9604(3)	37(1)
C(03)	3144(6)	4960(5)	9819(3)	53(2)
C(04)	2425(7)	4720(5)	9399(4)	61(2)
C(05)	2210(6)	5303(4)	8755(3)	47(2)
C(06)	2743(5)	6146(4)	8540(3)	28(1)
C(10)	4814(5)	7486(4)	9135(3)	34(1)
C(11)	5448(5)	8323(4)	8720(3)	29(1)
C(12)	6956(5)	9212(4)	8843(3)	32(1)
C(13)	9030(5)	9517(5)	8465(3)	50(2)
C(14)	9310(7)	10056(6)	7714(4)	72(2)
C(15)	8588(6)	7782(4)	8233(3)	48(2)
C(16)	8942(7)	7021(5)	8845(4)	62(2)
O(10)	4048(3)	7218(2)	8695(2)	30(1)
O(11)	5152(5)	8757(4)	8149(2)	66(1)
N(10)	6290(4)	8458(4)	9034(3)	43(1)
N(11)	8120(4)	8871(3)	8524(2)	35(1)
S(10)	6375(1)	10496(1)	9094(1)	48(1)
C(20)	1962(4)	6448(4)	7427(3)	26(1)
C(21)	1827(4)	7208(4)	6773(2)	24(1)
C(22)	1140(4)	7268(3)	5635(3)	26(1)
C(23)	16(5)	7873(4)	4638(3)	39(1)
C(24)	347(6)	8868(5)	4249(3)	49(2)
C(25)	-972(5)	8230(4)	6019(3)	41(1)
C(26)	-1810(5)	7489(5)	6280(4)	55(2)
O(20)	2539(3)	6812(2)	7942(2)	31(1)
O(21)	2401(4)	7924(3)	6652(2)	38(1)
N(20)	1060(4)	7014(3)	6384(2)	29(1)
N(21)	124(4)	7777(3)	5438(2)	29(1)
S(20)	2443(1)	6853(1)	4929(1)	34(1)

C(31)	5790(4)	9821(3)	5923(2)	23(1)
C(32)	6408(4)	10579(3)	5572(3)	25(1)
C(33)	7051(4)	10447(4)	4813(3)	28(1)
C(34)	7100(4)	9577(4)	4407(3)	30(1)
C(35)	6509(4)	8790(4)	4768(3)	26(1)
C(36)	5882(4)	8917(3)	5527(2)	22(1)
C(40)	4781(5)	10858(4)	7051(3)	31(1)
C(41)	3528(5)	11007(4)	7575(3)	29(1)
C(42)	2151(5)	12062(4)	8522(3)	31(1)
C(43)	101(5)	13173(5)	8991(3)	48(2)
C(44)	-910(7)	12725(7)	8871(4)	81(2)
C(45)	1324(6)	13340(4)	7653(3)	43(1)
C(46)	1069(7)	12697(5)	7047(3)	64(2)
O(40)	5054(3)	9888(2)	6653(2)	28(1)
O(41)	2898(3)	10331(2)	7585(2)	31(1)
N(40)	3191(4)	11892(3)	7959(2)	34(1)
N(41)	1235(4)	12826(3)	8401(2)	34(1)
S(40)	2047(1)	11390(1)	9372(1)	41(1)
C(50)	5491(5)	7186(3)	5599(3)	28(1)
C(51)	5337(4)	6368(3)	6234(3)	24(1)
C(52)	5392(5)	4590(3)	6456(3)	30(1)
C(55)	7154(6)	4683(5)	6962(4)	51(2)
C(56)	7032(7)	5210(6)	7705(4)	71(2)
O(50)	5299(3)	8183(2)	5948(2)	26(1)
O(51)	4967(4)	6650(2)	6912(2)	37(1)
N(50)	5596(4)	5413(3)	5961(2)	28(1)
N(51)	6087(4)	4251(3)	6929(2)	40(1)
S(50)	4262(1)	3996(1)	6356(1)	36(1)
C(60)	1550(6)	8783(5)	9413(3)	45(1)
O(60)	1918(4)	9059(3)	8628(2)	41(1)
C(53A)	6102(15)	3217(12)	7375(12)	44(4)
C(54A)	5206(12)	3444(8)	8142(6)	63(4)
C(53B)	5680(30)	3500(20)	7510(20)	44(4)
C(54B)	6710(20)	2534(16)	7395(14)	80(7)
O(70)	137(8)	5176(6)	6624(5)	97(3)
C(70)	278(12)	4906(8)	5829(9)	111(5)
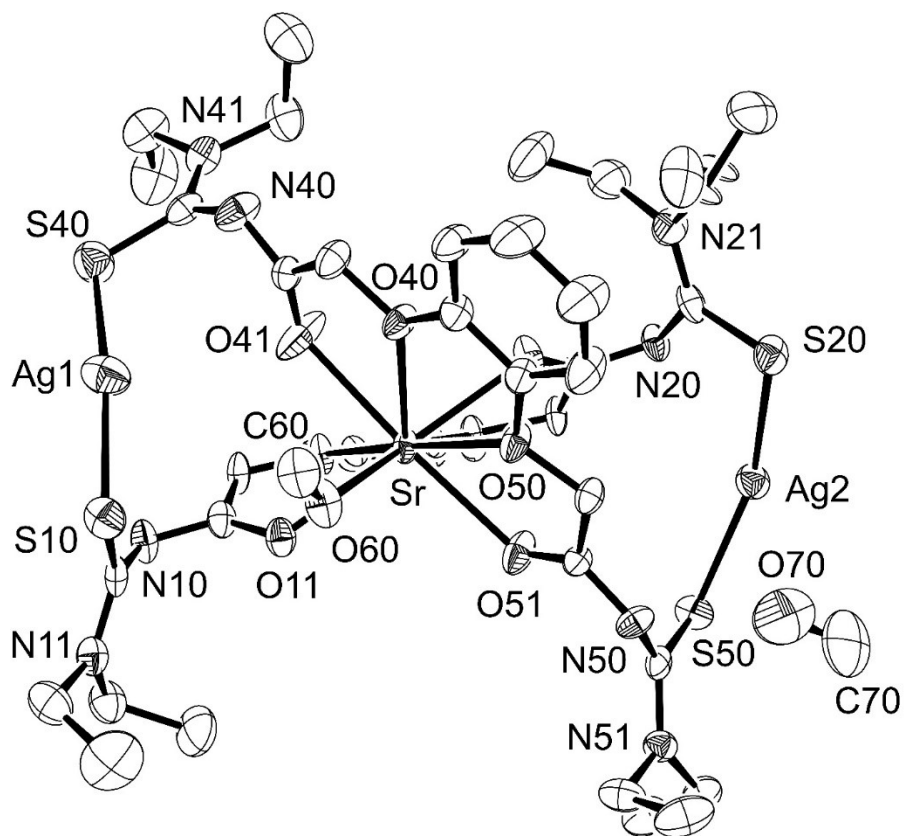
Figure 33: Ellipsoid plot (50% probability) of $\{(CH_3OH)Sr \subset [Ag_2(L^3)_2]\} \cdot 0.75\ CH_3OH$.

34. $\{Ca \subset [Ag_2(L^3)_2]\}_2 \cdot CH_3OH$

Table 69. Crystal data and structure refinement for $\{Ca \subset [Ag_2(L^3)_2]\}_2 \cdot CH_3OH$.

Empirical formula	$C_{81}H_{116}O_{17}N_{16}S_8Ag_4Ca_2$
Formula weight	2354.01
Measurement instrument	STOE IPDS 2T
Temperature	200(2) K
Wavelength	0.71073 Å
Crystal system	Monoclinic
Space group	P 2_1/c
Unit cell dimensions	a = 13.563(1) Å $\quad$ $\alpha = 90°$.
	b = 33.829(2) Å $\quad$ $\beta = 116.04(1)°$.
	c = 25.258(2) Å $\quad$ $\gamma = 90°$.
Volume	10412.5(15) $Å^3$
Z	4
Density (calculated)	1.502 g/cm^3
Absorption coefficient	1.066 mm^{-1}
F(000)	4824
Crystal size	0.184 x 0.054 x 0.03 mm^3
Theta range for data collection	1.776 to 25.000°.
Index ranges	-16<=h<=14, -40<=k<=40, -27<=l<=30
Reflections collected	51890
Independent reflections	18216 [R(int) = 0.1251]
Completeness to theta = 25.000°	99.4 %
Absorption correction	None
Refinement method	Full-matrix least-squares on F^2
Data / restraints / parameters	18214 / 22 / 1200
Goodness-of-fit on F^2	0.880
Final R indices [I>2sigma(I)]	R1 = 0.0632, wR2 = 0.1346
R indices (all data)	R1 = 0.1494, wR2 = 0.1605
Extinction coefficient	0.00149(9)
Largest diff. peak and hole	1.073 and -0.656 $e/Å^3$

Table 70. Atomic coordinates (x 10^4) and equivalent isotropic displacement parameters (Å^2 x 10^3) for {Ca $\subset$ [Ag$_2$(L^3)$_2$]}$_2$ · CH$_3$OH. U(eq) is defined as one third of the trace of the orthogonalized U^{ij} tensor.

	x	y	z	U(eq)
Ag(1)	2705(1)	8703(1)	1644(1)	83(1)
Ag(2)	7496(1)	6425(1)	1379(1)	59(1)
Ag(3)	5252(1)	9364(1)	2527(1)	63(1)
Ag(4)	10648(1)	11411(1)	2153(1)	54(1)
Ca(1)	4975(1)	7540(1)	1469(1)	44(1)
Ca(2)	8107(1)	10302(1)	2455(1)	46(1)
C(01)	6212(7)	8278(2)	994(4)	46(2)
C(02)	6793(7)	8618(3)	1013(4)	55(2)
C(03)	7284(9)	8654(3)	642(5)	70(3)
C(04)	7245(8)	8345(3)	274(5)	76(3)
C(05)	6657(8)	8007(3)	262(5)	68(3)
C(06)	6139(7)	7977(2)	618(4)	46(2)
C(10)	5804(8)	8515(2)	1770(4)	59(2)
C(11)	5327(7)	8366(2)	2172(4)	49(2)
C(12)	4723(8)	8515(3)	2857(4)	56(2)
C(13)	4911(11)	8230(4)	3794(5)	90(4)
C(14)	4339(14)	7835(4)	3625(5)	139(7)
C(15)	6518(9)	8279(3)	3557(5)	80(3)
C(16)	6865(11)	7861(4)	3549(6)	115(5)
O(10)	5691(4)	8216(2)	1350(2)	49(1)
O(11)	5091(6)	8004(2)	2169(3)	65(2)
N(10)	5155(7)	8627(2)	2496(3)	59(2)
N(11)	5343(7)	8348(2)	3370(3)	63(2)
S(10)	3389(3)	8641(1)	2680(1)	90(1)
C(20)	5687(7)	7296(2)	366(4)	55(2)
C(21)	5124(7)	6950(2)	514(4)	47(2)
C(22)	4927(8)	6283(3)	429(4)	59(2)
C(23)	3734(10)	5694(3)	215(7)	113(5)
C(24)	4258(13)	5402(5)	20(9)	161(8)
C(25)	3235(10)	6259(4)	-518(5)	92(4)
C(26)	2282(11)	6451(5)	-480(7)	131(5)
O(20)	5524(4)	7650(2)	626(2)	45(1)
O(21)	4735(5)	7007(2)	870(3)	58(2)

N(20)	5129(6)	6633(2)	237(4)	64(2)
N(21)	4006(7)	6088(2)	57(4)	73(2)
S(20)	5765(2)	6075(1)	1089(1)	65(1)
C(31)	3990(7)	7021(2)	2336(4)	44(2)
C(32)	3297(7)	6868(2)	2553(4)	54(2)
C(33)	3643(8)	6571(3)	2974(4)	59(2)
C(34)	4688(8)	6439(3)	3193(4)	62(3)
C(35)	5432(8)	6589(3)	2989(4)	59(2)
C(36)	5066(7)	6880(2)	2565(4)	48(2)
C(40)	2691(7)	7489(3)	1703(4)	55(2)
C(41)	2498(7)	7737(2)	1163(4)	51(2)
C(42)	1264(7)	8180(3)	511(5)	58(2)
C(43)	144(9)	8316(4)	-551(5)	96(4)
C(44)	-934(11)	8519(6)	-659(7)	170(9)
O(40)	3715(4)	7287(2)	1883(2)	47(1)
O(41)	3171(5)	7742(2)	958(3)	66(2)
N(40)	1539(6)	7927(2)	960(4)	63(2)
N(41)	551(7)	8055(3)	-24(4)	72(2)
S(40)	1687(3)	8660(1)	604(1)	81(1)
C(50)	6791(6)	6904(3)	2512(4)	56(2)
C(51)	7341(7)	7137(2)	2201(4)	48(2)
C(52)	8838(7)	7176(2)	2014(4)	53(2)
C(53)	9671(10)	7660(3)	2823(6)	89(4)
C(54)	8947(12)	8024(4)	2742(7)	124(5)
O(50)	5696(4)	7051(2)	2316(3)	53(2)
O(51)	6842(5)	7415(2)	1872(3)	65(2)
N(50)	8339(6)	7017(2)	2330(4)	61(2)
N(51)	9522(7)	7480(2)	2262(4)	70(2)
S(50)	8701(2)	6967(1)	1375(1)	68(1)
C(61)	9104(7)	9479(2)	2016(4)	51(2)
C(62)	9566(8)	9113(3)	2025(5)	67(3)
C(63)	9999(8)	9025(3)	1636(5)	70(3)
C(64)	9943(8)	9293(3)	1228(5)	70(3)
C(65)	9471(7)	9668(3)	1200(4)	60(2)
C(66)	9072(7)	9749(2)	1602(4)	47(2)
C(70)	8525(9)	9302(3)	2750(5)	72(3)
C(71)	8088(7)	9501(3)	3150(4)	54(2)
C(72)	7363(8)	9338(3)	3800(4)	63(3)
C(73)	7627(12)	9360(5)	4838(6)	113(4)

C(74)	7136(14)	9013(4)	4956(8)	147(6)
C(75)	9110(10)	9153(5)	4577(6)	107(4)
C(76)	9217(11)	8695(6)	4512(7)	137(6)
O(70)	8667(5)	9599(2)	2387(3)	57(2)
O(71)	8171(5)	9870(2)	3206(3)	62(2)
N(70)	7765(7)	9242(2)	3419(4)	66(2)
N(71)	7965(8)	9282(3)	4361(4)	85(3)
S(70)	6045(2)	9517(1)	3558(1)	74(1)
C(80)	8817(7)	10437(2)	1339(4)	51(2)
C(81)	8308(7)	10808(2)	1447(4)	44(2)
O(80)	8583(4)	10113(2)	1618(2)	50(1)
O(81)	7899(5)	10804(2)	1798(3)	54(2)
N(80)	8367(5)	11103(2)	1122(3)	49(2)
C(82)	8074(6)	11479(2)	1213(3)	40(2)
C(85)	6808(7)	12035(2)	798(4)	61(3)
C(86)	7285(9)	12327(3)	508(5)	83(3)
C(83)	6518(8)	11400(3)	248(4)	71(3)
C(84)	5691(9)	11149(4)	346(5)	103(4)
N(81)	7181(6)	11626(2)	784(3)	55(2)
S(80)	8893(2)	11754(1)	1808(1)	55(1)
C(91)	7226(7)	10946(2)	3229(4)	43(2)
C(92)	6583(7)	11127(2)	3458(4)	48(2)
C(93)	7020(7)	11427(2)	3869(4)	52(2)
C(94)	8077(8)	11544(3)	4047(4)	61(3)
C(95)	8759(7)	11360(3)	3835(4)	54(2)
C(96)	8322(7)	11059(2)	3431(4)	45(2)
C(100)	5797(7)	10511(2)	2615(4)	49(2)
C(101)	5499(7)	10253(2)	2082(4)	49(2)
C(102)	3969(7)	9927(2)	1355(4)	56(2)
C(103)	2560(9)	9791(3)	347(4)	86(4)
C(104)	1445(9)	9718(4)	337(6)	100(4)
C(10A)	2750(30)	10508(9)	821(13)	73(6)
C(11A)	3500(30)	10716(10)	593(15)	113(8)
C(10B)	3300(20)	10463(8)	646(10)	73(6)
C(11B)	2560(30)	10699(9)	796(15)	113(8)
O(100)	6885(4)	10653(2)	2808(2)	45(1)
O(101)	6262(5)	10119(2)	1972(3)	59(2)
N(100)	4445(6)	10205(2)	1779(3)	61(2)
N(101)	3243(8)	10054(2)	836(4)	93(3)

|				
S(100)	4178(2)	9431(1)	1479(1)	61(1)
C(110)	10001(7)	10969(3)	3358(4)	56(2)
C(111)	10479(6)	10705(2)	3049(4)	43(2)
O(110)	8895(4)	10846(2)	3193(2)	48(1)
O(111)	9989(4)	10400(2)	2793(3)	58(2)
C(112)	11935(7)	10648(3)	2786(4)	50(2)
C(113)	12582(8)	10135(3)	3530(4)	63(2)
C(114)	11966(10)	9734(3)	3415(6)	105(4)
C(115)	13073(7)	10123(3)	2691(5)	65(3)
C(116)	12300(9)	9870(3)	2158(6)	94(4)
N(110)	11427(5)	10837(2)	3088(3)	49(2)
N(111)	12472(6)	10316(2)	2982(3)	55(2)
S(110)	11866(2)	10872(1)	2165(1)	57(1)
C(120)	3979(15)	4745(7)	4270(8)	60(5)
O(120)	3569(9)	4547(3)	3803(8)	73(5)
C(130)	1482(11)	5328(4)	514(6)	34(4)
O(130)	723(11)	5230(4)	698(5)	70(4)
C(45A)	310(20)	7620(6)	-122(19)	95(11)
C(46A)	-574(18)	7506(7)	78(11)	130(10)
C(45B)	-140(50)	7691(12)	-130(50)	95(11)
C(46B)	300(40)	7370(14)	-400(20)	140(30)
C(55A)	10186(11)	7646(4)	1984(6)	104(4)
C(56A)	9575(16)	7943(4)	1528(10)	127(8)
C(55B)	10186(11)	7646(4)	1984(6)	104(4)
C(56B)	10880(50)	7935(15)	2320(30)	127(8)
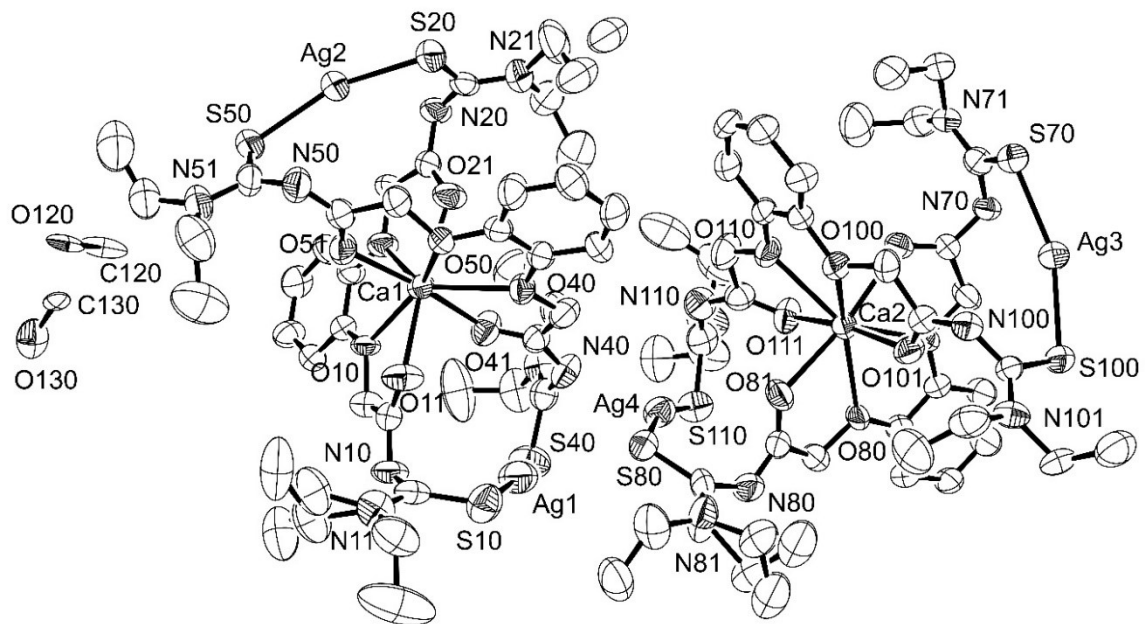
Figure 34: Ellipsoid plot (50% probability) of $\{Ca \subset [Ag_2(L^3)_2]\}_2 \cdot CH_3OH$.

35. {Ba ⊂ [Hg₂(L³)₃]} · CH₃OH

Table 71. Crystal data and structure refinement for {Ba ⊂ [Hg₂(L³)₃]} · CH₃OH.

Empirical formula	$C_{61}H_{88}O_{13}N_{12}S_6Hg_2Ba$
Formula weight	1928.35
Measurement instrument	STOE IPDS 2T
Temperature	200(2) K
Wavelength	0.71073 Å
Crystal system	Monoclinic
Space group	C 2/c
Unit cell dimensions	a = 21.762(1) Å $\quad$ α = 90°.
	b = 15.962(6) Å $\quad$ β = 110.09(5)°.
	c = 23.192(2) Å $\quad$ γ = 90°.
Volume	7566(8) Å³
Z	4
Density (calculated)	1.693 g/cm³
Absorption coefficient	4.793 mm⁻¹
F(000)	3815
Crystal size	0.300 x 0.287 x 0.270 mm³
Theta range for data collection	3.381 to 25.000°.
Index ranges	-25<=h<=25, -16<=k<=18, -27<=l<=27
Reflections collected	28803
Independent reflections	6629 [R(int) = 0.0504]
Completeness to theta = 25.000°	99.7 %
Absorption correction	None
Refinement method	Full-matrix least-squares on F²
Data / restraints / parameters	6629 / 0 / 436
Goodness-of-fit on F²	1.059
Final R indices [I>2sigma(I)]	R1 = 0.0244, wR2 = 0.0550
R indices (all data)	R1 = 0.0275, wR2 = 0.0562
Largest diff. peak and hole	1.207 and -1.585 e/Å³

Table 72. Atomic coordinates (x 10^4) and equivalent isotropic displacement parameters (Å^2 x 10^3) for {Ba $\subset$ [Hg$_2$(L^3)$_3$]} · CH$_3$OH. U(eq) is defined as one third of the trace of the orthogonalized U^{ij} tensor.

	x	y	z	U(eq)
Hg	3362(1)	4856(1)	782(1)	34(1)
Ba	5000	5038(1)	2500	27(1)
C(01)	3580(1)	6220(2)	3041(1)	32(1)
C(02)	3054(2)	6724(2)	3021(2)	44(1)
C(03)	2773(2)	6665(3)	3475(2)	58(1)
C(04)	3001(2)	6091(3)	3935(2)	59(1)
C(05)	3520(2)	5575(3)	3956(2)	47(1)
C(06)	3816(1)	5634(2)	3515(1)	32(1)
C(10)	3558(2)	6732(2)	2077(1)	34(1)
C(11)	3893(1)	6633(2)	1610(1)	31(1)
C(12)	3650(1)	6843(2)	550(1)	34(1)
C(13)	3649(2)	7409(3)	-444(2)	52(1)
C(14)	3060(2)	7131(4)	-970(2)	73(1)
C(15)	3305(2)	8279(3)	285(2)	61(1)
C(16)	3860(3)	8851(3)	626(3)	88(2)
O(10)	3902(1)	6278(1)	2624(1)	32(1)
O(11)	4445(1)	6328(2)	1750(1)	43(1)
N(10)	3538(1)	6984(2)	1070(1)	36(1)
N(11)	3532(1)	7463(2)	143(1)	42(1)
S(10)	3890(1)	5878(1)	331(1)	42(1)
C(20)	4600(2)	4625(2)	4045(1)	37(1)
C(21)	5176(1)	4128(2)	4010(1)	31(1)
C(22)	5948(1)	3141(2)	4595(1)	35(1)
C(23)	6541(2)	1867(2)	5109(2)	47(1)
C(24)	6502(2)	1216(3)	4628(2)	69(1)
C(25)	5403(2)	2158(2)	5069(2)	49(1)
C(26)	5417(2)	2488(3)	5681(2)	67(1)
O(20)	4342(1)	5151(1)	3520(1)	34(1)
O(21)	5353(1)	4202(2)	3561(1)	43(1)
N(20)	5413(1)	3615(2)	4493(1)	39(1)
N(21)	5977(1)	2436(2)	4914(1)	41(1)
S(20)	6636(1)	3346(1)	4387(1)	39(1)
C(31)	4662(1)	2476(2)	2451(2)	37(1)

C(32)	4341(2)	1719(2)	2397(2)	53(1)
C(33)	4669(2)	968(2)	2446(2)	69(1)
C(40)	3670(2)	3211(2)	2231(2)	42(1)
C(41)	3364(1)	4060(2)	2036(1)	31(1)
C(42)	2309(1)	4633(2)	1600(1)	33(1)
C(43)	1265(2)	5361(2)	1479(2)	49(1)
C(44)	707(2)	5048(3)	931(3)	76(1)
C(45)	1650(2)	4165(3)	2201(2)	55(1)
C(46)	1960(2)	4498(4)	2845(2)	85(2)
O(40)	4364(1)	3245(1)	2411(1)	35(1)
O(41)	3701(1)	4683(1)	2040(1)	36(1)
N(40)	2715(1)	4016(2)	1884(1)	38(1)
N(41)	1761(1)	4712(2)	1740(1)	40(1)
S(40)	2384(1)	5300(1)	1033(1)	42(1)
C(50)	5000	8264(5)	2500	97(2)
O(50)	5220(4)	7977(4)	2094(4)	80(2)
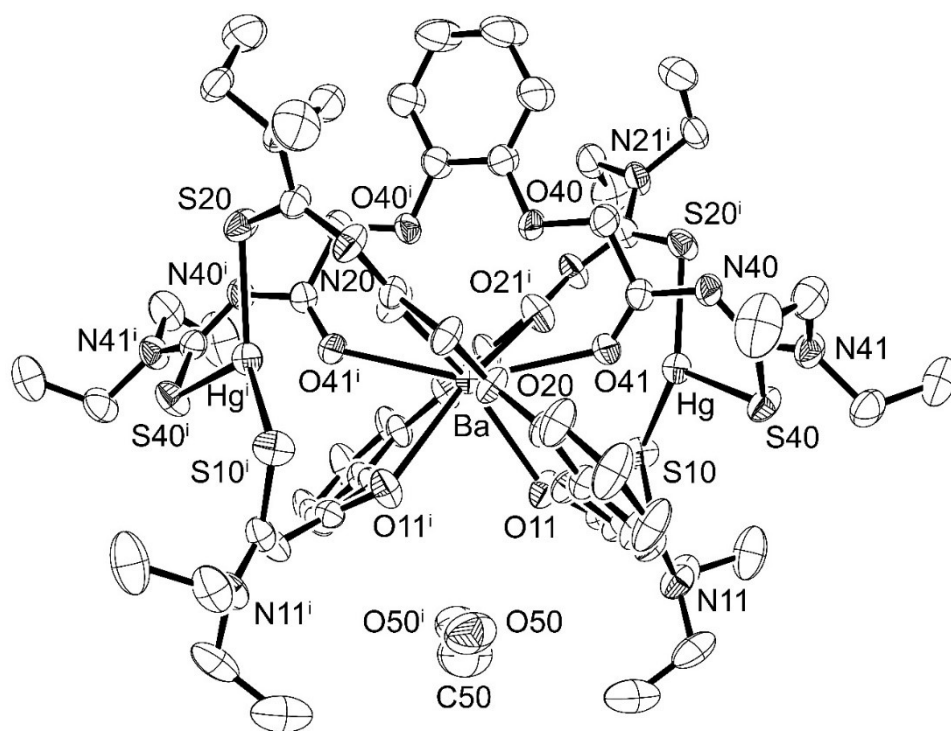
Figure 35: Ellipsoid plot (50% probability) of $\{Ba \subset [Hg_2(L^3)_3]\} \cdot CH_3OH$.

36. $\{Sr \subset [Hg_2(L^3)_3]\} \cdot CH_3OH$

Table 73. Crystal data and structure refinement for $\{Sr \subset [Hg_2(L^3)_3]\} \cdot CH_3OH$.

Empirical formula	$C_{61}H_{88}O_{13}N_{12}S_6Hg_2Sr$
Formula weight	1878.63
Measurement instrument	STOE IPDS 2T
Temperature	200(2) K
Wavelength	0.71073 Å
Crystal system	Monoclinic
Space group	C 2/c
Unit cell dimensions	a = 21.652(2) Å $\quad$ $\alpha = 90°$.
	b = 16.112(2) Å $\quad$ $\beta = 111.36(1)°$.
	c = 23.067(2) Å $\quad$ $\gamma = 90°$.
Volume	7494(1) Å^3
Z	4
Density (calculated)	1.665 g/cm^3
Absorption coefficient	5.028 mm^{-1}
F(000)	3743
Crystal size	0.184 x 0.054 x 0.03 mm^3
Theta range for data collection	1.679 to 25.000°.
Index ranges	-25<=h<=25, -19<=k<=19, -27<=l<=27
Reflections collected	29961
Independent reflections	6599 [R(int) = 0.1475]
Completeness to theta = 25.000°	99.9 %
Absorption correction	Integration
Max. and min. transmission	0.5171 and 0.4179
Refinement method	Full-matrix least-squares on F^2
Data / restraints / parameters	6599 / 0 / 435
Goodness-of-fit on F^2	0.883
Final R indices [I>2sigma(I)]	R1 = 0.0497, wR2 = 0.0818
R indices (all data)	R1 = 0.1042, wR2 = 0.0956
Largest diff. peak and hole	0.711 and -1.589 e/Å^3

Table 74. Atomic coordinates (x 10^4) and equivalent isotropic displacement parameters (Å^2 x 10^3) for $\{Sr \subset [Hg_2(L^3)_3]\} \cdot CH_3OH$. U(eq) is defined as one third of the trace of the orthogonalized U^{ij} tensor.

	x	y	z	U(eq)
Hg	3371(1)	4838(1)	810(1)	40(1)
Sr	5000	5065(1)	2500	36(1)
C(01)	6388(4)	6301(6)	1943(4)	41(2)
C(02)	6895(4)	6846(6)	1955(4)	46(2)
C(03)	7155(5)	6804(7)	1489(5)	56(3)
C(04)	6940(5)	6227(7)	1032(5)	65(3)
C(05)	6433(4)	5675(6)	1013(5)	50(3)
C(06)	6155(4)	5719(5)	1468(4)	39(2)
C(10)	3576(4)	6766(5)	2068(4)	40(2)
C(11)	3900(4)	6596(5)	1604(4)	34(2)
C(12)	3649(4)	6792(5)	528(4)	34(2)
C(13)	3622(5)	7321(6)	-489(5)	56(3)
C(14)	3019(5)	7026(8)	-1011(5)	74(3)
C(15)	3291(5)	8221(6)	231(5)	57(3)
C(16)	3829(7)	8804(6)	561(7)	88(4)
O(10)	6072(3)	6342(3)	2363(3)	39(2)
O(11)	4431(3)	6224(4)	1744(3)	46(2)
N(10)	3551(4)	6958(4)	1055(3)	39(2)
N(11)	3527(4)	7402(5)	111(4)	46(2)
S(10)	3871(1)	5829(1)	313(1)	47(1)
C(20)	5405(4)	4636(5)	985(4)	44(2)
C(21)	4846(4)	4142(5)	1055(4)	35(2)
C(22)	4077(5)	3110(5)	501(4)	42(2)
C(23)	3474(5)	1841(6)	-4(5)	52(3)
C(24)	3512(6)	1205(6)	493(6)	76(4)
C(25)	4625(5)	2119(6)	45(5)	55(3)
C(26)	4630(6)	2454(7)	-553(6)	75(4)
O(20)	5653(2)	5209(4)	1488(2)	39(1)
O(21)	4665(3)	4268(3)	1501(3)	43(2)
N(20)	4616(3)	3583(4)	593(4)	46(2)
N(21)	4050(4)	2401(4)	201(4)	46(2)
S(20)	3382(1)	3329(1)	696(1)	45(1)
C(31)	4673(4)	2523(5)	2483(5)	42(2)

C(32)	4343(5)	1777(6)	2450(6)	64(3)
C(33)	4676(6)	1019(6)	2466(7)	80(4)
C(40)	3686(4)	3281(6)	2328(5)	47(2)
C(41)	3393(4)	4128(6)	2110(4)	37(2)
C(42)	2322(4)	4700(5)	1632(4)	44(2)
C(43)	1238(5)	5391(6)	1435(5)	56(3)
C(44)	688(5)	4996(8)	901(6)	91(4)
C(45)	1667(5)	4285(6)	2267(5)	62(3)
C(46)	1970(6)	4677(10)	2884(6)	98(5)
O(40)	4381(3)	3277(3)	2455(3)	45(2)
O(41)	3752(3)	4724(4)	2097(3)	43(1)
N(40)	2734(3)	4099(5)	1954(4)	45(2)
N(41)	1761(3)	4791(5)	1765(3)	46(2)
S(40)	2384(1)	5306(2)	1042(1)	49(1)
C(50)	5000	8234(13)	2500	103(7)
O(50)	4792(9)	7977(10)	2976(10)	95(6)
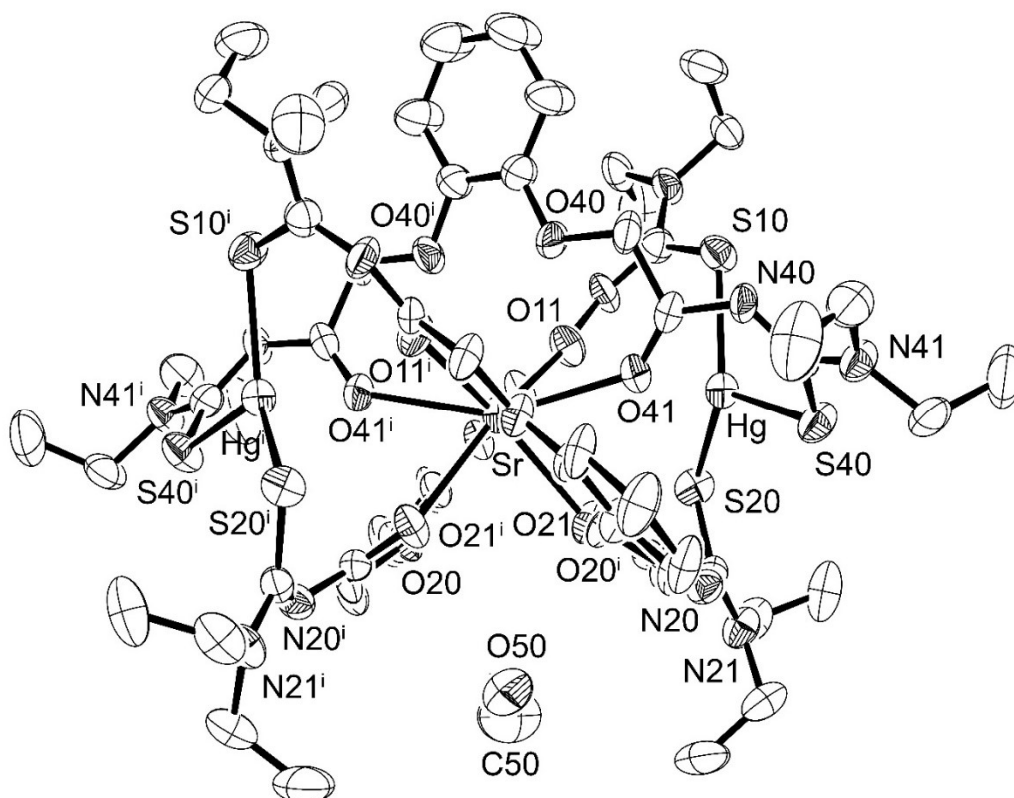
Figure 36: Ellipsoid plot (50% probability) of $\{Sr \subset [Hg_2(L^3)_3]\} \cdot CH_3OH$.